NASA CR-114741

A FORWARD SPEED EFFECTS STUDY ON JET NOISE FROM SEVERAL SUPPRESSOR NOZZLES IN THE NASA/AMES 40- BY 80-FOOT WIND TUNNEL

Final Report

by

M.R. Beulke
W.S. Clapper
E.O. McCann
H.M. Morozumi

GENERAL ELECTRIC COMPANY

Prepared For

National Aeronautics and Space Administration

NASA-Ames Research Center
Contract NAS2-7457

NASA CR-114741

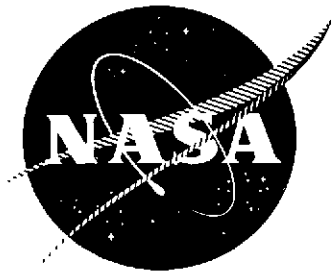

A FORWARD SPEED EFFECTS STUDY ON JET NOISE FROM SEVERAL SUPPRESSOR NOZZLES IN THE NASA/AMES 40- BY 80-FOOT WIND TUNNEL

Final Report

by

M.R. Beulke
W.S. Clapper
E.O. McCann
H.M. Morozumi

GENERAL ELECTRIC COMPANY

Prepared For

National Aeronautics and Space Administration

NASA-Ames Research Center
Contract NAS2-7457

1.0 ABSTRACT

A test program was conducted in the NASA/Ames 40 by 80 Foot Wind Tunnel to evaluate the effect of relative velocity on the jet noise signature of a conical ejector, auxiliary inlet ejector, 32 spokes and 104 tube nozzle with and without an acoustically treated shroud. The freestream velocities in the wind tunnel were varied from 0 to 103.6 m/sec (300 ft/sec) for exhaust jet velocities of 259.1 m/sec (850 ft/sec) to 609.6 m/sec (2000 ft/sec). Reverberation corrections for the wind tunnel were developed and the procedure is explained. In conjunction with wind tunnel testing the nozzles were also evaluated on an outdoor test stand. The wind tunnel microphone arrays were duplicated during the outdoor testing. The data were then extrapolated for comparisons with data measured using a microphone array placed on a 30.5 meter (100 ft) arc. Using these data as a basis, farfield to nearfield arguments are presented with regards to the data measured in the wind tunnel. Finally, comparisons are presented between predictions made using existing methods and the measured data.

The results of the study indicate that significant changes in the jet noise signature can be measured in the freestream environment simulated by using a wind tunnel. The magnitude of the change is a function of freestream velocity, acoustic angle and jet velocity. The comparison of the static and "wind on" data indicates that a complex suppressor such as the 104 tube nozzle does not become ineffective in a relative velocity environment.

Finally, recommendations are made for techniques that could be used to improve the wind tunnel for acoustic measurements.

2.0 TABLE OF CONTENTS

TABLE OF CONTENTS - Continued

LIST OF ILLUSTRATIONS, TABLES, AND SYMBOLS

Symbol	
A_{E8}	Effective nozzle area
C/A	Cart air
CM,cm	Centimeters
dB	Decible, re: 0.0002 dynes/cm^2
EANG	Angle of attack of engine
EGA	Extra ground attenuation
FF	Far field
FPS,ft/sec	Feet per second
FT,ft,'	Feet
Hz	Hertz
IN,in,"	Inches
in^2	Square inches
^oK	Degrees Kelvin
KgPS	Kilograms per second
M,m	Meters
M^2	Square meters
MPS,m/sec	Meter per second
NF	Near field
OASPL	Overall sound pressure level, calculated by summation of sound pressure levels at each 1/3 octave
OAPWL	Overall sound power level, calculated by summation of sound power levels at each 1/3 octave
PNdB,PNL	Perceived noise level in dB
PPS	Pounds per second
PWL	Sound power level, re: 10^{-13} watts

Symbol	
P_8/P_o	Exhaust nozzle total pressure divided by ambient pressure
Q	Dynamic head
^oR	Degrees Rankine
% RH	Ambient atmospheric relative humidity in percent
RPM	Revolutions per minute
SPL	Sound pressure level, re: 0.0002 dynes/cm^2
T_8	Total temperature of jet exhaust
T_o	Ambient temperature
V_o, V_T	Ambient air velocity
V_8	Velocity of jet exhaust
W_8	Total weight flow of engine
^{o}	Degrees-angular measure
Θ_I	Acoustic angle in degrees, referenced to engine inlet

SUMMARY

A J85 turbojet engine was used for wind tunnel and outdoor testing of a conical ejector, auxiliary inlet ejector (AIE), 32 spoke, 104 tube and 104 tube nozzle with an acoustically treated shroud. The objective of the program was to evaluate the NASA/Ames 40 by 80 - Foot Wind Tunnel (12.2 x 24.4 meters) as a fixed frame facility to be used for determining inflight effects.

To fulfill the program objective four test programs were conducted. These test programs and the nozzles evaluated may be summarized as follows:

Isolated Nacelle Wind Tunnel Test	-	concical ejector, AIE
Wing/Nacelle Wind Tunnel Test	-	conical ejector, 104 tube nozzle with and without an acoustically treated shroud
Outdoor Isolated Nacelle Static Test	-	conical ejector, AIE, 32-spoke, 104 tube nozzle with and without an acoustically treated shroud
Wing/Nacelle Outdoor Static Test	-	conical ejector, 104 tube nozzle with and without acoustically treated shroud

The difference between the wing/nacelle and isolated nacelle tests was that the noise signature of the nozzles was evaluated in an installed mode during the wing/nacelle test series. During the wind tunnel test programs, data were measured on 4.2 and 5.5 meter (13.8* and 18 ft) sidelines for jet velocities ranging from 259.1 m/sec (850 ft/sec) through 609.6 m/sec (2000 ft/sec). The simulated freestream velocities in the wind tunnel varied from zero to 103.6 m/sec (340 ft/sec). The tunnel background noise was measured for each simulated freestream condition and the data were corrected for this effect. The wind tunnel microphones arrays were duplicated during the outdoor static testing. The outdoor and wind tunnel static data were then compared to determine a set of wind tunnel reverberation corrections. Using these corrections, all wind tunnel data were corrected for reverberation effects. Also during the outdoor testing, data were measured on a 30.5 meter (100 ft) arc using microphones at the source (engine) centerline height.

*In this report, this sideline will be referred to as a nominal 13 foot sideline.

Using this farfield data, comparisons are made with extrapolated nearfield outdoor data (corrected for ground reflections) which were measured using the simulated wind tunnel microphone arrays. The purpose of these comparisons was to determine if the microphone arrays in the wind tunnel were in the farfield or nearfield region.

The data were analyzed and presented on the basis of OAPWL, one-third octave band PWL spectra, peak OASPL, OASPL and PNL directivity, and one-third octave band SPL spectra. The results of the program indicate that substantial reduction in the jet noise signature of conical ejector and complex suppressor nozzles can be measured as the simulated freestream velocity in the wind tunnel increases. The jet velocity at which this effect can be measured is a function of nozzle type, freestream velocity, jet velocity and the proximity of the microphone array to the noise source.

Analytical predictions are also made using existing techniques for the conical ejector nozzle and 104 tube nozzle. These predictions were compared to data on the basis of OAPWL, one-third octave band PWL spectra, and one-third octave band SPL spectra for the conical nozzle. The predictions for the 104 tube nozzle were done on the basis of peak OASPL, PNL and the peak one-third octave band SPL spectra. In general, agreement between the measured and predicted results is good.

5.0 INTRODUCTION

Need for Technology

One of the critical technology areas that must be defined is the effect of flight on the noise suppression characteristics of complex exhaust nozzle systems. This technology is essential if the true noise signature of the suppressor is to be determined in the actual environment that the suppressor must function.

The conventional technique used to evaluate the inflight suppression characteristics was to conduct flight testing using flying test beds. Unfortunately, this method has many inherent disadvantages if parametric studies are to be conducted similar to the type done during static testing. The hardware required for flight testing is extremely expensive. The control of the important variables such as aircraft speed, altitude, and exact aircraft position relative to the microphone location is extremely difficult.

One technique that would enable the evaluation of scale model configurations would be to use a wind tunnel to simulate freestream environment. This system would eliminate several of the disadvantages inherent in flight testing. It could be used to determine the change in the noise signature of the exhaust jet due to the changes in the turbulent mixing process because of the freestream environment. Recognizing the need to evaluate the wind tunnel as a test facility for forward speed effects, a test program was conducted in the NASA Ames 40 by 80 - Foot Wind Tunnel (12.2 x 24.4 meters).

Purpose of the Program

The program objective was to evaluate the wind tunnel as a technique by measuring the changes in the jet noise signature of a conical ejector, auxiliary inlet ejector and 104 tube nozzle with and without an acoustically treated shroud due to changes in freestream velocity in the 40 by 80 - Foot Wind Tunnel. These measurements were conducted for a wide range of jet velocities.

In addition to the wind tunnel testing, the test nozzles were also evaluated statically outdoors and these data were then compared with static data measured in the wind tunnel to determine the effects of reverberation on the measured data.

For comparisons with the measured data, predictions were also made using existing analytical and semi-empirical methods.

The purpose of this report is to document the results of the test program and present the comparisons of the predicted and measured data.

6.0 DESCRIPTION OF ENGINE AND NOZZLE CONFIGURATIONS

The General Electric J85 Engine was used in conjunction with the five nozzles that were evaluated during the test program. The J85-13 was used for the isolated nacelle wind test series and the J85-5 was used for the remaining tests. Presented on Figure 6.1 is a schematic of the engine and a tabulation defining the number of blades in each stage of the compressor and turbine. The engine stations for the J85 engine are defined on Figure 6.2.

Five nozzle configurations were used in conjunction with the J85 engine. These configurations were:

a. Conical ejector nozzle - Figure 6.3

b. Auxiliary inlet ejector nozzle (AIE) - Figure 6.4

c. 104 Elliptical tube nozzle - Figure 6.5

d. 104 Elliptical tube nozzle with an acoustically treated shroud - Figure 6.6

e. 32-Spoke area ratio - Figure 6.7

Each of the five engine nozzle configurations were tested in the isolated nacelle mode and the wing nacelle mode. The difference between the isolated nacelle and wing nacelle installation is illustrated by comparing Figures 7.1 and 6.3, respectively.

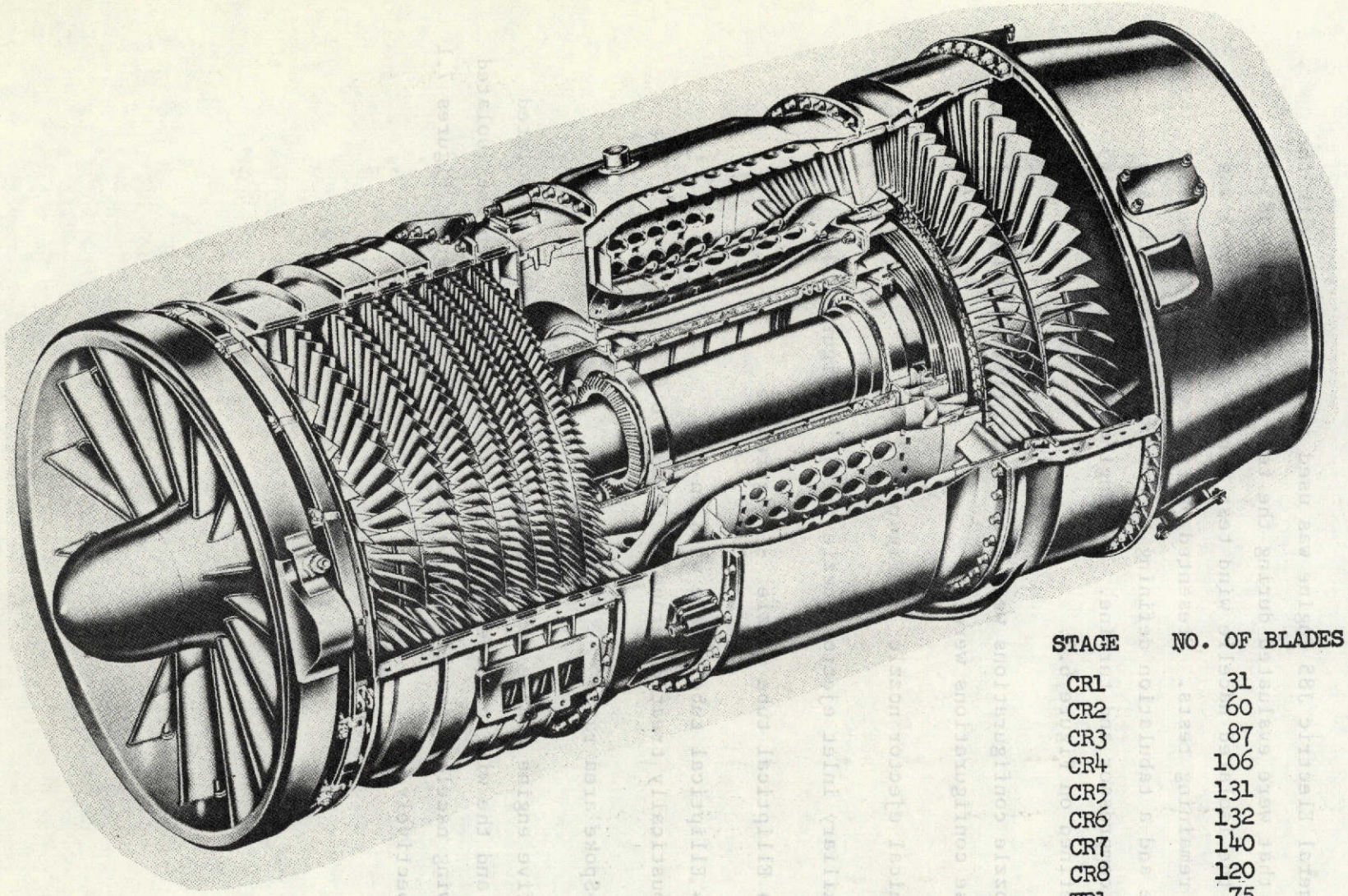

STAGE	NO. OF BLADES
CR1	31
CR2	60
CR3	87
CR4	106
CR5	131
CR6	132
CR7	140
CR8	120
TR1	75
TR2	55

FIGURE 6.1- CROSS SECTION OF J85 ENGINE

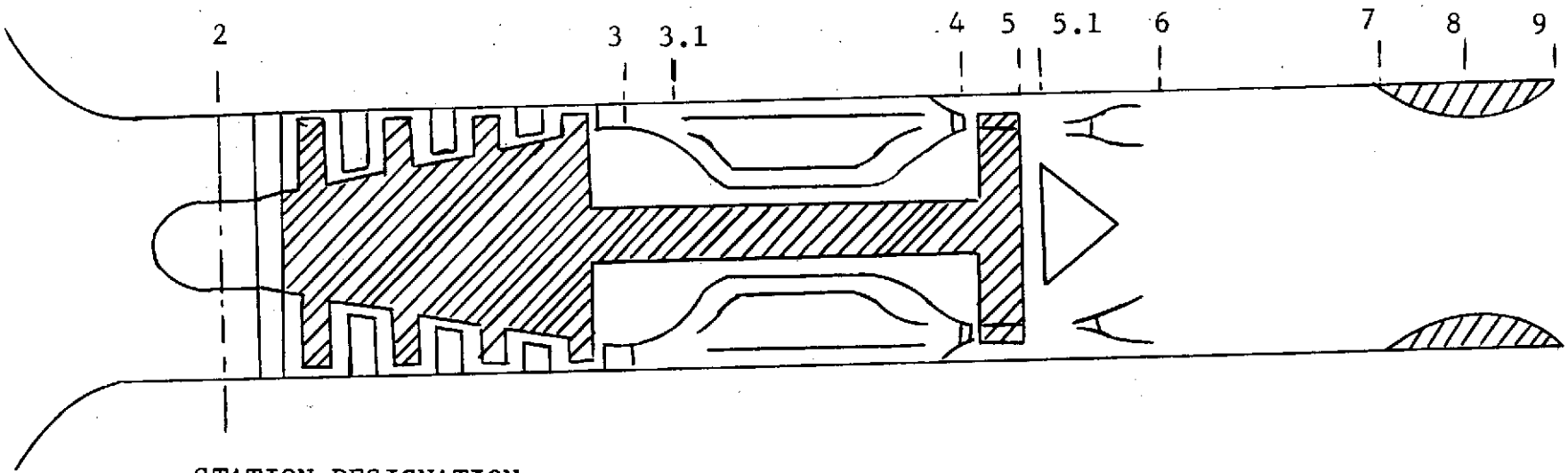

STATION DESIGNATION

2 Compressor Inlet
3 Compressor Outlet
3.1 Diffuser Inlet
4 Turbine Inlet
5 Turbine Outlet
5.1 Turbine Outlet - Average condition including cooling and leakage
6 Tailpipe Inlet - Upstream of afterburner
7 Tailpipe Outlet - Jet nozzle inlet
8 Jet Nozzle Throat
9 Jet Nozzle Outlet

FIGURE 6.2 - ENGINE STATIONS FOR THE J85 ENGINE

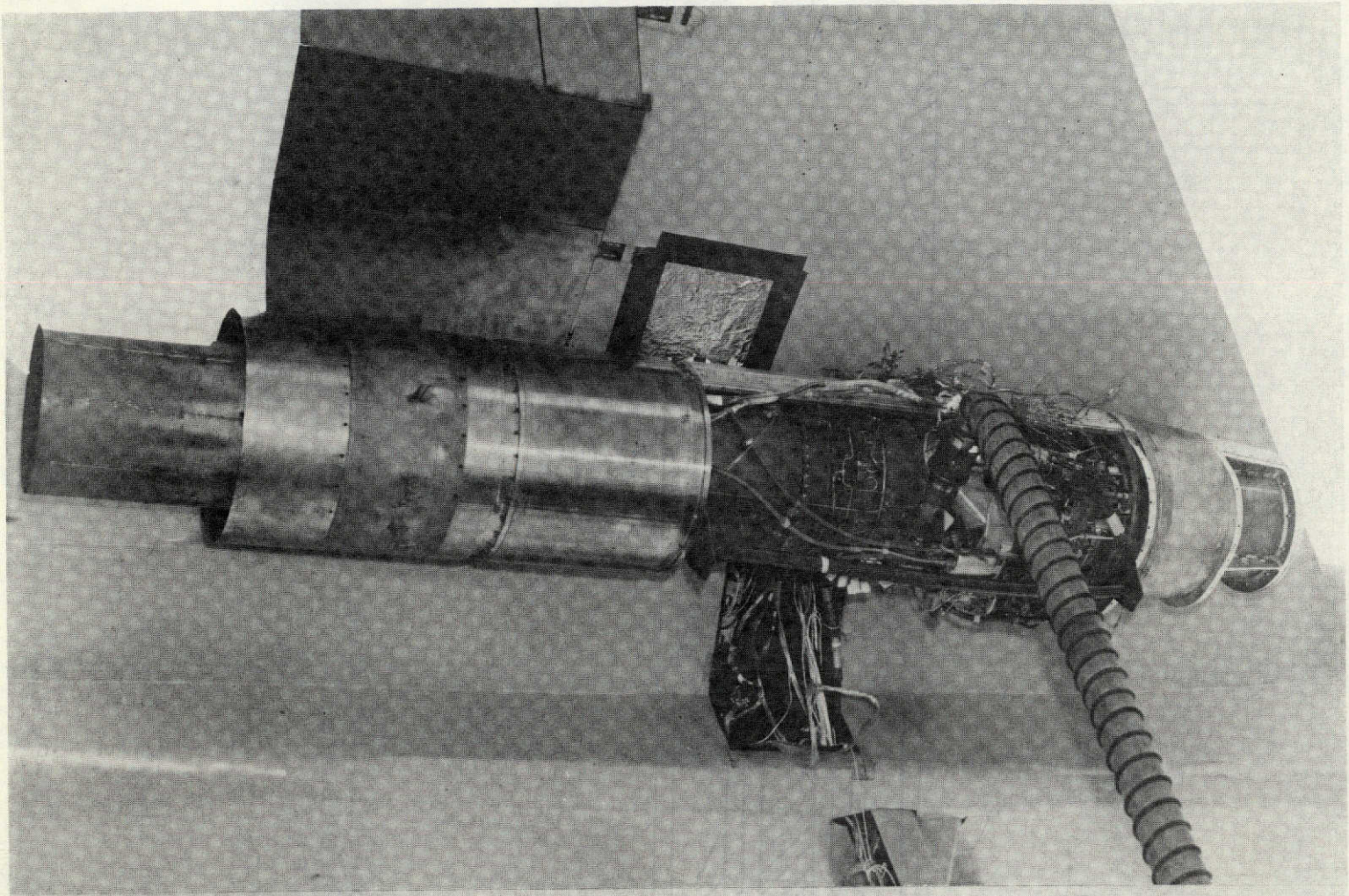

WING/NACELLE INSTALLATION - CONICAL EJECTOR NOZZLE

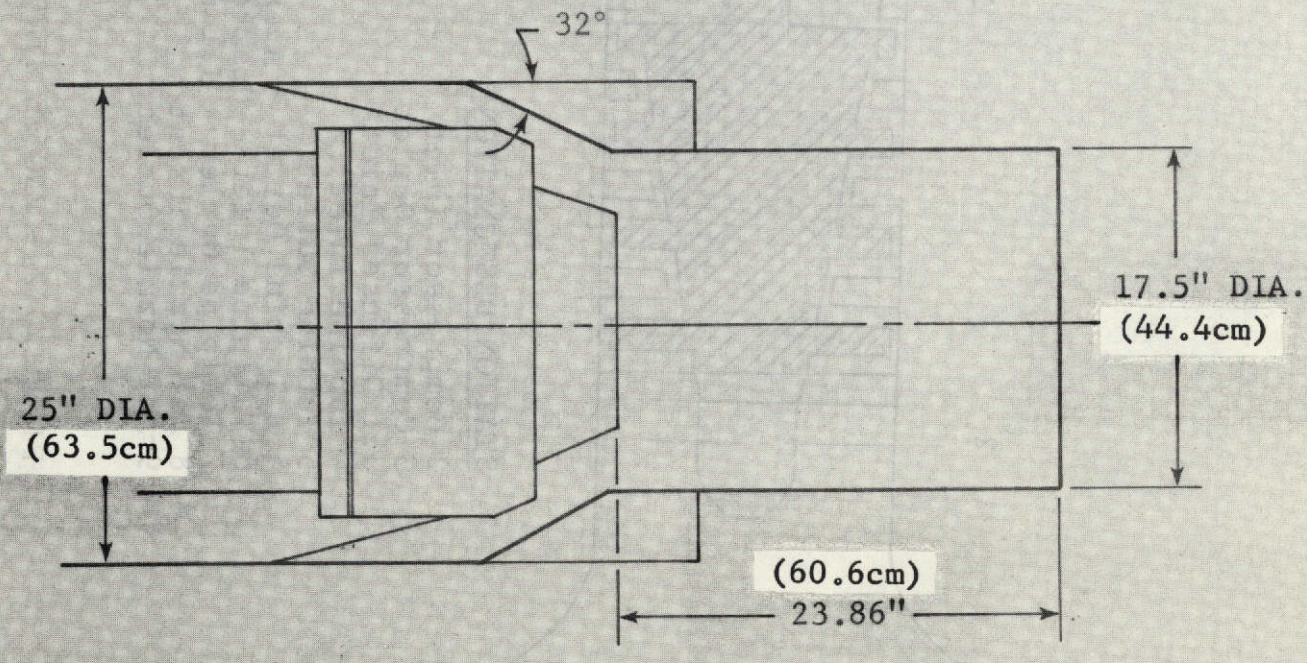

FIGURE 6.3 - SCHEMATIC OF CONICAL EJECTOR NOZZLE

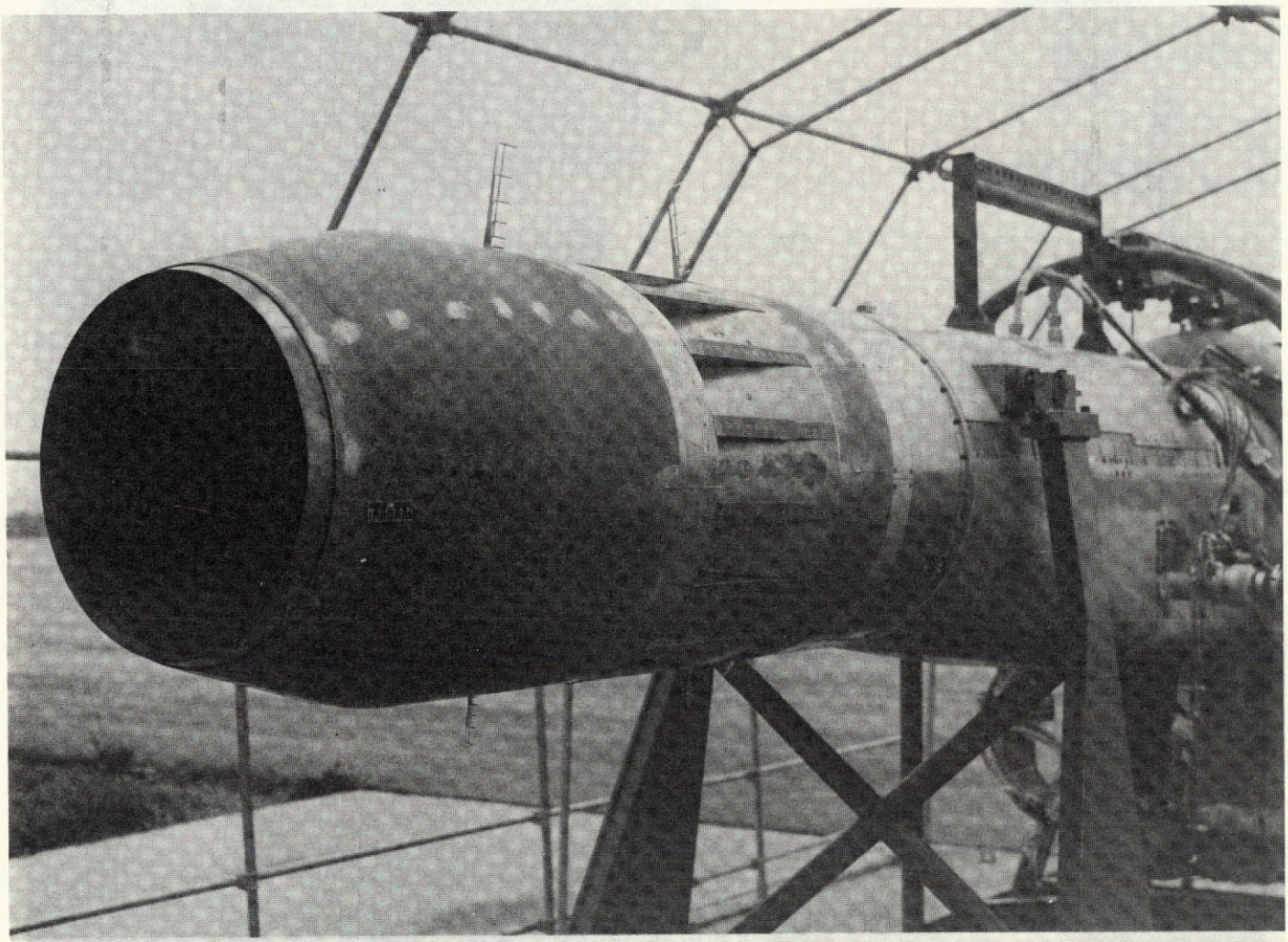

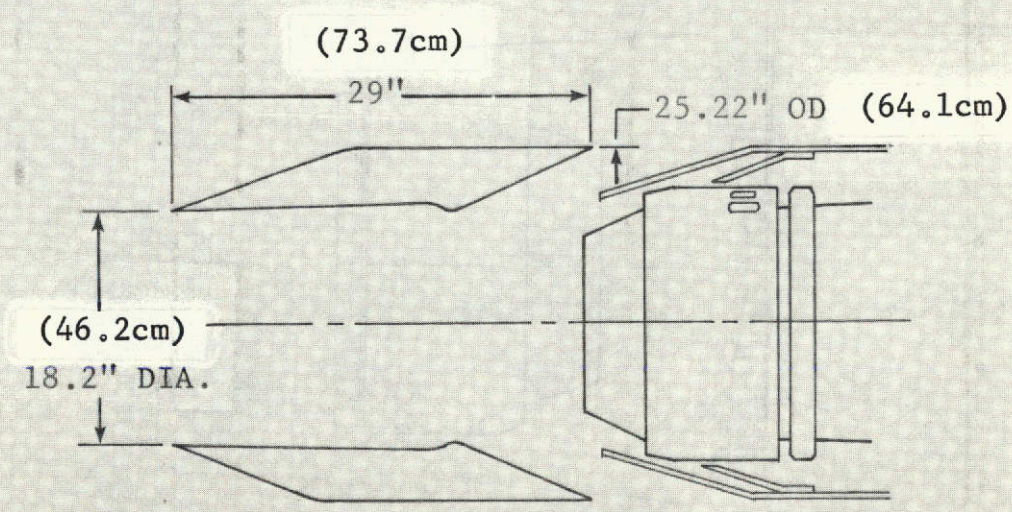

FIGURE 6.4 - AUXILIARY INLET EJECTOR NOZZLE

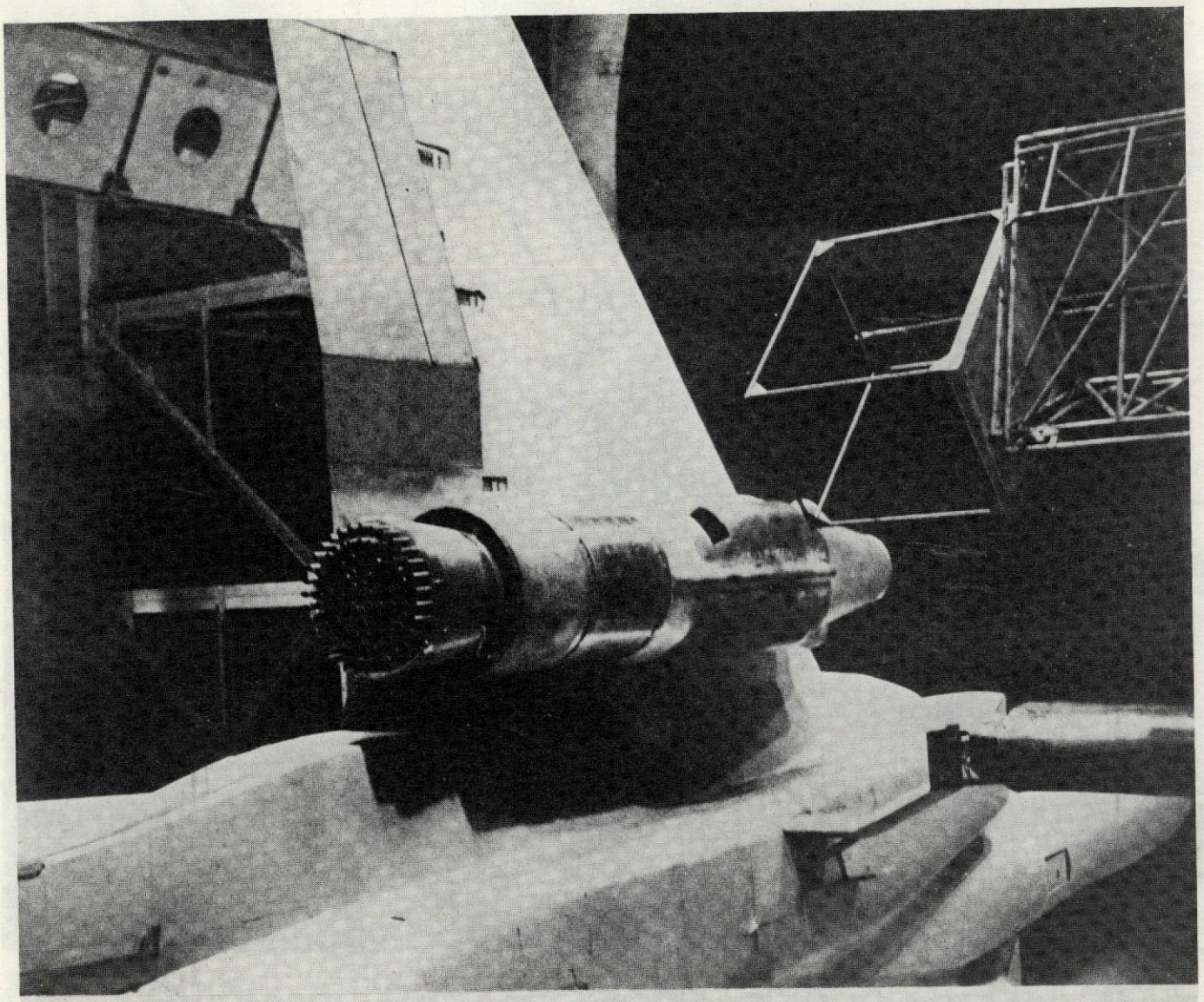

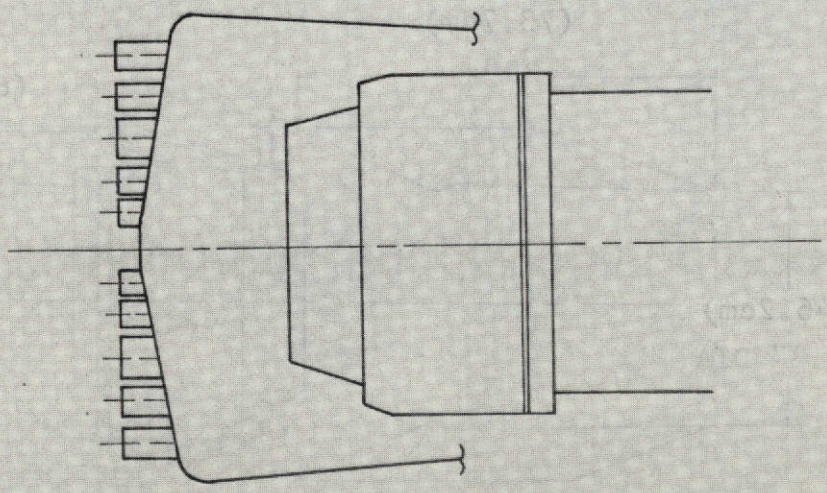

FIGURE 6.5 - 104 ELLIPTICAL TUBE NOZZLE

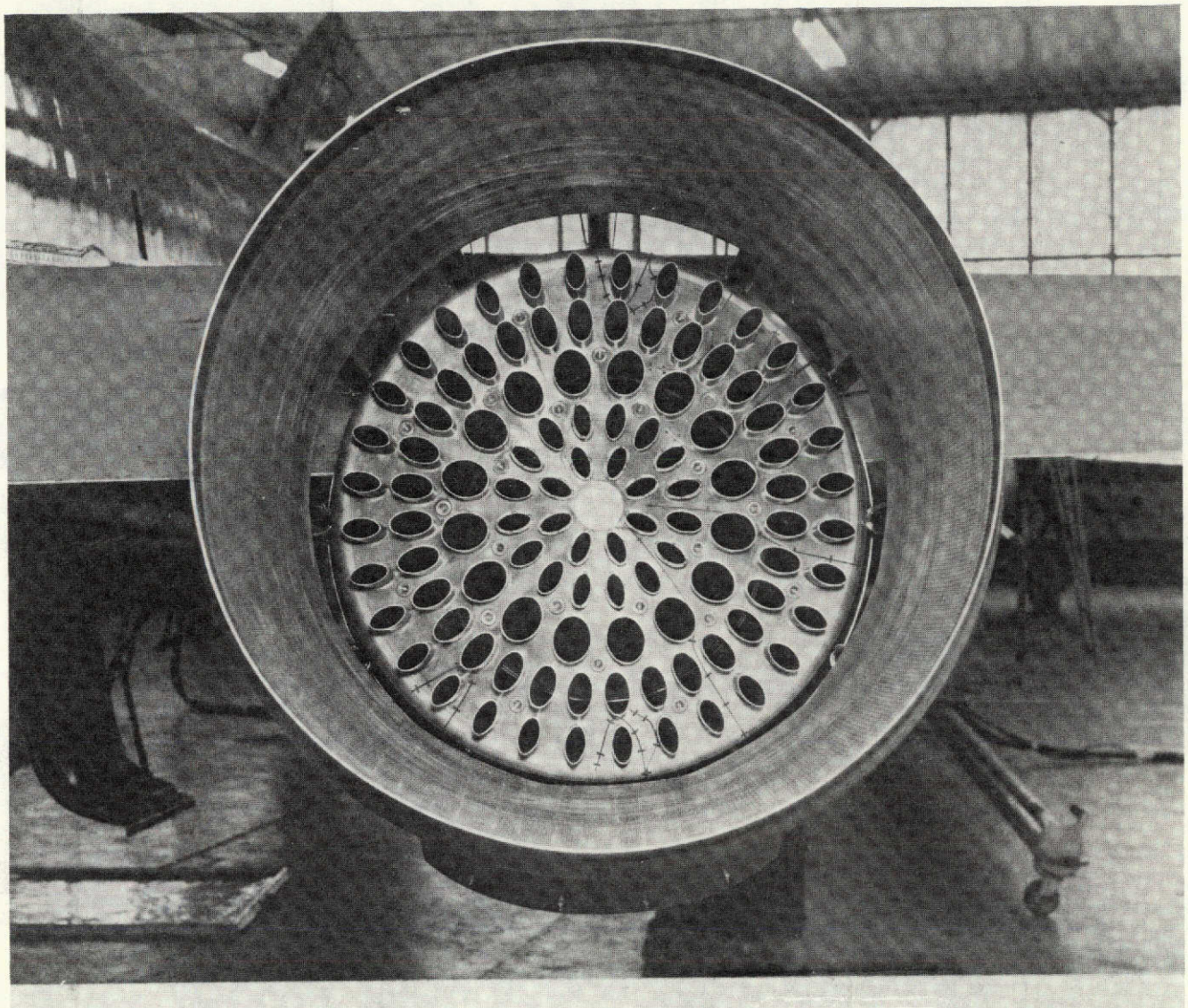

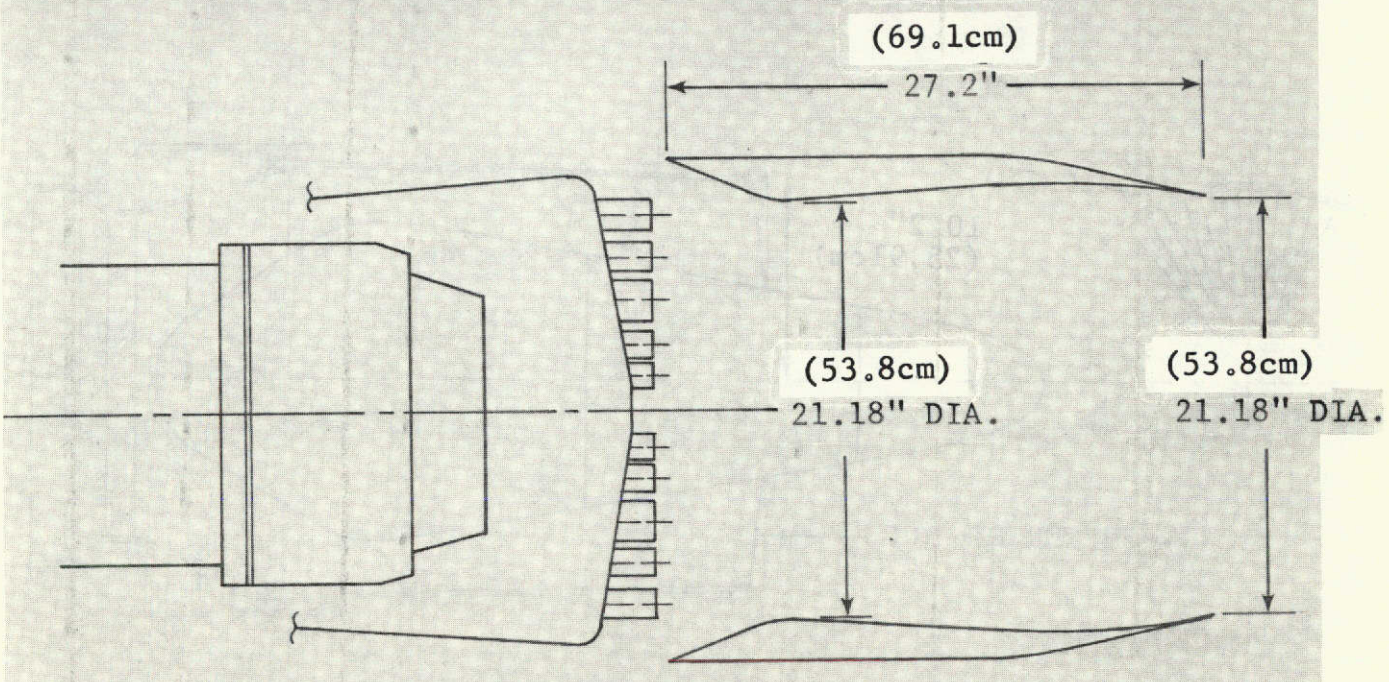

FIGURE 6.6 - 104 ELLIPTICAL TUBE NOZZLE WITH ACOUSTICALLY TREATED SHROUD

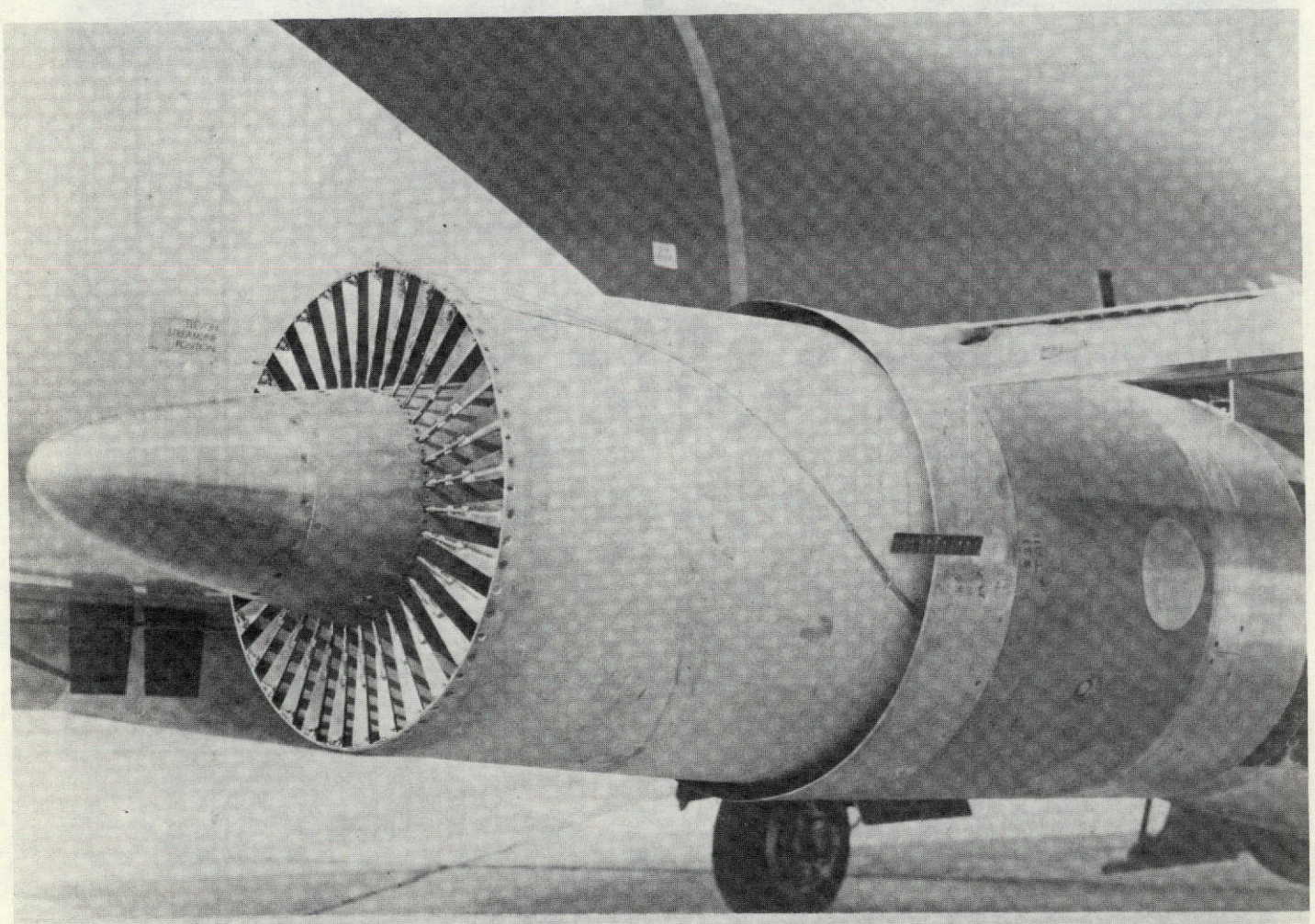

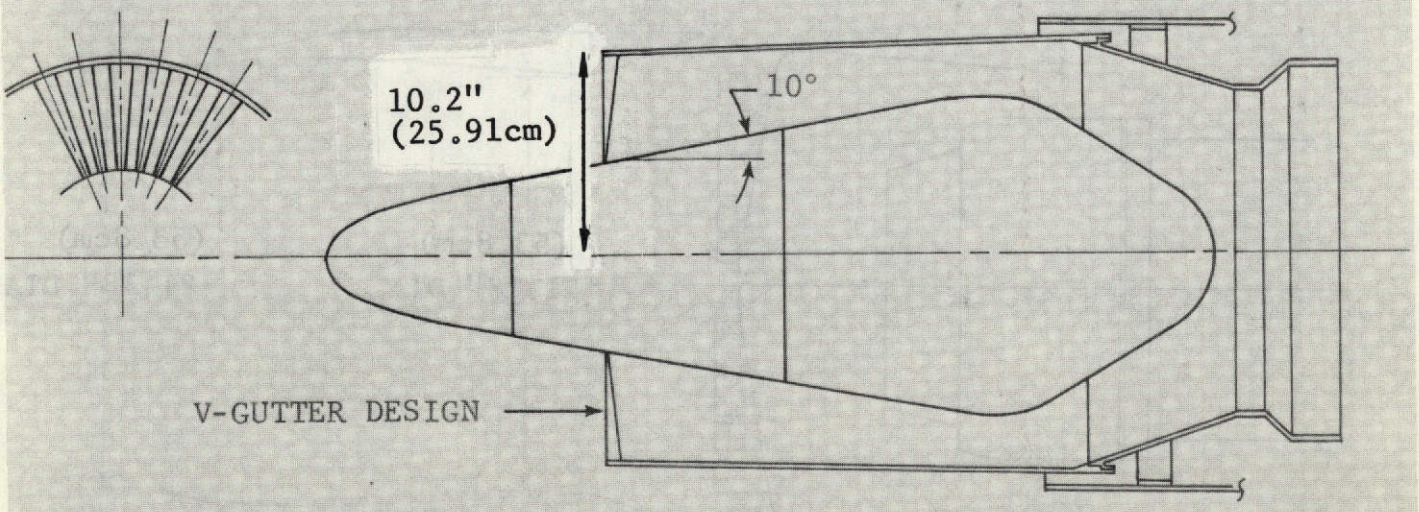

FIGURE 6.7 - 32-SPOKE NOZZLE

7.0 DESCRIPTION OF TEST SETUP

7.1 Isolated Nacelle Wind Tunnel Test

The isolated nacelle wind tunnel test defined as test number 423 was conducted with the J85-13 engine (No. 243-832). The test was conducted in the 40 by 80 - Foot Wind Tunnel. The engine centerline was positioned 6.0 meters (19.8 feet) above the wind tunnel floor and laterally in line with the wind tunnel centerline. Mounting of the engine on the test/thrust stand is presented on Figure 7-1. The two front struts provided the main support and a rear strut was used for stabilization. The rear strut also was used to change engine angle of attack. For static testing in the wind tunnel, a "rounded lip" or bellmouth inlet was used. For "wind on" testing, a "sharp lip" or flight inlet was used.

Prior to engine installation in the wind tunnel, a microphone reference plane was established normal to the tunnel flow and 4.3 meters (14 feet) aft of the front lift wire. Using the intersection of the engine centerline and the microphone reference plane as a focal point, two sideline nearfield microphone arrays were established. Figure 7-2 defines each microphone location with regard to microphone number. Presented on Figure 7-3 is the acoustic angle and acoustic path length for each microphone. All angles and distance identification for each microphone are based on the engine inlet being defined as zero degrees and the sound field focal point as being at the center of the exit plane of the exhaust nozzle. Since the height of the engine was different than estimated 6.0 m vs. 5.8 m (19.8' vs. 20') and the exhaust plane of the conical nozzle was 12.7 cm (five inches) forward of the reference plane, the microphone locations were slightly different than originally planned. Also, the location of the nozzle exit plane varied as a function of nozzle configuration. That is why there are slight differences between the acoustic angles for each of the configurations.

7.2 Isolated Nacelle Outdoor Static Test

The outdoor portion of the isolated nacelle test was designated Test A73 and was performed using a J85-5 engine. The engine was mounted using a support structure similar to that used in the wind tunnel test series. The engine centerline height was 6.1 meters (20 feet) above ground level. A photograph showing this test setup is presented on Figure 7-4.

The microphone arrays were positioned relative to a microphone reference plane that was established 2.1 meters (7 feet) aft of the center of the front support ball socket. This caused the exhaust plane of the conical nozzle to be identical to the microphone reference plane. As a result, there was a slight diffference between the microphone arrays in the wind tunnel and those that were used in the outdoor test, however, the maximum error was less than two degrees and would have a negligible effect. The locations of the exhaust planes of the other nozzles relative to the microphone reference plane are defined on Figure 7.5. Also, defined on Figure 7.5 are the locations of the nearfield microphones relative to the microphone reference plane. Because the exhaust plane of each of the five nozzles is different in relation to the microphone reference plane, the acoustic path lengths are slightly different for each configuration. However, this effect is extremely small. This conclusion is supported by the tabulation of acoustic angle and path length for each configuration presented on Figure 7.6.

The farfield microphone array consisted of twelve microphones that were located on a 30.5 meter (100 foot) radius. The reference point for this radius was the exit plane of the conical nozzle. The microphones were located in a horizontal plane through the engine centerline. Presented on Figure 7.7 is a picture of the acoustic arena and a schematic defining the microphone locations.

7.3 Wing Nacelle Outdoor Static Test

The J85-5 engine was used for the wing/nacelle outdoor static test. This test was designated test B73. The engine was mounted under the right wing of an aircraft model with the engine centerline 6.1 meters (20 feet) above the ground and laterally 2.1 meters (82 inches) from the centerline of the aircraft model. This installation is presented on Figure 7.8. The model was supported with a tripod structure similar to the isolated nacelle test.

The nearfield microphones were again established relative to a microphone reference plane perpendicular to the engine centerline and in the exhaust plane of the conical ejector nozzle. All microphones were mounted in a horizontal plane 1.8 meters (6 feet) above the ground. Figure 7.9 shows each microphone

location relative to the microphone reference plane. Defined on Figure 7.10 are the acoustic angle and path length for each microphone for all the configurations that were tested.

The farfield microphone array was again setup on a 30.5 meter (100 foot) radius referenced to the center of the conical nozzle exit plane. The array consisted of ten microphones. The microphones were mounted in the horizontal plane of the engine centerline. The locations of these microphones are defined on Figure 7.11.

7.4 Wing/Nacelle Wind Tunnel Test

The wing/nacelle wind tunnel test was designated test number 428. This test was conducted in the 40 by 80 - Foot Wind Tunnel using a J85-5 engine mounted under the wing of an aircraft test model. This aircraft model was identical to the one used for the outdoor wing nacelle test series.

The model was supported by a tripod structure with the engine centerline 6.1 meters (19.9 feet) above the wind tunnel floor. A photograph of the installation is presented on Figure 7.12.

For static testing in the wind tunnel, a bellmouth inlet was used. During the "wind on" testing, a flight inlet was used and the lower part of the engine nacelle was replaced with a "bath tub" section, Figure 7.13, to allow cooling air to flow in the cavity between the engine and the nacelle.

The microphone array was installed relative to a reference plane 7.6 meters (24.8 feet) aft of the front lift wire which coincided with the exhaust plane of the conical ejector nozzle. A schematic of the microphone array is presented on Figure 7.14. It should be noted that microphones one through seven and fourteen were alternately staggered $\pm$ 10.2 cm (4 inches) on each side of the engine centerline. This was to keep the downstream microphones from being in the wake produced by the upstream microphones. The acoustic angles and path lengths for each of the nozzles evaluated during this phase of testing are defined on Figure 7.15. The slight differences between each of the nozzles are due to where the nozzle exhaust plane fell in relation to the microphone reference plane.

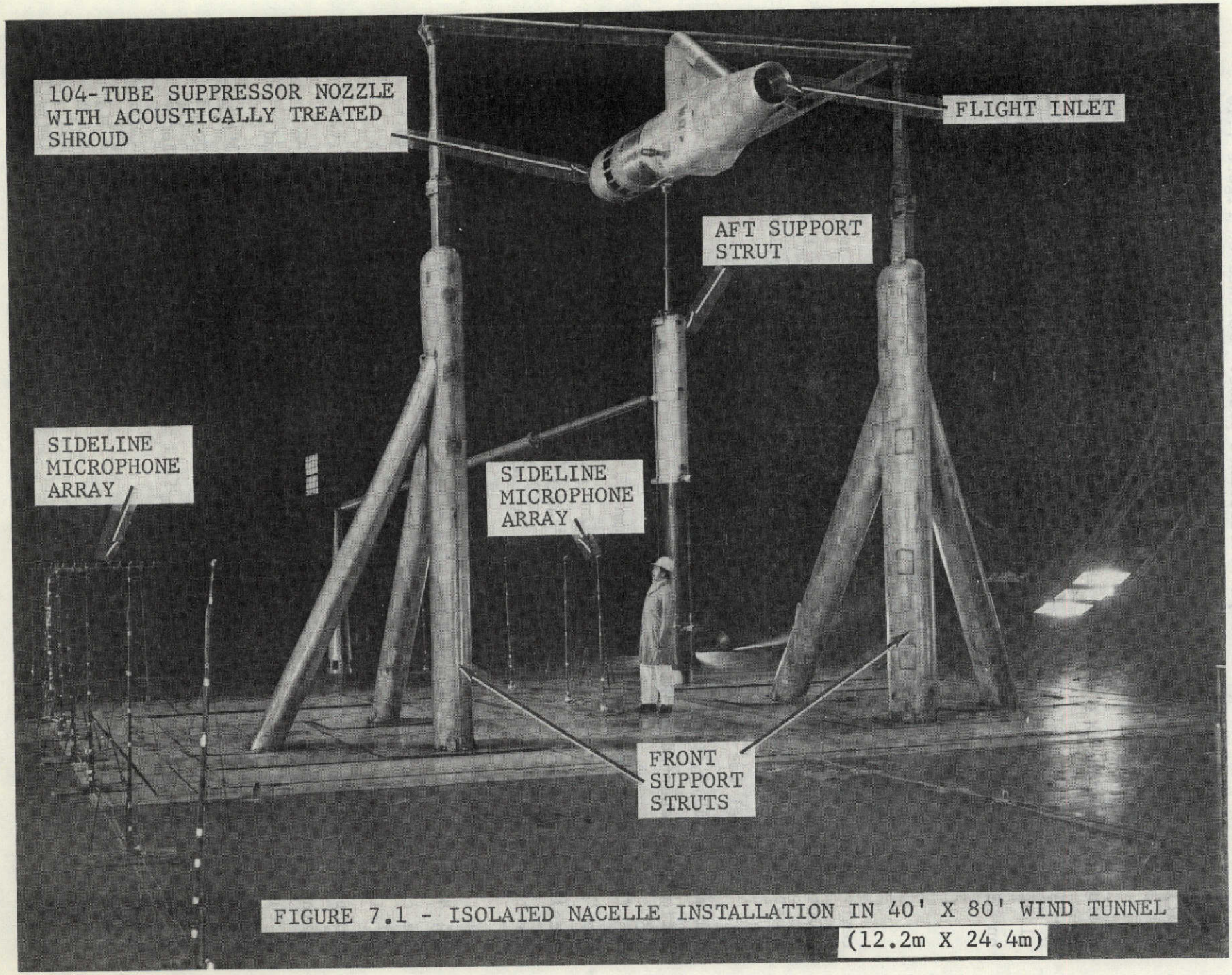

FIGURE 7.1 - ISOLATED NACELLE INSTALLATION IN 40' X 80' WIND TUNNEL (12.2m X 24.4m)

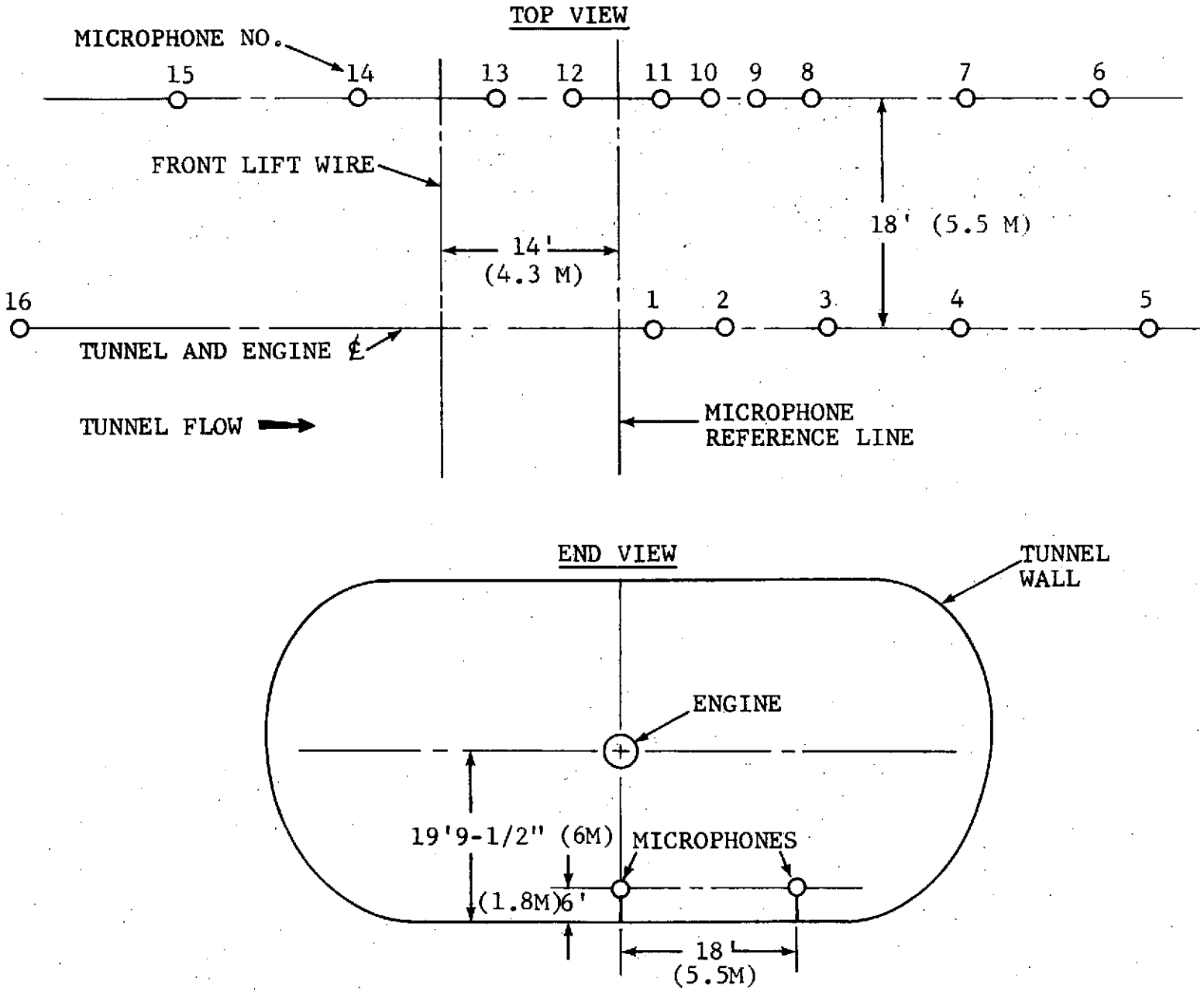

FIGURE 7.2 - DEFINITION OF MICROPHONE LOCATIONS - ISOLATED NACELLE WIND TUNNEL TEST

MIC NO.	CONICAL NOZZLE		AIE NOZZLE	
	ACOUSTIC ANGLE REF. ENGINE INLET (DEGREES)	ACOUSTIC PATH LENGTH (FEET, METERS)	ACOUSTIC ANGLE REF. ENGINE INLET (DEGREES)	ACOUSTIC PATH LENGTH (FEET, METERS)
1	101.3	14.1, 4.3	99.6	14.0, 4.3
2	119.9	15.9, 4.8	118.5	15.7, 4.8
3	139.1	21.1, 6.4	138.3	20.7, 6.3
4	157.5	35.9, 10.9	157.2	35.5, 10.8
5	169.5	75.4, 23	169.4	75.0, 22.9
16	13.0	61.2, 18.7	12.9	61.6, 18.8
6	159.7	65.5, 20	159.6	65.1, 19.8
7	149.8	45.0, 13.8	149.5	44.7, 13.6
8	130.1	29.6, 9	129.5	29.4, 9
9	120.3	26.3, 8	119.5	26.1, 8
10	110.4	24.2, 7.4	109.4	24.1, 7.3
11	101.0	23.1, 7	100.0	23.0, 7
12	81.0	23.0, 7	80.0	23.0, 7
13	61.3	25.8, 7.9	60.5	26.1, 8
14	41.0	34.6, 10.5	40.6	34.9, 10.6
15	30.8	44.3, 13.5	30.5	44.7, 13.6

FIGURE 7.3 - ISOLATED NACELLE WIND TUNNEL TEST
DEFINITION OF MICROPHONE LOCATION

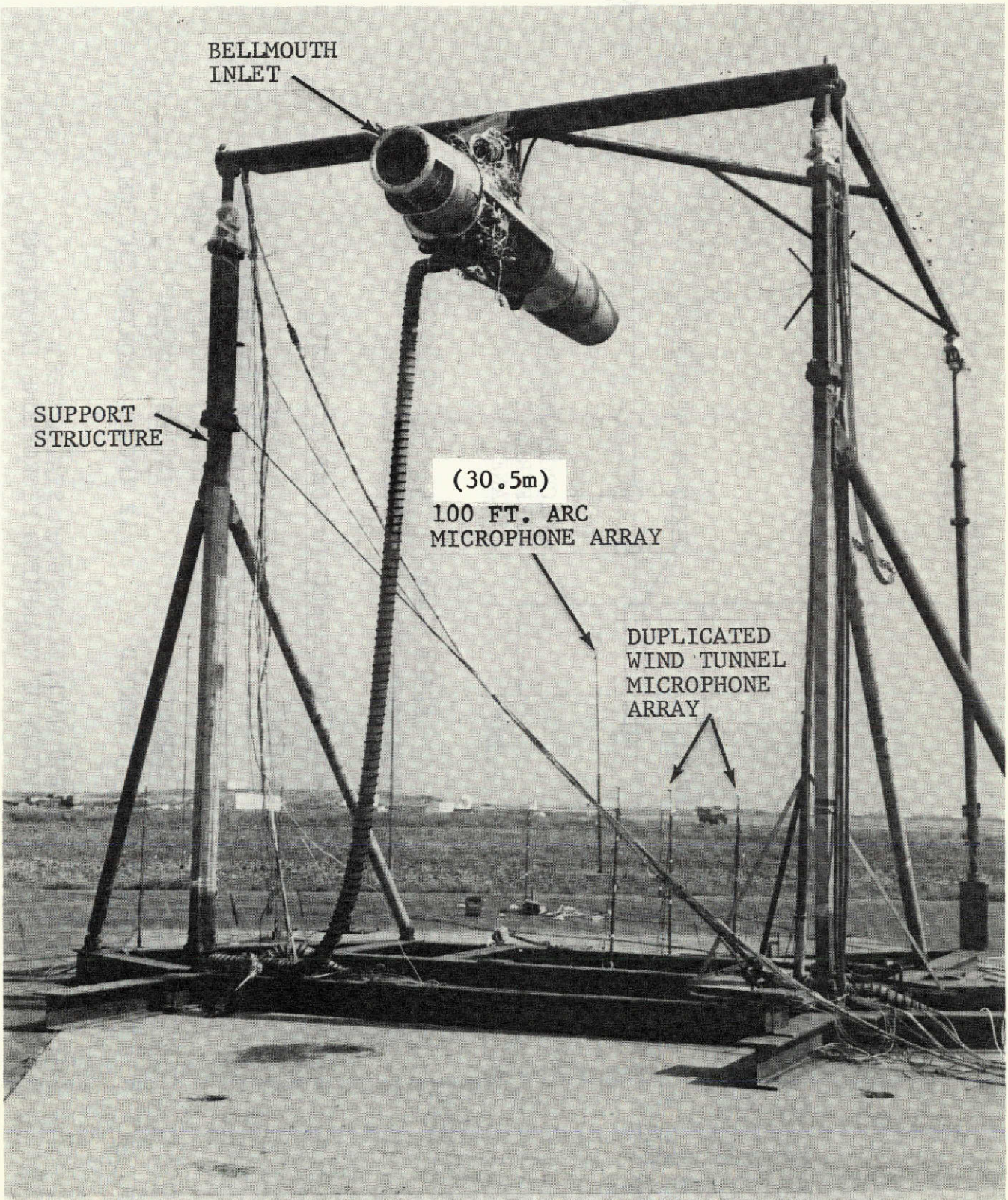

FIGURE 7.4 - ISOLATED NACELLE INSTALLATION - OUTDOOR STATIC TEST

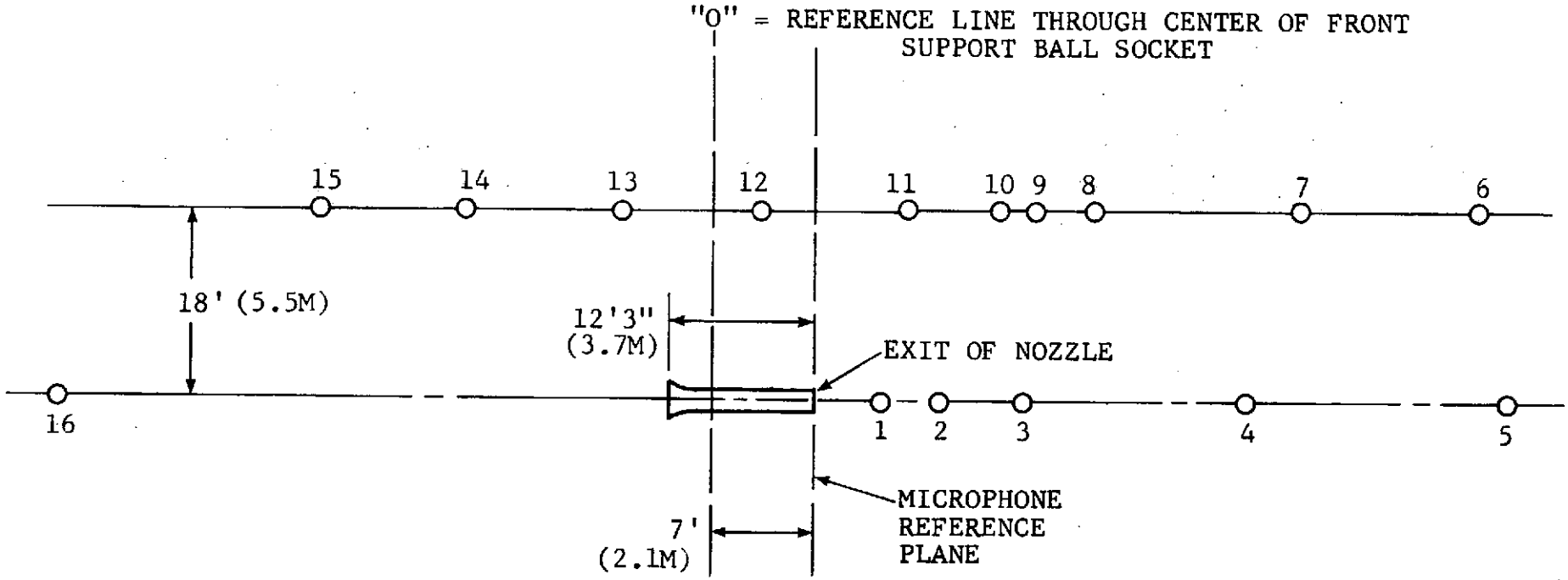

PLANE VIEW

ALL MIC HEIGHTS TO BE 6' FROM GROUND (1.8M)

NOZZLE LENGTHS REFERENCE TO CONICAL NOZZLE

CONFIGURATION	LENGTH
AIE	5 INCHES LONGER (12.7CM)
32 SPOKE	2.5 INCHES LONGER (6.4CM)
104 TUBE WITH SHROUD	0 INCHES LONGER
104 TUBE WITHOUT SHROUD	12 INCHES SHORTER (30.5CM)

FIGURE 7.5 - ISOLATED NACELLE OUTDOOR STATIC TEST DEFINITION OF NEARFIELD MICROPHONE LOCATIONS

MIC NO.	CONICAL NOZZLE		AIE NOZZLE		104-TUBE NOZZLE WITHOUT SHROUD		104-TUBE NOZZLE WITH SHROUD		32-SPOKE NOZZLE	
	ANGLE (DEGREES) REF. 0° AT ENGINE INLET	ACOUSTIC PATH LENGTH (FT.,METERS)	ANGLE (DEGREES) REF. 0° AT ENGINE INLET	ACOUSTIC PATH LENGTH (FT.,METERS)	ANGLE (DEGREES) REF. 0° AT ENGINE INLET	ACOUSTIC PATH LENGTH (FT.,METERS)	ANGLE (DEGREES) REF. 0° AT ENGINE INLET	ACOUSTIC PATH LENGTH (FT.,METERS)	ANGLE (DEGREES) REF. 0° AT ENGINE INLET	ACOUSTIC PATH LENGTH (FT.,METERS)
1	99.6	14.0, 4.3	98.1	13.9, 4.2	103.6	14.2, 4.3	99.6	14.0, 4.3	98.8	14.0, 4.3
2	118.5	15.7, 4.8	117.3	15.5, 4.7	121.6	16.2, 4.9	118.5	15.7, 4.8	117.9	15.6, 4.8
3	138.3	20.7, 6.3	137.6	20.5, 6.2	140.1	21.5, 6.6	138.3	20.7, 6.3	138.0	20.6, 6.3
4	157.2	35.5, 10.8	156.9	35.2, 10.7	157.8	36.5, 11.1	157.2	35.5, 10.8	157.0	35.3, 10.8
5	169.4	75.0, 22.9	169.3	74.7, 22.8	169.5	76.0, 23.2	169.4	75.0, 22.9	169.4	74.8, 22.8
16	12.9	61.6, 18.8	12.9	61.9, 18.9	12.2	60.6, 18.5	12.9	61.6, 18.8	12.9	61.8, 18.8
6	159.6	65.1, 19.8	159.5	64.7, 19.7	159.9	66.0, 20.1	159.6	65.1, 19.8	159.5	64.9, 19.8
7	149.5	44.7, 13.6	149.3	44.4, 13.5	150.1	45.6, 13.9	149.5	44.7, 13.6	149.4	44.5, 13.6
8	129.5	29.4, 9.0	128.9	29.1, 8.9	130.9	30.0, 9.1	129.5	29.4, 9.0	129.1	29.2, 8.9
9	119.5	26.1, 8.0	118.8	25.9, 7.9	121.4	26.6, 8.1	119.5	26.1, 8.0	119.1	25.9, 7.9
10	109.4	24.1, 7.3	108.6	99.1, 30.2	111.6	24.4, 7.4	109.4	24.1, 7.3	109.0	24.0, 7.3
11	100.0	23.0, 7.0	99.1	23.0, 7.0	102.4	23.2, 7.1	100.0	23.0, 7.0	99.5	23.0, 7.0
12	80.0	23.0, 7.0	79.1	23.1, 7.0	82.5	22.9, 7.0	80.0	23.0, 7.0	79.5	23.1, 7.0
13	60.5	26.1, 8.0	59.8	26.2, 8.0	62.4	25.6, 7.8	60.5	26.1, 8.0	60.1	26.2, 8.0
14	40.6	34.9, 10.6	40.2	35.2, 10.7	41.6	34.1, 10.4	40.6	34.9, 10.6	40.3	34.0, 10.4
15	30.5	44.7, 13.6	30.2	45.0, 13.7	31.2	43.8, 13.4	30.5	44.7, 13.6	30.4	44.9, 13.7

FIGURE 7.6 - ISOLATED NACELLE OUTDOOR STATIC TEST

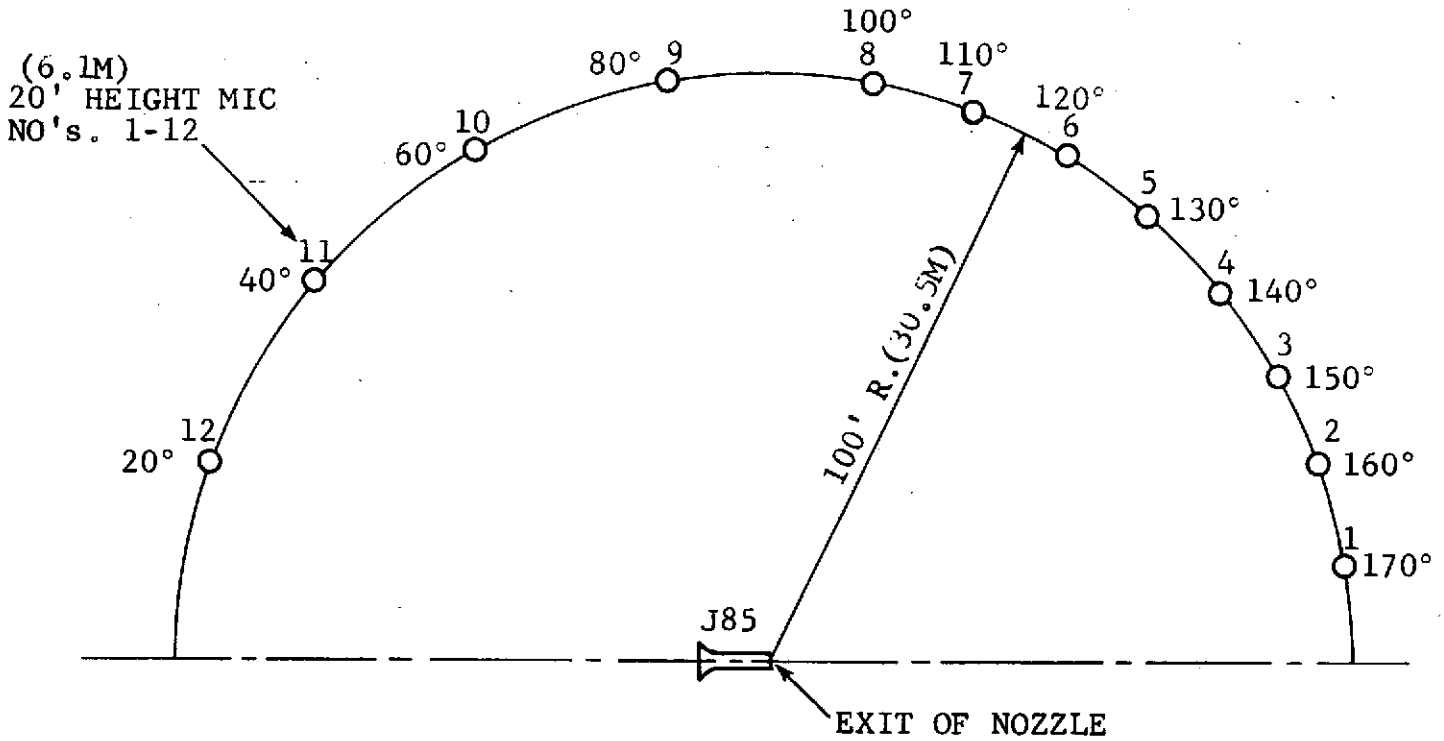

FIGURE 7.7 - ISOLATED NACELLE OUTDOOR STATIC TEST
DEFINITION OF FARFIELD MICROPHONE LOCATIONS

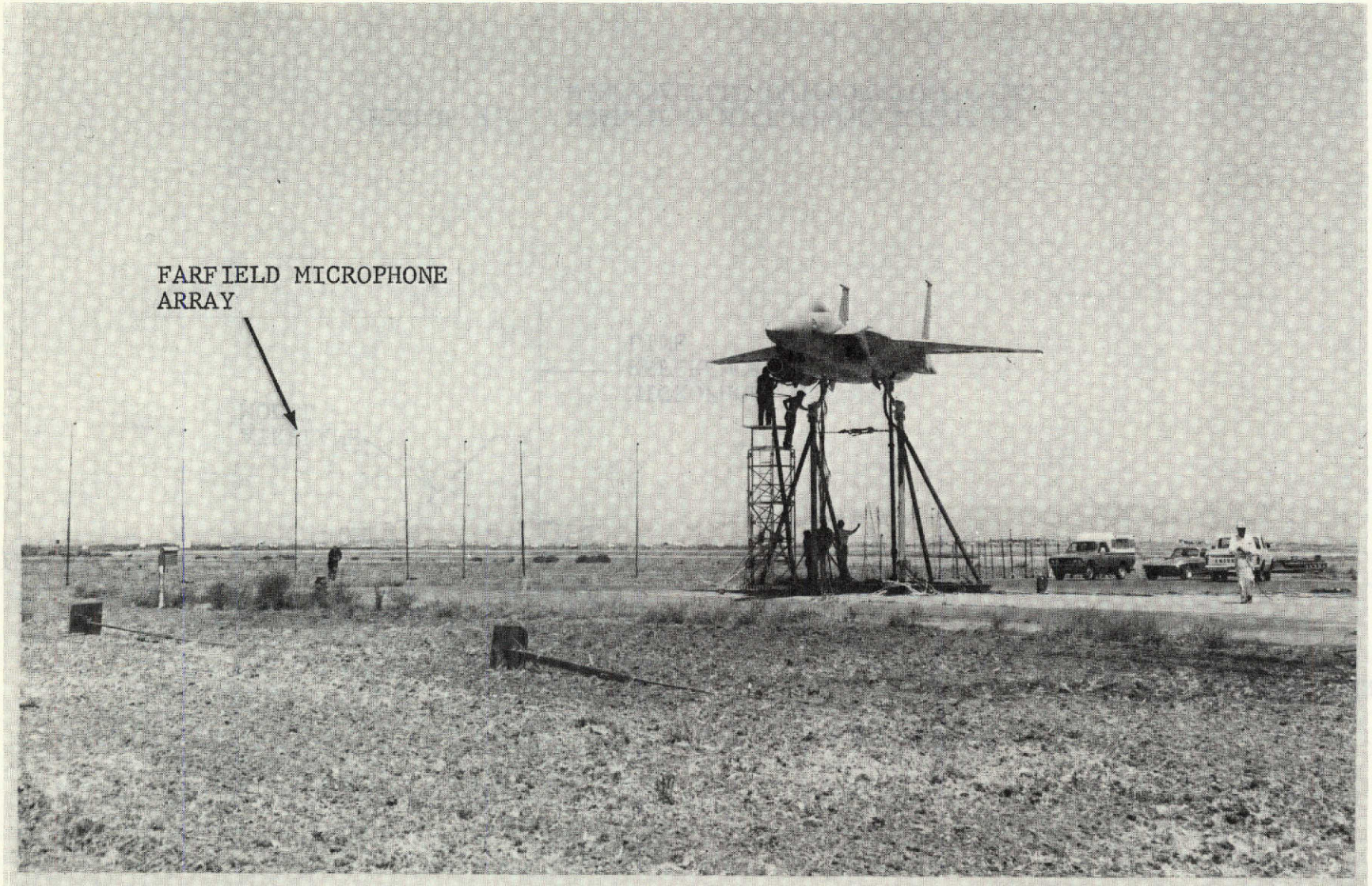

FIGURE 7.8 - WING/NACELLE INSTALLATION OUTDOOR STATIC TEST

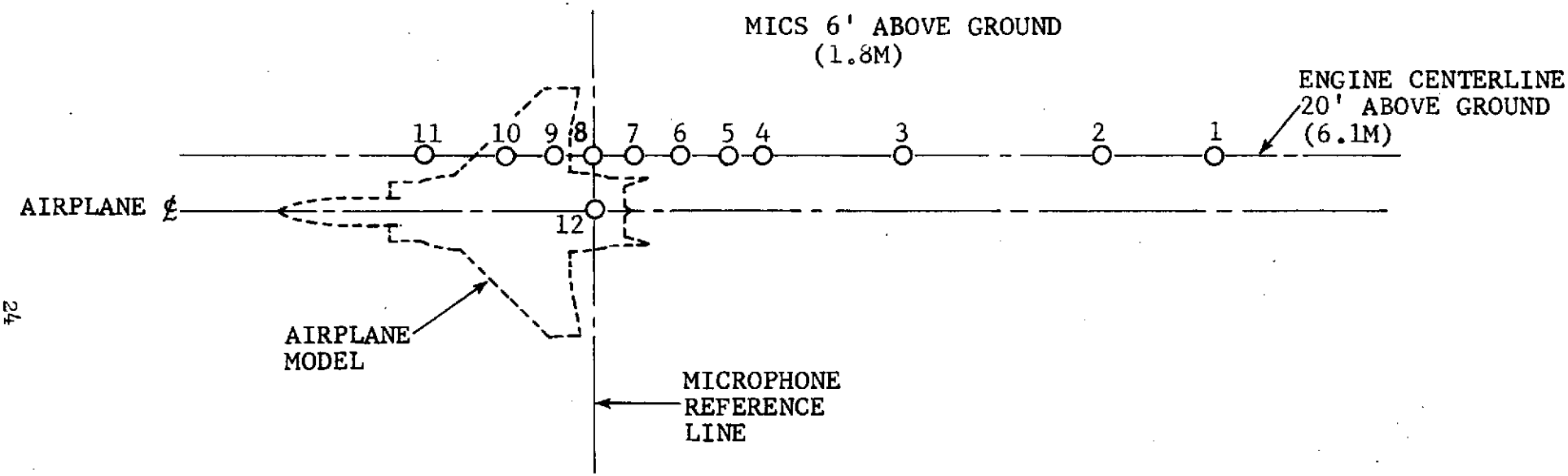

FIGURE 7.9 - NEARFIELD MICROPHONE LOCATIONS
WING/NACELLE OUTDOOR STATIC TEST

MIC NO.	CONICAL NOZZLE		32-SPOKE NOZZLE		104-TUBE NOZZLE WITHOUT SHROUD		104-TUBE NOZZLE WITH SHROUD	
	ANGLE (DEGREES) REF. 0° AT ENGINE INLET	ACOUSTIC PATH LENGTH (FT.,METERS)	ANGLE (DEGREES) REF. 0° AT ENGINE INLET	ACOUSTIC PATH LENGTH (FT.,METERS)	ANGLE (DEGREES) REF. 0° AT ENGINE INLET	ACOUSTIC PATH LENGTH (FT.,METERS)	ANGLE (DEGREES) REF. 0° AT ENGINE INLET	ACOUSTIC PATH LENGTH (FT.,METERS)
1	161.3	43.6, 13.3	161.2	43.4, 13.2	161.7	44.6, 13.6	161.3	43.6, 13.3
2	156.8	35.6, 10.9	159.4	39.8, 12.1	160.0	40.9, 12.5	159.5	39.9, 12.2
3	145.9	25.0, 7.6	145.6	24.8, 7.6	147.1	25.8, 7.9	145.9	25.0, 7.6
4	137.9	20.9, 6.4	125.9	17.3, 5.3	129.0	18.0, 5.5	126.4	17.4, 5.3
5	126.4	17.4, 5.3	121.1	16.4, 5.0	124.6	17.0, 5.2	121.8	16.5, 5.0
6	110.3	14.9, 4.5	109.5	14.8, 4.5	113.8	15.3, 4.7	110.3	14.9, 4.5
7	100.5	14.2, 4.3	99.6	14.2, 4.3	104.4	14.5, 4.4	100.5	14.2, 4.3
8	90.0	14.0, 4.3	89.1	14.0, 4.3	94.1	14.0, 4.3	90.0	14.0, 4.3
9	79.5	14.2, 4.3	78.7	14.3, 4.4	83.5	14.1, 4.3	79.5	14.2, 4.3
10	69.7	14.9, 4.5	69.0	15.0, 4.6	73.4	14.6, 4.6	69.7	14.9, 4.5
11	53.6	17.4, 5.3	53.0	17.5, 5.3	56.3	16.8, 5.1	53.6	17.4, 5.3
12	90.0	15.6, 4.8	89.2	15.6, 4.8	93.7	15.6, 4.8	90.0	15.6, 4.8

FIGURE 7.10 - WING/NACELLE OUTDOOR TEST

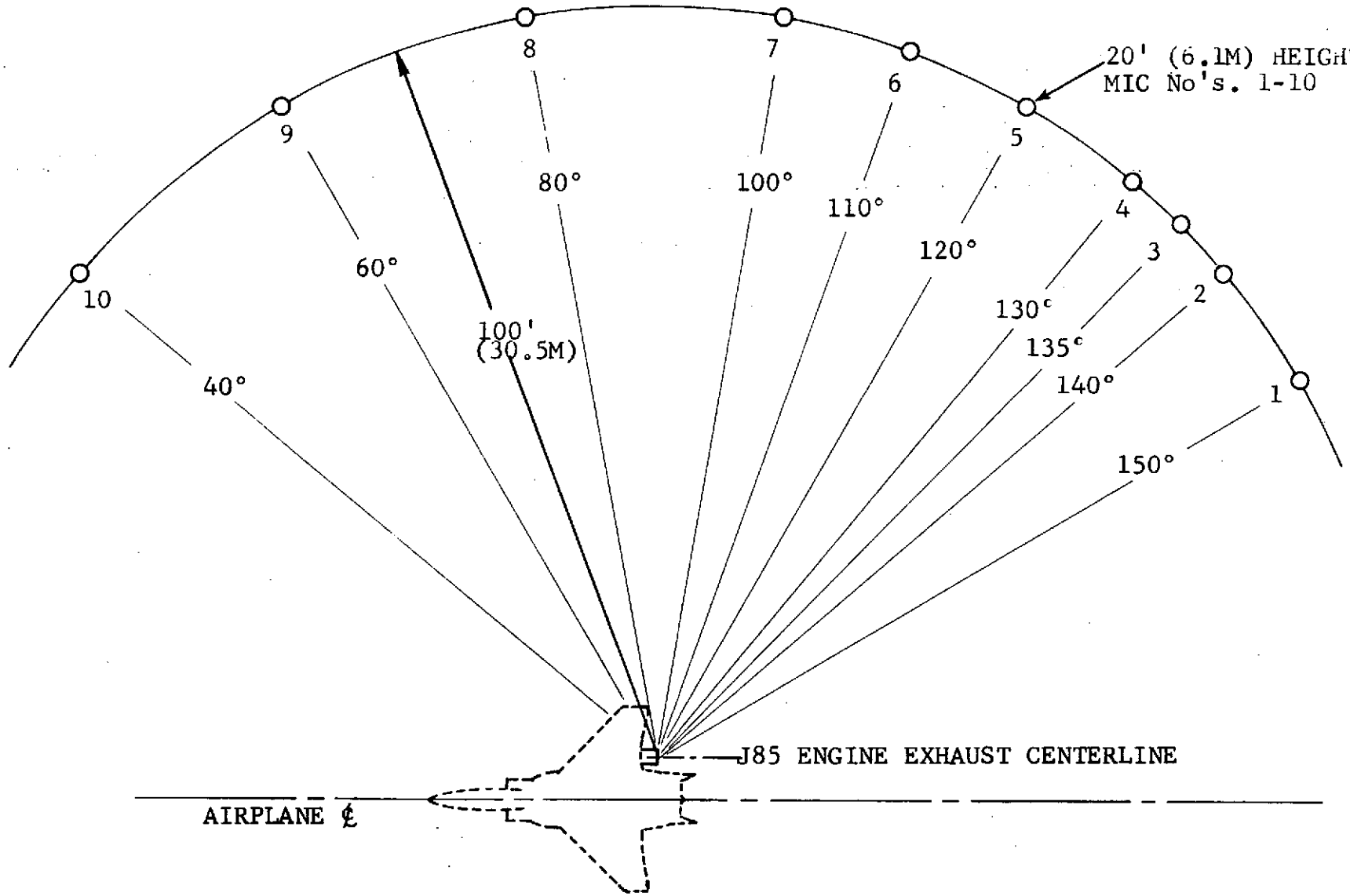

FIGURE 7.11 - AST ON-LINE MICROPHONE POSITIONS
FAR FIELD, 100' RADIUS
(30.5M)

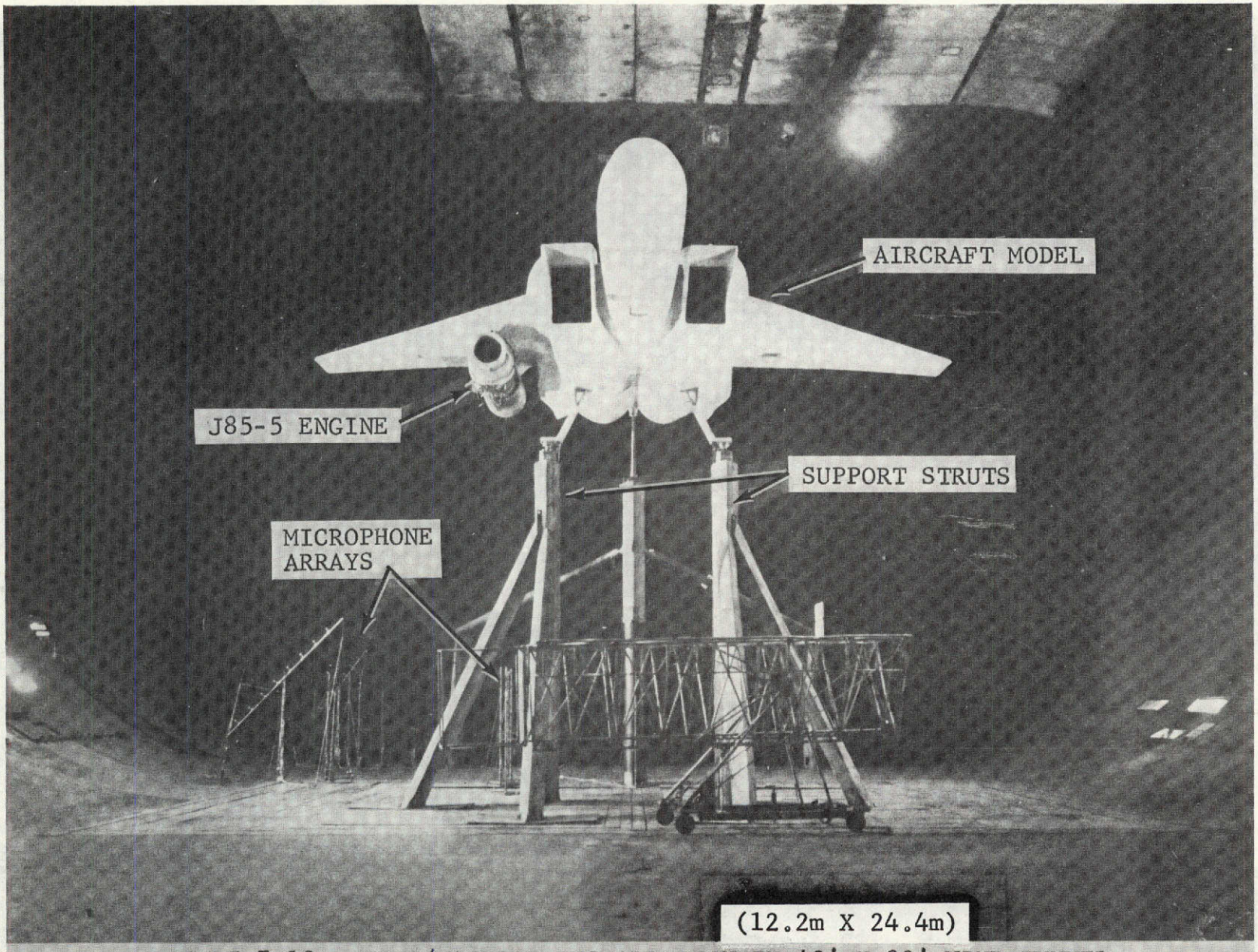

FIGURE 7.12 - WING/NACELLE INSTALLATION IN 40' X 80' WIND TUNNEL

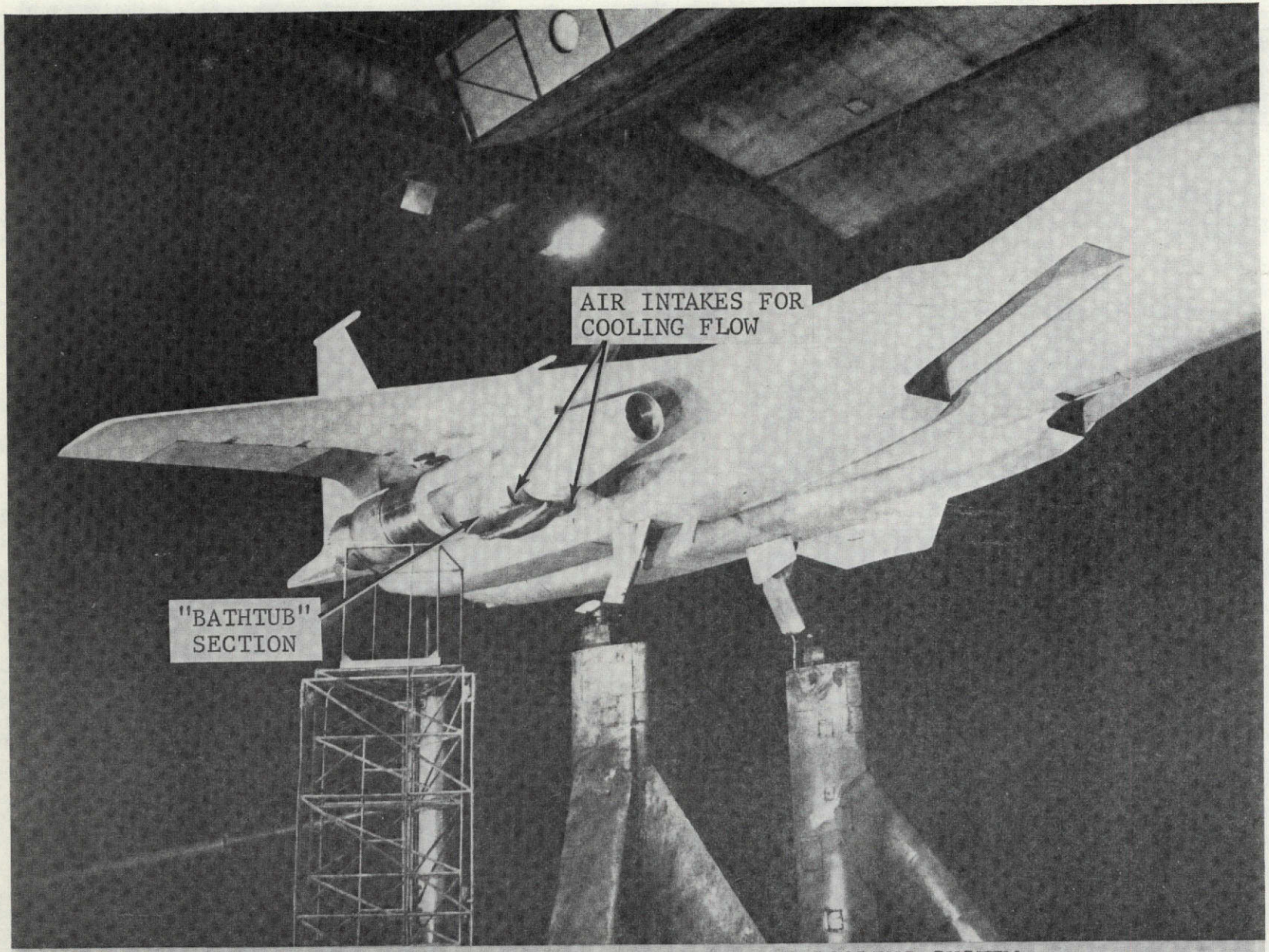

FIGURE 7.13 - IDENTIFICATION OF NACELLE COOLING SYSTEM

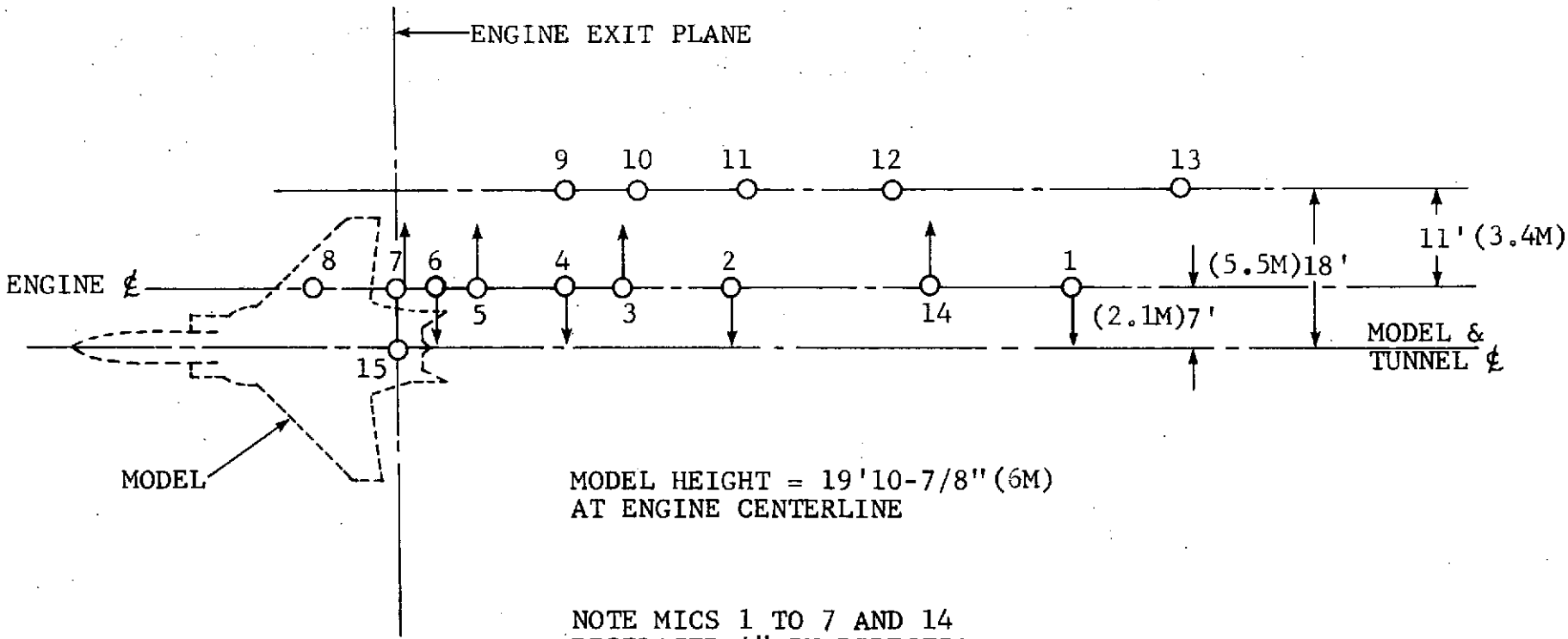

FIGURE 7.14 - DEFINITION OF MICROPHONE LOCATIONS
WING/NACELLE WIND TUNNEL TEST

MIC NO.	CONICAL NOZZLE		AIE NOZZLE		104-TUBE NOZZLE WITHOUT SHROUD		104-TUBE NOZZLE WITH SHROUD		32-SPOKE NOZZLE	
	ANGLE (DEGREES) REF. 0° AT ENGINE INLET	ACOUSTIC PATH LENGTH (FT.,METERS)	ANGLE (DEGREES) REF. 0° AT ENGINE INLET	ACOUSTIC PATH LENGTH (FT.,METERS)	ANGLE (DEGREES) REF. 0° AT ENGINE INLET	ACOUSTIC PATH LENGTH (FT.,METERS)	ANGLE (DEGREES) REF. 0° AT ENGINE INLET	ACOUSTIC PATH LENGTH (FT.,METERS)	ANGLE (DEGREES) REF. 0° AT ENGINE INLET	ACOUSTIC PATH LENGTH (FT.,METERS)
1	161.4	43.6, 13.3	161.2	43.3, 13.2	161.8	44.6, 13.6	161.4	43.6, 13.3	161.3	43.4, 13.2
2	146.1	24.9, 7.6	145.6	24.6, 7.5	147.3	25.7, 7.8	146.1	24.9, 7.6	145.8	24.7, 7.5
3	135.0	19.7, 6.0	134.2	19.4, 5.9	137.0	20.4, 6.2	135.0	19.7, 6.0	134.6	19.5, 5.9
4	126.6	17.3, 5.3	125.6	17.1, 5.2	129.2	17.9, 5.5	126.6	17.3, 5.3	126.0	17.2, 5.2
5	110.4	14.8, 4.5	109.0	14.7, 4.5	113.9	15.2, 4.6	110.4	14.8, 4.5	109.6	14.8, 4.5
6	100.5	14.2, 4.3	99.0	14.1, 4.3	104.5	14.4, 4.3	100.5	14.2, 4.3	99.7	14.1, 4.3
7	90.0	13.9, 4.2	88.5	13.9, 4.2	94.1	14.0, 4.3	90.0	13.9, 4.2	89.1	13.9, 4.2
8	69.6	14.8, 4.5	68.3	15.0, 4.6	73.3	14.5, 4.4	69.6	14.8, 4.5	68.9	14.9, 4.5
9	119.4	20.4, 6.2	118.5	20.2, 6.2	121.8	20.9, 6.4	119.4	20.4, 6.2	118.9	20.2, 6.2
10	126.8	22.1, 6.7	126.0	21.9, 6.7	128.8	22.7, 6.9	126.8	22.1, 6.7	126.3	22.0, 6.7
11	140.2	27.7, 8.4	139.7	27.4, 8.4	141.4	28.4, 8.7	140.2	27.7, 8.4	139.9	27.5, 8.4
12	149.4	34.9, 10.6	149.1	34.5, 10.5	150.2	35.7, 10.9	149.4	34.9, 10.6	149.2	34.7, 10.6

FIGURE 7.15 - WING/NACELLE WIND TUNNEL TEST

8.0 ACOUSTIC DATA ACQUISITION, CALIBRATION AND PROCESSING

The acoustic data acquisition system for both the wind tunnel and outdoor tests consisted of the following components:

- o Bruel-Kjaer microphones
- o Bruel-Kjaer signal conditioning and power supply
- o Two Ampex FR1300A 14 track tape recorder operating at 76 cm (30 inches) a second with a center frequency of 54 KHz.

A schematic of the system is presented on Figure 8.1.

All wind tunnel microphone arrays and duplicated wind tunnel arrays for outdoor testing were fitted with a Bruel-Kjaer nose cone model 0052E. The microphone was oriented to point directly into the tunnel flow. During the outdoor testing, the farfield microphones were fitted with the Bruel-Kjaer UA0207 wind screen and oriented to point at the noise source.

The free field frequency response of each microphone head was taken from a pressure response calibration curve (recorded automatically by the electrostatic actuator method) which was supplied by the microphone manufacture. Also supplied were the free field characteristics for various angles of incidence for microphones with nose cones and wind screens.

Prior to initiation of testing, a frequency response of each data channel (with the microphone head removed) was made by the insertion of a Hewlett-Packard Pseudo-Random Pink Noise Generator into each cathode follower. The response was recorded on magnetic tape.

Prior to and at the end of each test run, an absolute calibration of 124 dB at 250 Hz was made by the insertion of a Bruel-Kjaer pistonphone, model 4220, on each microphone and recording the signal on magnetic tape.

The one-third octave band data processing for the outdoor and wind tunnel data consisted of correcting for system response characteristics only. This processing was done at General Electric's Edward Flight Test Center. The Data Processing system consisted of a General Radio Real Time Analyzer, Honeywell 316 and SDS 930 computers. Figure 8.2 depicts schematically the entire

processing system. Thirty-two second averaging time was used for data processing with data for each microphone sampled from the same period of time for each data point by the use of a tape recorder shuttling system reading time code from the data tapes.

Before data processing could be initiated, however, the total data acquisition and reduction system frequency response characteristics had to be determined and made available in the computer for final data processing. The first step in this process was to analyze the Pink Noise calibration tapes through the analyzer for each data channel. Then the response characteristics were determined for the total system as referenced to 250 Hz (frequency of the pistonphone) for each 1/3 octave band. The final correction then made was to include in these the corrections for non-uniformity in the Pink Noise generator itself, the microphones cartridge and windscreen/nose cones corrections where applicable.

With the above corrections now available and stored in the computer for each data channel, final 1/3 octave data processing was made by determining absolute sound pressure levels for each measuring location. This data was then extrapolated to 61 and 91.4 meter (200 and 300 foot) sidelines* assuming standard day (59°, 70% relative humidity) conditions as per SAE ARP 866. The extrapolations were done with and without extra ground attenuation effects as per SAE AIR 923. For a wind tunnel data processing, standard day conditions were assumed because the absolute numbers could not be measured while the wind tunnel was in operation. The assumption would cause minimal error because the acoustic propagation path length is extremely small.

Following the first processing of wind tunnel data, it became quite apparent that for certain combinations of high freestream velocity and low engine speed, the flow noise would contaminate the noise signature of the J85 engine. Presented on Figure 8.3 are examples of how the flow noise contaminates the engine noise signature for minimum and maximum operating conditions. To further correct the data for high background noise levels, the data was input into the General Electric time sharing computer system. In this system, the measured data were corrected for background noise. These corrections were made for the appropriate wind tunnel J85 combinations. The technique used was to antilogarithmetically subtract the background noise level from the jet noise signa-

*A sideline is defined as an imaginary line parallel to the engine centerline. A 61 meter sideline is 61 meters from the engine centerline.

ture produced by the J85 engine. The corrections would only be done if the J85 noise signature was 4 dB greater than the background noise. If this difference was less than 3 dB, the resultant engine noise level could not be determined and a zero is printed on the data tabulation sheet. Data tabulation from this process were then obtained containing new spectra corrected for background noise levels. Using these spectra, PNdB and OASPL levels were calculated. These levels should be used in conjuntion with the spectra to determine if enough of the one-third octave band spectra is available to allow the calculation of meaningful values for PNdB and OASPL.

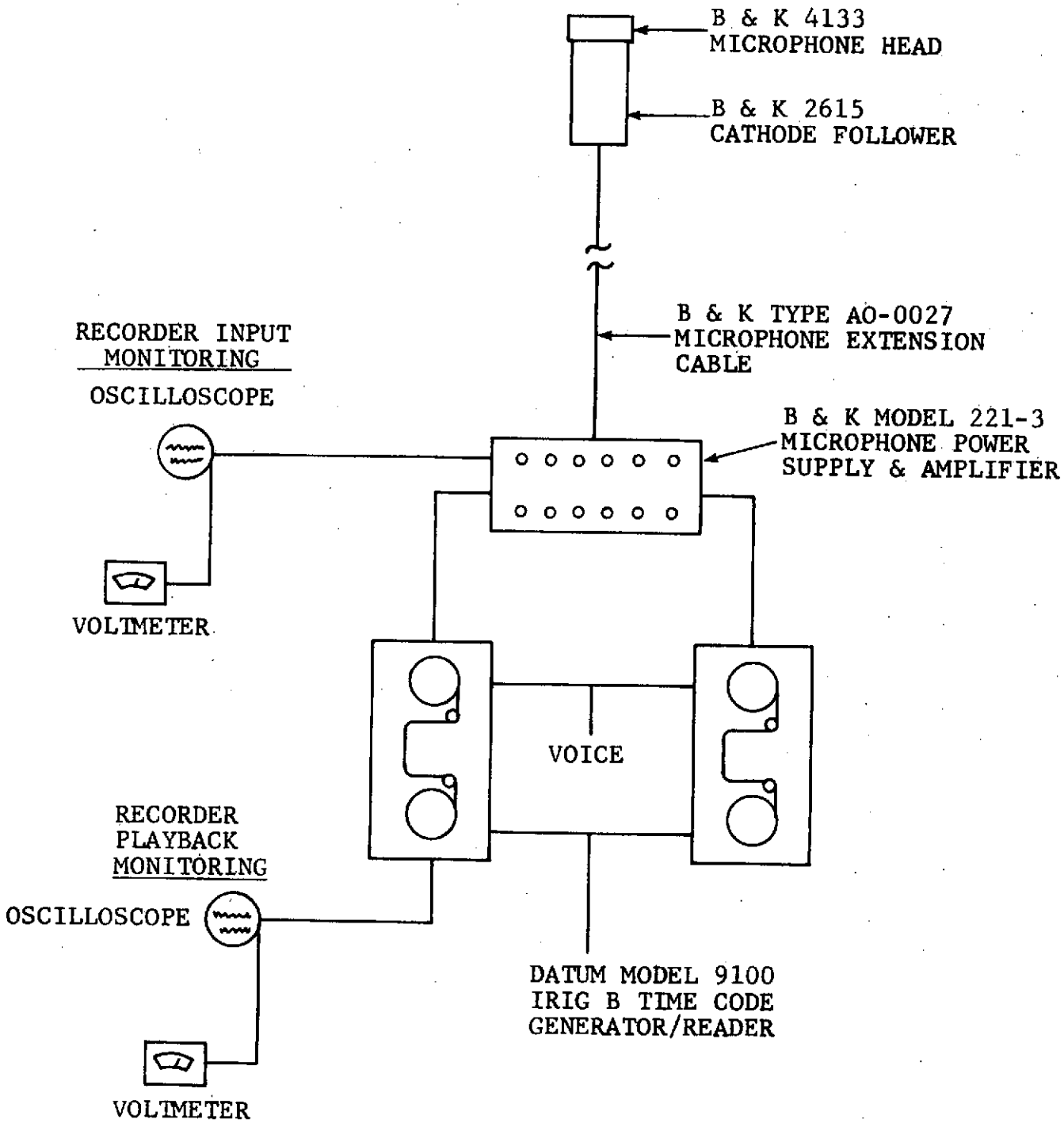

FIGURE 8.1 - ACOUSTIC DATA ACQUISITION SYSTEM

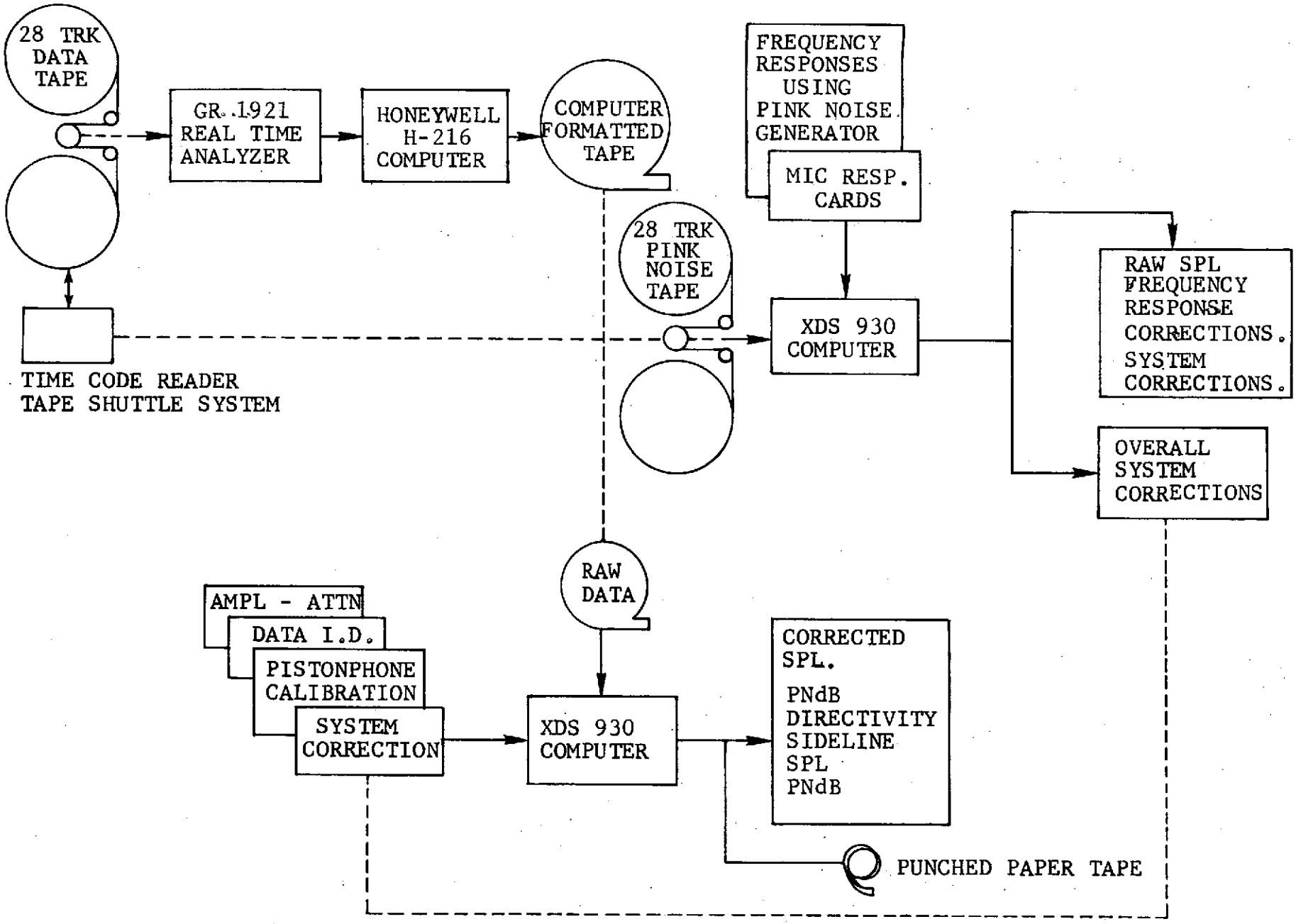

FIGURE 8.2 - GENERAL ELECTRIC ACOUSTIC DATA PROCESSING SYSTEM

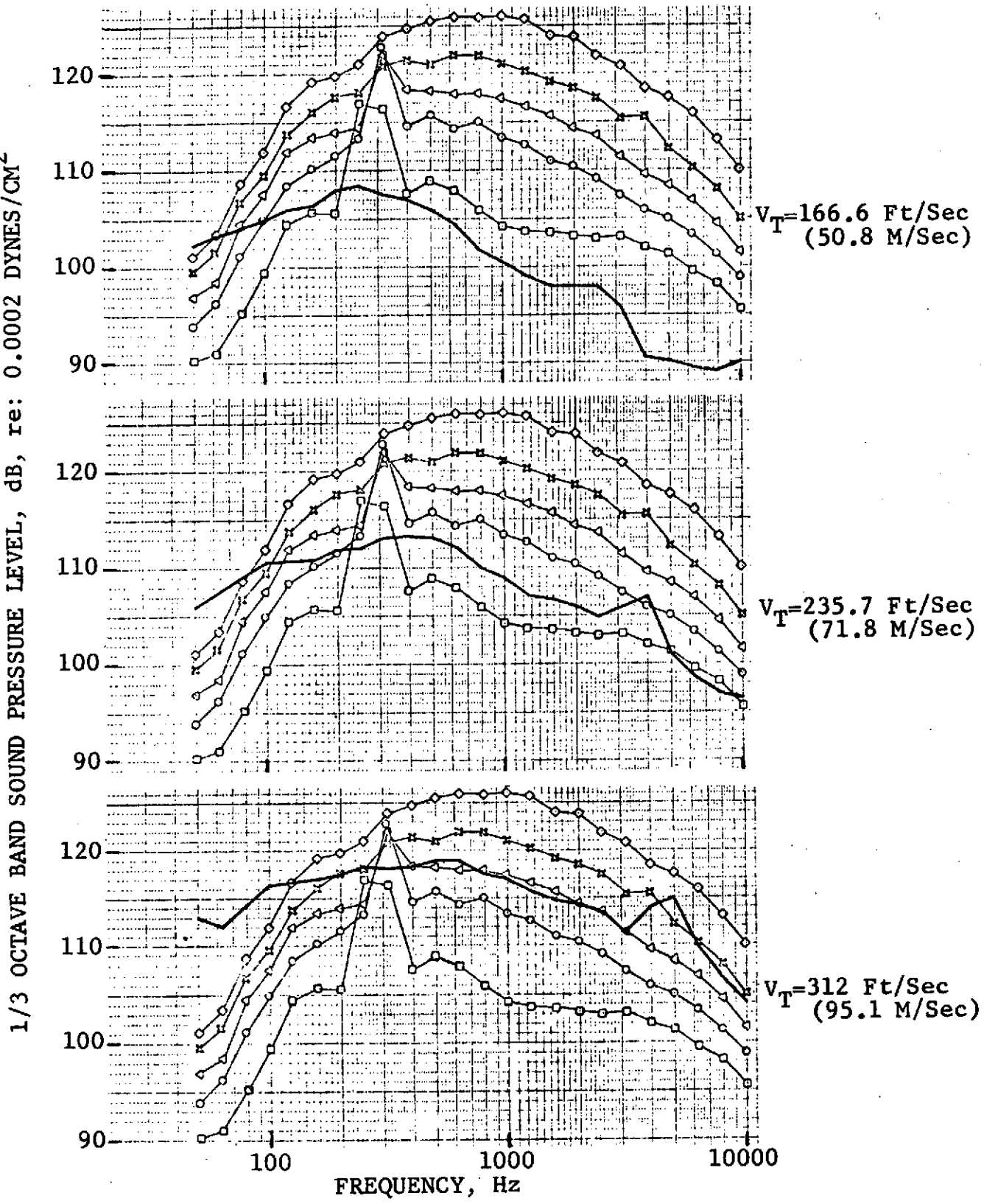

- Acoustic Path Length = 29.4 Ft. (9M)
- θ_I = 130°
- Conical Ejector Nozzle

FIGURE 8.3 - COMPARISON OF ENGINE STATIC DATA WITH TUNNEL BACKGROUND NOISE LEVELS

9.0 ENGINE CYCLE DATA

On the following pages are tables (English and Metric units) summarizing the cycle parameters of the J85 engine. These measurements were reduced and supplied by NASA. The data is presented for each of the tests in the following order:

1. Isolated nacelle outdoor static test
2. Isolated nacelle wind tunnel test
3. Wing nacelle outdoor static test
4. Wing nacelle wind tunnel test

TABLE 9.1

ISOLATED NACELLE OUTDOOR STATIC TEST
CYCLE DATA

Nozzle	Data Point	V_8 FPS	T_{T8} °R	W_8 PPS	P_8/P_o -	A_{E8} In.^{2}	RPM -	T_o °R	V_o FPS	Data Type
Conical Ejector	403	695	1140	29.94	1.133	115.71	13940	519.0	0	FF
	404	1075	1275	38.34	1.313	135.63	14889	519.4	0	
	405	1375	1356	43.41	1.532	135.91	15659	519.7	0	
	406	1580	1518	44.95	1.661	137.68	16247	522.0	0	
	407	1914	1716	45.72	1.957	126.79	16593	520.4	0	
	502	706	1182	30.83	1.132	121.48	13810	520.9	0	NF
	503	1146	1316	38.02	1.351	132.81	14891	521.4	0	
	504	1325	1356	43.05	1.484	139.09	15602	523.2	0	
	505	1586	1562	45.00	1.643	141.46	16311	521.8	0	
	506	1905	1746	45.40	1.918	129.58	16543	522.3	0	
	508	1827	1750	45.67	1.811	138.20	16608	523.2	0	
AIE	703	1017	1212	30.66	1.291	107.97	14146	521.6	0	FF
	704	1182	1284	35.10	1.390	118.28	14487	521.6	0	
	705	1322	1320	38.16	1.498	120.92	15034	523.0	0	
	706	1653	1500	43.73	1.763	125.93	16160	523.1	0	
	707	1727	1500	44.23	1.863	120.61	16474	523.5	0	
	602	1035	1203	30.83	1.306	107.08	14130	519.1	0	NF
	603	1175	1266	34.38	1.391	114.51	14460	519.3	0	
	604	1307	1320	38.71	1.484	124.06	15033	520.0	0	
	605	1646	1500	44.23	1.753	128.26	16161	519.7	0	
	606	1903	1716	44.17	1.940	124.07	16509	519.9	0	
32 Spoke	1502	885	1351	26.36	1.187	106.58	11696	515.5	0	FF
	1503	1343	1415	32.66	1.474	109.08	14124	514.5	0	
	1504	1526	1448	37.51	1.643	113.80	14847	515.0	0	
	1505	1730	1550	41.68	1.828	117.75	15456	516.4	0	
	1506	1996	1750	45.24	2.053	121.27	16283	518.6	0	
	1507	1949	1712	38.97	2.013	105.42	16254	520.5	0	
	1602	884	1323	26.25	1.192	104.66	11772	518.2	0	NF
	1603	1319	1370	32.57	1.472	107.15	14094	517.7	0	
	1604	1517	1426	37.38	1.646	112.3	14831	518.6	0	
	1605	1732	1554	42.08	1.827	119.13	15450	520.0	0	
	1606	1949	1716	45.13	2.010	122.37	16315	519.5	0	

Nozzle	Data Point	V_8 FPS	T_{T8} °R	W_8 PPS	P_8/P_o -	A_{E8} In.^{2}	RPM -	T_o °R	V_o FPS	Data Type
104 Tube Without Shroud	1402	888	1292	26.45	1.198	103.18	12415	515.0	0	FF
	1403	1325	1371	34.60	1.477	113.10	14380	515.0	0	
	1404	1545	1461	38.71	1.656	116.64	14992	515.5	0	
	1405	1618	1509	40.10	1.712	118.91	15157	515.5	0	
	1406	1763	1583	42.11	1.848	118.60	15474	515.9	0	
	1407	1872	1626	43.68	1.971	117.00	15765	515.9	0	
	1408	1968	1689	44.69	2.067	116.45	15972	518.6	0	
	1409	1948	1723	45.05	2.002	122.48	16085	518.6	0	
	1302	867	1217	26.52	1.201	100.10	12433	513.2	0	NF
	1303	1322	1333	30.56	1.491	97.56	13358	512.3	0	
	1304	1528	1422	38.65	1.661	114.54	14978	513.2	0	
	1305	1749	1555	42.29	1.851	117.87	15462	512.7	0	
	1306	1916	1646	44.53	2.032	117.00	15881	513.6	0	
	1307	1999	1729	45.35	2.079	119.00	16198	514.5	0	
104 Tube With Shroud	1002	858	1231	26.83	1.194	102.67	12659	516.4	0	FF
	1003	1305	1326	32.07	1.479	103.03	14395	517.7	0	
	1004	1548	1446	34.50	1.668	102.81	14970	517.7	0	
	1005	1604	1440	35.18	1.741	100.22	15126	518.2	0	
	1006	1770	1563	36.46	1.873	100.80	15436	518.2	0	
	1007	1896	1674	43.53	1.965	118.89	15687	520.0	0	
	1008	1914	1687	44.31	1.981	120.50	15925	520.0	0	
	1009	1686	1704	44.54	1.674	144.15	16031	520.9	0	
	1102	896	1314	26.51	1.199	104.36	12565	522.7	0	NF
	1103	1325	1379	34.51	1.473	113.46	14378	522.3	0	
	1104	1530	1468	39.56	1.635	121.08	15108	522.3	0	
	1005	1744	1568	41.85	1.834	118.23	15405	524.1	0	
	1106	2002	1744	44.32	2.068	117.41	15951	524.1	0	

TABLE 9.2

ISOLATED NACELLE OUTDOOR STATIC TEST

CYCLE DATA

Nozzle	Data Point	V_8 MPS	T_{T8} °K	W_8 K_gPS	P_8/P_o -	A_{E8} M^2	RPM -	T_o °K	V_o MPS	Data Type
Conical	403	211.8	633	13.58	1.133	.07465	13940	288	0	FF
Ejector	404	327.7	708	17.39	1.313	.08750	14889	288	0	
	405	419.1	753	19.69	1.532	.08768	15659	288	0	
	406	481.6	843	20.39	1.661	.08882	16247	290	0	
	407	583.4	953	20.74	1.957	.08180	16593	289	0	
	502	215.2	657	13.98	1.132	.07837	13810	289	0	NF
	503	349.3	731	17.25	1.351	.08568	14891	290	0	
	504	403.9	753	19.53	1.484	.08973	15602	291	0	
	505	483.4	868	20.41	1.643	.09126	16311	290	0	
	506	580.6	970	20.59	1.918	.08360	16543	290	0	
	508	556.9	972	20.72	1.811	.08916	16608	291	0	
AIE	703	310.0	673	13.91	1.291	.06966	14146	290	0	FF
	704	360.3	713	15.92	1.390	.07631	14487	290	0	
	705	403.0	733	17.31	1.498	.07801	15034	291	0	
	706	503.8	833	19.84	1.763	.08124	16160	291	0	
	707	526.4	833	20.06	1.863	.07781	16474	291	0	
	602	315.5	668	13.98	1.306	.06908	14130	288	0	NF
	603	358.1	703	15.59	1.391	.07387	14460	288	0	
	604	398.4	733	17.56	1.484	.08004	15033	289	0	
	605	501.7	833	20.06	1.753	.08274	16161	289	0	
	606	580.0	953	20.04	1.940	.08004	16509	289	0	
32 Spoke	1502	269.8	751	11.96	1.187	.06876	11696	286	0	FF
	1503	409.4	786	14.81	1.474	.07037	14124	286	0	
	1504	465.1	804	17.01	1.643	.07342	14847	286	0	
	1505	527.3	861	18.91	1.828	.07596	15456	287	0	
	1506	608.4	972	20.52	2.053	.07824	16283	288	0	
	1507	594.1	951	17.68	2.013	.06801	16254	289	0	
	1602	269.4	735	11.91	1.192	.06752	11772	288	0	NF
	1603	402.0	761	14.77	1.472	.06913	14094	288	0	
	1604	462.4	792	16.96	1.646	.07245	14831	288	0	
	1605	527.9	863	19.09	1.827	.07685	15450	289	0	
	1606	594.1	953	20.47	2.010	.07895	16315	289	0	

Nozzle	Data Point	V_8 MPS	T_{T8} °K	W_8 KgPS	P_8/P_o -	A_{E8} M^2	RPM -	T_o °K	V_o MPS	Data Type
104 Tube	1402	270.7	718	12.00	1.198	.06657	12415	286	0	FF
Without	1403	403.9	762	15.69	1.477	.07296	14380	286	0	
Shroud	1404	470.9	812	17.56	1.656	.07525	14992	286	0	
	1405	493.2	838	18.19	1.712	.07671	15157	286	0	
	1406	537.4	879	19.10	1.848	.07651	15474	287	0	
	1407	570.6	903	19.81	1.971	.07548	15765	287	0	
	1408	599.9	938	20.27	2.067	.07513	15972	288	0	
	1409	593.8	957	20.43	2.002	.07902	16085	288	0	
	1302	264.3	676	12.03	1.201	.06458	12433	285	0	NF
	1303	403.0	741	13.86	1.491	.06294	13358	285	0	
	1304	465.7	790	17.53	1.661	.07389	14978	285	0	
	1305	533.1	864	19.18	1.851	.07604	15462	285	0	
	1306	584.0	914	20.20	2.032	.07548	15881	285	0	
	1307	609.3	961	20.57	2.079	.07677	16198	286	0	
104 Tube	1002	261.5	684	12.17	1.194	.06624	12659	287	0	FF
With	1003	397.8	737	14.55	1.479	.06647	14395	288	0	
Shroud	1004	471.8	803	15.65	1.668	.06633	14970	288	0	
	1005	488.9	800	15.96	1.741	.06466	15126	288	0	
	1006	539.5	868	16.54	1.873	.06503	15436	288	0	
	1007	577.9	930	19.75	1.965	.07667	15687	289	0	
	1008	583.4	937	20.10	1.981	.07774	15925	289	0	
	1009	513.9	947	20.20	1.674	.09300	16031	289	0	
	1102	273.1	730	12.03	1.199	.06733	12565	290	0	NF
	1103	403.9	766	15.65	1.473	.07320	14378	290	0	
	1104	466.3	816	17.94	1.635	.07811	15108	290	0	
	1105	531.6	871	18.98	1.834	.07627	15405	291	0	
	1106	610.2	969	20.10	2.068	.07575	15951	291	0	

TABLE 9.3

ISOLATED NACELLE WIND TUNNEL TEST
CYCLE DATA

Nozzle	Data Point	V_8 FPS	T_{T8} °R	W_8 PPS	P_8/P_o -	$AE8_2$ In.^{2}	RPM -	T_o °R	V_o FPS	Data Type
Conical Ejector	301	866	1169	28.43	1.210	103.96	13533	528	18.6	NF
	302	1254	1275	35.40	1.455	112.64	14494	528	18.5	
	303	1465	1337	38.61	1.642	111.69	15119	528	16.0	
	304	1666	1448	43.45	1.820	118.17	15724	530	20.2	
	305	1961	1665	45.04	2.079	115.46	16327	530	21.4	
	306	1520	1401	38.10	1.665	111.36	15048	533	20.6	
	307	1528	1410	37.92	1.669	111.00	15020	535	19.2	
	308	1529	1410	37.67	1.670	110.23	14992	537	19.5	
	401	765	1140	27.94	1.164	106.38	13435	516	148.7	NF
	402	1230	1302	32.62	1.423	108.97	14367	520	149.8	
	409	1389	1374	39.25	1.537	124.89	15078	525	150.7	
	413	1859	1653	40.95	1.928	114.56	15484	529	150.3	
	501	1888	1662	41.97	1.964	115.64	16160	540	171.6	NF
	505	849	1219	31.45	1.192	123.46	13310	548	247.1	
	509	1329	1349	33.09	1.491	109.52	14331	553	248.1	
	513	1554	1433	38.01	1.685	114.96	15071	556	248.0	
	601	1983	1673	43.69	2.109	117.08	16179	538	330.0	NF
	605	1971	1671	41.43	2.090	112.27	15628	558	337.9	
	609	1903	1658	37.78	1.991	107.14	14964	570	340.1	
	613	1462	1437	32.49	1.579	107.83	14242	578	341.9	
	617	1207	1386	27.18	1.374	101.78	13276	582	342.1	
	621	1919	1674	39.05	2.002	110.71	15620	574	339.4	
AIE	701	1073	1329	27.93	1.296	102.12	13437	534	14.7	NF
	704	1237	1386	31.84	1.396	110.54	14334	534	14.7	
	705	1366	1419	35.98	1.494	118.17	15004	534	14.7	
	709	1762	1671	39.83	1.783	119.49	15724	538	14.7	
	710	1758	1674	41.00	1.775	123.67	16112	539	14.8	
	901	980	1293	*	1.263	*	*	*	150	NF
	902	1210	1410	*	1.389	*	*	*	150	
	903	1300	1464	*	1.452	*	*	*	150	
	904	1621	1671	*	1.666	*	*	*	150	
	905	1676	1671	*	1.729	*	*	*	150	

Nozzle	Data Point	V_8 FPS	T_{T8} °R	W_8 PPS	P_8/P_o -	$AE8_2$ In.^{2}	RPM -	T_o °R	V_o FPS	Data Type
AIE	1001	995	1275	*	1.277	*	*	*	250	NF
	1002	1220	1392	*	1.401	*	*	*	250	
	1003	1322	1464	*	1.464	*	*	*	250	
	1004	1638	1608	*	1.716	*	*	*	250	
	1005	1698	1662	*	1.773	*	*	*	250	
	1006	1070	1316	*	1.318	*	*	*	250	
	1101	1075	1217	29.11	1.331	106.09	13520	520	327	NF
	1102	1452	1343	34.54	1.623	108.74	14366	527	330	
	1103	1508	1437	36.03	1.629	117.13	15069	533	332	
	1104	1694	1671	38.59	1.701	130.06	15765	539	332	
	1105	1622	1671	39.19	1.623	138.59	15867	542	335	
	1113	-	-	-	-	-	-	560	340	
	1114	-	-	-	-	-	-	520	250	
	1115	-	-	-	-	-	-	560	150	
	1116	-	-	-	-	-	-	520	0	

*Data not available

TABLE 9.4

ISOLATED NACELLE WIND TUNNEL TEST
CYCLE DATA

Nozzle	Data Point	V_8 MPS	T_{T8} °K	W_8 KgPS	P_8/P_o -	A_{E8} M^2	RPM -	T_o °K	V_o MPS	Data Type
Conical Ejector	301	264.0	649	12.90	1.210	.06707	13533	293	5.7	NF
	302	382.2	708	16.06	1.455	.07267	14494	293	5.6	
	303	446.5	743	17.51	1.642	.07206	15119	293	4.9	
	304	507.8	804	19.71	1.820	.07624	15724	294	6.2	
	305	597.7	925	20.43	2.079	.07449	16327	294	6.5	
	306	463.3	778	17.28	1.665	.07184	15048	296	6.3	
	307	465.7	783	17.20	1.669	.07161	15020	297	5.9	
	308	466.0	783	17.09	1.670	.07111	14992	298	5.9	
	401	233.2	633	12.67	1.164	.06863	13435	287	45.3	NF
	405	374.9	723	14.80	1.423	.07030	14367	289	45.7	
	409	423.4	763	17.80	1.537	.08057	15078	292	45.9	
	413	566.6	918	18.58	1.928	.07391	15484	294	45.8	
	501	575.5	923	19.04	1.964	.07460	16160	300	52.3	NF
	505	258.8	677	14.27	1.192	.07965	13310	304	75.3	
	509	405.1	749	15.01	1.491	.07066	14331	307	75.6	
	513	473.7	796	17.24	1.685	.07416	15071	309	75.6	
	601	604.4	929	19.82	2.109	.07553	16179	299	100.6	NF
	605	600.8	928	18.79	2.090	.07243	15628	310	103.0	
	609	580.0	921	17.14	1.991	.06912	14964	317	103.7	
	613	445.6	798	14.74	1.579	.06956	14242	321	104.2	
	617	367.9	770	12.33	1.374	.06566	13276	323	104.3	
	621	584.9	930	17.71	2.002	.07142	15620	319	103.5	
AIE	701	327.1	738	12.67	1.296	.06588	13437	297	4.5	NF
	704	377.0	770	14.44	1.396	.07131	14334	297	4.5	
	705	416.4	788	16.32	1.494	.07624	15004	297	4.5	
	709	537.1	928	18.07	1.783	.07709	15724	299	4.5	
	710	535.8	930	18.60	1.775	.07978	16112	299	4.5	
	901	299	718	*	1.263	*	*	*	45.7	NF
	902	369	783	*	1.389	*	*	*	45.7	
	903	396	813	*	1.452	*	*	*	45.7	
	904	494	928	*	1.666	*	*	*	45.7	
	905	511	928	*	1.729	*	*	*	45.7	

Nozzle	Data Point	V_8 MPS	T_{T8} °K	W_8 KgPS	P_8/P_o -	A_{E8} M^2	RPM -	T_o °K	V_o MPS	Data Type
AIE	1001	303	708	*	1.277	*	*	*	76	NF
	1002	372	773	*	1.401	*	*	*	76	
	1003	403	813	*	1.464	*	*	*	76	
	1004	499	893	*	1.716	*	*	*	76	
	1005	518	923	*	1.773	*	*	*	76	
	1006	326	731	*	1.318	*	*	*	76	
	1101	327.7	676	13.20	1.331	.06844	13520	289	99.7	NF
	1102	442.6	746	15.67	1.623	.07015	14366	293	100.6	
	1103	459.6	798	16.34	1.629	.07556	15069	296	101.2	
	1104	516.3	928	17.50	1.701	.08391	15765	299	101.2	
	1105	494.4	928	17.78	1.623	.08941	15867	301	102.1	
	1113	-	-	-	-	-	-	310	104	
	1114	-	-	-	-	-	-	288	76	
	1115	-	-	-	-	-	-	310	45.7	
	1116	-	-	-	-	-	-	288	0	

*Data not available

TABLE 9.5

WING NACELLE OUTDOOR STATIC TEST CYCLE DATA

Nozzle	Data Point	V_8 FPS	T_{T8} °R	W_8 PPS	P_8/P_o -	A_{E8_2} In.^{2}	RPM -	T_o °R	V_o FPS	Data Type
32 Spoke	102	1150	1397	28.33	1.329	103.99	13366	518.2	0	FF
	103	1407	1465	34.99	1.511	115.84	14435	515.9	0	
	104	1729	1572	42.69	1.81	122.44	15508	518.2	0	
	105	1819	1617	42.23	1.899	122.68	15812	517.7	0	
	106	1990	1749	45.47	2.045	122.08	16324	518.6	0	
	202	1157	1386	28.03	1.337	101.78	13318	524.1	0	NF
	203	1418	1461	34.02	1.523	111.44	14333	524.1	0	
	204	1750	1563	41.72	1.845	116.94	15403	526.4	0	
	205	1846	1617	43.36	1.940	117.68	15709	526.4	0	
	206	2021	1781	44.75	2.064	120.12	16212	526.8	0	
104 Tube With Shroud	302	1292	1387	34.76	1.441	117.45	14479	515.9	0	FF
	303	1507	1482	38.30	1.602	120.55	15018	516.4	0	
	304	1741	1589	41.73	1.813	120.38	15518	516.4	0	
	305	1810	1634	42.48	1.874	120.33	15637	517.3	0	
	306	2008	1756	44.15	2.068	117.76	16150	518.6	0	
	402	1218	1329	34.63	1.402	117.55	14459	516.8	0	NF
	403	1440	1428	37.97	1.561	120.21	14984	517.5	0	
	404	1687	1563	41.53	1.762	122.18	15471	518.0	0	
	405	1750	1590	42.21	1.824	121.01	15589	519.9	0	
	406	1920	1716	44.12	1.965	122.20	16114	520.6	0	
104 Tube Without Shroud	602	1314	1387	34.18	1.460	113.86	14410	520.0	0	FF
	603	1506	1453	37.66	1.617	116.00	14934	520.5	0	
	604	1755	1604	41.49	1.821	119.53	15475	521.4	0	
	605	1823	1634	42.11	1.891	118.04	15623	521.8	0	
	606	2019	1782	43.85	2.060	118.09	16041	523.2	0	
	502	1304	1375	33.63	1.457	111.72	14306	522.7	0	NF
	503	1501	1456	37.04	1.610	114.78	14824	523.6	0	
	504	1755	1595	40.69	1.827	116.51	15371	525.0	0	
	505	1819	1626	42.02	1.892	117.41	15567	525.5	0	
	506	2023	1769	43.61	2.079	115.90	16059	525.5	0	
Conical Ejector	1202	1929	1738	45.49	1.960	126.52	16923	517.3	0	FF
	1203	1850	1662	44.82	1.908	125.13	16375	518.2	0	
	1204	1646	1532	44.64	1.731	131.57	16259	517.3	0	
	1205	1665	1545	44.61	1.746	130.95	16232	517.3	0	
	1206	1270	1321	39.32	1.450	127.92	15144	517.7	0	
	1207	1006	1226	33.05	1.280	117.12	14193	517.7	0	
	1208	1954	1734	45.18	2.000	122.89	16579	520.0	0	
	1302	1979	1765	44.64	2.012	121.83	16483	522.3	0	NF
	1303	1861	1681	44.03	1.908	123.55	16049	523.6	0	
	1304	1674	1557	44.27	1.749	130.11	16197	524.1	0	
	1305	1281	1522	38.24	1.456	124.30	15001	521.4	0	
	1306	1036	1256	31.70	1.292	112.68	14001	524.5	0	

TABLE 9.6

WING NACELLE OUTDOOR STATIC TEST

CYCLE DATA

Nozzle	Data Point	V_8 MPS	T_{T8} °K	W_8 KgPS	P_8/P_o -	$AE8$ M^2	RPM -	T_o °K	V_o MPS	Data Type
32 Spoke	102	350.5	776	12.85	1.329	.06709	13366	288	0	FF
	103	428.9	814	15.87	1.511	.07473	14435	287	0	
	104	527.0	873	19.36	1.810	.07899	15508	288	0	
	105	554.4	898	19.16	1.899	.07915	15812	288	0	
	106	606.6	972	20.63	2.045	.07876	16324	288	0	
	202	352.7	770	12.71	1.337	.06566	13318	291	0	NF
	203	432.2	812	15.43	1.523	.07189	14333	291	0	
	204	533.4	868	18.92	1.845	.07544	15403	292	0	
	205	562.7	898	19.67	1.940	.07592	15709	292	0	
	206	616.0	989	20.30	2.064	.07749	16212	293	0	
104 Tube With Shroud	302	393.8	771	15.77	1.441	.07577	14479	287	0	FF
	303	459.3	823	17.37	1.602	.07777	15018	287	0	
	304	530.7	883	18.93	1.813	.07766	15518	287	0	
	305	551.7	908	19.27	1.874	.07763	15637	287	0	
	306	612.0	976	20.03	2.068	.07597	16150	288	0	
	402	371.3	738	15.71	1.402	.07584	14459	287	0	NF
	403	438.9	793	17.22	1.561	.07755	14984	287	0	
	404	514.2	868	18.84	1.762	.07882	15471	288	0	
	405	533.4	883	19.15	1.824	.07807	15589	289	0	
	406	585.2	953	20.01	1.965	.07884	16114	289	0	
104 Tube Without Shroud	602	400.5	771	15.50	1.460	.07345	14410	289	0	FF
	603	459.0	807	17.08	1.617	.07484	14934	289	0	
	604	534.9	891	18.82	1.821	.07711	15475	290	0	
	605	555.7	908	19.10	1.891	.07615	15623	290	0	
	606	615.4	990	19.89	2.060	.07618	16041	291	0	
	502	397.5	764	15.25	1.457	.07207	14306	290	0	NF
	503	457.5	809	16.80	1.610	.07405	14824	291	0	
	504	534.9	886	18.46	1.827	.07516	15371	292	0	
	505	554.4	903	19.06	1.892	.07575	15567	292	0	
	506	616.6	983	19.78	2.079	.07477	16059	292	0	

Nozzle	Data Point	V_8 MPS	$TT8$ °K	W_8 KgPS	P_8/P_o -	A_{E8} M^2	RPM -	T_o °K	V_o MPS	Date Type
Conical Ejector	1202	588.0	966	20.63	1.960	.08162	16923	287	0	FF
	1203	563.9	923	20.33	1.908	.08073	16375	288	0	
	1204	501.7	851	20.25	1.731	.08488	16259	287	0	
	1205	507.5	858	20.24	1.746	.08448	16232	287	0	
	1206	387.1	734	17.84	1.450	.08253	15144	288	0	
	1207	306.6	681	14.99	1.280	.07556	14193	288	0	
	1208	595.6	963	20.49	2.000	.07928	16579	289	0	
	1302	603.2	981	20.25	2.012	.07860	16483	290	0	NF
	1303	567.2	934	19.97	1.908	.07971	16049	291	0	
	1304	510.2	865	20.08	1.749	.08394	16197	291	0	
	1305	390.5	846	17.35	1.456	.08019	15001	290	0	
	1306	315.8	698	14.38	1.292	.07269	14001	291	0	

TABLE 9.7

WING NACELLE WIND TUNNEL TEST
CYCLE DATA

Nozzle	Data Point	V_8 FPS	T_{T8} °R	W_8 PPS	P_8/P_o -	A_{E8} In.^{2}	RPM -	T_o °R	V_o FPS	Data Type
Conical Ejector	201	1910	1712	42.68	1.954	120.55	16106	527	169	NF
	202	1753	1609	42.25	1.814	124.43	15951	529	169	
	203	1347	1400	37.35	1.484	125.06	15274	534	170	
	204	1331	1399	37.16	1.471	125.52	15280	534	170	
	301	1973	1716	43.87	2.048	122.90	16410	532	293	NF
	302	1717	1552	43.06	1.808	128.81	15978	534	293	
	303	1976	1722	43.01	2.048	120.39	16174	546	304	
	304	1753	1579	41.01	1.836	122.37	15614	547	305	
	401	1949	1736	43.69	1.992	124.02	16401	534	251	NF
	402	1733	1563	42.2	1.822	123.99	15832	541	252	
	403	1357	1399	37.72	1.494	124.12	15156	545	251	
	500	-	-	-	-	-	-	-	0	NF
	501	1986	1746	46.2	2.041	123.36	16690	523	0	
	502	1655	1521	44.95	1.75	134.3	16118	524	0	
	503	1294	1336	38.74	1.465	125.37	15006	526	0	
AIE	601	1996	1731	46.07	2.072	120.07	16544	523	0	NF
	602	1656	1501	45.14	1.766	128.19	16097	525	0	
	603	1326	1351	38.0	1.488	121.2	14916	529	0	
	701	1989	1741	43.6	2.051	119.22	16146	537	250	NF
	702	1761	1595	42.36	1.835	123.65	15731	540	250	
	703	1404	1590	36.44	1.529	120.07	15029	545	250	
	704	1968	1702	42.5	2.054	116.47	15773	549	304	
	801	1934	1740	43.38	1.966	121.39	16415	536	167	NF
	802	1755	1601	42.56	1.823	122.87	15859	530	167	
	803	1410	1441	36.75	1.525	120.18	15160	541	169	
	804	1410	1442	36.67	1.516	120.66	15160	541	168	

Nozzle	Data Point	V_8 FPS	T_{T8} °R	W_8 PPS	P_8/P_o -	A_{E8} In.^{2}	RPM -	T_o °R	V_o FPS	Data Type
104 Tube With Shroud	901	2030	1765	44.62	2.096	116.82	16050	532	0	NF
	902	1728	1560	41.59	1.818	117.64	15429	532	0	
	903	1473	1394	37.41	1.615	112.35	14890	538	0	
	1001	1929	1702	42.37	1.992	116.3	15867	530	167	NF
	1002	1778	1609	39.93	1.849	114.72	15493	534	168	
	1003	1541	1509	36.4	1.624	115.15	15108	535	170	
	1004	1947	1694	43.39	2.027	116.31	15756	540	142	
	1005	1766	1593	40.35	1.845	115.13	15352	545	140	
	1006	1541	1490	36.62	1.634	113.89	14970	548	139	
	1007	1894	1603	41.89	2.029	110.85	15565	554	221	
	1008	1813	1615	38.41	1.892	111.91	15275	555	307	
	1009	1594	1513	35.07	1.681	111.18	14851	558	309	
104 Tube Without Shroud	1101	1947	1716	42.95	2.007	117.49	15992	526	166	
	1102	1765	1612	40.13	1.827	116.82	15522	531	168	
	1103	1527	1506	36.44	1.61	116.15	15115	534	169	
	1104	1979	1715	42.76	2.059	116.28	15830	536	252	
	1105	1778	1595	39.6	1.859	114.82	15373	539	251	
	1106	1547	1497	35.95	1.637	114.47	14972	542	252	
	1107	1958	1690	41.83	2.049	115.25	15637	547	306	
	1108	1804	1585	38.83	1.905	111.35	15341	552	307	
	1109	1557	1497	34.89	1.648	112.26	14827	556	308	
	1201	2027	1716	45.69	2.14	111.45	16238	518	0	NF
	1202	1715	1550	42.4	1.807	120.12	15493	518	0	
	1203	1480	1438	37.79	1.597	116.47	14898	524	0	
32 Spoke	1301	2026	1719	45.51	2.135	111.41	16530	523	0	
	1302	1742	1563	41.58	1.834	117.33	15458	528	0	
	1303	1417	1443	34.24	1.53	111.08	14449	529	0	
	1401	1915	1694	42.78	1.977	118.86	16091	527	168	NF
	1402	1778	1621	40.45	1.839	118.07	15547	531	169	
	1403	1442	1481	33.18	1.536	110.6	14569	534	168	
	1404	1893	1572	42.68	2.058	111.66	15970	536	250	
	1405	1777	1602	39.87	1.852	117.09	15394	539	252	
	1406	1460	1478	32.83	1.556	110.05	14494	543	252	
	1407	1961	1691	42.02	2.052	116.45	15796	547	307	
	1408	1798	1609	38.91	1.876	114.94	15292	552	308	
	1409	1454	1452	32.05	1.563	107.72	14348	554	309	

TABLE 9.8

WING NACELLE WIND TUNNEL TEST
CYCLE DATA

Nozzle	Data Point	V_8 MPS	T_{T8} °K	W_8 K_gPS	P_8/P_o -	A_{E8} M^2	RPM -	T_o °K	V_o MPS	Data Type
Conical	201	582.2	951	19.36	1.954	.0778	16106	293	51.5	NF
Ejector	202	534.3	894	19.16	1.814	.0803	15951	294	51.5	
	203	410.6	778	16.94	1.484	.0807	15274	297	51.8	
	204	405.7	777	16.86	1.471	.0810	15280	297	51.8	
	301	601.4	953	19.90	2.048	.0788	16410	296	89.3	NF
	302	523.3	862	19.53	1.808	.0831	15978	297	89.3	
	303	602.3	957	19.51	2.048	.0777	16174	303	92.6	
	304	534.3	877	18.60	1.836	.0789	15614	304	92.9	
	401	594.1	964	19.82	1.992	.0800	16401	297	76.5	NF
	402	528.2	868	19.14	1.822	.0799	15832	301	76.8	
	403	413.6	777	17.11	1.494	.0801	15156	303	76.5	
	500	-	-	-	-	-	-	-	0	NF
	501	605.3	970	20.96	2.041	.0796	16690	288	0	
	502	504.4	845	20.39	1.75	.0841	16118	291	0	
	503	394.4	742	17.57	1.465	.0809	15006	292	0	
AIE	601	608.4	962	20.90	2.072	.0775	16544	291	0	NF
	602	504.7	834	20.48	1.766	.0827	16097	291	0	
	603	404.2	751	17.24	1.488	.0782	14916	294	0	
	701	606.2	967	19.78	2.051	.0769	16146	298	76.2	NF
	702	536.8	886	19.21	1.835	.0798	15731	300	76.2	
	703	427.9	883	16.53	1.529	.0775	15029	303	76.2	
	704	599.8	946	19.28	2.054	.0752	15773	305	92.7	
	705	545.3	890	18.59	1.87	.0771	15526	307	92.7	
	801	589.5	967	19.68	1.966	.0783	16415	298	50.9	NF
	802	534.9	889	19.30	1.823	.0793	15859	294	50.9	
	803	429.8	801	16.67	1.525	.0775	15160	301	51.5	
	804	429.8	801	16.63	1.516	.0779	15160	301	51.2	
104 Tube W/Shroud	901	618.7	981	20.24	2.096	.0754	16050	296	0	NF
	902	526.7	867	18.86	1.818	.0760	15424	292	0	
	903	448.9	774	16.97	1.615	.0725	14890	299	0	

Nozzle	Data Point	V_8 MPS	T_{T8} °K	W_8 K_gPS	P_8/P_o -	A_{E8} M^2	RPM -	T_o °K	V_o MPS	Data Type
104 Tube W/Shroud	1001	588	946	19.22	1.992	.0750	15867	294	50.9	NF
	1002	541.9	894	18.11	1.849	.0740	15493	297	51.2	
	1003	469.7	838	16.51	1.624	.0743	15108	297	51.8	
	1004	593.4	941	19.68	2.027	.0750	15756	300	43.3	
	1005	538.3	885	18.30	1.845	.0743	15352	303	42.7	
	1006	469.7	828	16.61	1.634	.0735	14970	304	42.4	
	1007	577.3	891	19.00	2.029	.0715	15565	308	67.4	
	1008	552.6	897	17.42	1.892	.0722	15275	308	93.6	
	1009	485.9	840	15.91	1.681	.0717	14851	310	94.2	
104 Tube W/O Shroud	1101	593.4	953	19.48	2.007	.0758	15992	292	50.6	
	1102	537.9	896	18.20	1.827	.0754	15522	295	51.2	
	1103	465.4	837	16.53	1.61	.0749	15115	297	51.5	
	1104	603.2	953	19.40	2.059	.0750	15830	298	76.8	
	1105	541.9	886	17.96	1.859	.0740	15373	299	76.5	
	1106	471.5	832	16.31	1.637	.0739	14972	301	76.8	
	1107	596.8	939	18.97	2.049	.0744	15637	304	93.3	
	1108	549.9	881	17.61	1.905	.0718	15341	307	93.6	
	1109	474.6	832	15.83	1.648	.0724	14827	309	93.9	
	1201	617.8	953	20.72	2.14	.0720	16238	288	0	NF
	1202	522.7	861	19.23	1.807	.0775	15493	288	0	
	1203	451.1	799	17.14	1.597	.0751	14898	291	0	
32 Spoke	1301	617.5	955	20.64	2.135	.0719	16530	291	0	NF
	1302	530.9	868	18.86	1.834	.0757	15458	293	0	
	1303	431.9	802	15.53	1.530	.0717	14444	294	0	
	1401	583.7	941	19.40	1.977	.0769	16091	293	51.2	NF
	1402	541.9	901	18.35	1.839	.0762	15547	295	51.5	
	1403	439.5	823	15.18	1.536	.0714	14569	297	51.2	
	1404	577	873	19.36	2.058	.0720	15970	298	76.2	
	1405	541.6	890	18.08	1.852	.0755	15394	299	76.8	
	1406	445	821	14.89	1.556	.0710	14494	302	76.8	
	1407	597.7	939	19.06	2.052	.0751	15796	304	93.6	
	1408	548	894	17.65	1.876	.0741	15292	307	93.9	
	1409	443	807	14.54	1.563	.0695	14348	308	94.2	

10.0 ACOUSTIC DATA ANALYSIS

10.1 Wind Tunnel Acoustic Data

10.1.1 Reverberation Corrections

When a source is generating noise in a semi-reverberant environment such as a wind tunnel, three noise regions results. The regions may be termed "nearfield", "farfield", and "reverberant." Figure 10.1 defines the outer edge of the nearfield region as extending a distance "A" from the noise source. The value of "A" is usually three to four times the wavelength of the noise that is being monitored. Between points, "A" and "B", the farfield region exists. The "farfield" is defined as a region where doubling in distance causes the sound pressure level at a given frequency to decrease by 6 dB if air attenuations corrections are made. The extent of the farfield region is the distance "B" where the reflected noise from the walls of the wind tunnel begins to contaminate the direct noise field. The reverberant field is defined as the regions where this contaimination occurs. It should be noted that in a semi-reverberant room, the effects of reverberation vary as a function of acoustic angle, frequency, and the distance from the noise source.

In order to successfully perform acoustic measurements in a wind tunnel to determine the effects of freestream velocity on the noise produced by the exhaust stream, the noise measurements made in the wind tunnel must be corrected for reverberation effects. To determine the magnitude of the corrections, two procedures were used.

The first technique was to use a dodecahedron sound source and perform measurements in the NASA/AMES 40' by 80' Foot Wind Tunnel as well as an anechoic environment. This technique is described in detail in Reference 10.1. The corrections determined using this procedure are presented in Figures 10.2 through 10.9.

The second technique to determine reverberation corrections was to compare outdoor static test data to wind tunnel static test data at equivalent microphone locations and engine power settings. The acoustic data from the outdoor static tests were corrected to freefield using a ground reflection model developed by Hoch and Thomas, Reference 10.2. This

was done for several acoustic data points representing a jet velocity range from 305 to 610 meters/sec (1000 to 2000 ft/sec). These outdoor freefield spectra were then compared to the wind tunnel static spectra at the same power setting and acoustic angle. The differences between the two spectra at the twenty-four one-third octave band frequencies were defined as the reverberation corrections. This procedure was used for both the isolated nacelle and wing/nacelle test series.

Presented on Figures 10.2 through 10.9 are the reverberation corrections for the 4 (13) and 5.5 meter (8 foot) sideline monitoring locations for the isolated nacelle wind tunnel test series. The corrections were calculated for both the conical ejector and AIE nozzle. The reverberation corrections were calculated at three power settings for the two nozzles and then averaged. The average values for the conical ejector and AIE nozzles were compared to determine if the corrections were a function of nozzle type. The comparisons indicated that the differences between the two configurations were negligible. These corrections were then compared to those obtained using the dodecahedron sound source. These comparisons are presented on Figures 10.2 through 10.9. The results of these comparisons indicate that at the peak jet noise angle of 130°, the dodecahedron corrections are much greater than those determined by the comparison of indoor and outdoor static data. This difference could be due to the following reasons:

- The dodecahedron sound source is a monopole omi-directional sound source, and has a spherical radiation pattern. The exhaust jet can be thought of as series of highly directional sources.
- The dodecahedron sound source was placed at one location in the 40 by 80 - Foot Wind Tunnel. The exhaust jet is not a point source but can be visualized as a series of point sources extending along the axis of the exhaust jet.

Because of these differences, the corrections determined using indoor to outdoor static data comparisons were used. These corrections are summarized on Tables 10.1 and 10.2.

The same procedure that was used to determine the reverberation corrections for the isolated nacelle test series was used for the wing nacelle test series. The corrections were determined for three nozzle configurations: conical ejector nozzle, 104 tube nozzle and 104 tube nozzle with an acoustically treated shroud. The corrections for each of the nozzles were averaged and then compared to determine if the corrections for a complex suppressor nozzle such as the 104 tube nozzle would be different from that of the conical ejector nozzle. The comparisons indicated only small differences. As a result, the average corrections for each nozzle were again averaged to determine the final set of reverberation corrections for the wing nacelle wind tunnel test series. These corrections are presented on Table 10.3. The reverberation corrections for the two separate test series cannot be compared because the micriphone arrays were not at the same locations in the wind tunnel. However, the following observations should be useful in further wind tunnel tests.

- Reverberation effects can be minimized by being close to the noise source.
- Reverberation effects do not appear to be strong functions of nozzle type or exhaust gas velocity.

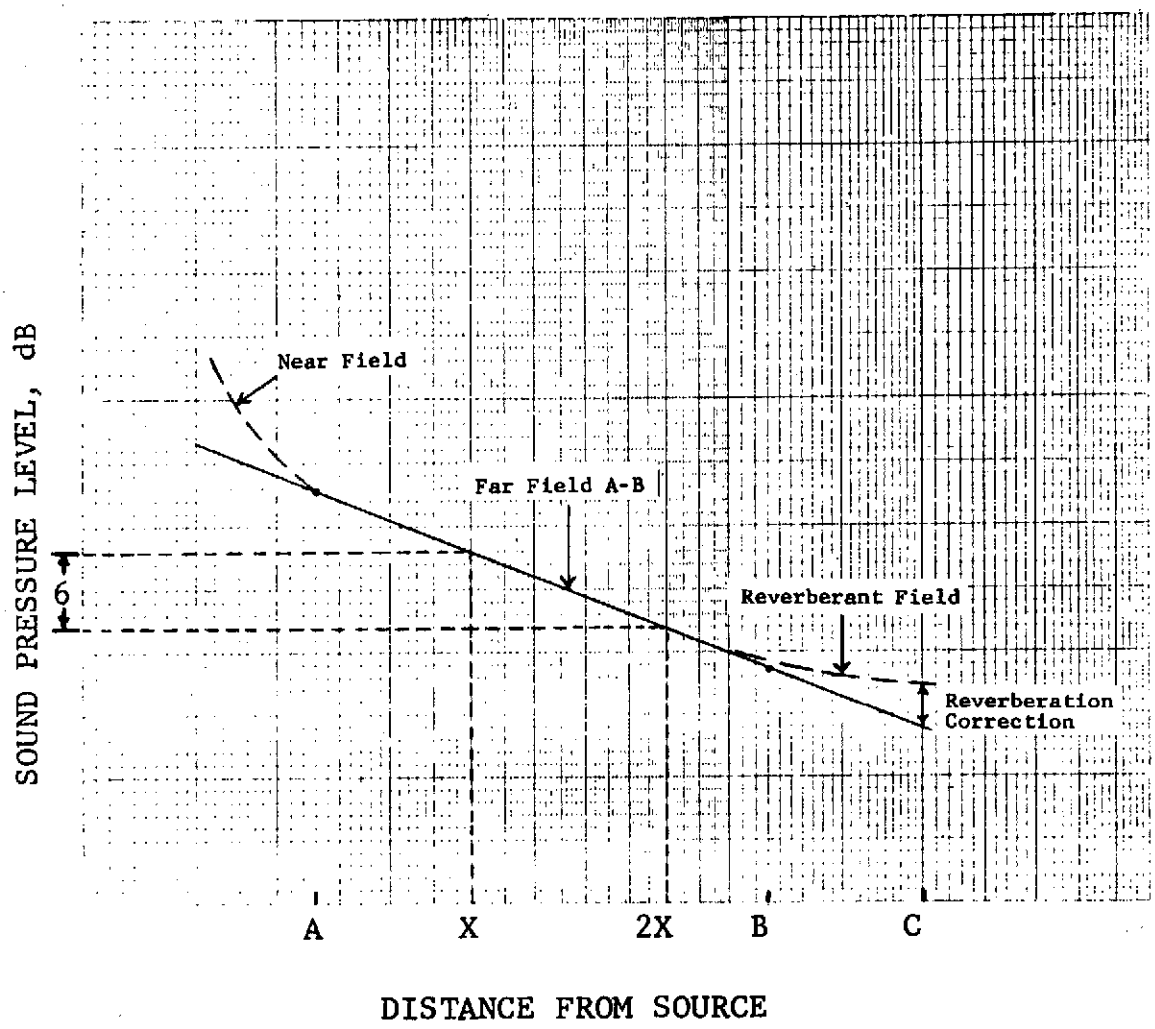

FIGURE 10.1 - REGIONS IN THE RADIATION FIELD OF A SEMI-REVERBERANT ENVIRONMENT

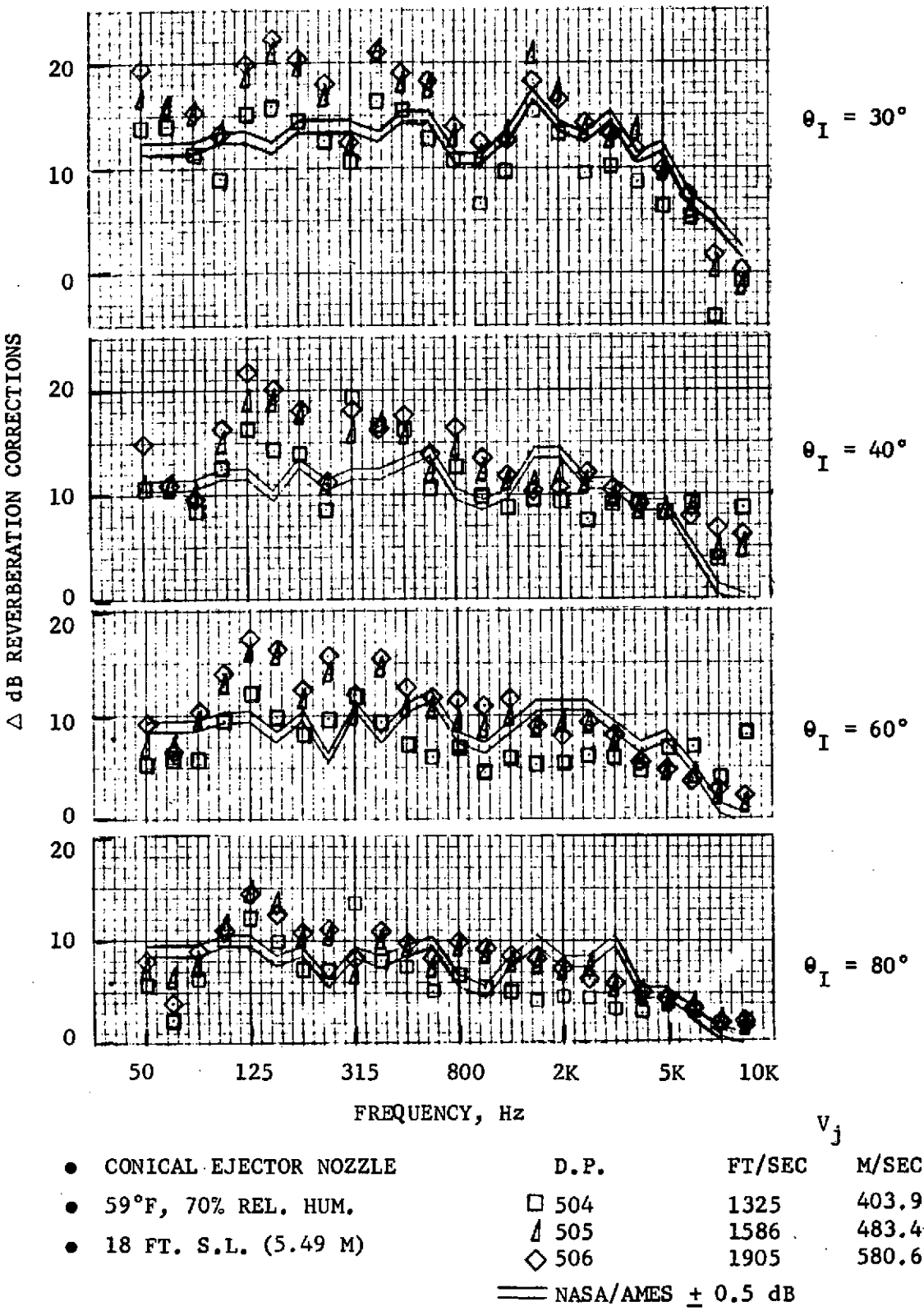

FIGURE 10.2 - REVERBERATION CORRECTIONS, ISOLATED NACELLE WIND TUNNEL TEST, CONICAL EJECTOR NOZZLE

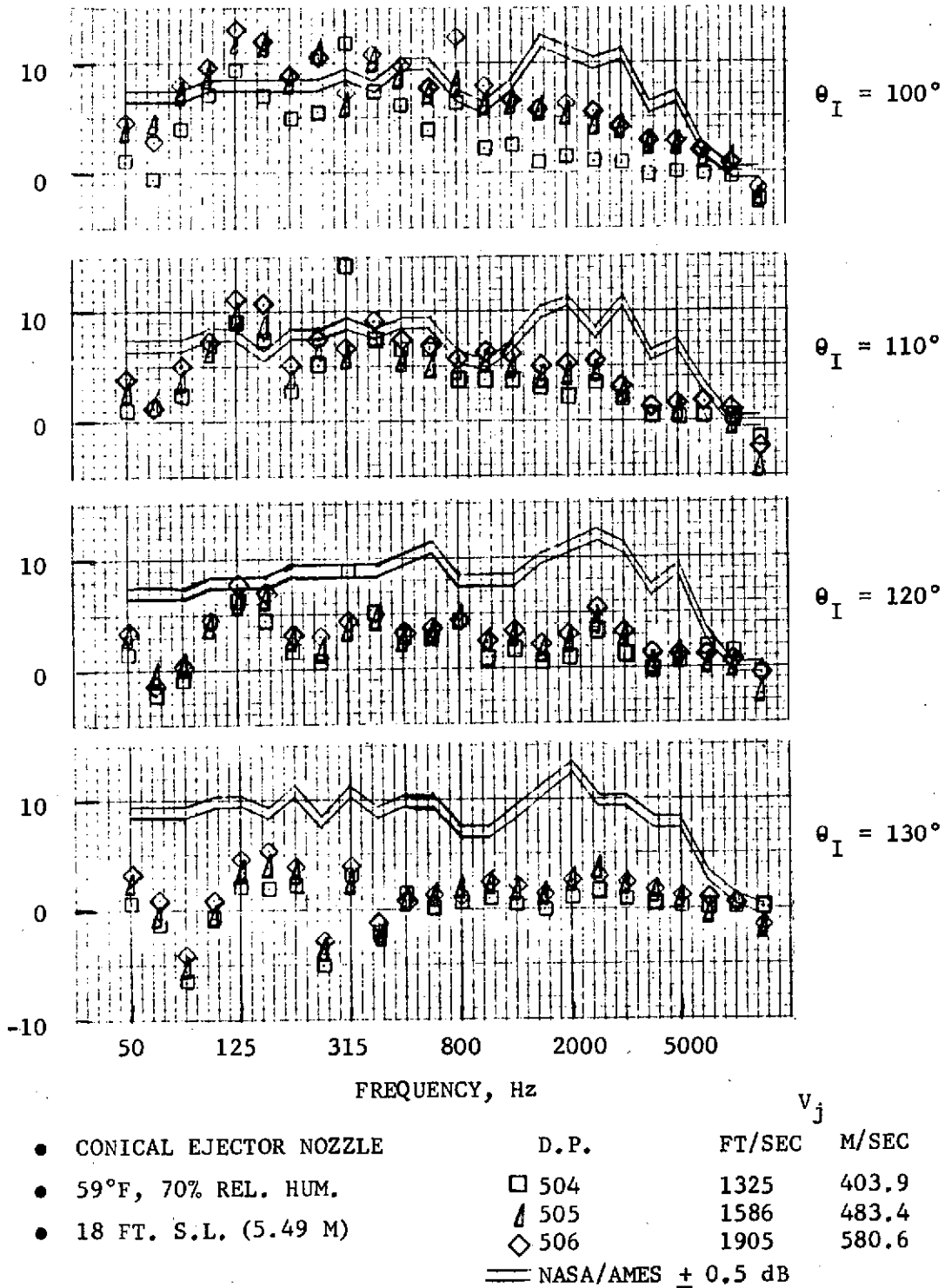

FIGURE 10.3 - REVERBERATION CORRECTIONS, ISOLATED NACELLE WIND TUNNEL TEST, CONICAL EJECTOR NOZZLE

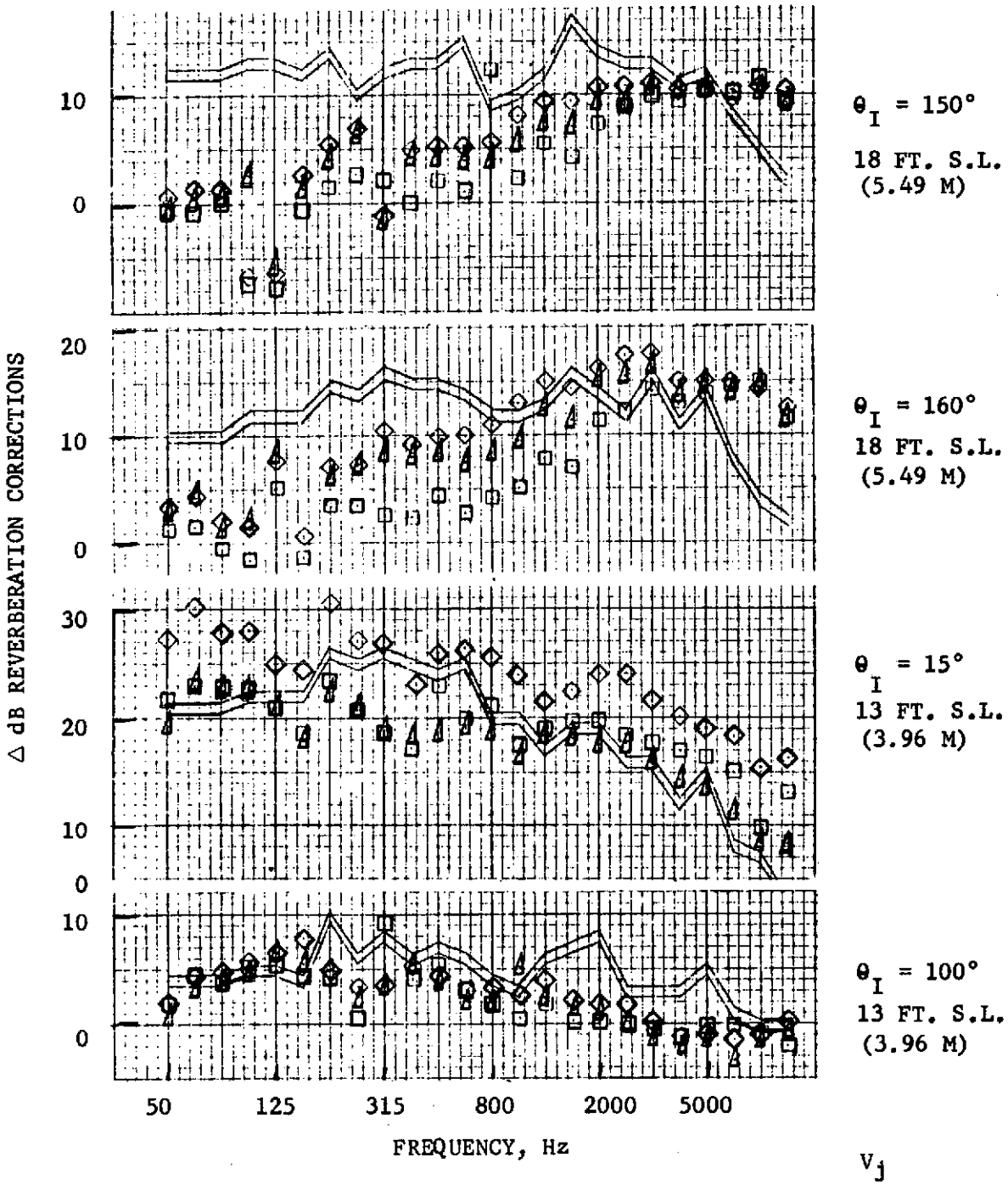

- CONICAL EJECTOR NOZZLE
- 59°F, 70% REL. HUM.

	D.P.	V_j FT/SEC	V_j M/SEC
□	504	1325	403.9
◁	505	1586	483.4
◇	506	1905	580.6

═══ NASA/AMES ± 0.5 dB

FIGURE 10.4 - REVERBERATION CORRECTIONS, ISOLATED NACELLE WIND TUNNEL TEST, CONICAL EJECTOR NOZZLE

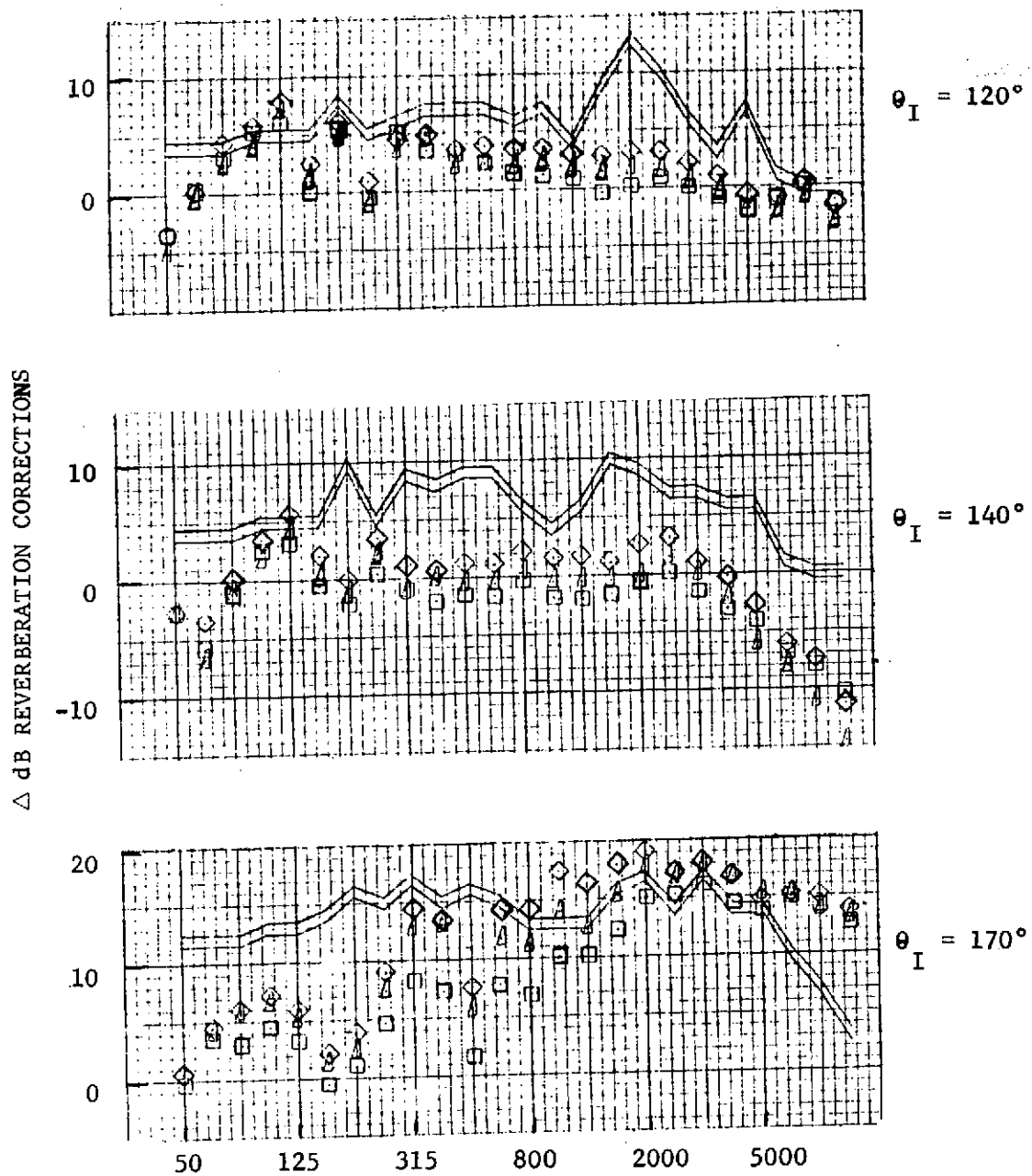

FIGURE 10.5 - REVERBERATION CORRECTIONS, ISOLATED NACELLE WIND TUNNEL TEST, CONICAL EJECTOR NOZZLE

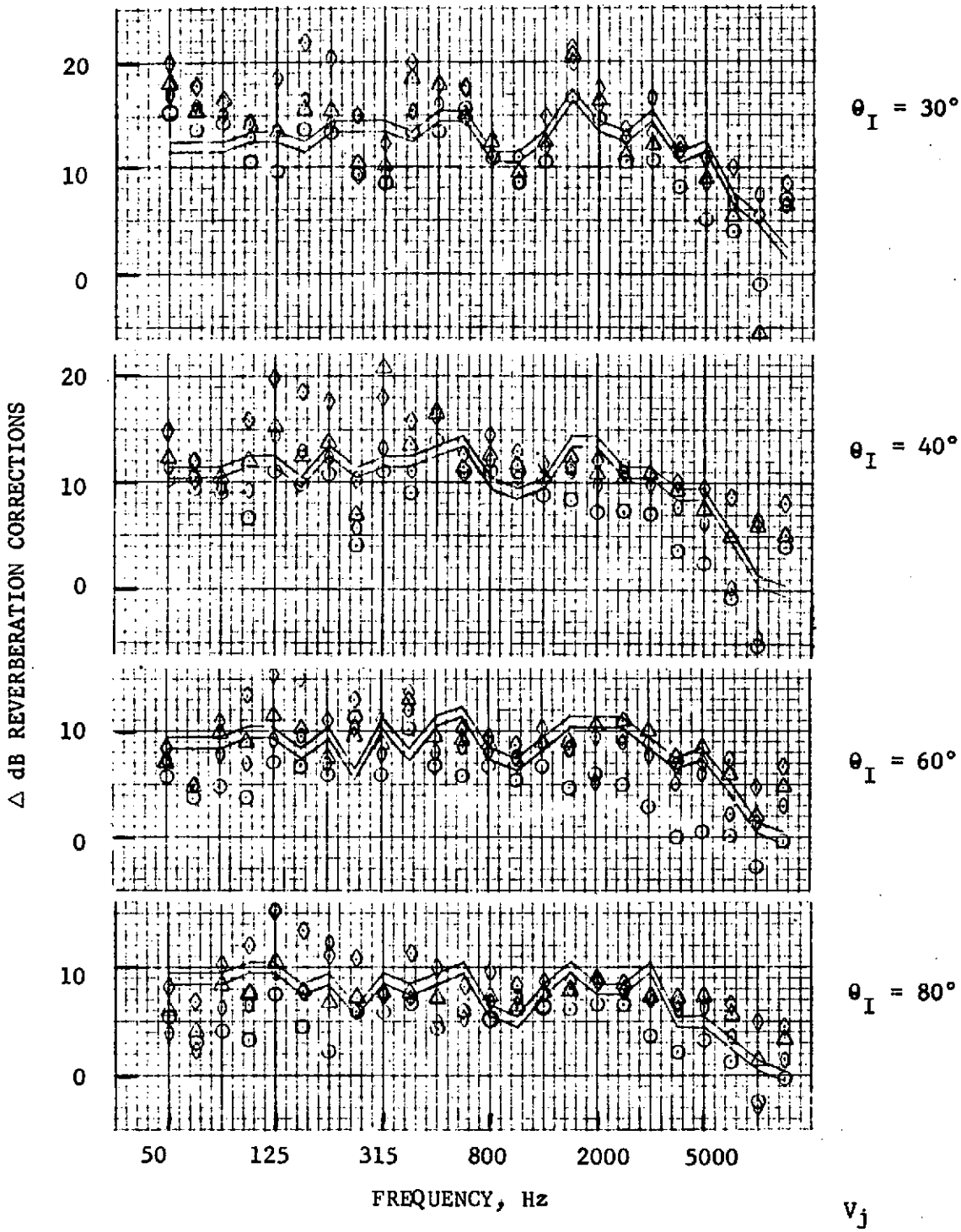

- AIE AUX NOZZLE
- 59°F, 70% REL. HUM.
- 18 FT. S.L. (5.49 M)

	D.P.	V_j FT/SEC	V_j M/SEC
O	602	1035	315.5
◊	603	1175	358.1
△	604	1307	398.4
◊	605	1646	501.7

NASA/AMES ± 0.5 dB

FIGURE 10.6 - REVERBERATION CORRECTIONS, ISOLATED NACELLE WIND TUNNEL TEST, AIE NOZZLE

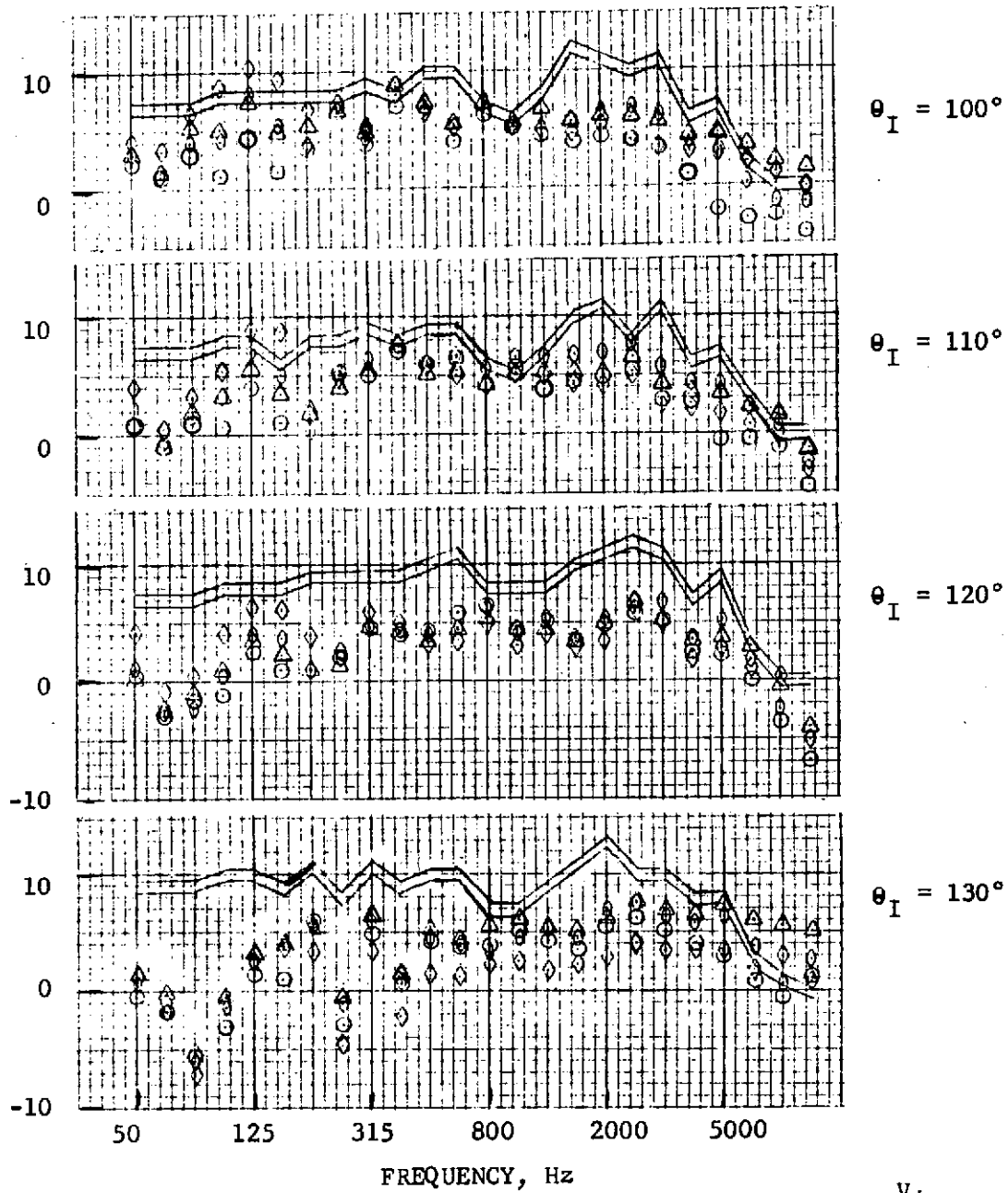

- AIE AUX NOZZLE
- 59°F, 70% REL. HUM.
- 18 FT. S.L. (5.49 M)

	D.P.	V_j FT/SEC	V_j M/SEC
○	602	1035	315.5
◊	603	1175	358.1
△	604	1307	398.4
◇	605	1646	501.7

═══ NASA/AMES ± 0.5 dB

FIGURE 10.7 - REVERBERATION CORRECTIONS, ISOLATED NACELLE WIND TUNNEL TEST, AIE NOZZLE

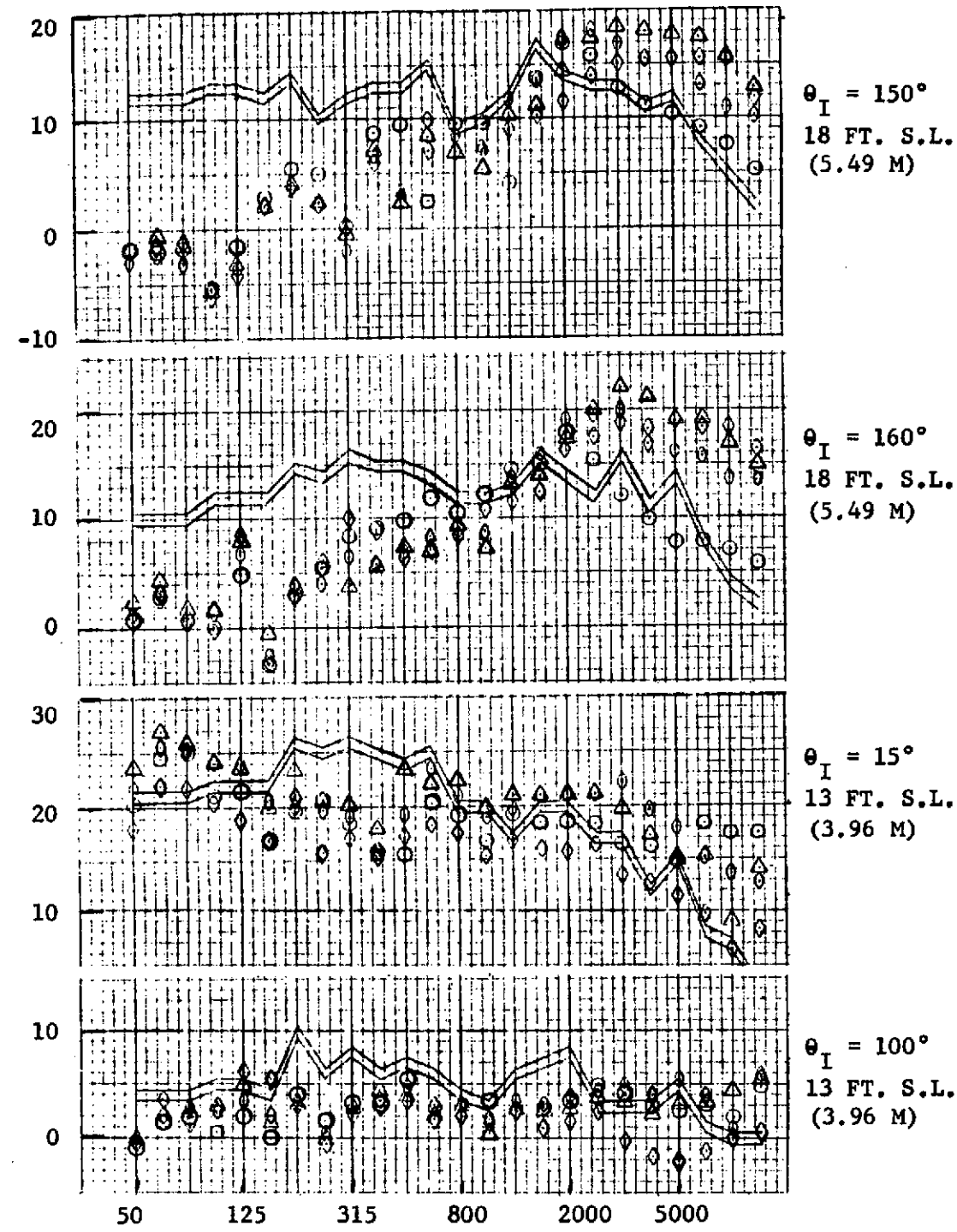

- AIE AUX NOZZLE
- 59°F, 70% REL. HUM.

	D.P.	V_j FT/SEC	V_j M/SEC
○	602	1035	315.5
◊	603	1175	358.1
△	604	1307	398.4
◊	605	1646	501.7

═══ NASA/AMES ± 0.5 dB

FIGURE 10.8 - REVERBERATION CORRECTIONS, ISOLATED NACELLE WIND TUNNEL TEST, AIE NOZZLE

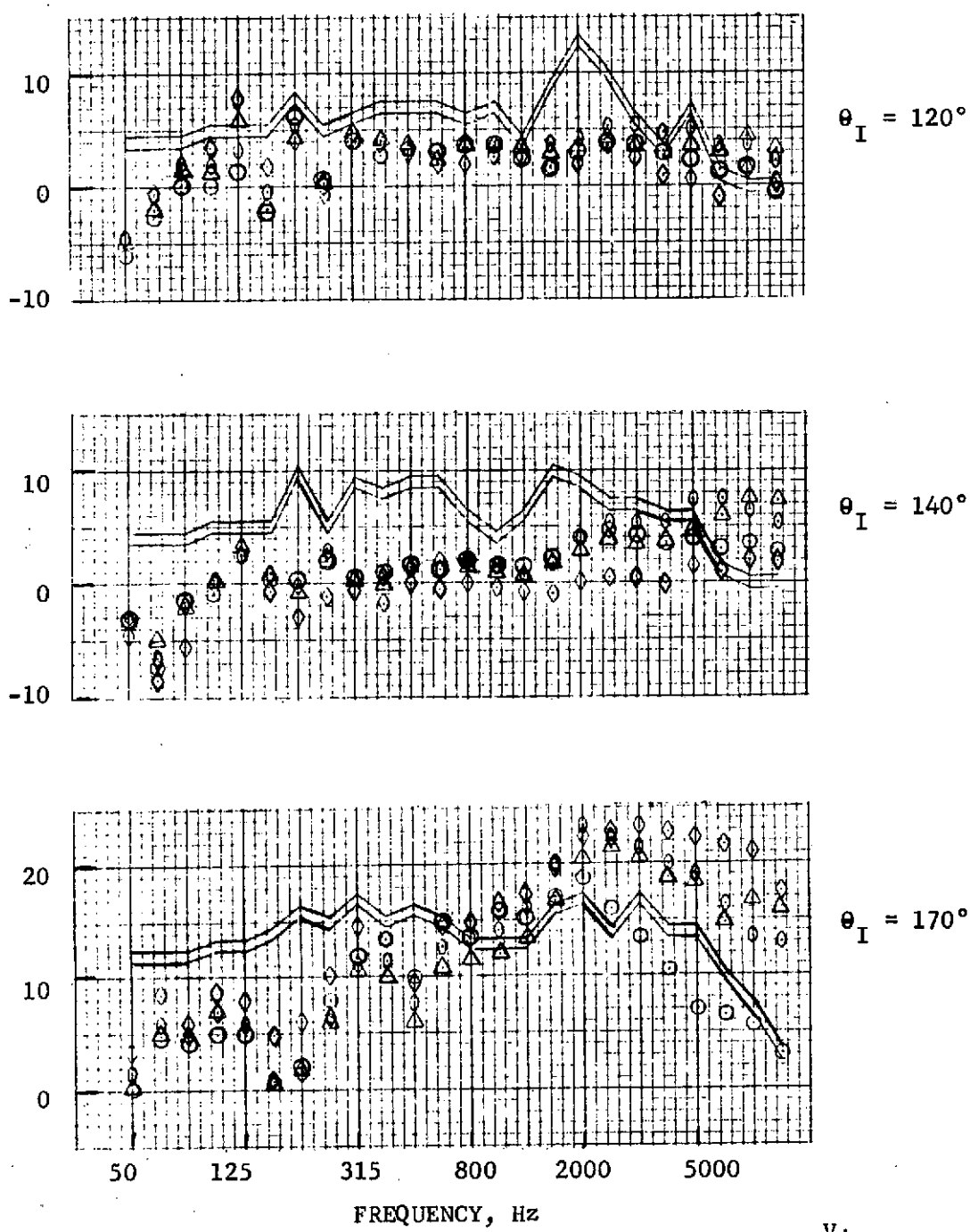

- AIE AUX NOZZLE
- 59°F, 70% REL. HUM.
- 13 FT. S.L. (3.96 M)

D.P.	V_j FT/SEC	V_j M/SEC
○ 602	1035	315.5
◊ 603	1175	358.1
△ 604	1307	398.4
◊ 605	1646	501.7

— NASA/AMES ± 0.5 dB

FIGURE 10.9 - REVERBERATION CORRECTIONS, ISOLATED NACELLE WIND TUNNEL TEST, AIE NOZZLE

TABLE 10.1

ISOLATED NACELLE WIND TUNNEL TEST

REVERBERATION CORRECTIONS FOR CONICAL EJECTOR NOZZLE AND AIE AUX. NOZZLE AT AN 18 FT (5.5 M) SIDELINE

ANGLE* (deg.) FREQ. (Hz)	159°	149°	130°	120°	110°	101°	81°	61°	41°	30°
50	3	0	2.0	3.0	2.5	4.0	7.0	6.0	10.5	16.0
63	4	0	1.0	-1.5	1.0	3.5	4.0	6.5	10.5	15.0
80	1.5	.5	-4.5	.5	4.0	7.5	8.0	10.0	9.0	15.0
100	2.0	-7.0	0	4.5	6.5	9.5	12.0	13.5	15.0	13.5
125	7.5	-7.0	3.0	7.0	10.0	12.0	14.5	16.5	19.0	20.0
160	6.5	+2.0	3.0	6.0	8.0	11.0	12.5	15.5	19.0	21.5
200	7.0	+4.5	3.0	2.5	3.5	8.0	10.5	12.0	17.5	20.0
250	7.0	6.5	-4.50	1.0	7.0	10.5	11.0	14.5	10.0	17.5
315	9.5	-1.5	3.0	3.5	6.0	7.0	7.5	12.0	17.5	12.0
400	8.0	4.5	-2.0	5.0	7.5	10.0	9.5	14.5	16.5	21.0
500	9.0	4.5	1.0	3.0	6.5	8.5	9.0	11.0	16.0	18.5
630	8.5	4.5	1.0	3.0	6.0	7.0	7.5	11.0	12.0	18.0
800	10.0	5.0	1.0	4.5	5.0	7.0	9.5	9.0	14.5	13.5
1000	10.0	6.0	1.5	2.0	5.5	7.0	9.0	8.5	12.0	11.5
1250	13.5	7.5	1.0	2.5	5.0	6.0	7.5	10.5	11.5	13.0
1600	12.0	7.5	.5	1.5	4.5	5.5	7.6	9.0	9.5	20.0
2000	15.0	9.5	2.0	2.5	4.5	6.0	7.0	8.5	10.5	16.5
2500	15.5	10.0	2.5	4.0	4.5	5.0	6.5	9.0	11.5	13.5
3150	17.0	10.0	1.5	2.5	2.0	4.0	5.5	7.5	9.5	13.0
4000	13.5	10.0	1.5	.5	1.0	3.0	5.0	5.5	9.0	12.0
5000	14.5	10.0	.5	1.0	1.0	2.5	4.0	4.5	8.5	10.0
6300	14.5	10.0	.5	.5	1.0	1.5	3.5	4.0	8.5	6.5
8000	14.0	11.0	0	1.0	0.0	.5	2.0	3.0	5.5	1.0
10000	12.5	10.0	-1.5	-1.0	-2.0	-2.0	2.0	1.5	5.5	-1.0

*Angle is reference to inlet

TABLE 10.2

ISOLATED NACELLE WIND TUNNEL TEST

REVERBERATION CORRECTIONS FOR CONICAL EJECTOR NOZZLE AND AIE AUX. NOZZLE AT A 13 FT (4 M) SIDELINE

ANGLE* (deg.) FREQ. (Hz)	101°	119°	139°	169°	13°
50	1.5	-4.0	-3.0	0.5	20.5
63	3.5	0	-6.0	4.0	23.0
80	4.0	3.0	-0.5	5.5	23.0
100	5.5	4.5	2.5	6.5	22.5
125	6.5	6.5	4.5	5.0	21.0
160	5.5	1.0	0	2.5	18.5
200	5.0	6.0	-1.5	3.5	23.0
250	2.5	0	2.5	7.5	21.0
315	3.5	4.5	-0.5	13.5	18.5
400	5.0	4.0	0	13.0	18.0
500	4.5	3.0	-0.5	6.5	18.5
630	2.5	3.0	0	13.0	19.5
800	2.5	2.0	0.5	11.5	19.0
1000	2.5	2.0	-1.0	14.0	17.5
1250	2.0	2.0	-0.5	13.5	19.0
1600	1.5	1.0	0	15.0	19.0
2000	1.0	1.5	0	17.5	19.5
2500	0	2.0	2.0	16.5	18.5
3150	-0.5	1.0	0	17.5	17.5
4000	-2.0	0	-3.0	16.0	16.5
5000	-1.0	-1.0	-5.5	14.5	16.0
6300	-1.5	-1.5	-8.0	15.0	15.0
8000	-1.5	0	-10.5	14.5	14.0
10000	-1.0	-2.0	-13.0	13.5	13.0

*Angle is reference to inlet

TABLE 10.3

WING NACELLE WIND TUNNEL TEST

REVERBERATION CORRECTIONS FOR CONICAL EJECTOR NOZZLE AND 104 TUBE NOZZLE WITH AND WITHOUT SHROUD AT A 13 FT (4 M) SIDELINE

ANGLE* (deg.) FREQ. (Hz)	162°	147°	127°	111°	101°	90°	70°
50	2.0	-3.3	-2.2	-0.4	3.4	2.9	2.4
63	1.2	-9.3	0.5	1.3	4.3	4.3	5.2
80	1.4	-4.3	6.2	4.7	7.1	7.2	7.7
100	9.5	0.6	7.6	5.1	6.8	6.5	8.0
125	5.1	3.8	9.3	6.6	7.0	6.3	7.9
160	2.9	4.3	2.6	4.7	7.7	8.1	8.1
200	5.0	-5.2	7.1	5.6	6.8	6.5	9.5
250	5.9	2.2	3.8	2.2	3.1	3.9	3.6
315	-2.5	0.3	6.8	3.7	4.1	3.9	5.7
400	7.0	3.4	5.7	4.2	5.6	5.4	7.5
500	6.1	2.5	6.3	3.8	5.2	5.7	6.9
630	7.6	2.8	4.6	4.1	4.1	4.5	6.1
800	8.1	1.9	5.6	3.0	4.2	4.8	5.4
1000	9.5	4.3	4.6	2.2	4.6	3.9	4.3
1250	10.0	4.5	5.2	3.1	4.3	4.0	4.6
1600	11.5	5.3	4.4	3.1	3.8	4.3	5.3
2000	11.6	5.3	4.3	3.0	3.7	3.8	6.4
2500	12.1	5.9	3.9	2.8	4.2	3.7	6.4
3150	11.3	6.0	3.1	1.8	3.2	2.4	4.7
4000	10.3	5.3	3.1	1.1	3.0	2.0	4.2
5000	10.6	5.1	2.9	0.2	2.0	2.5	3.4
6300	10.3	4.1	2.3	-0.4	0.7	0.9	1.8
8000	9.5	3.9	2.1	-1.1	-1.1	-1.3	-0.2
10000	8.5	3.4	1.1	-3.7	-1.1	-0.3	-0.9

*Angle is reference to inlet

10.1.2 Comparisons of Fairfield and Nearfield Acoustic Data

During the outdoor isolated nacelle static test the wind tunnel microphone arrays were duplicated. The data measured using these arrays served a two-fold purpose. The first, which was to determine reverberation corrections, was described in detail in Section 10.1.1. The second was to use this data in conjunction with the one-hundred foot arc data to determine if the wind tunnel microphone arrays were in the farfield or nearfield region.

To assure that the conclusions drawn from these comparisions were valid, both sets of nearfield and farfield data were corrected for ground effects using the technique described in Reference 10.2. The nearfield data were then extrapolated to a one-hundred foot arc using standard SAE procedures including Extra Ground Attenuations.

Although for valid comparisons the data had to be corrected for ground reflection, the corrections themselves introduce another degree of complexity into the problem. In the work that was done by Howes' in Reference 10.3 and Hoch and Thomas in Reference 10.2 the following assumptions are made.

"The instrumentation is assumed to lie in the farfield, i.e., at a long distance from the source. This requirement is met when the distance between the source and the instrumentation is simultaneously a multiple of the wave length of the sound studied and a multiple of the longest linear dimension of the source."

For the geometry of the isolated nacelle outdoor static test, the first null occurs at 63 Hz which is not a multiple of wave lengths away from the source. Therefore, the analysis is not valid in this region because the simulated wind tunnel microphones are not a multiple of wave lengths away from the noise source. The comparisons are presented on the basis of PNL, OASPL and 1/3 octave band sound pressure level spectra.

The results are presented for the three nozzles at high and low jet velocities. From studying Figures 10.10 through 10.33 the following trends should be noted:

- On the basis of PNdB and OASPL the maximum difference between the three sets of data is 4 dB at the high power setting. This trend is also supported for the data at the low power setting except for the data measured at 120°.
- Comparing the spectra at several acoustic angles for the conical ejector nozzle indicates that the overall agreement is good. The spectrum shapes are the same and since the measurements were not conducted simultaneously, limited data scatter is to be expected.
- For the 104 tube nozzle without the acoustically treated shroud the comparisons indicate larger differences on the basis of OASPL and PNdB for acoustic angles of 140 through 160°.
- The extreme differences at the acoustic angle of 170° can be explained by the fact that the microphone was extremely close to the edge of the exhaust plume.
- However, it should be noted that except for the 160 degree acoustic angle the agreement on a spectrum basis is extremely good except at low frequencies where the validity of the ground reflections are in question.
- The 104 tube nozzle with shroud exhibits the same trends as the other two nozzles.

In summary, the comparison between the various data indicate good agreement on a spectrum basis except in the regions below 250 Hz where ground reflection corrections are not valid.

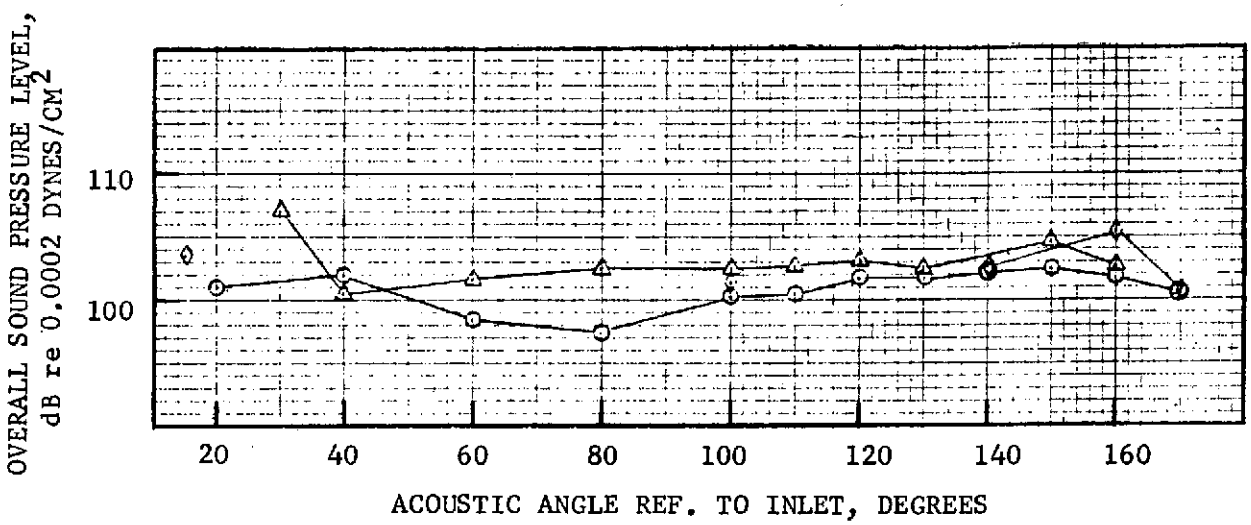

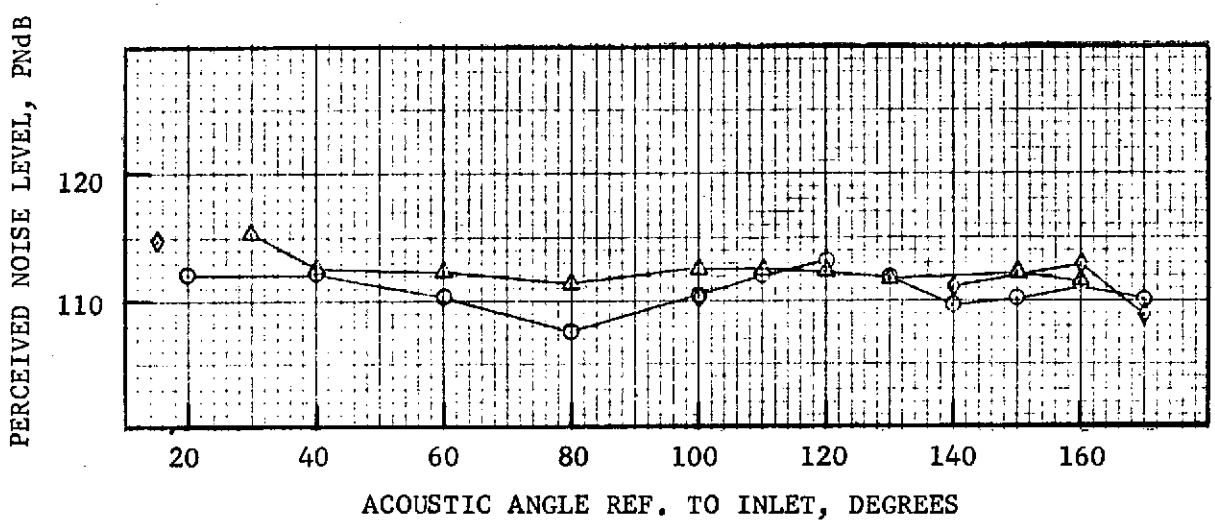

- CONICAL EJECTOR NOZZLE
- 59°F, 70% REL. HUM.
- 100 FT. ARC (30.5 M)
- V_j = 700 FT/SEC (213 M/SEC)

○ 20 FT. HIGH FARFIELD (6.1M)
△ 18 FT. NEARFIELD (5.49M)
◊ 13 FT. NEARFIELD (3.96M)

FIGURE 10.10 - ISOLATED NACELLE OUTDOOR STATIC TEST, FARFIELD/NEAR FIELD COMPARISON, OASPL AND PNdB DIRECTIVITY, CONICAL EJECTOR NOZZLE

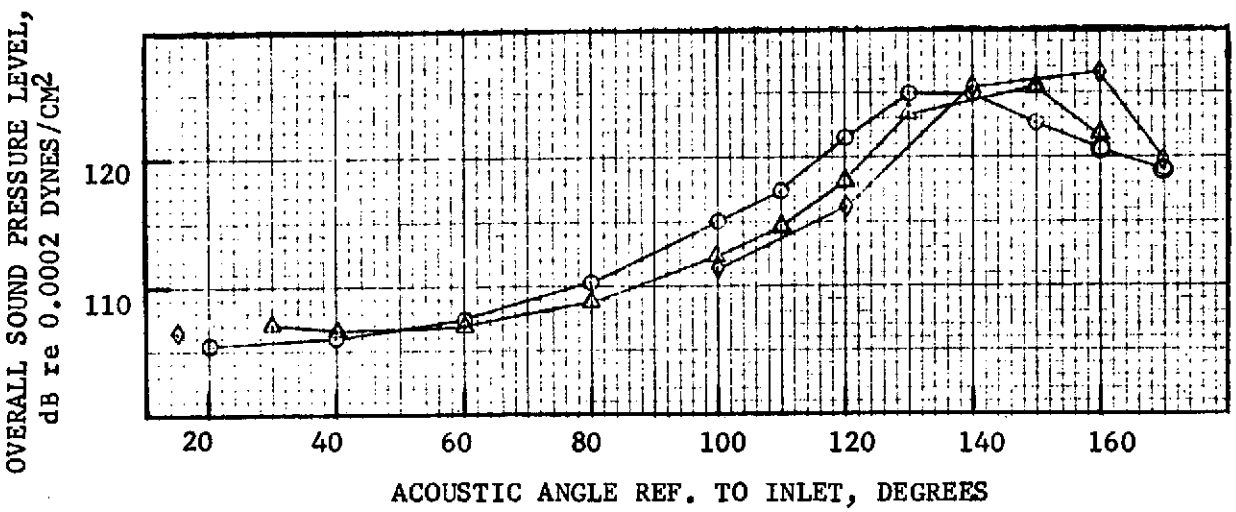

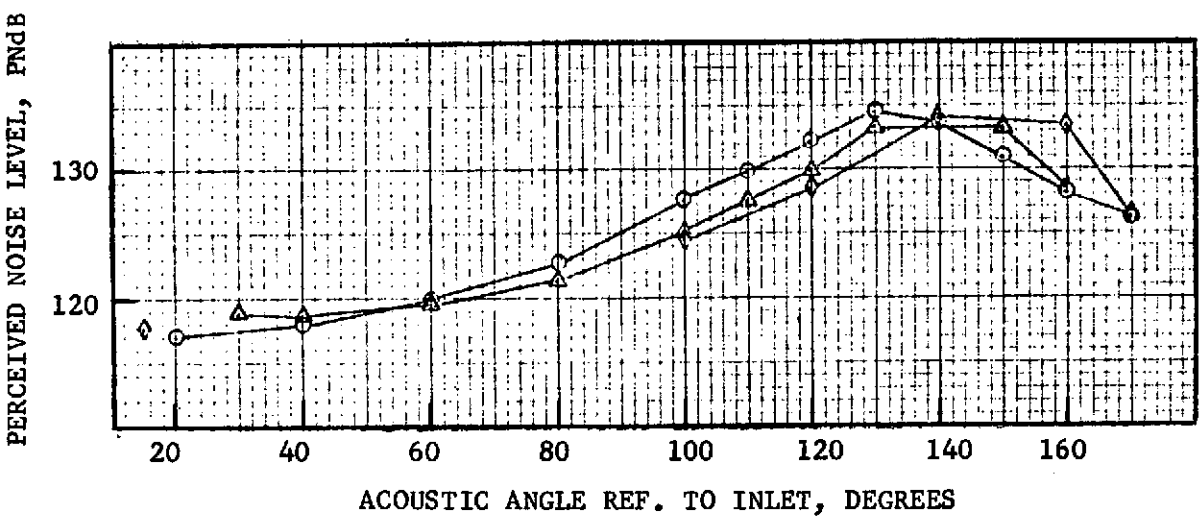

- CONICAL EJECTOR NOZZLE
- 59°F, 70% REL. HUM.
- 100 FT. ARC (30.5 M)
- V_j = 1910 FT/SEC (582 M/SEC)

○ 20 FT. HIGH FARFIELD (6.1M)
△ 18 FT. NEARFIELD (5.49M)
◊ 13 FT. NEARFIELD (3.96M)

FIGURE 10.11 - ISOLATED NACELLE OUTDOOR STATIC TEST, FARFIELD/NEAR FIELD COMPARISON, OASPL AND PNdB DIRECTIVITY, CONICAL EJECTOR NOZZLE

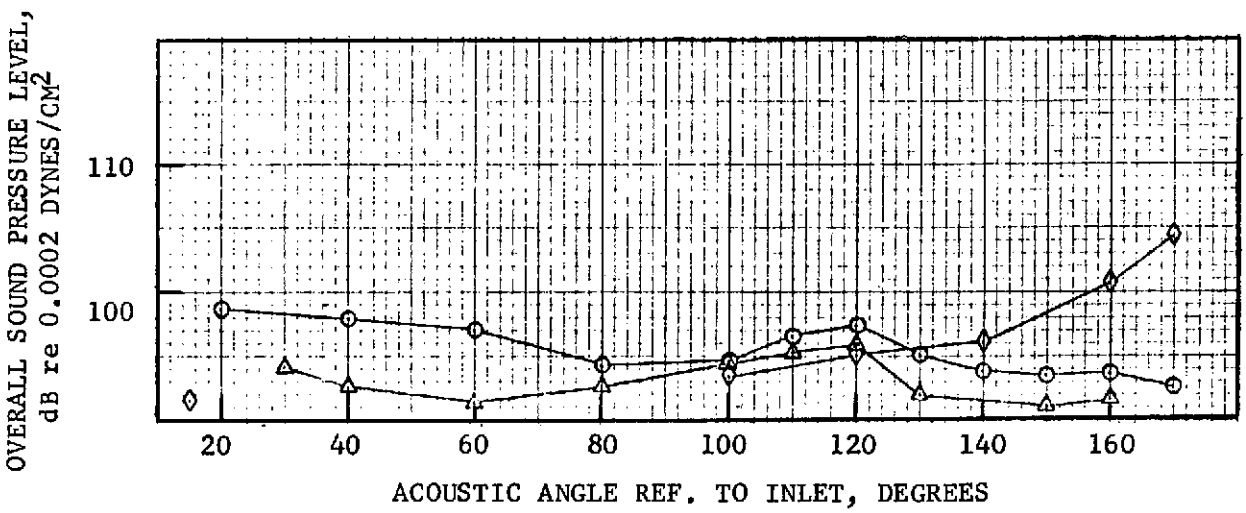

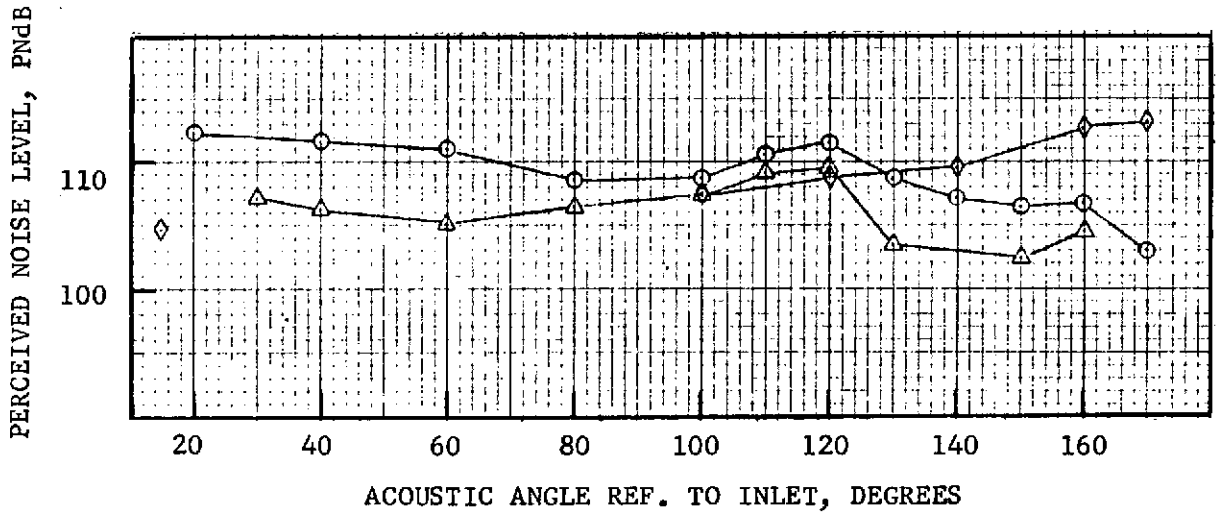

- 104 TUBE NOZZLE W/O SHROUD
- 59°F, 70% REL. HUM.
- 100 FT. ARC (30.5 M)
- V_j = 875 FT/SEC (267 M/SEC)

○ 20 FT. HIGH FARFIELD (6.1M)
△ 18 FT. NEARFIELD (5.49M)
◊ 13 FT. NEARFIELD (3.96M)

FIGURE 10.12 - ISOLATED NACELLE OUTDOOR STATIC TEST, FARFIELD/NEAR FIELD COMPARISON, OASPL AND PNdB DIRECTIVITY, 104-TUBE NOZZLE WITHOUT SHROUD

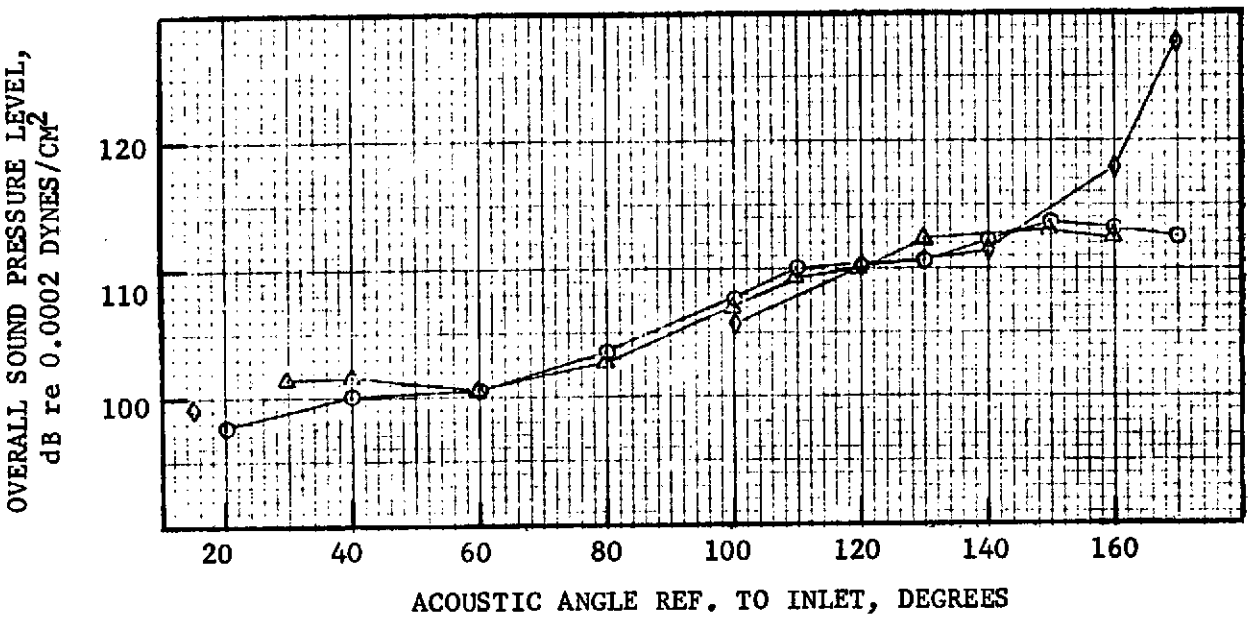

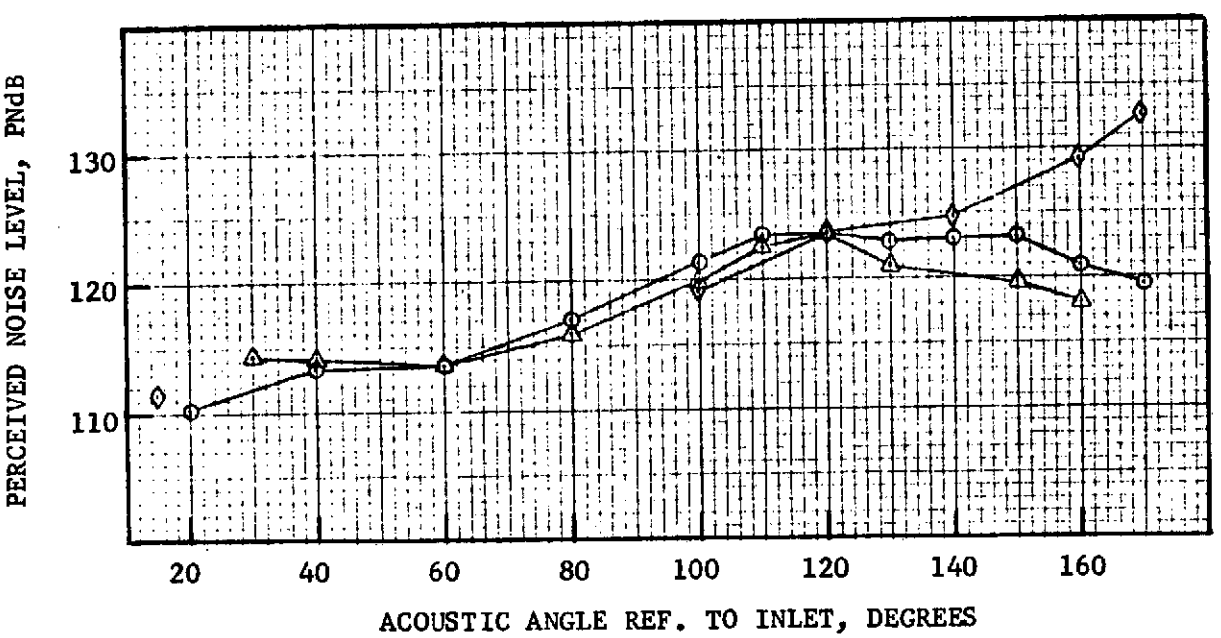

- 104 TUBE NOZZLE W/O SHROUD
- 59°F, 70% REL. HUM.
- 100 FT. ARC (30.5 M)
- V_j = 1985 FT/SEC (605 M/SEC)

○ 20 FT. HIGH FARFIELD (6.1M)
△ 18 FT. NEARFIELD (5.49M)
◊ 13 FT. NEARFIELD (3.96M)

FIGURE 10.13 - ISOLATED NACELLE OUTDOOR STATIC TEST, FARFIELD/NEAR FIELD COMPARISON, OASPL AND PNdB DIRECTIVITY, 104-TUBE NOZZLE WITHOUT SHROUD

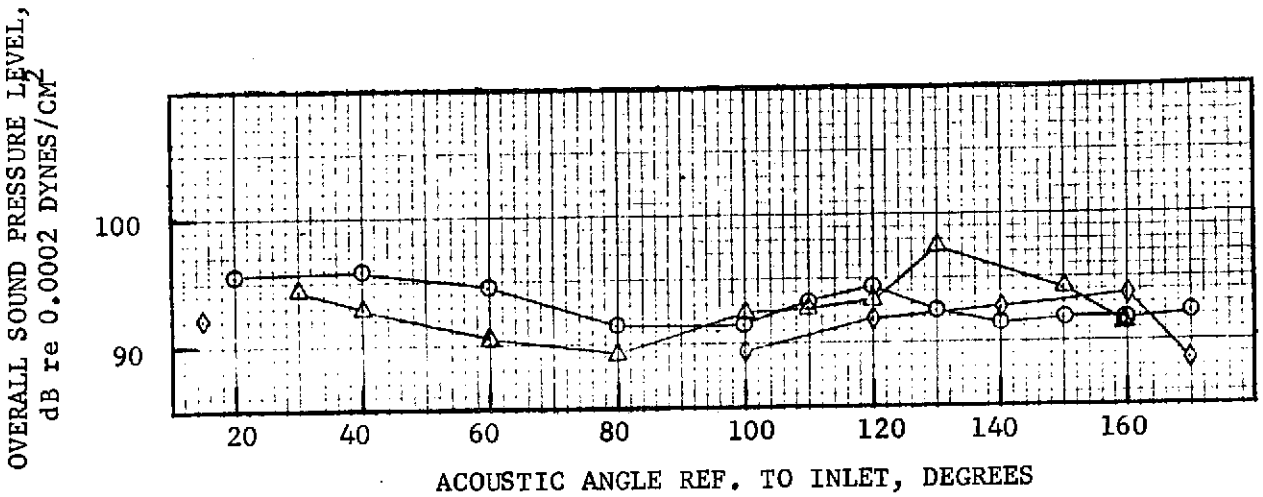

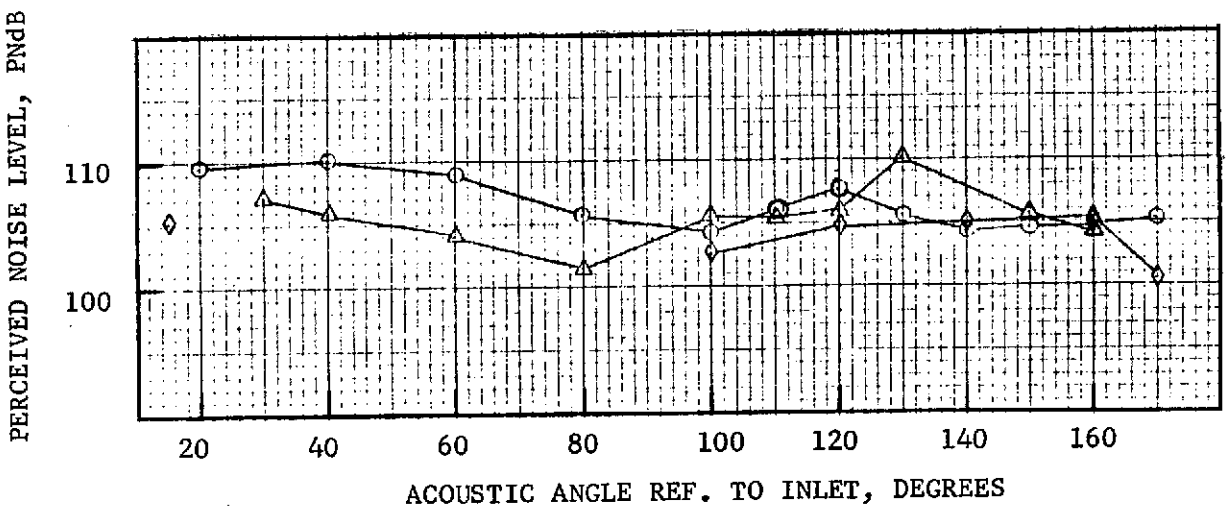

- 104 TUBE NOZZLE W/SHROUD
- 59°F, 70% REL. HUM.
- 100 FT. ARC (30.5 M)
- V_j = 880 FT/SEC (268 M/SEC)

○ 20 FT. HIGH FARFIELD (6.1M)
△ 18 FT. NEARFIELD (5.49M)
◊ 13 FT. NEARFIELD (3.96M)

FIGURE 10.14 - ISOLATED NACELLE OUTDOOR STATIC TEST, FARFIELD/NEAR FIELD COMPARISON, OASPL AND PNdB DIRECTIVITY, 104-TUBE NOZZLE WITH SHROUD

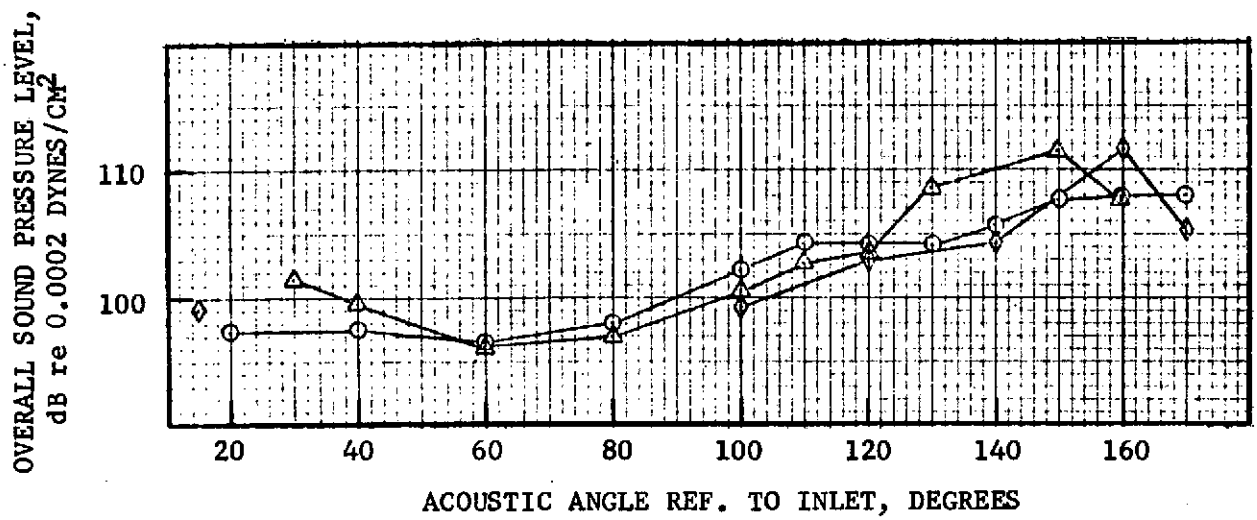

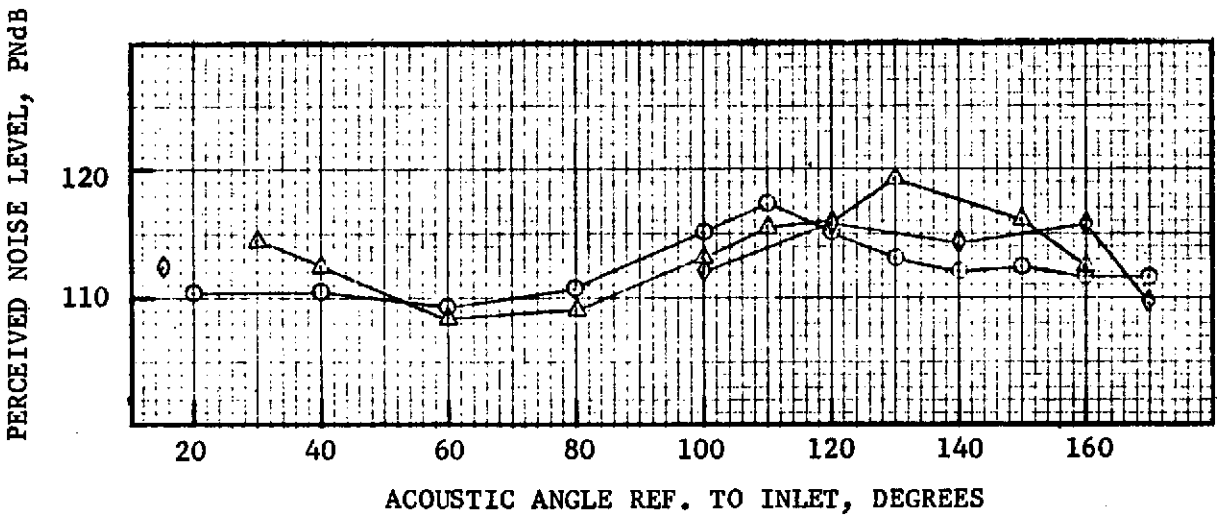

- 104 TUBE NOZZLE W/SHROUD
- 59°F, 70% REL. HUM.
- 100 FT. ARC (30.5 M)
- V_j = 1755 FT/SEC (535 M/SEC)

○ 20 FT. HIGH FARFIELD (6.1M)
△ 18 FT. NEARFIELD (5.49M)
◊ 13 FT. NEARFIELD (3.96M)

FIGURE 10.15 - ISOLATED NACELLE OUTDOOR STATIC TEST, FARFIELD/NEAR FIELD COMPARISON, OASPL AND PNdB DIRECTIVITY, 104-TUBE NOZZLE WITH SHROUD

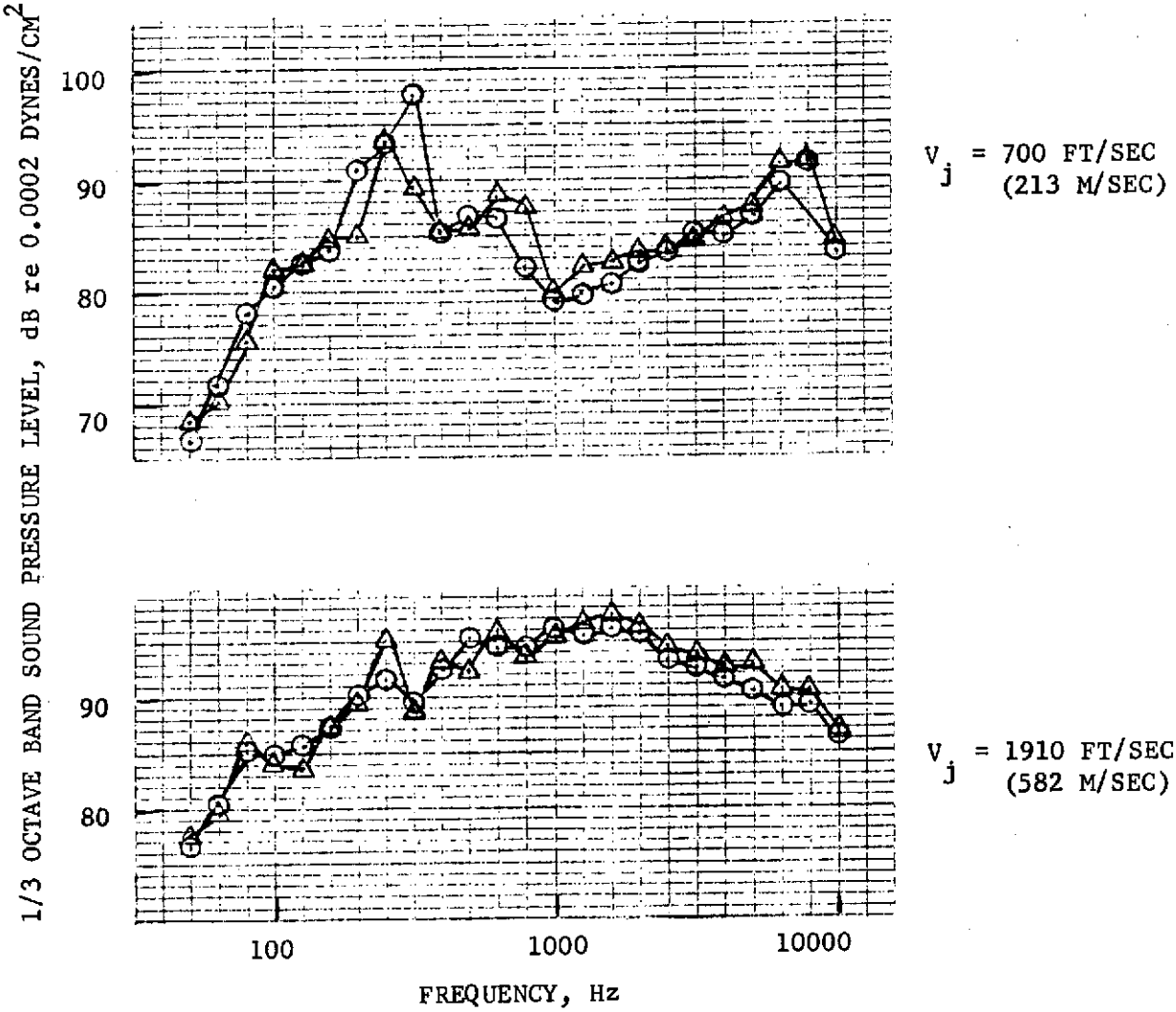

- CONICAL EJECTOR NOZZLE
- 59°F, 70% REL. HUM.
- 100 FT. ARC (30.5 M)
- $\theta_I = 40°$

○ 20 FT. HIGH FARFIELD (6.1 M)
△ 18 FT. NEARFIELD (5.49 M)
◊ 13 FT. NEARFIELD (3.96 M)

FIGURE 10.16 - ISOLATED NACELLE OUTDOOR STATIC TEST, FARFIELD/NEAR FIELD COMPARISON, 1/3 OCTAVE BAND SPECTRA, CONICAL EJECTOR NOZZLE

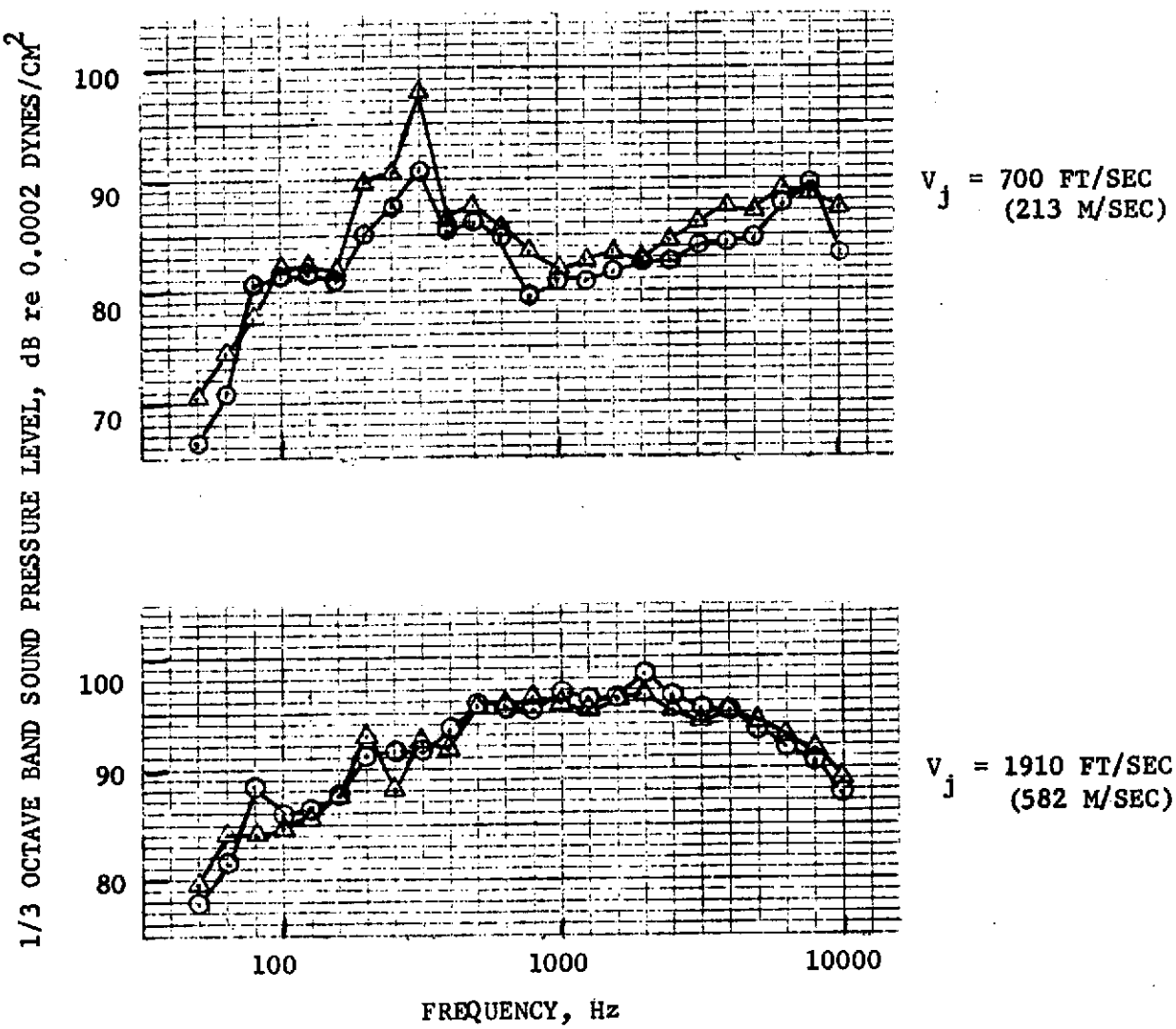

- CONICAL EJECTOR NOZZLE
- 59°F, 70% REL. HUM.
- 100 FT. ARC (30.5 M)
- $\theta_I = 60°$

○ 20 FT. HIGH FARFIELD (6.1 M)
△ 18 FT. NEARFIELD (5.49 M)
◊ 13 FT. NEARFIELD (3.96 M)

FIGURE 10.17 - ISOLATED NACELLE OUTDOOR STATIC TEST, FARFIELD/NEAR FIELD COMPARISON, 1/3 OCTAVE BAND SPECTRA, CONICAL EJECTOR NOZZLE

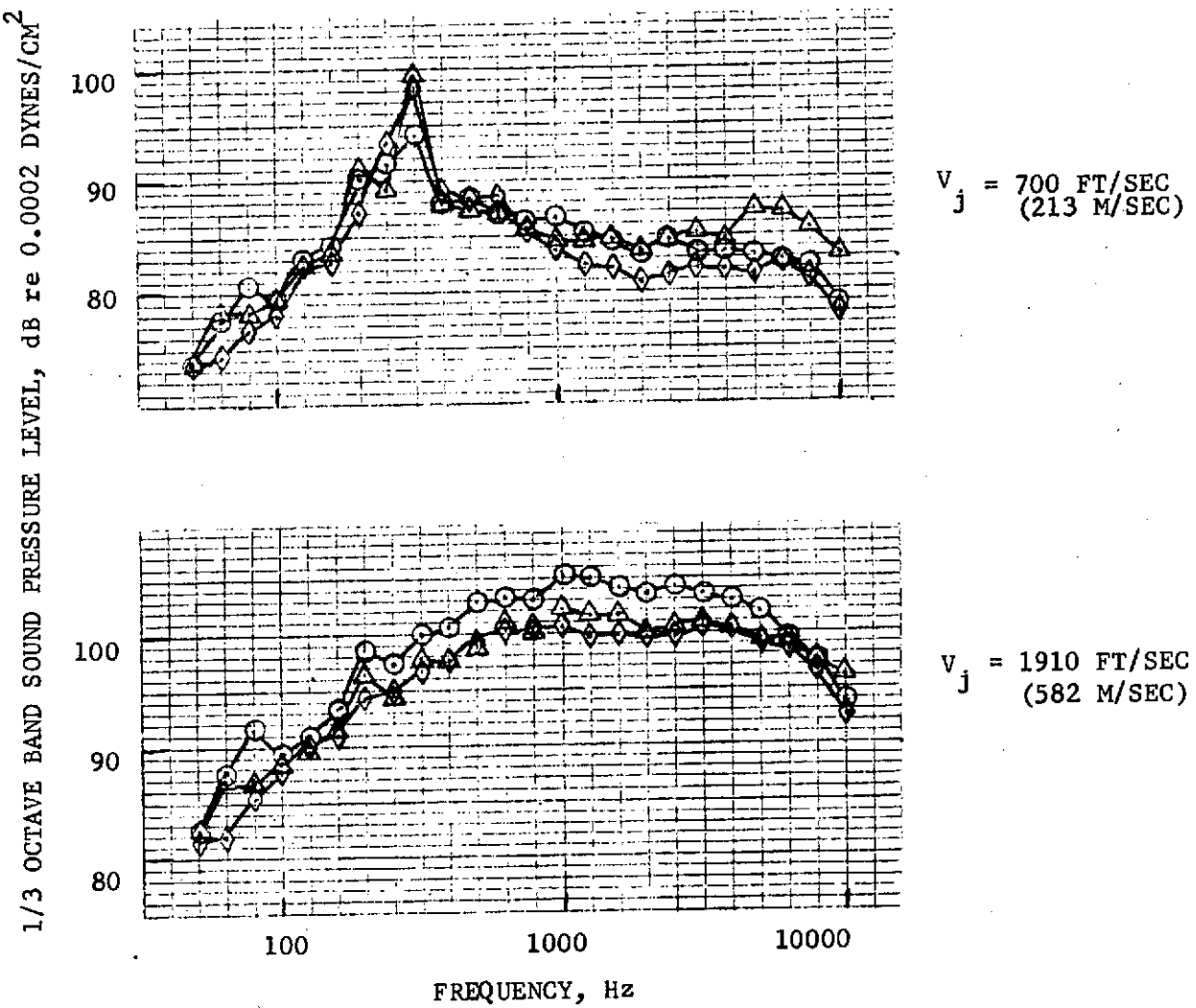

- CONICAL EJECTOR NOZZLE
- 59°F, 70% REL. HUM.
- 100 FT. ARC (30.5 M)
- θ_I = 100°

○ 20 FT. HIGH FARFIELD (6.1 M)
△ 18 FT. NEARFIELD (5.49 M)
◊ 13 FT. NEARFIELD (3.96 M)

FIGURE 10.18 - ISOLATED NACELLE OUTDOOR STATIC TEST, FARFIELD/NEAR FIELD COMPARISON, 1/3 OCTAVE BAND SPECTRA, CONICAL EJECTOR NOZZLE

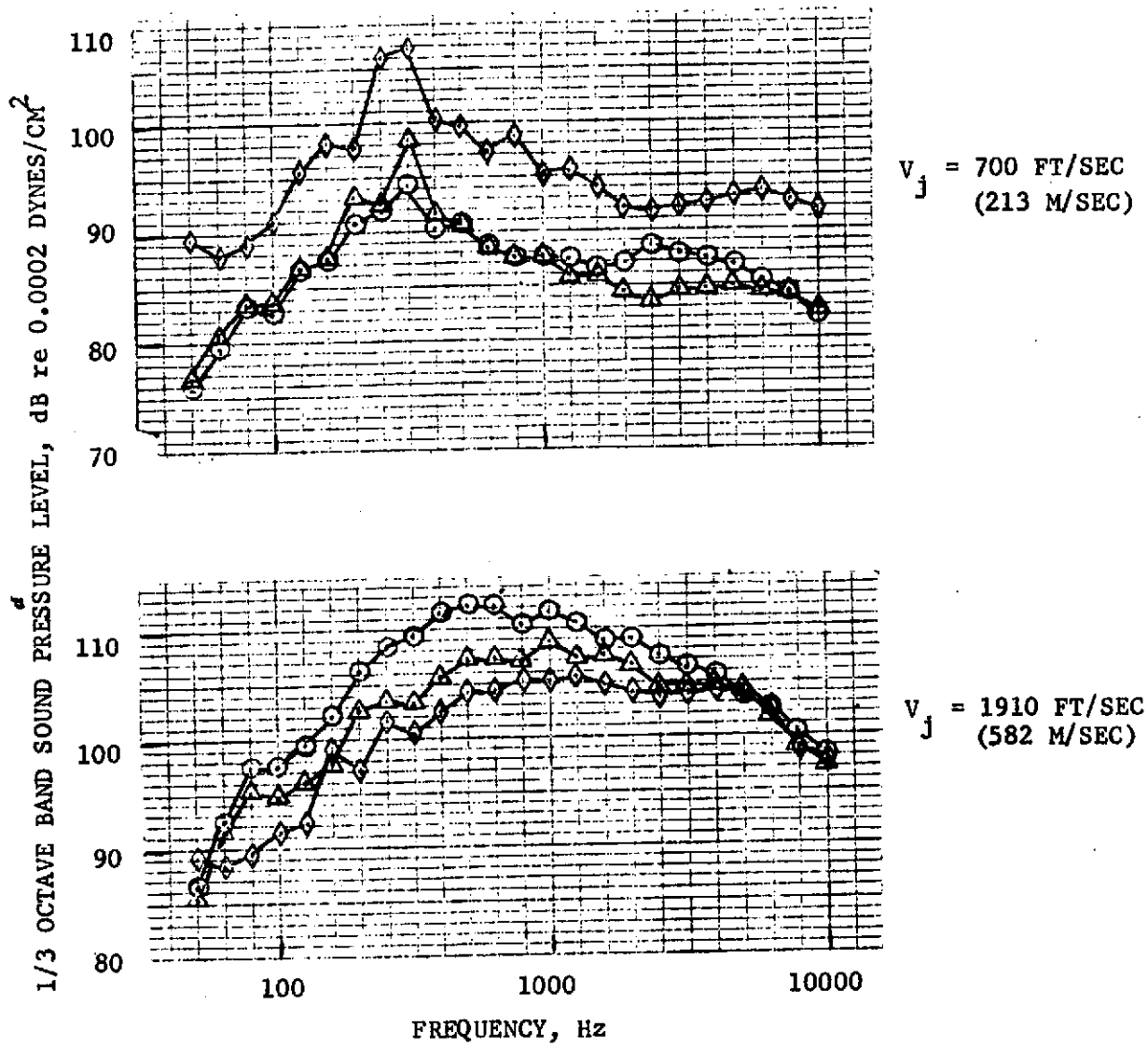

- CONICAL EJECTOR NOZZLE
- 59°F, 70% REL. HUM.
- 100 FT. ARC (30.5 M)
- θ_I = 120°

○ 20 FT. HIGH FARFIELD (6.1 M)
△ 18 FT. NEARFIELD (5.49 M)
◊ 13 FT. NEARFIELD (3.96 M)

FIGURE 10.19 - ISOLATED NACELLE OUTDOOR STATIC TEST, FARFIELD/NEAR FIELD COMPARISON, 1/3 OCTAVE BAND SPECTRA, CONICAL EJECTOR NOZZLE

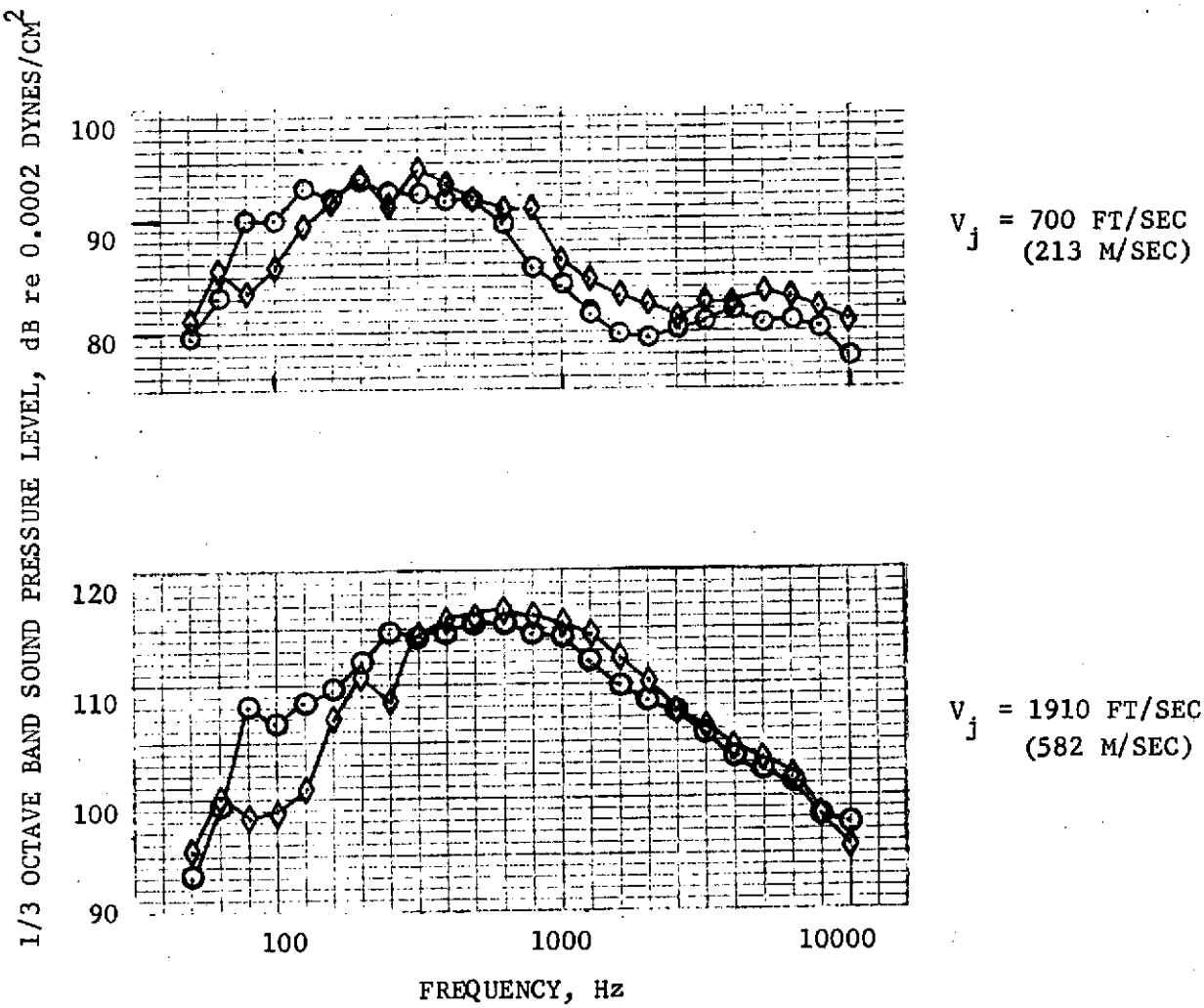

- CONICAL EJECTOR NOZZLE
- 59°F, 70% REL. HUM.
- 100 FT. ARC (30.5 M)
- $\theta_I = 140°$

○ 20 FT. HIGH FARFIELD (6.1 M)
△ 18 FT. NEARFIELD (5.49 M)
◇ 13 FT. NEARFIELD (3.96 M)

FIGURE 10.20 - ISOLATED NACELLE OUTDOOR STATIC TEST, FARFIELD/NEAR FIELD COMPARISON, 1/3 OCTAVE BAND SPECTRA, CONICAL EJECTOR NOZZLE

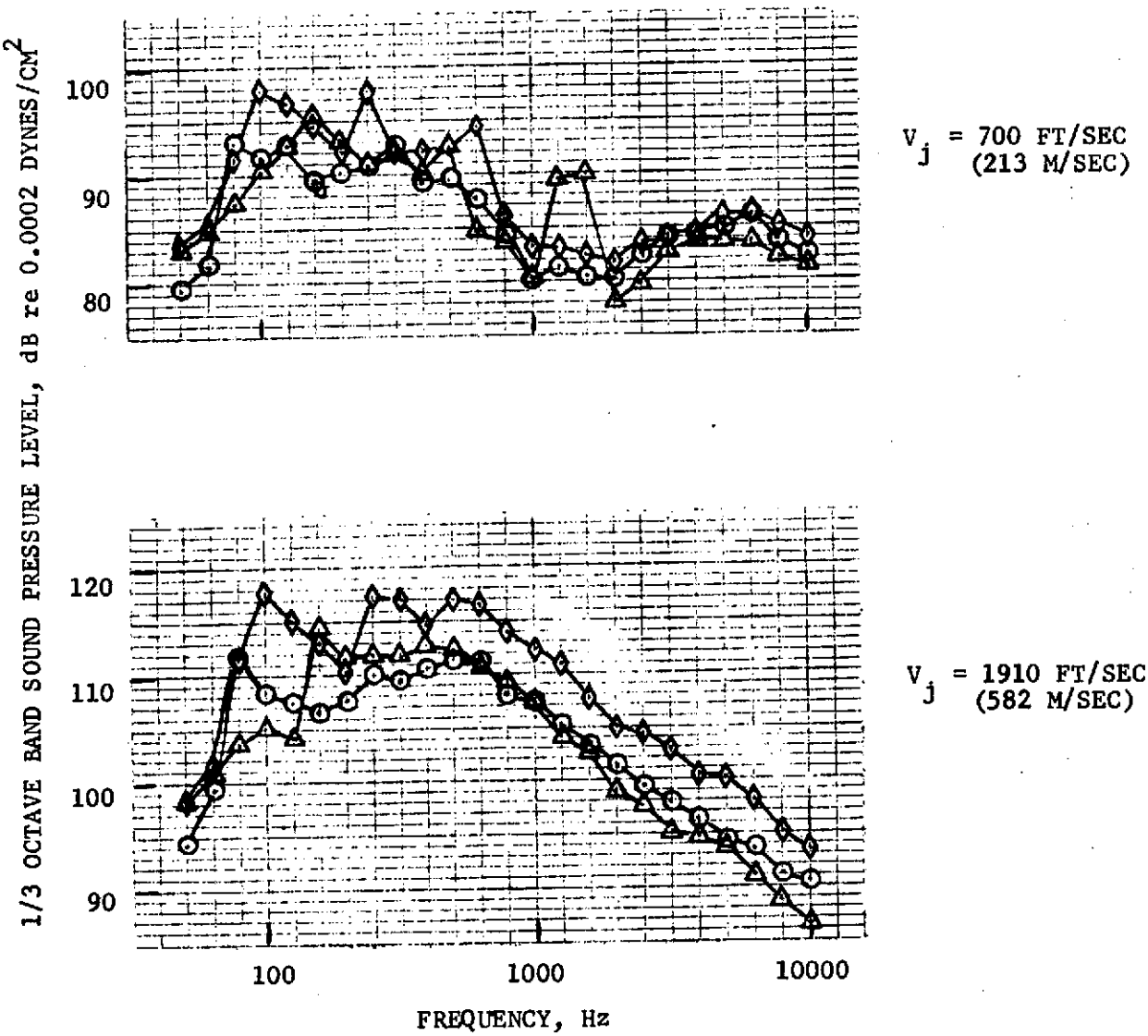

FIGURE 10.21 - ISOLATED NACELLE OUTDOOR STATIC TEST, FARFIELD/NEAR FIELD COMPARISON, 1/3 OCTAVE BAND SPECTRA, CONICAL EJECTOR NOZZLE

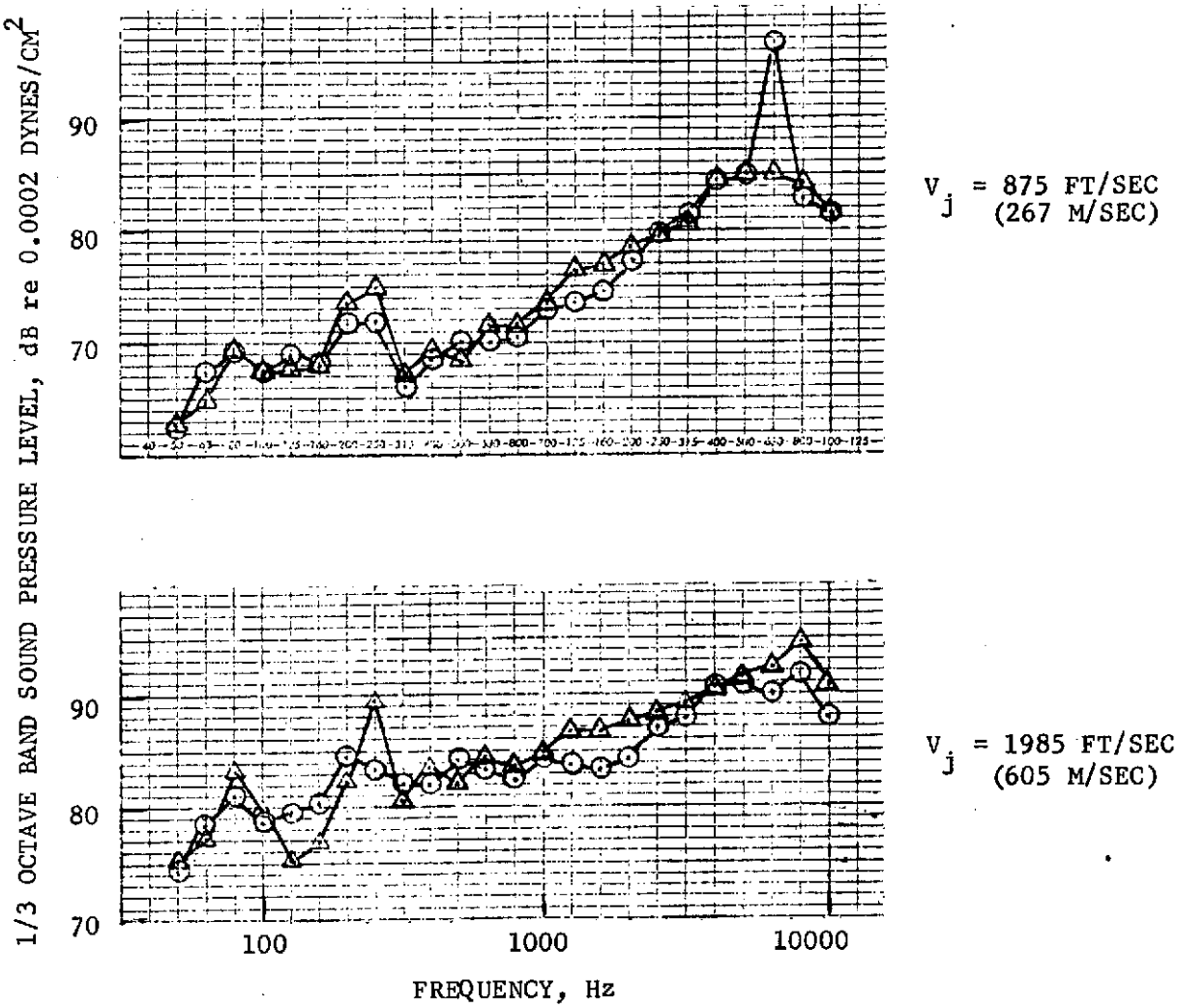

- 104 TUBE NOZZLE W/O SHROUD
- 59°F, 70% REL. HUM.
- 100 FT. ARC (30.5 M)
- θ_I = 40°

○ 20 FT. HIGH FARFIELD (6.1 M)
△ 18 FT. NEARFIELD (5.49 M)
◇ 13 FT. NEARFIELD (3.96 M)

FIGURE 10.22 - ISOLATED NACELLE OUTDOOR STATIC TEST, FARFIELD/NEAR FIELD COMPARISON, 1/3 OCTAVE BAND SPECTRA, 104-TUBE NOZZLE W/O SHROUD

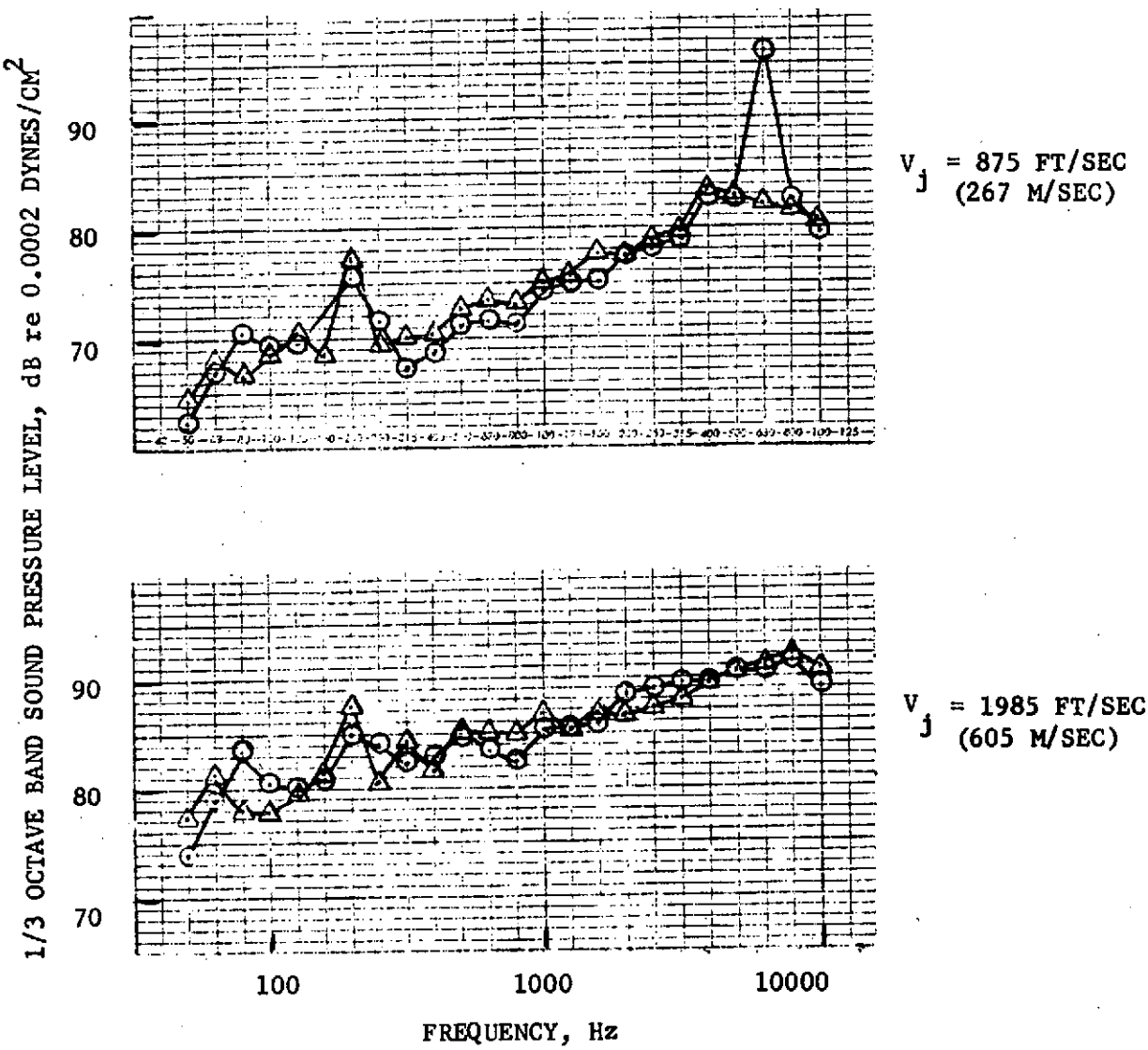

- 104 TUBE NOZZLE W/O SHROUD
- 59°F, 70% REL. HUM.
- 100 FT. ARC (30.5 M)
- θ_I = 60°

○ 20 FT. HIGH FARFIELD (6.1 M)
△ 18 FT. NEARFIELD (5.49 M)
◊ 13 FT. NEARFIELD (3.96 M)

FIGURE 10.23 - ISOLATED NACELLE OUTDOOR STATIC TEST, FARFIELD/NEAR FIELD COMPARISON, 1/3 OCTAVE BAND SPECTRA, 104-TUBE NOZZLE W/O SHROUD

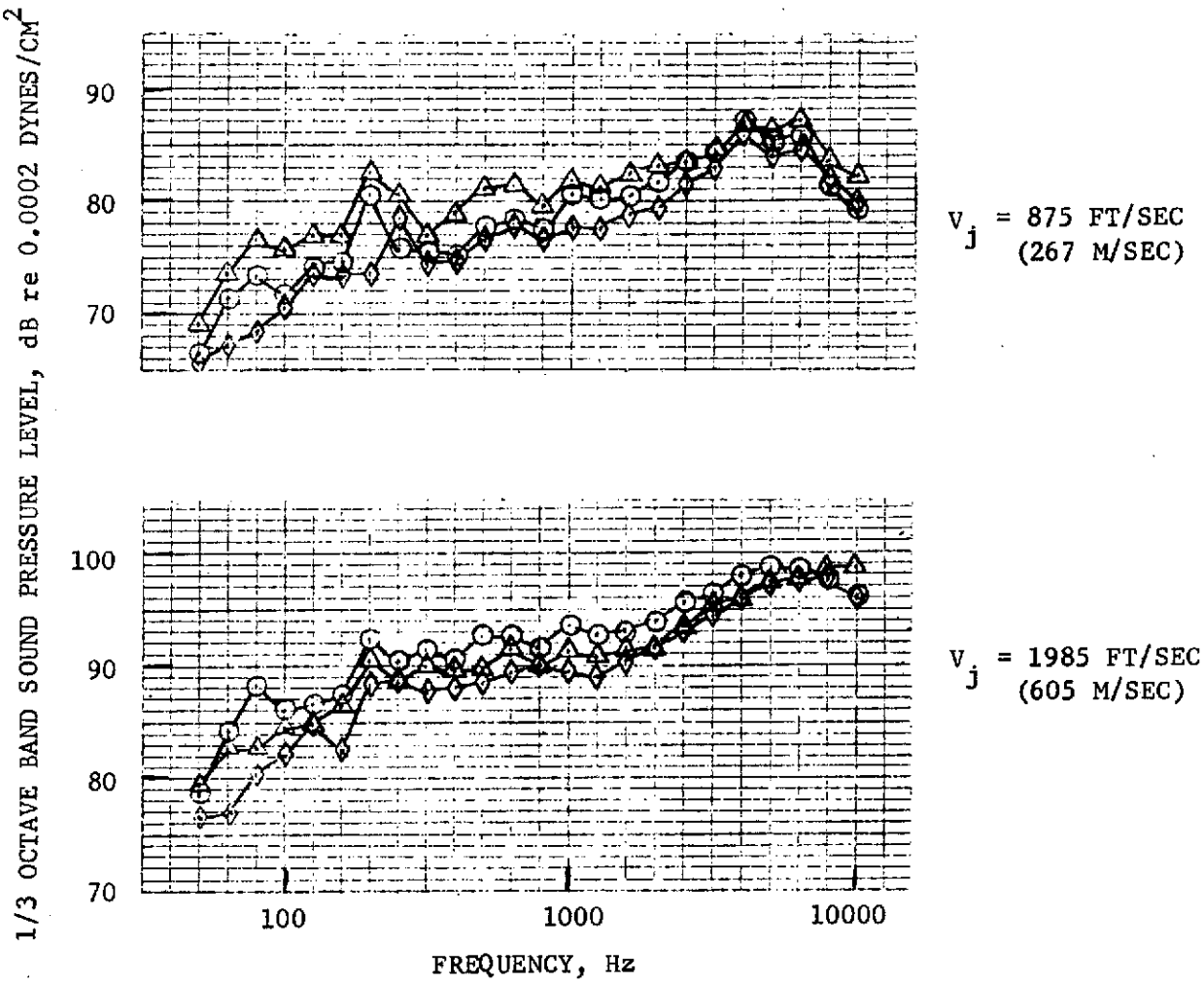

- 104 TUBE NOZZLE W/O SHROUD
- 59°F, 70% REL. HUM.
- 100 FT. ARC (30.5 M)
- θ_I = 100°

○ 20 FT. HIGH FARFIELD (6.1 M)
△ 18 FT. NEARFIELD (5.49 M)
◇ 13 FT. NEARFIELD (3.96 M)

FIGURE 10.24 - ISOLATED NACELLE OUTDOOR STATIC TEST, FARFIELD/NEAR FIELD COMPARISON, 1/3 OCTAVE BAND SPECTRA, 104-TUBE NOZZLE W/O SHROUD

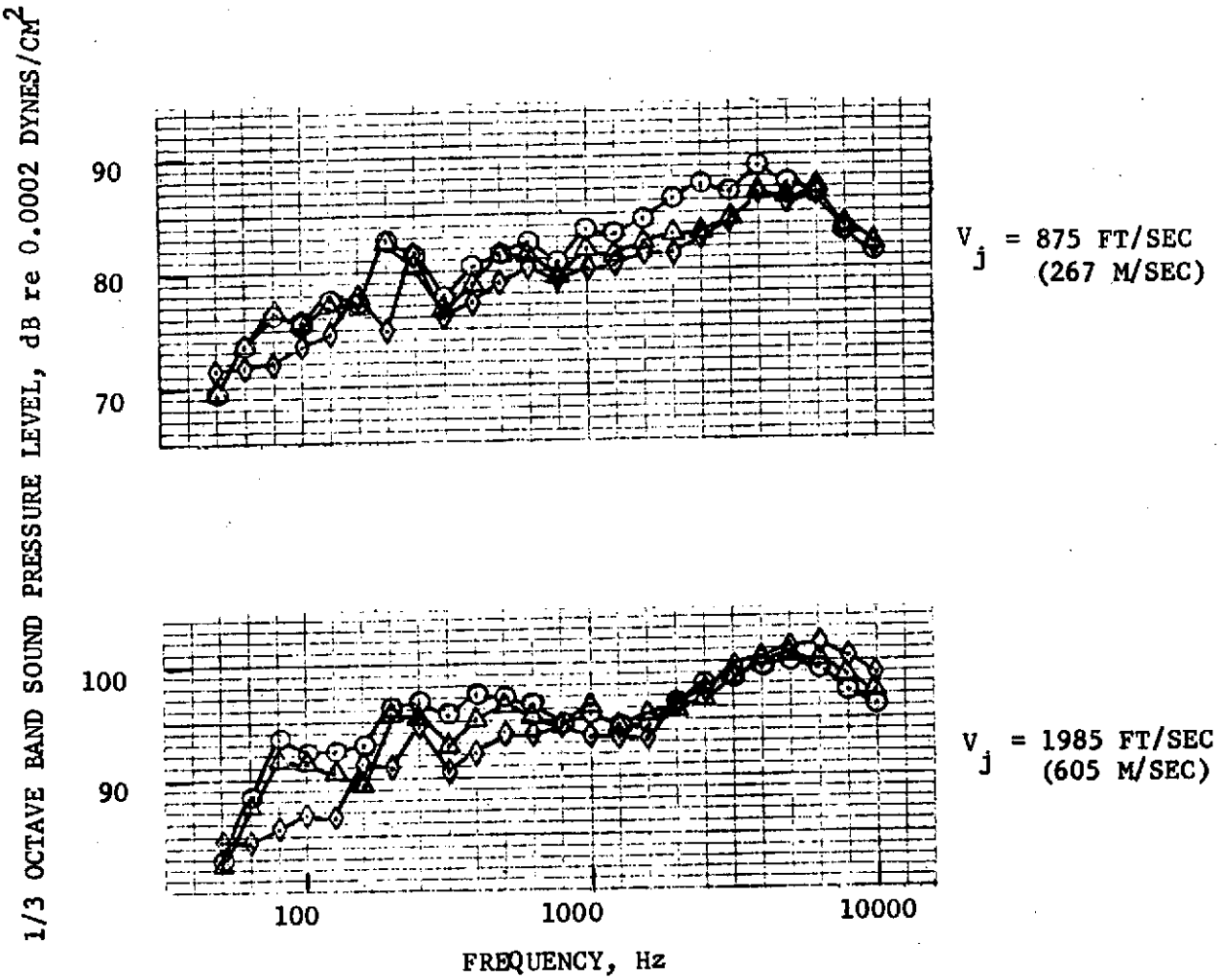

- 104 TUBE NOZZLE W/O SHROUD
- 59°F, 70% REL. HUM.
- 100 FT. ARC (30.5 M)
- θ_I = 120°

○ 20 FT. HIGH FARFIELD (6.1 M)
△ 18 FT. NEARFIELD (5.49 M)
◊ 13 FT. NEARFIELD (3.96 M)

FIGURE 10.25 - ISOLATED NACELLE OUTDOOR STATIC TEST, FARFIELD/NEAR FIELD COMPARISON, 1/3 OCTAVE BAND SPECTRA, 104-TUBE NOZZLE W/O SHROUD

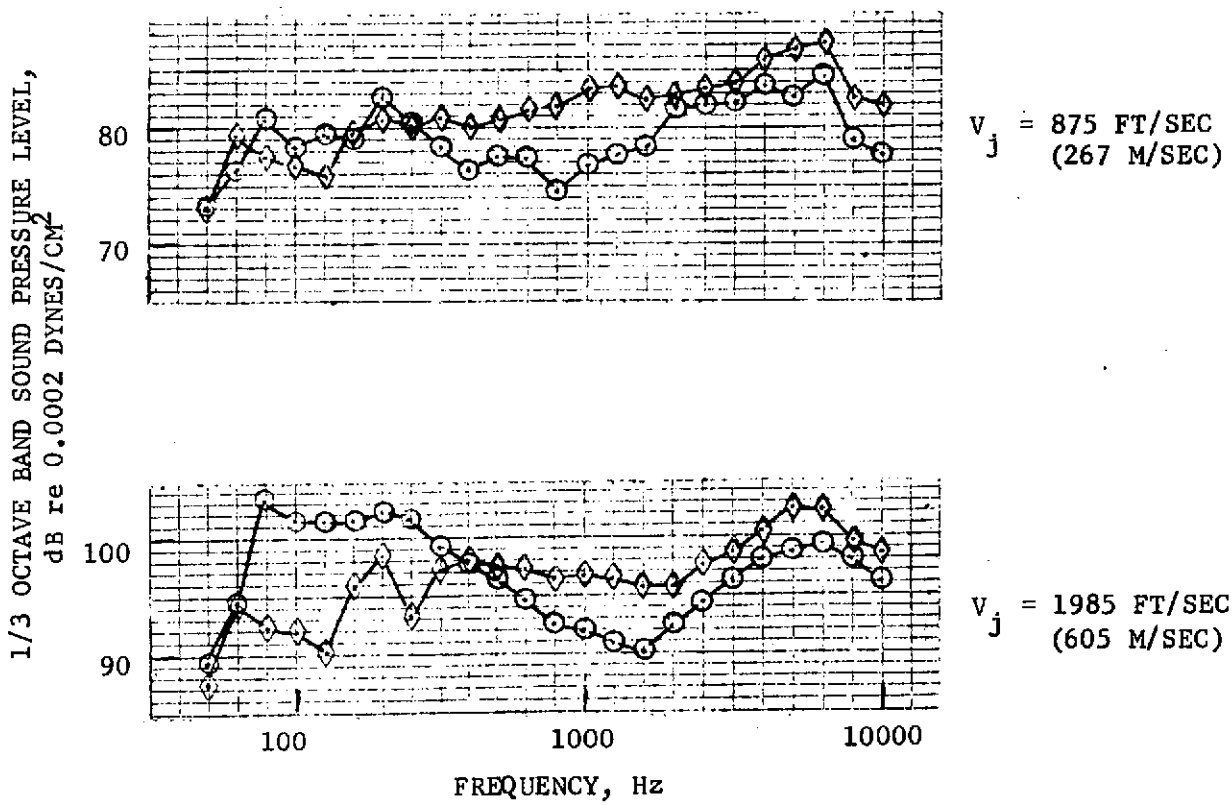

- 104 TUBE NOZZLE W/O SHROUD
- 59°F, 70% REL. HUM.
- 100 FT. ARC (30.5 M)
- θ_I = 140°

○ 20 FT. HIGH FARFIELD (6.1 M)
△ 18 FT. NEARFIELD (5.49 M)
◇ 13 FT. NEARFIELD (3.96 M)

FIGURE 10.26 - ISOLATED NACELLE OUTDOOR STATIC TEST, FARFIELD/NEAR FIELD COMPARISON, 1/3 OCTAVE BAND SPECTRA, 104-TUBE NOZZLE W/O SHROUD

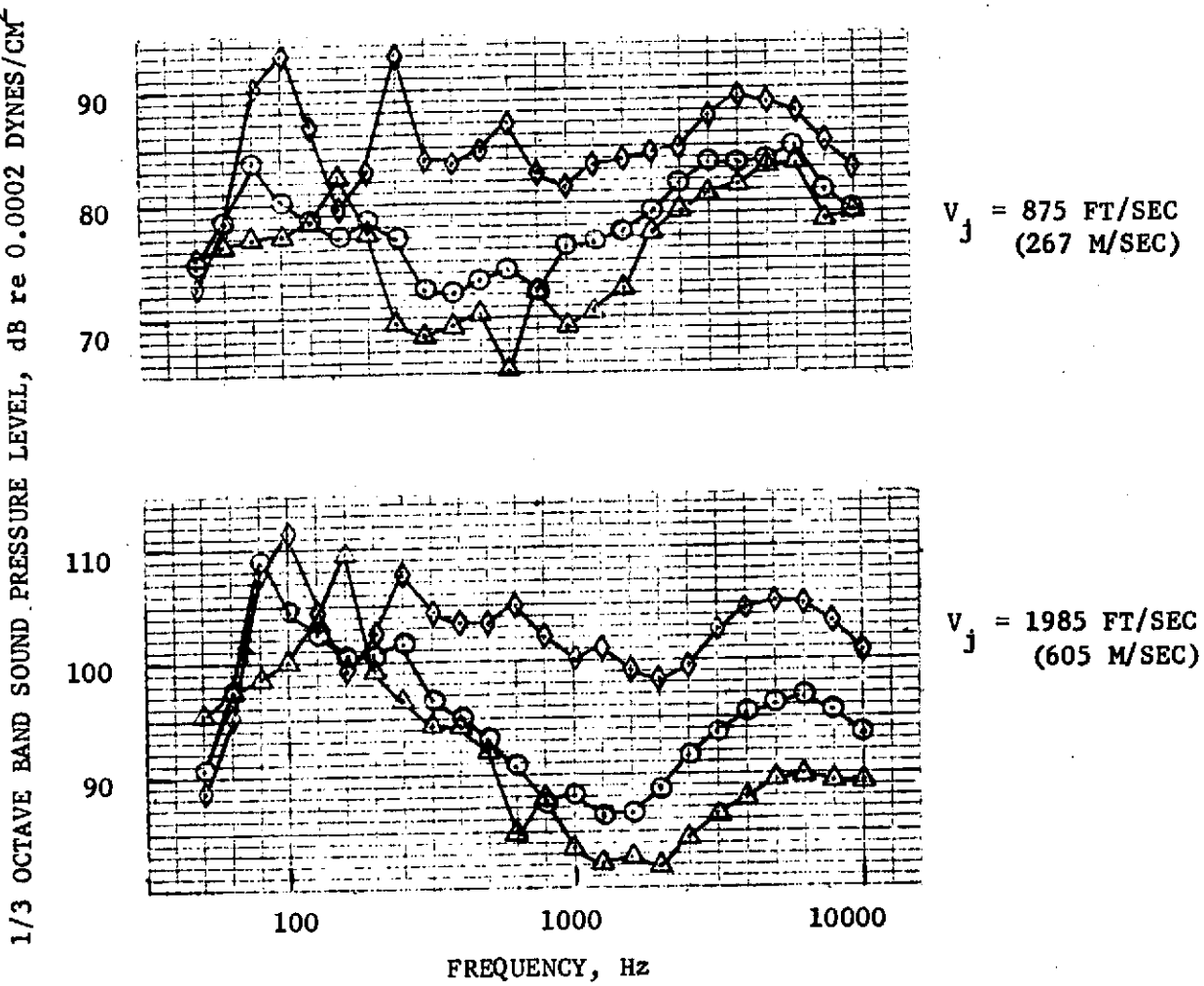

- 104 TUBE NOZZLE W/O SHROUD
- 59°F, 70% REL. HUM.
- 100 FT. ARC (30.5 M)
- θ_I = 160°

○ 20 FT. HIGH FARFIELD (6.1 M)
△ 18 FT. NEARFIELD (5.49 M)
◊ 13 FT. NEARFIELD (3.96 M)

FIGURE 10.27 - ISOLATED NACELLE OUTDOOR STATIC TEST, FARFIELD/NEAR FIELD COMPARISON, 1/3 OCTAVE BAND SPECTRA, 104-TUBE NOZZLE W/O SHROUD

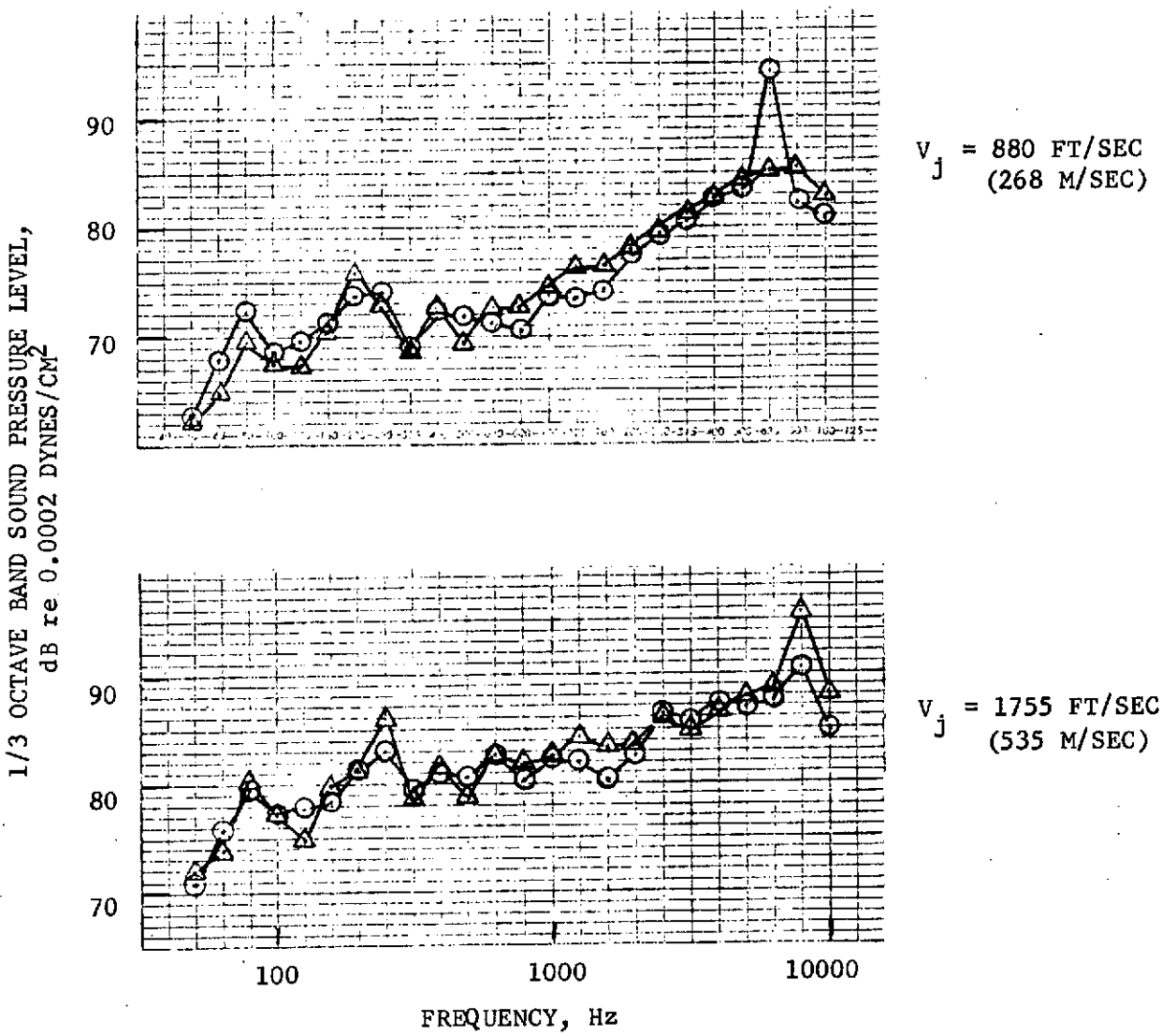

- 104 TUBE NOZZLE W/SHROUD
- 59°F, 70% REL. HUM.
- 100 FT. ARC (30.5 M)
- θ_I = 40°

⊙ 20 FT. HIGH FARFIELD (6.1 M)
△ 18 FT. NEARFIELD (5.49 M)
◊ 13 FT. NEARFIELD (3.96 M)

FIGURE 10.28 - ISOLATED NACELLE OUTDOOR STATIC TEST, FARFIELD/NEAR FIELD COMPARISON, 1/3 OCTAVE BAND SPECTRA, 104-TUBE NOZZLE WITH SHROUD

C-7

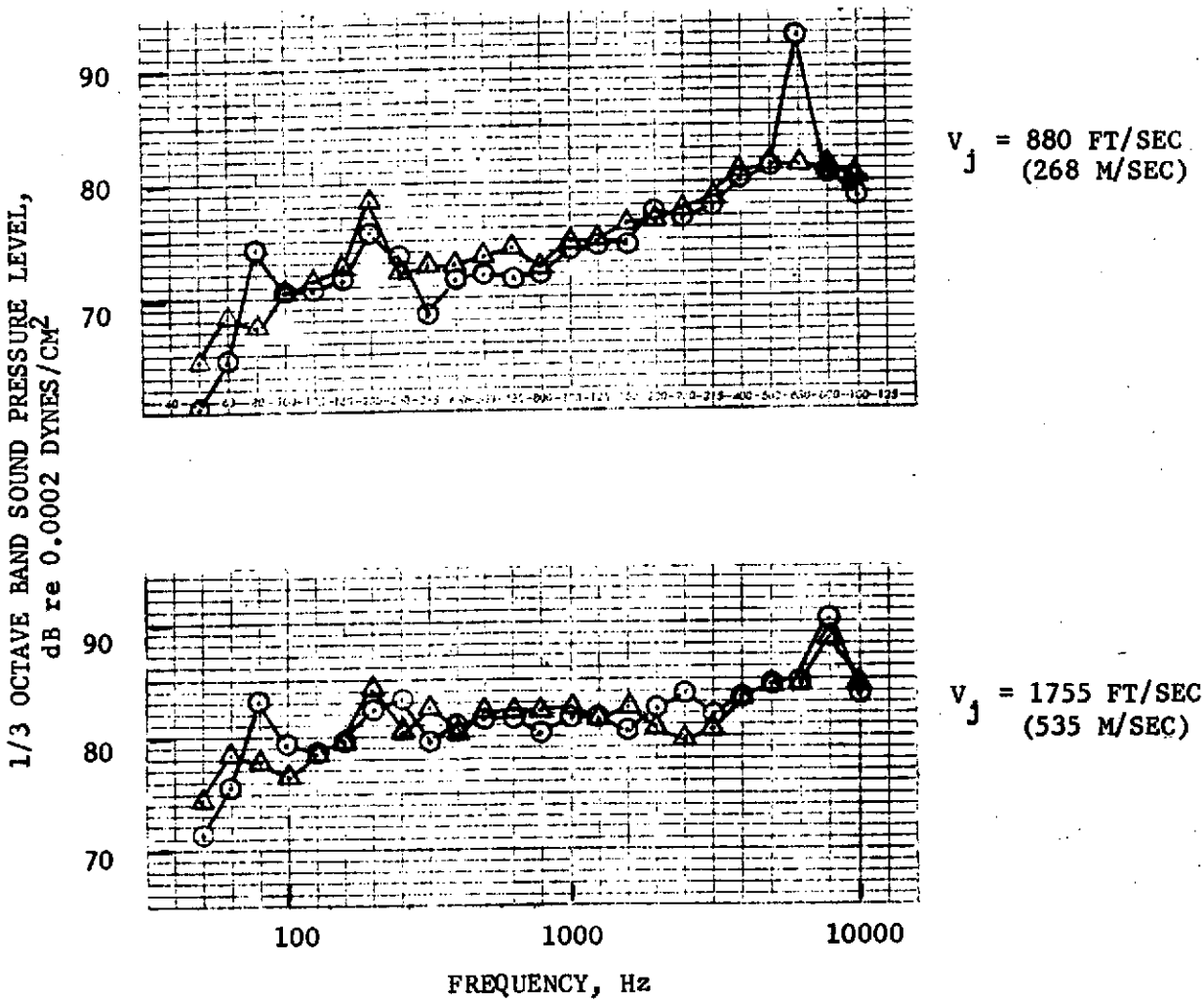

- 104 TUBE NOZZLE W/SHROUD
- 59°F, 70% REL. HUM.
- 100 FT. ARC (30.5 M)
- θ_I = 60°

○ 20 FT° HIGH FARFIELD (6.1 M)
△ 18 FT. NEARFIELD (5.49 M)
◊ 13 FT. NEARFIELD (3.96 M)

FIGURE 10.29 - ISOLATED NACELLE OUTDOOR STATIC TEST, FARFIELD/NEAR FIELD COMPARISON, 1/3 OCTAVE BAND SPECTRA, 104-TUBE NOZZLE WITH SHROUD

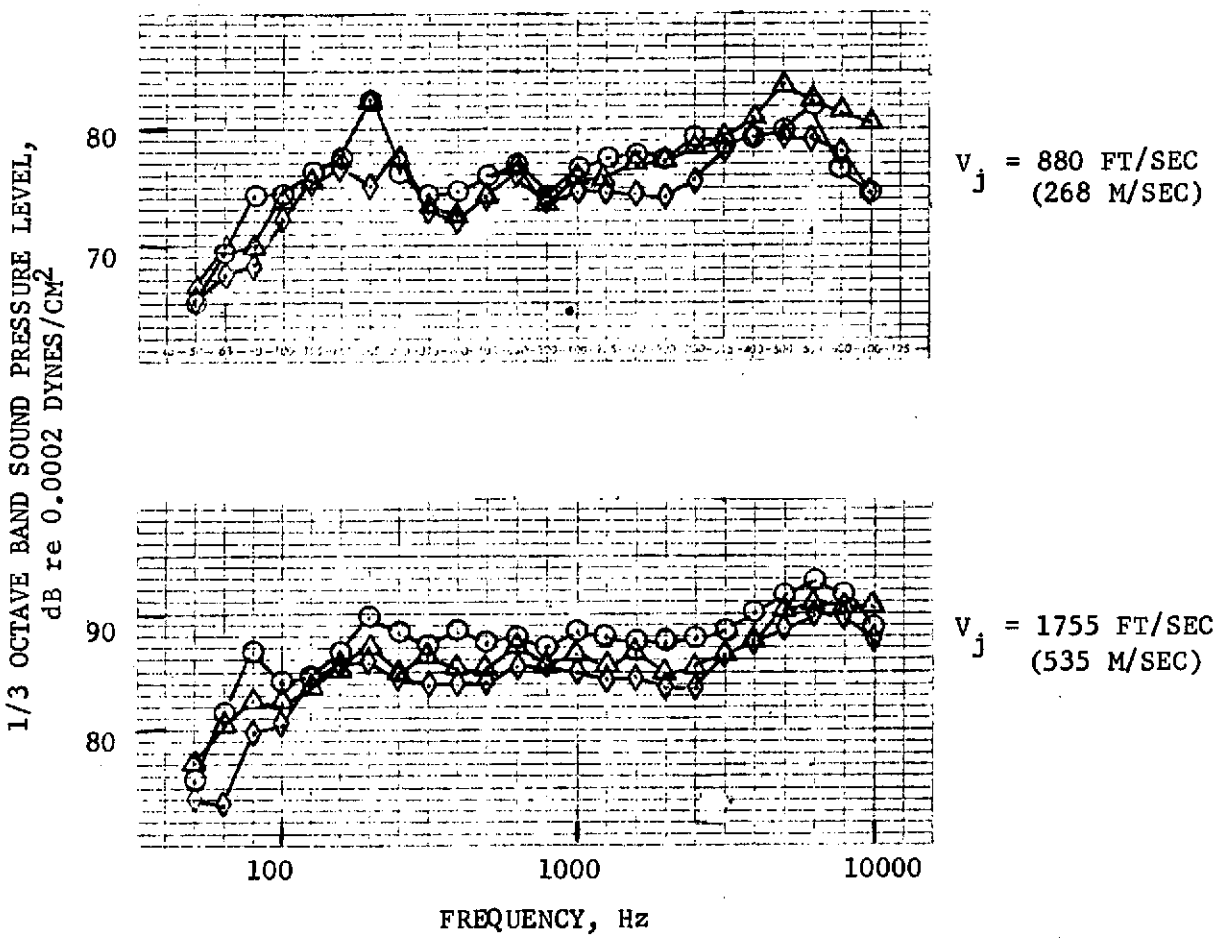

- 104 TUBE NOZZLE W/SHROUD
- 59°F, 70% REL. HUM.
- 100 FT. ARC (30.5 M)
- θ_I = 100°

○ 20 FT. HIGH FARFIELD (6.1 M)
△ 18 FT. NEARFIELD (5.49 M)
◊ 13 FT. NEARFIELD (3.96 M)

FIGURE 10.30 - ISOLATED NACELLE OUTDOOR STATIC TEST, FARFIELD/NEAR FIELD COMPARISON, 1/3 OCTAVE BAND SPECTRA, 104-TUBE NOZZLE WITH SHROUD

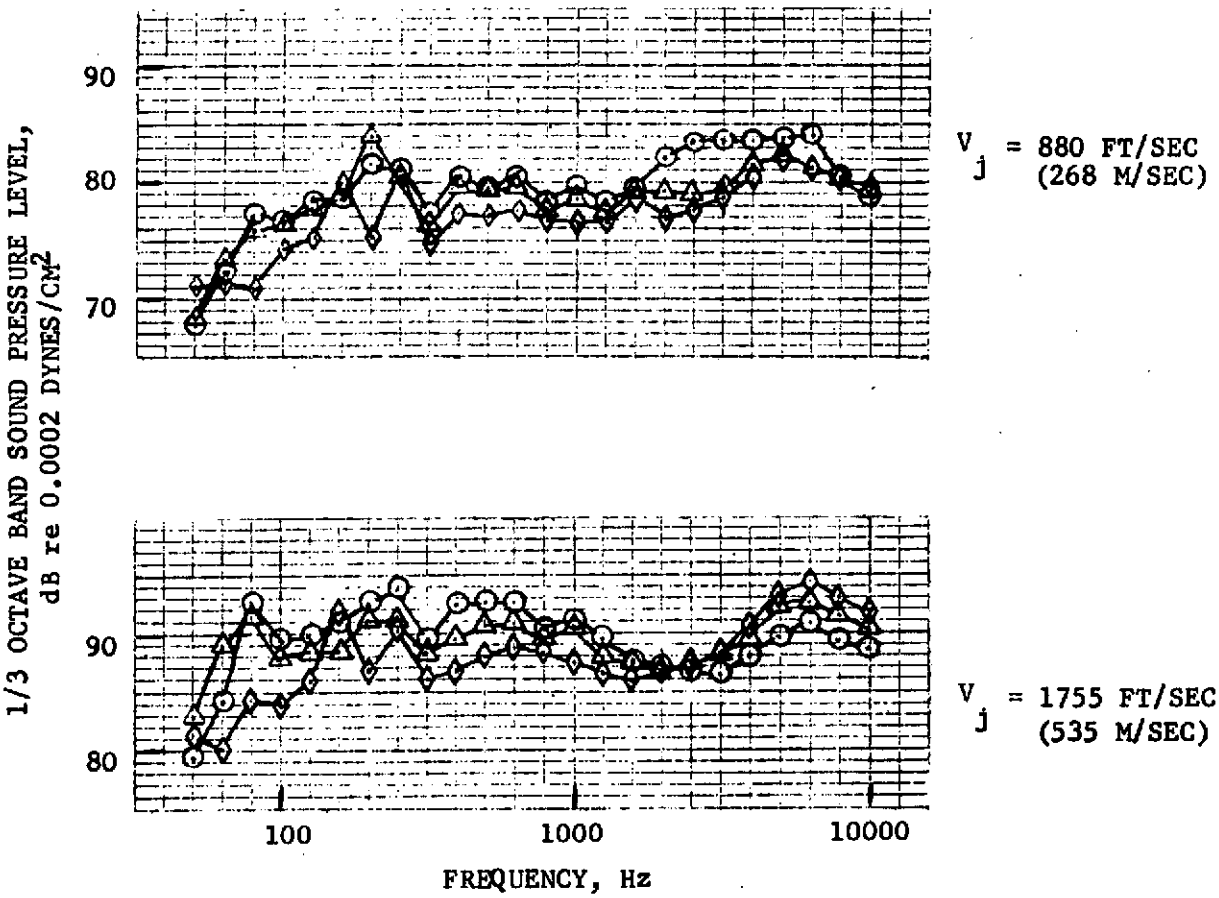

- 104 TUBE NOZZLE W/SHROUD
- 59°F, 70% REL. HUM.
- 100 FT. ARC (30.5 M)
- θ_I = 120°

○ 20 FT. HIGH FARFIELD (6.1 M)
△ 18 FT. NEARFIELD (5.49 M)
◊ 13 FT. NEARFIELD (3.96 M)

FIGURE 10.31 - ISOLATED NACELLE OUTDOOR STATIC TEST, FARFIELD/NEAR FIELD COMPARISON, 1/3 OCTAVE BAND SPECTRA, 104-TUBE NOZZLE WITH SHROUD

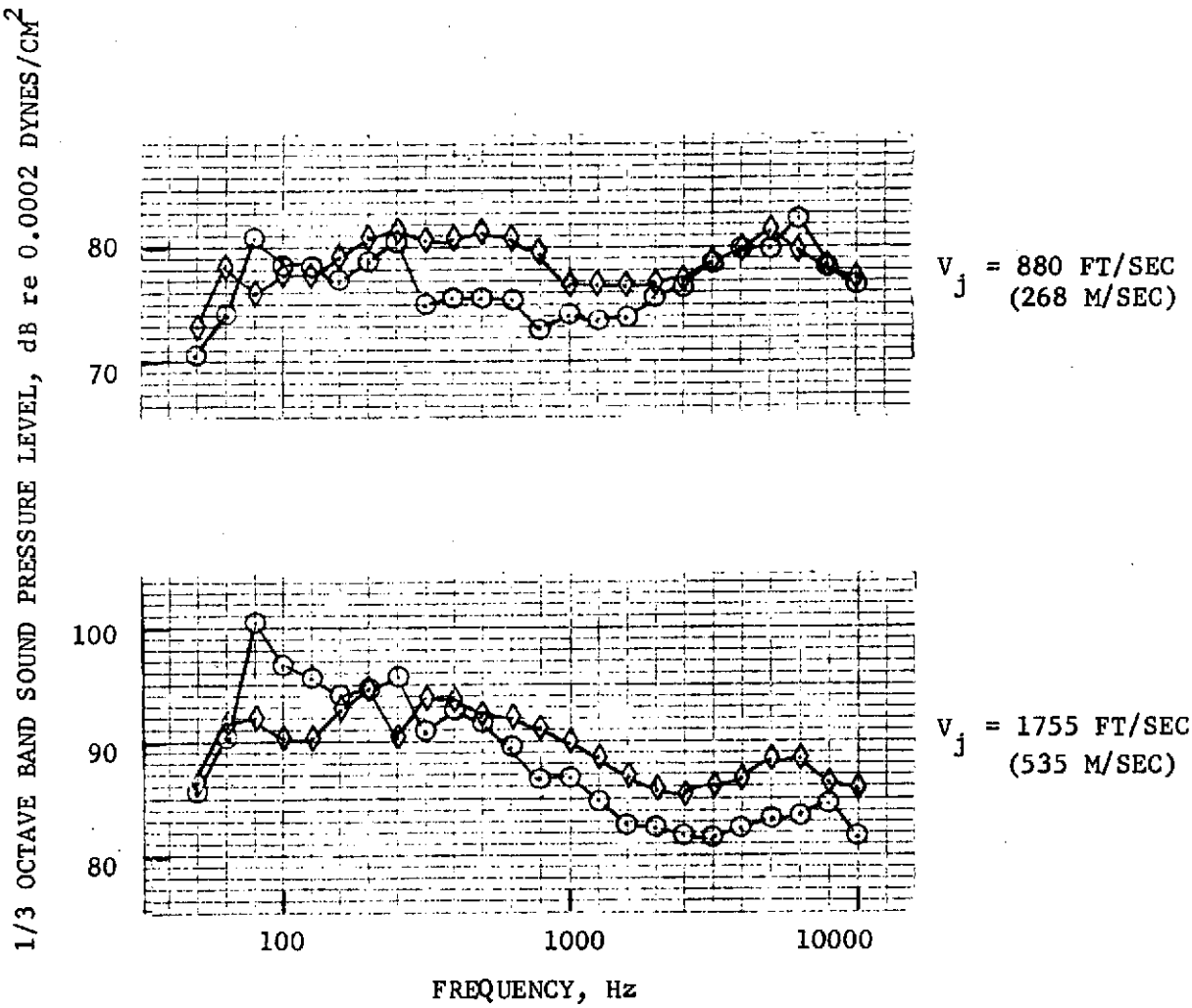

- 104 TUBE NOZZLE W/SHROUD
- 59°F, 70% REL. HUM.
- 100 FT. ARC (30.5 M)
- $\theta_I = 140°$

○ 20 FT. HIGH FARFIELD (6.1 M)
△ 18 FT. NEARFIELD (5.49 M)
◊ 13 FT. NEARFIELD (3.96 M)

FIGURE 10.32 - ISOLATED NACELLE OUTDOOR STATIC TEST, FARFIELD/NEAR FIELD COMPARISON, 1/3 OCTAVE BAND SPECTRA, 104-TUBE NOZZLE WITH SHROUD

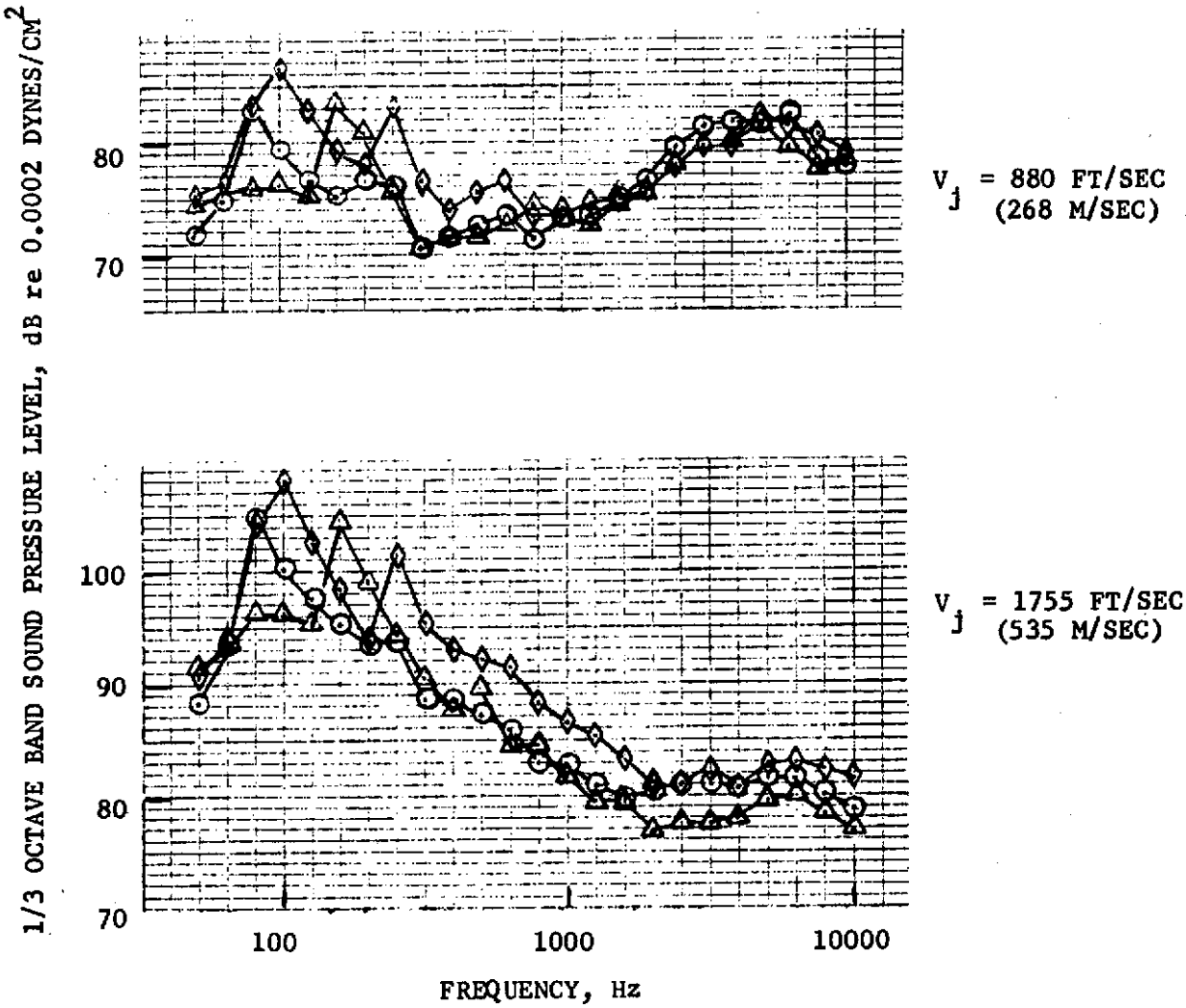

- 104 TUBE NOZZLE W/SHROUD
- 59°F, 70% REL. HUM.
- 100 FT. ARC (30.5 M)
- θ_I = 160°

○ 20 FT. HIGH FARFIELD (6.1 M)
△ 18 FT. NEARFIELD (5.49 M)
◇ 13 FT. NEARFIELD (3.96 M)

FIGURE 10.33 - ISOLATED NACELLE OUTDOOR STATIC TEST, FARFIELD/NEAR FIELD COMPARISON, 1/3 OCTAVE BAND SPECTRA, 104-TUBE NOZZLE WITH SHROUD

10.1.3 Relative Velocity Effects

10.1.3.1 Isolated Nacelle Wind Tunnel Test

The isolated nacelle wind tunnel test data were analyzed for the conical ejector and AIE nozzles. These measurements were conducted in the NASA/Ames 40 by 80 Foot Wind Tunnel. The material is presented in a manner that illustrates the effect of relative velocity on the noise signature of each nozzle. The method of presentation is to show the effect of free stream velocity on the following acoustic parameters:

- Peak OASPL at various jet velocities
- OASPL and PNL directivity patterns
- One-third octave band sound pressure spectra at several acoustic angles

All data presented in this section were corrected for background noise and reverberation effects. The procedure used to correct for reverberation effects is described in detail in Section 10.1.1. The estimates of the repeatability of the data measured in the wind tunnel are summarized in reference 10.4.

Figures 10.34 and 10.35 show graphs of peak overall sound pressure level as a function of jet velocity at different free stream velocities for the conical ejector and AIE nozzles. These peak overall sound pressure levels occurred at acoustic angles of 130-150 degrees, reference to inlet. A summary of the results for the two sidelines at two jet velocities is presented below:

	5.49 M (18 Ft) Sideline Data			3.96 M (13 Ft) Sideline Data		
			V_j = 610 M/sec (2000 Ft/sec)			
V_o MPS,FPS	Peak OASPL CON	AIE	ΔdB Suppression*	Peak OASPL CON	AIE	ΔdB Suppression*
0,0	136	134	2	141	140	1
46,150	132	134	-2	137	138	-1
76,250	128	132	-4	134	136	-2
104,340	128	129	-1	135	135	0
			V_j = 396 M/Sec (396 Ft/Sec)			
0,0	126	123	3	130	128	2
46,150	122	121	1	126	126	0
76,250	117	119	-2	124	125	-1
104,340	115	116	-1	122	123	-1

*Suppression of AIE nozzle relative to conical ejector nozzle

From the above table it can be seen that the AIE nozzle provides some noise reduction during static operation (wind off). Generally, when external flow is present (relative velocity effect), the AIE nozzle increases the noise level relative to the conical ejector nozzle. It is also evident from the above table that the 5.49 and 3.96 meter (18 and 13 foot) sidelines give generally the same trend in noise level differences for the two different jet velocities.

Presented on Figures 10.36 through 10.47 are the directivity patterns for each of the configurations on the basis of OASPL and PNL. Because of background noise contamination at select cases of low jet velocity and high free stream velocity, only a limited portion of the spectra is defined. Due to this problem a criteria was established to define the validity of the OASPL and PNL levels that were calculated for the spectra corrected for background noise. The criteria used was that if the spectra was defined 6 dB below the peak one-third octave band sound pressure level, the calculated OASPL and PNL values were assumed to be representative and used in the anlaysis. The data presented on Figures 10.36 through 10.47 indicate several trends which may be summarized as follows:

- o OASPL and PNL levels decreased as the free stream velocity increased.

- The data at the low jet velocity of 259 m/sec (850 ft/sec) is not conclusive and this is due to contamination by turbomachinery noise.

- The noise level reduction caused by the addition of the free stream velocity was largest at the angle of peak jet noise and less at the angles in the forward noise quadrant.

To evaluate how the free stream velocity affects the suppression characteristics of the AIE nozzle relative to the conical ejector nozzle, the OASPL and PNL levels are tabulated on Tables 10.4 and 10.5 for three acoustic angles. The comparisons presented were made for data corrected to exhaust jet velocities of 376 m/sec (1235 ft/sec) and 518 m/sec (1700 ft/sec).

The comparisons indicate that the effectiveness of the AIE nozzle as a suppressor in a relative velocity environment is inconclusive with regards to the magnitude of suppression in a relative velocity field. This result may indicate that the validity of the aforementioned criteria of analysis (minimum of 6 dB between maximum and minimum SPL's - page 88) is questionable. The criteria does not take into account the required location of the SPL's in the spectra, e.g., high or low frequencies. This later observation may be particularly relevant when one considers that background noise contamination is the greatest at low frequencies. In light of the fact that PNdB is frequency biased, it is reasonable to question the above nozzle suppression analysis for low jet velocity and high free stream velocity. To assure that valid trends were being observed, a detailed analysis on the basis of 1/3 OBSPL was conducted to give more representative information of AIE nozzle suppression relative to the conical ejector nozzle.

Presented on Figures 10.48 through 10.77 are the spectra for the two nozzles at the 5.49 and 3.96 meter (18 and 13 foot) sidelines. Tabulated on Tables 10.6 and 10.7 are the 1/3 OBSPL for the two nozzles and sidelines at four acoustic angles. Also shown on the table is the amount of suppression the AIE nozzle gives relative to the conical ejector nozzle at each of the frequencies. The data presented on Tables 10.6 and 10.7 are for corrected

exhaust jet velocities of 405 and 518 meters/second (1330 and 1700 feet per second), respectively. Four representative frequencies were selected for presentation in tabular form. From studying the spectra and plots the following conclusions are relevant.

- The one-third octave band sound pressure levels generally decrease as the free stream velocity increases for each of the nozzles.
- The peak frequency of the noise spectra does not shift as the free stream velocity increases. This peak occurs in the 500 Hz to 1000 Hz range.
- The general trend supported by the data presented on Tables 10.6 and 10.7 is that the amount of suppression attributed to the AIE nozzle relative to the conical nozzle decreases as the free stream velocity increases.
- Background noise is most apparent at conditions of low jet velocity, high free stream velocity and for the 5.49 meter (18 foot) sideline microphone array.

In summary, the addition of the free stream velocity causes a definite change in the jet noise signature of both the configurations that were evaluated.

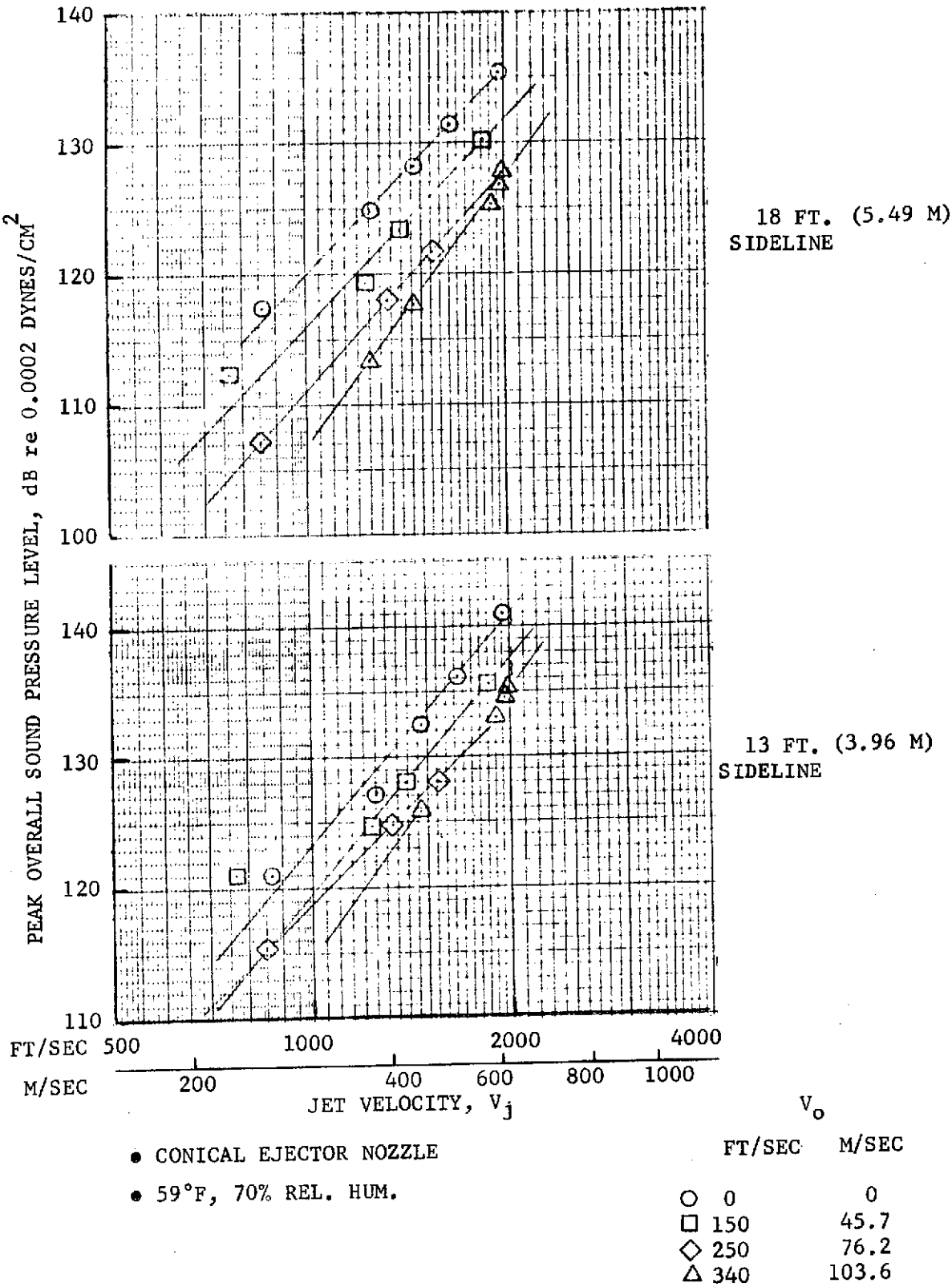

FIGURE 10.34 - ISOLATED NACELLE WIND TUNNEL TEST, PEAK OASPL VS V_J, CONICAL EJECTOR NOZZLE

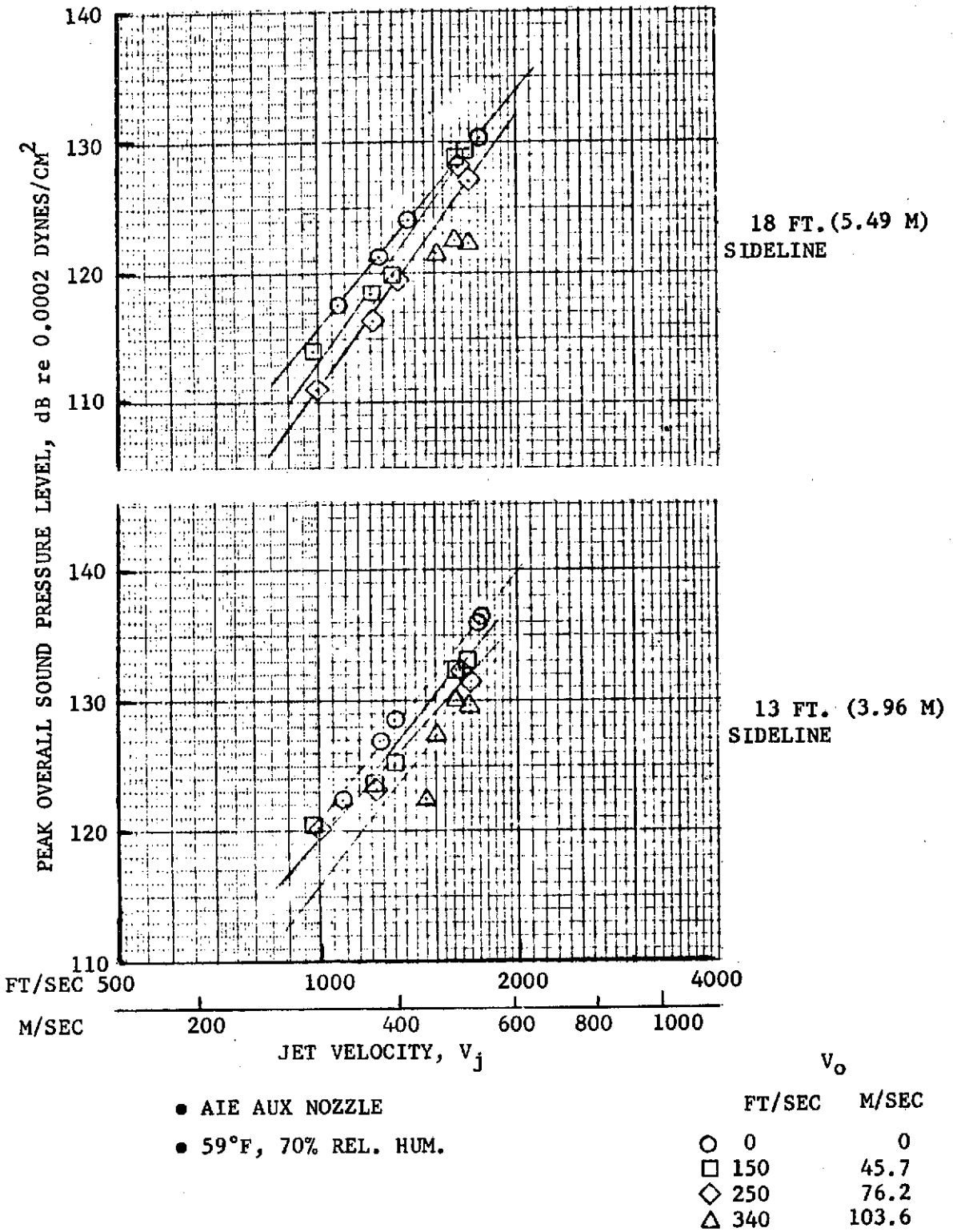

FIGURE 10.35 - ISOLATED NACELLE WIND TUNNEL TEST, PEAK OASPL VS V_J, AIE NOZZLE

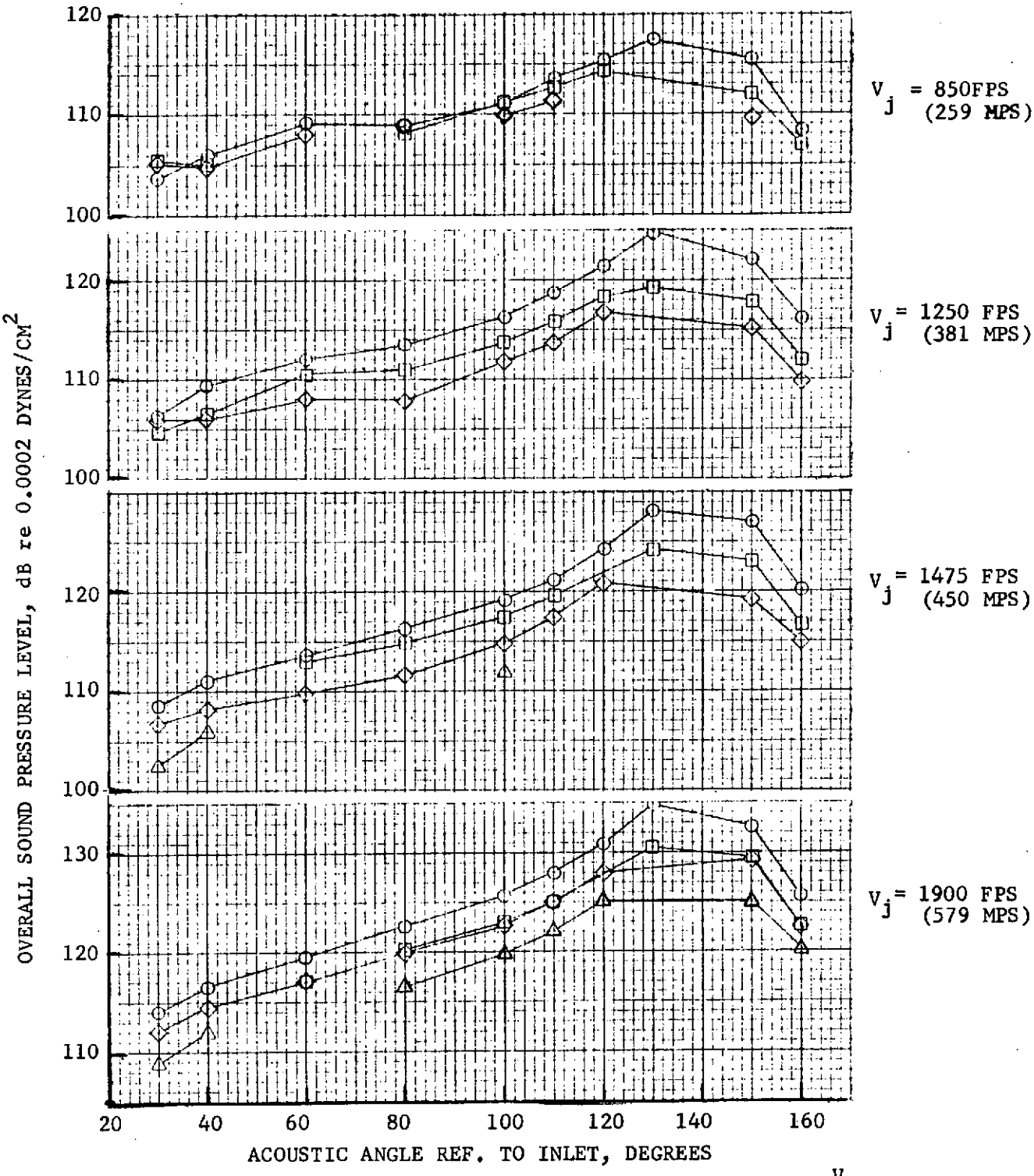

- CONICAL EJECTOR NOZZLE
- 18 FT. S.L. (5.49 M)
- 59°F, 70% REL. HUM.

FIGURE 10.36 - ISOLATED NACELLE WIND TUNNEL TEST, OASPL DIRECTIVITY, CONICAL EJECTOR NOZZLE

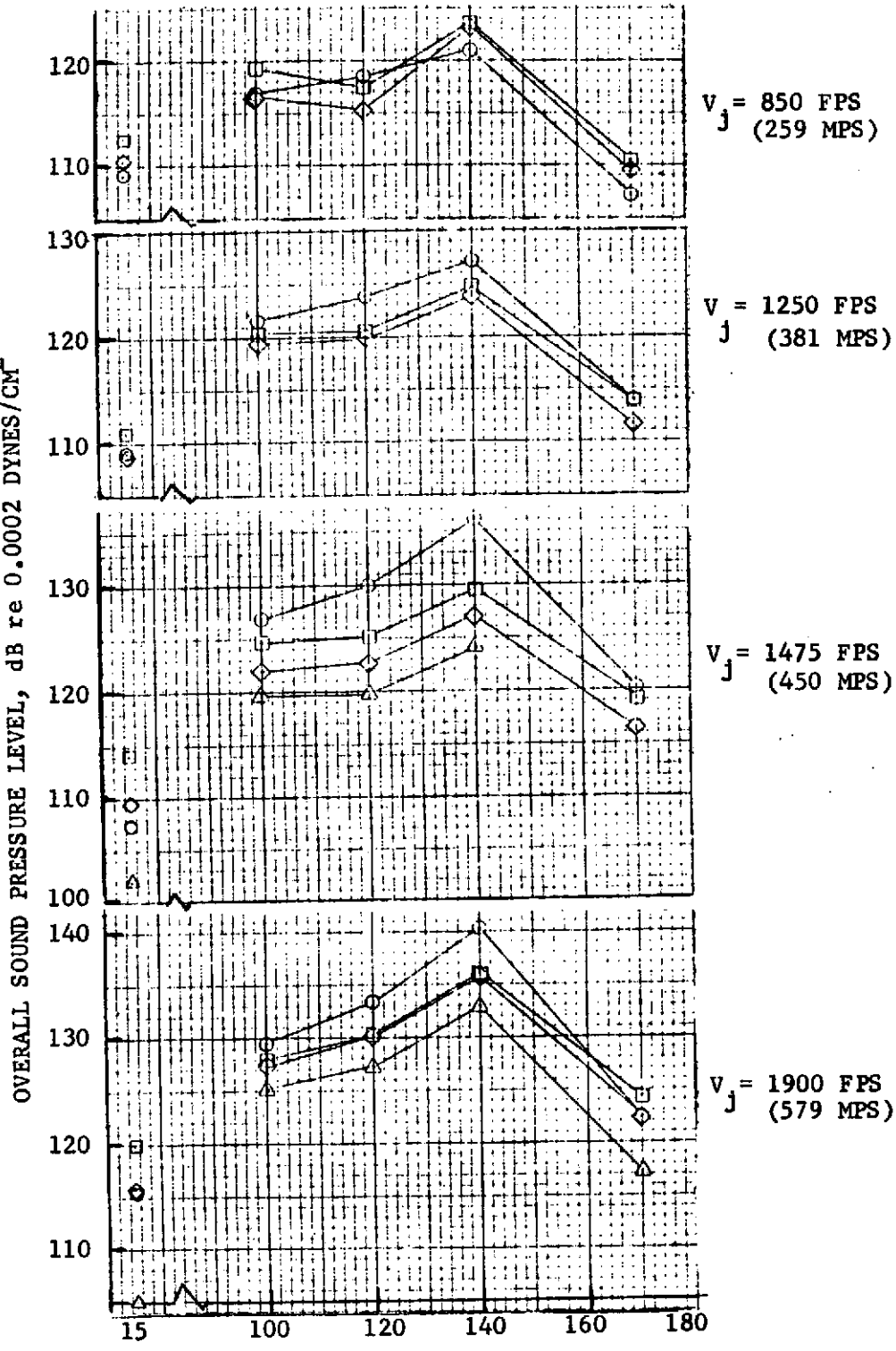

- CONICAL EJECTOR NOZZLE
- 13 FT. S.L. (3.96 M)
- 59°F, 70% REL. HUM.

V_o FT/SEC	V_o M/SEC
○ 0	0
□ 150	45.7
◇ 250	76.2
△ 340	103.6

FIGURE 10.37 - ISOLATED NACELLE WIND TUNNEL TEST, OASPL DIRECTIVITY, CONICAL EJECTOR NOZZLE

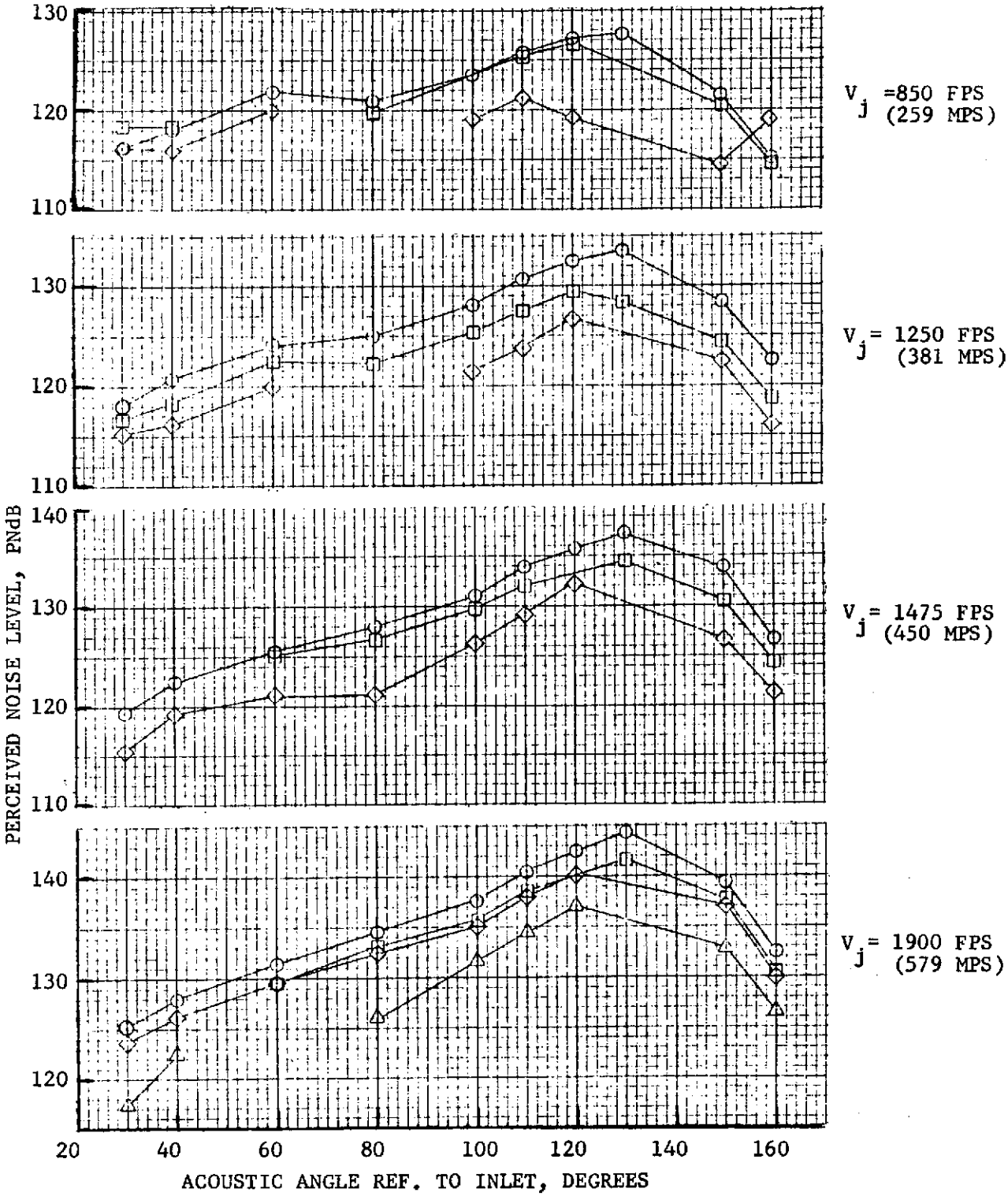

- CONICAL EJECTOR NOZZLE
- 18 FT. S.L. (5.49 M)
- 59°F, 70% REL. HUM.

	V_o FT/SEC	V_o M/SEC
○	0	0
□	150	45.7
◇	250	76.2
△	340	103.6

FIGURE 10.38 - ISOLATED NACELLE WIND TUNNEL TEST, PNdB DIRECTIVITY, CONICAL EJECTOR NOZZLE

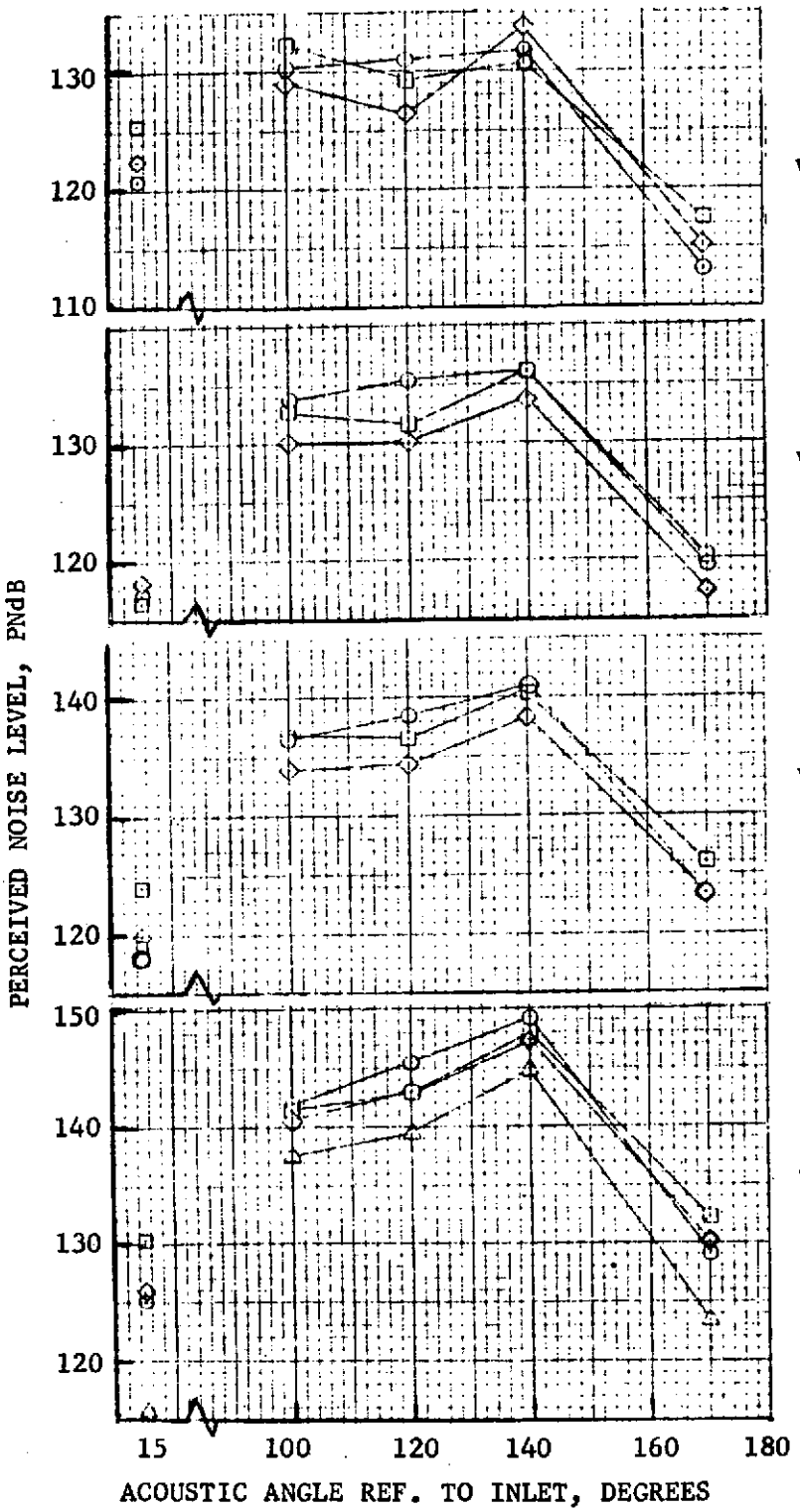

- CONICAL EJECTOR NOZZLE
- 13 FT. S.L. (3.96 M)
- 59°F, 70% REL. HUM.

V_o	FT/SEC	M/SEC
○	0	0
□	150	45.7
◇	250	76.2
△	340	103.6

FIGURE 10.39 - ISOLATED NACELLE WIND TUNNEL TEST, PNdB DIRECTIVITY, CONICAL EJECTOR NOZZLE

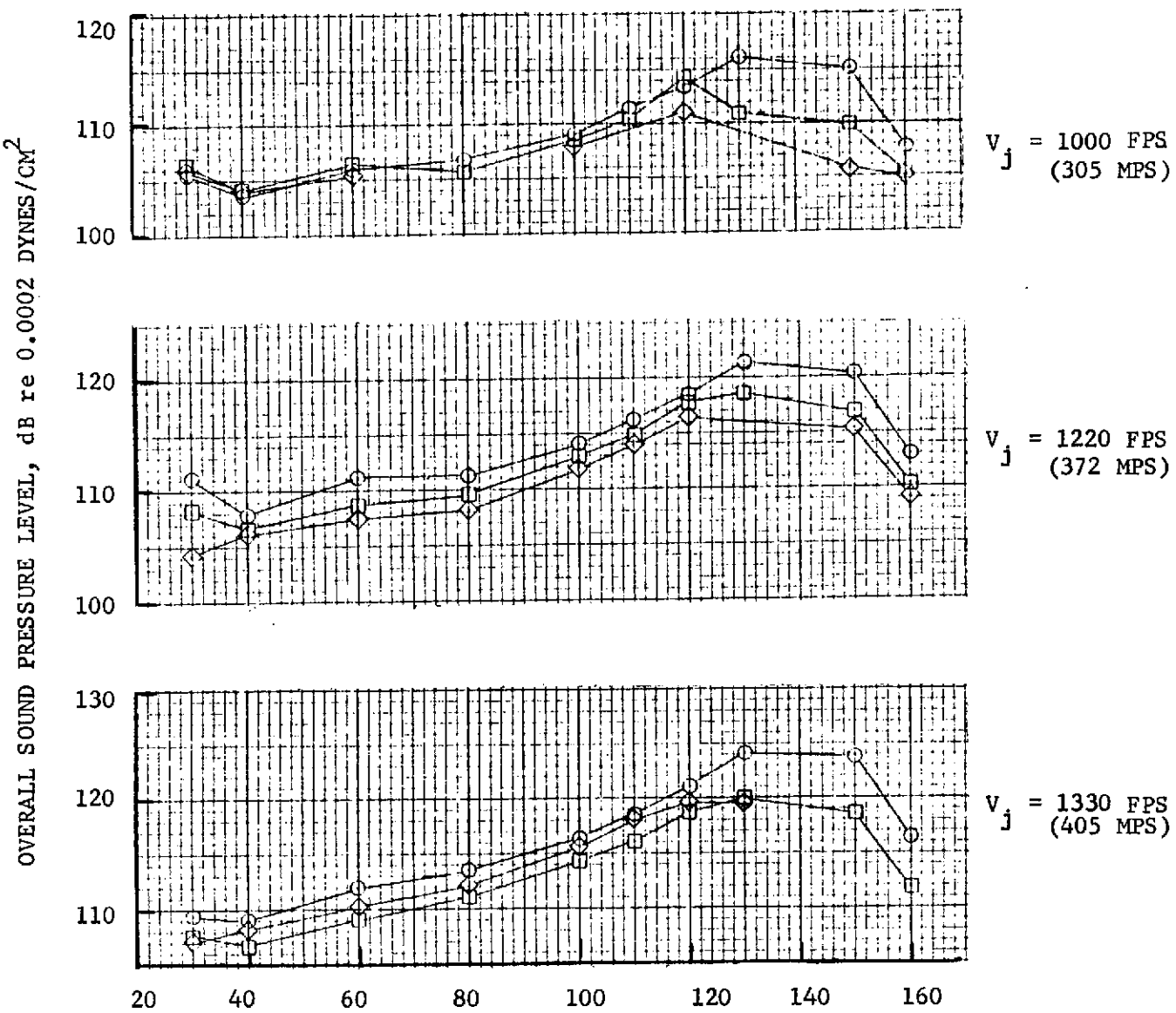

- AIE AUX NOZZLE
- 18 FT. S.L. (5.49 M)
- 59°F, 70% REL. HUM.

	V_o FT/SEC	V_o M/SEC
○	0	0
□	150	45.7
◇	250	76.2
△	340	103.6

FIGURE 10.40 - ISOLATED NACELLE WIND TUNNEL TEST, OASPL DIRECTIVITY, AIE NOZZLE

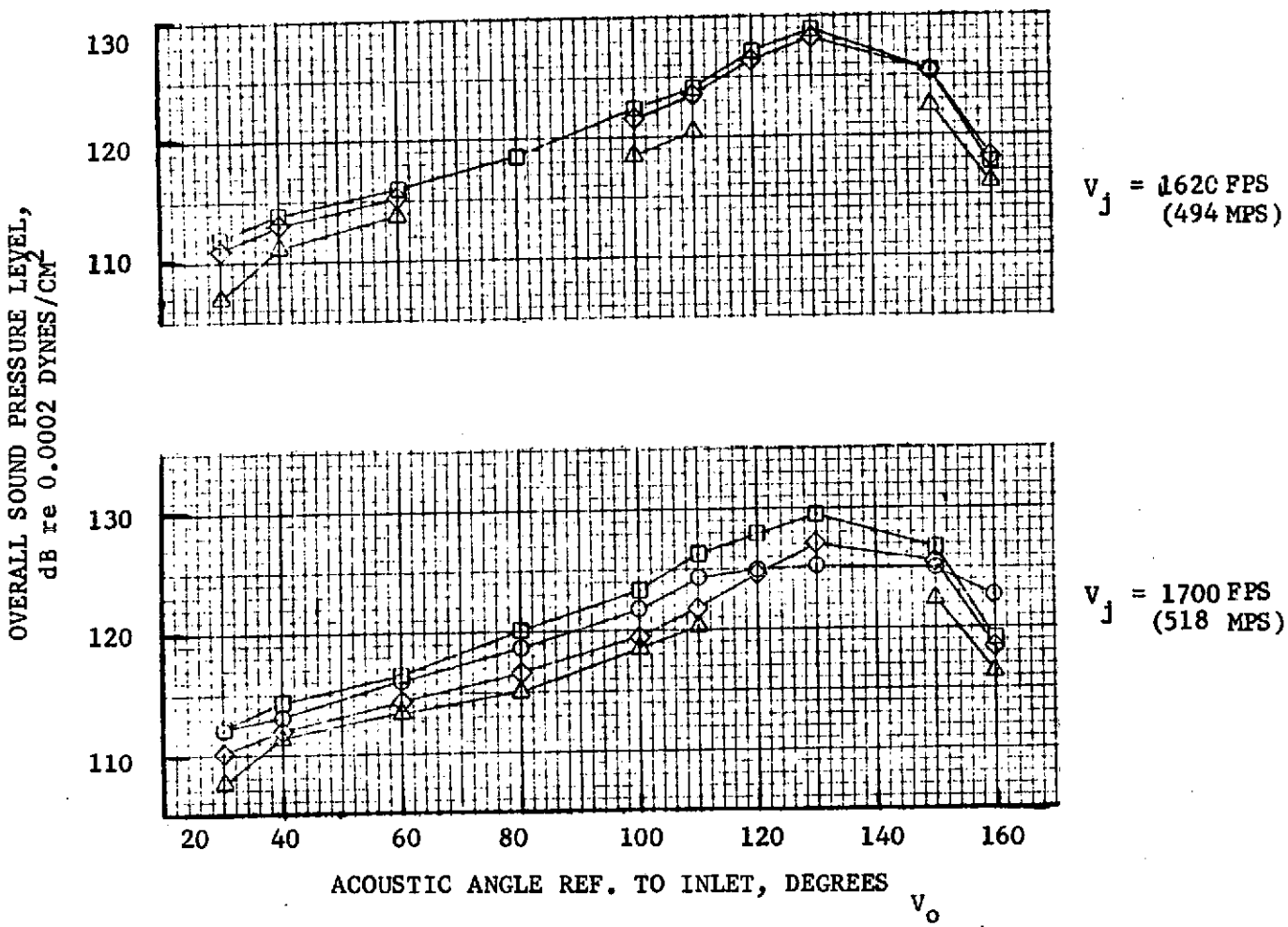

FIGURE 10.41 - ISOLATED NACELLE WIND TUNNEL TEST, OASPL DIRECTIVITY, AIE NOZZLE

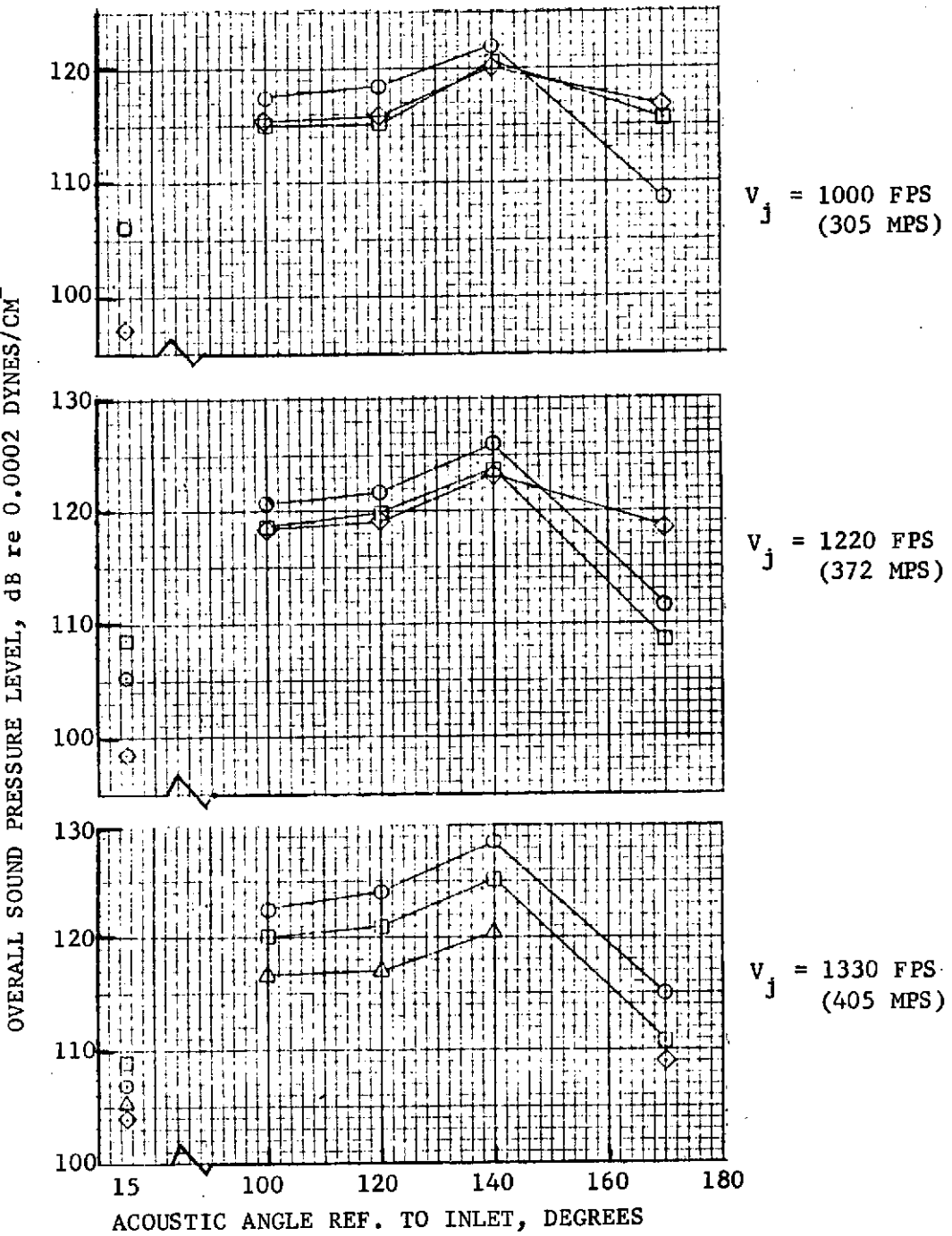

- AIE AUX NOZZLE
- 13 FT. S.L. (3.96 M)
- 59°F, 70% REL. HUM.

	V_o FT/SEC	V_o M/SEC
○	0	0
□	150	45.7
◇	250	76.2
△	340	103.6

FIGURE 10.42 - ISOLATED NACELLE WIND TUNNEL TEST, OASPL DIRECTIVITY, AIE NOZZLE

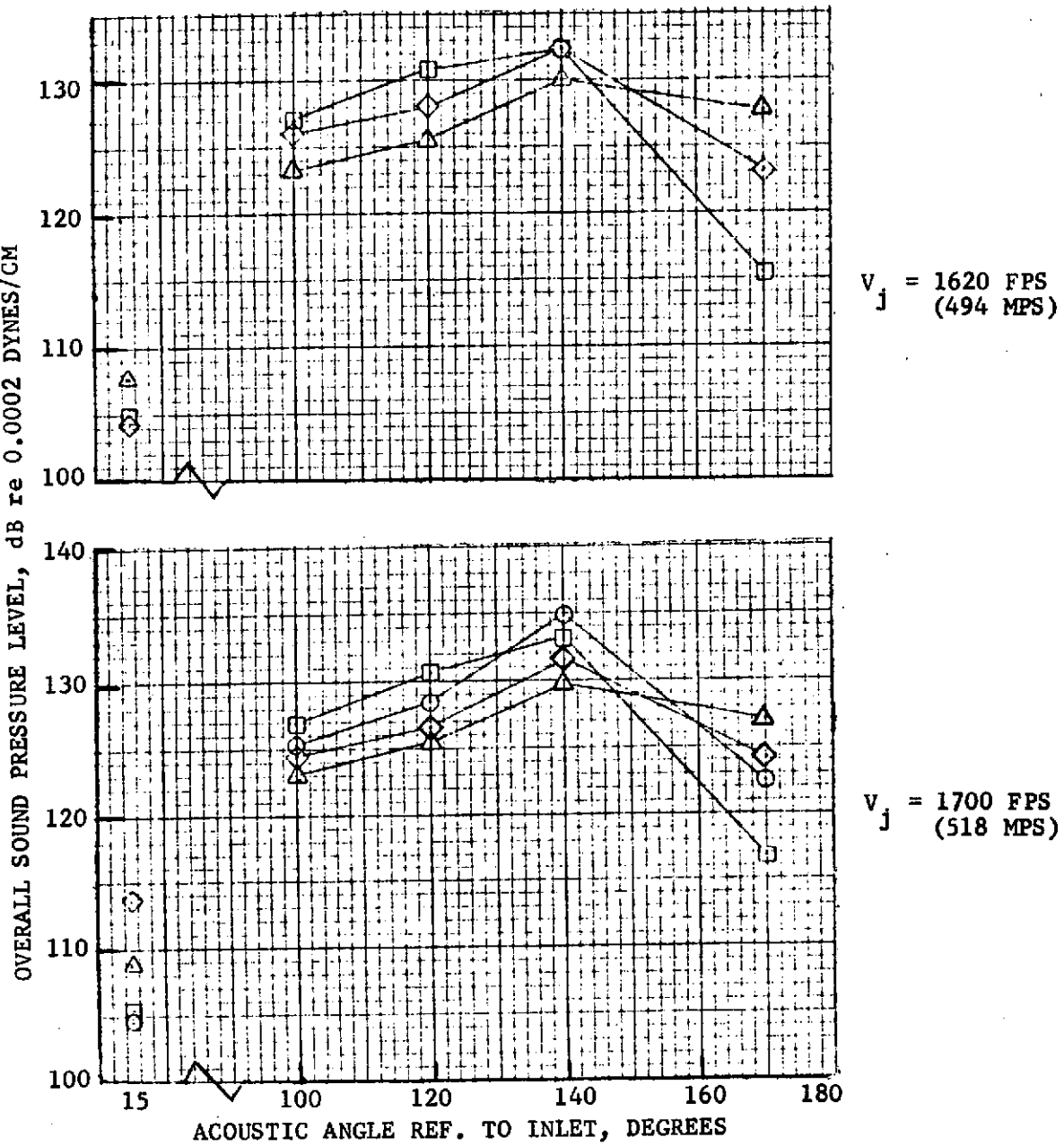

- AIE AUX NOZZLE
- 13 FT. S.L.(3.96 M)
- 59°F, 70% REL. HUM.

	V_o FT/SEC	V_o M/SEC
○	0	0
□	150	45.7
◇	250	76.2
△	340	103.6

FIGURE 10.43 - ISOLATED NACELLE WIND TUNNEL TEST, OASPL DIRECTIVITY, AIE NOZZLE

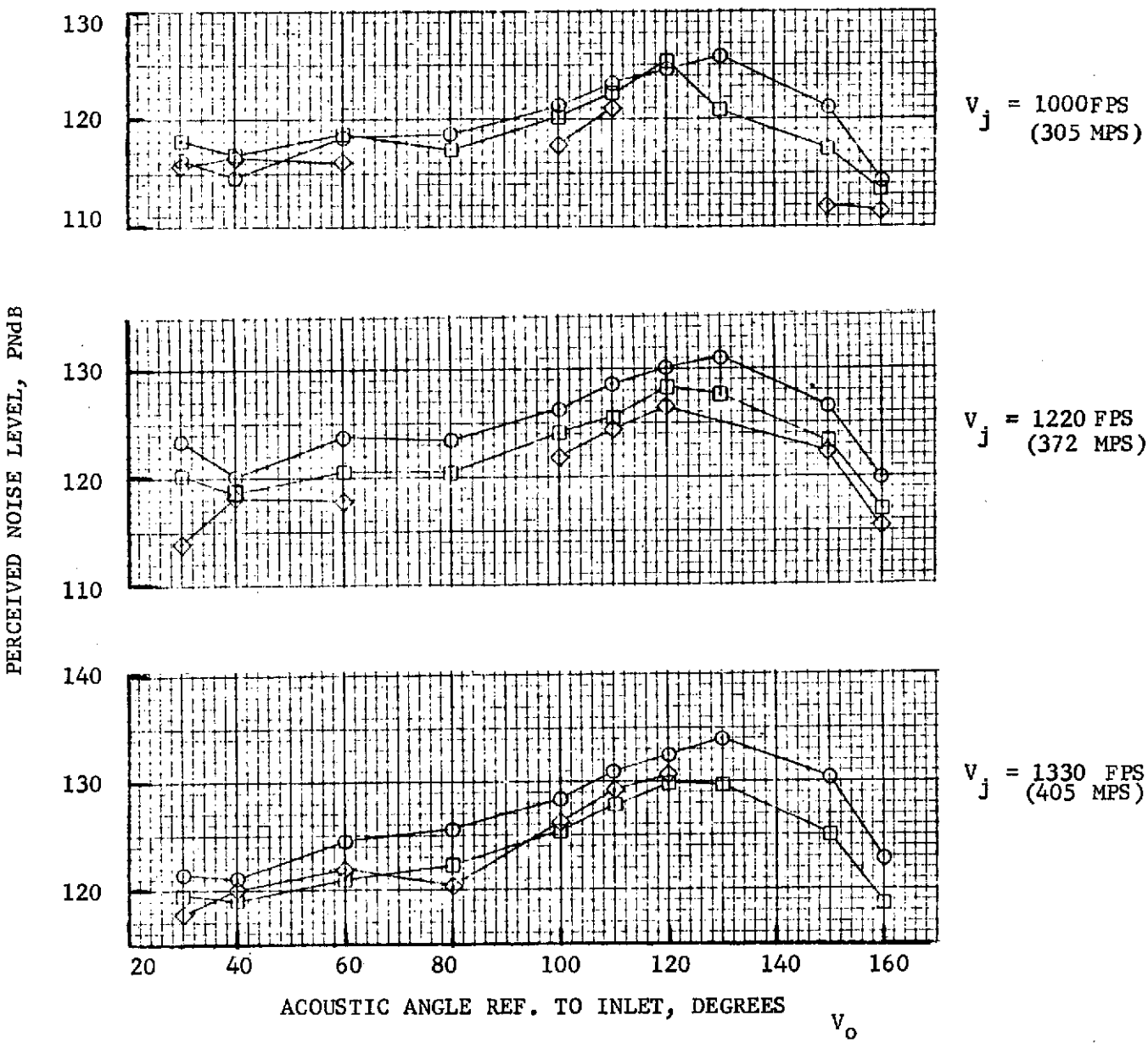

- AIE AUX NOZZLE
- 18 FT. S.L. (5.49 M)
- 59°F, 70% REL. HUM.

V_o FT/SEC	V_o M/SEC
○ 0	0
□ 150	45.7
◇ 250	76.2
△ 340	103.6

FIGURE 10.44 - ISOLATED NACELLE WIND TUNNEL TEST, PNdB DIRECTIVITY, AIE NOZZLE

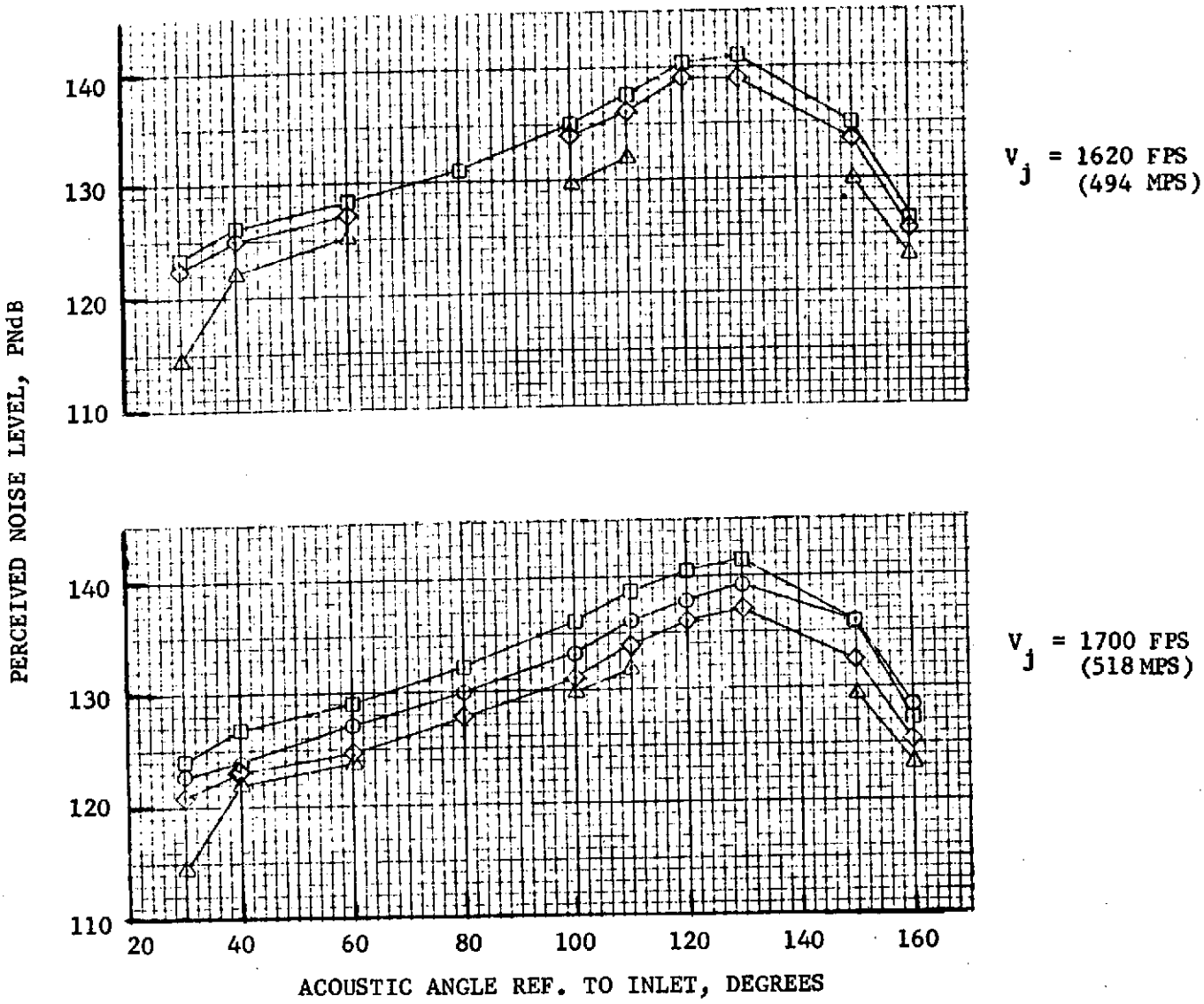

FIGURE 10.45 - ISOLATED NACELLE WIND TUNNEL TEST, PNdB DIRECTIVITY, AIE NOZZLE

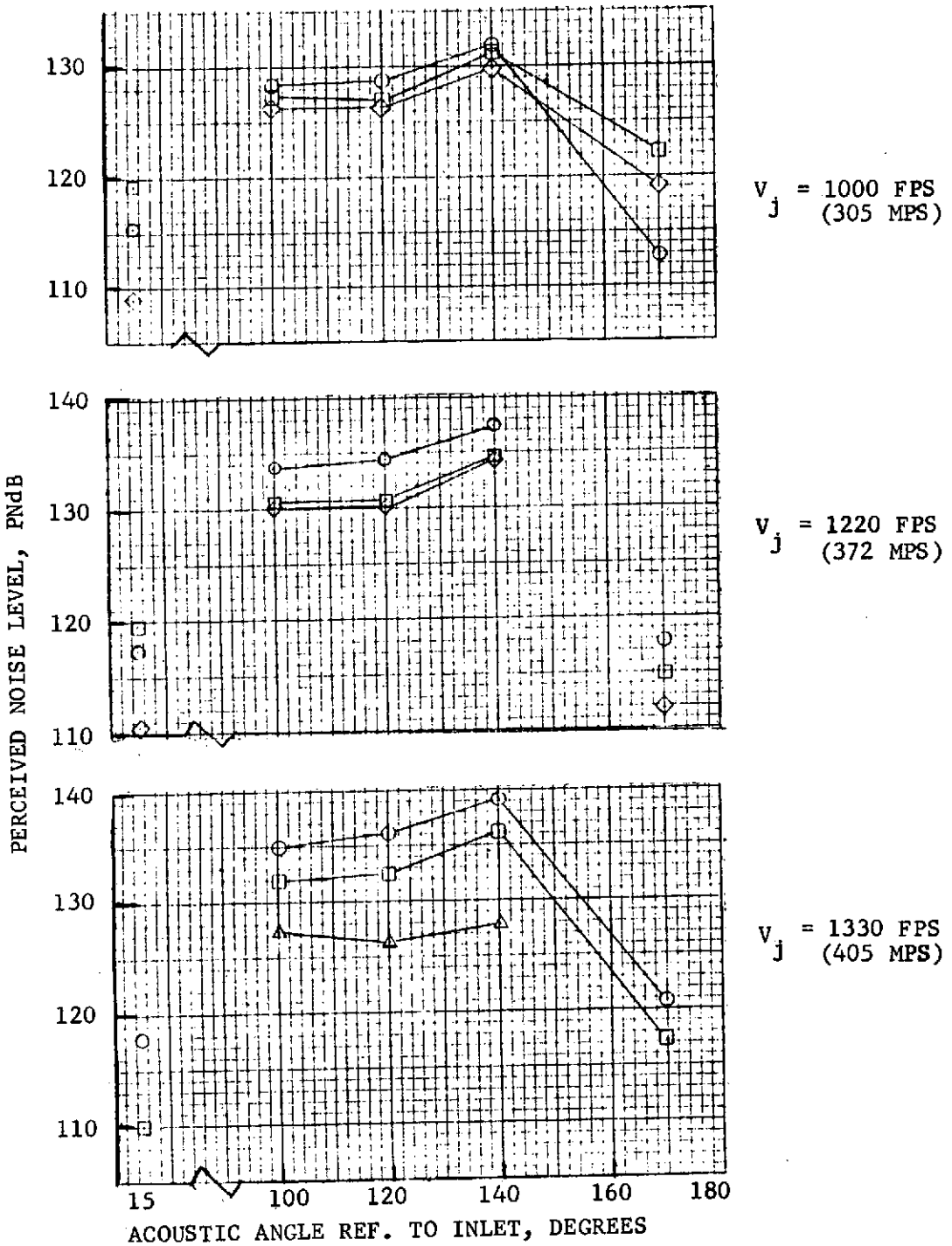

- AIE AUX NOZZLE
- 13 FT. S.L. (3.96 M)
- 59°F, 70% REL. HUM.

	FT/SEC	M/SEC
○	0	0
□	150	45.7
◇	250	76.2
△	340	103.6

FIGURE 10.46 - ISOLATED NACELLE WIND TUNNEL TEST, PNdB DIRECTIVITY, AIE NOZZLE

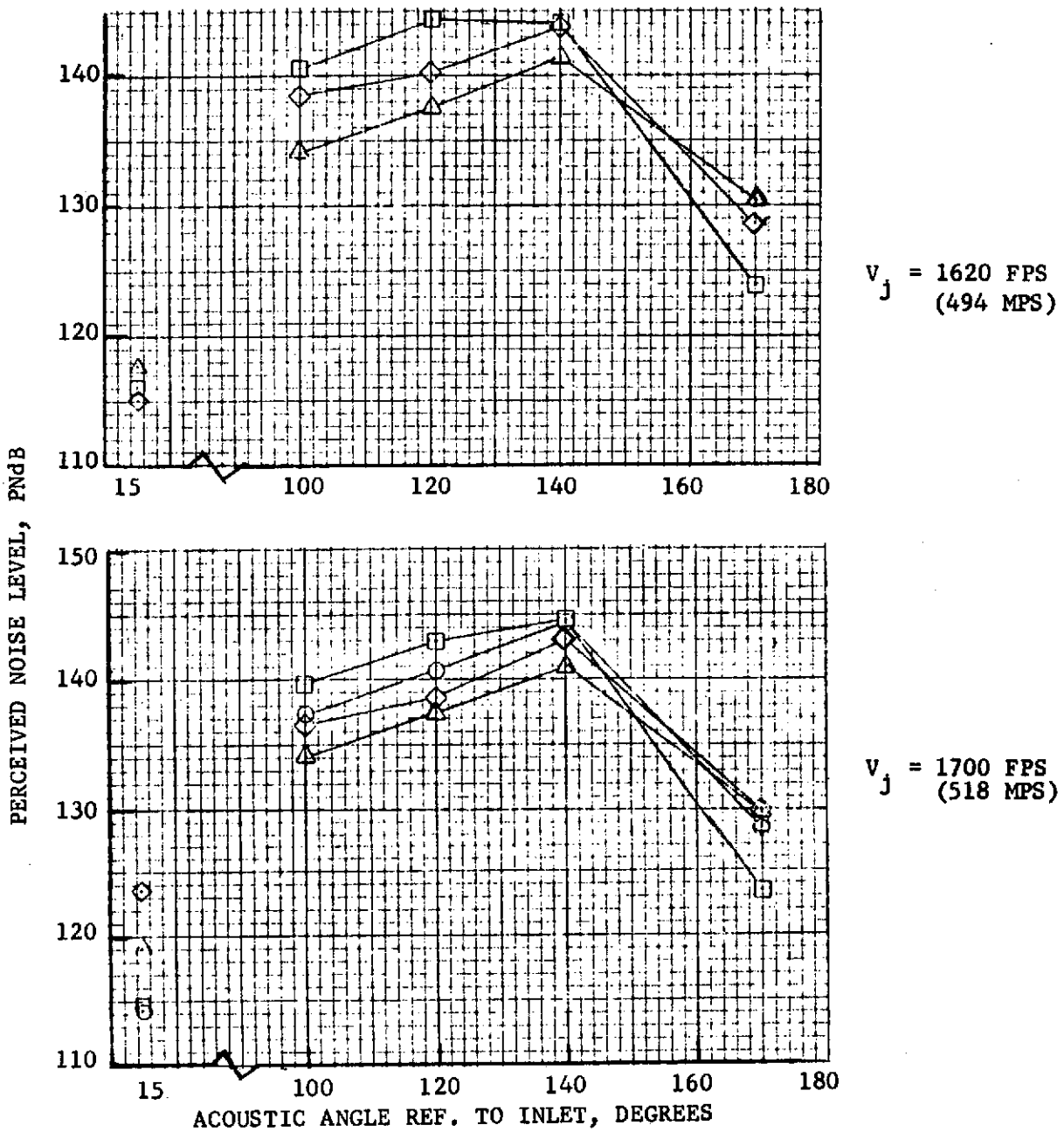

FIGURE 10.47 - ISOLATED NACELLE WIND TUNNEL TEST, PNdB DIRECTIVITY, AIE NOZZLE

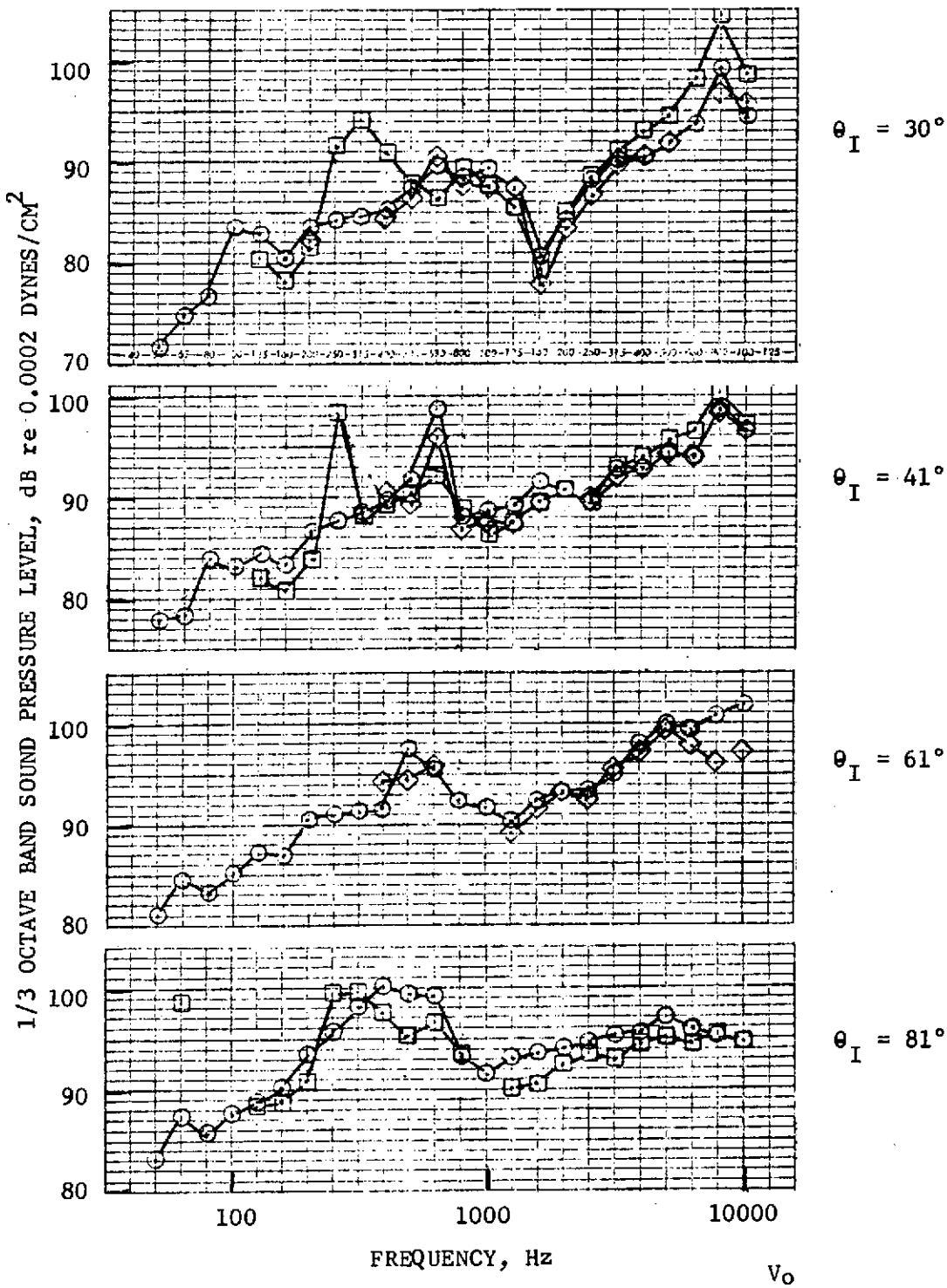

- CONICAL EJECTOR NOZZLE
- 18 FT. S.L. (5.49 M)
- V_j = 850 FT/SEC (259 M/SEC)
- 59°F, 70% REL. HUM.

	V_o FT/SEC	V_o M/SEC
○	0	0
□	150	45.7
◇	250	76.2
△	340	103.6

FIGURE 10.48 - ISOLATED NACELLE WIND TUNNEL TEST, 1/3 OCTAVE BAND SPECTRA, CONICAL EJECTOR NOZZLE

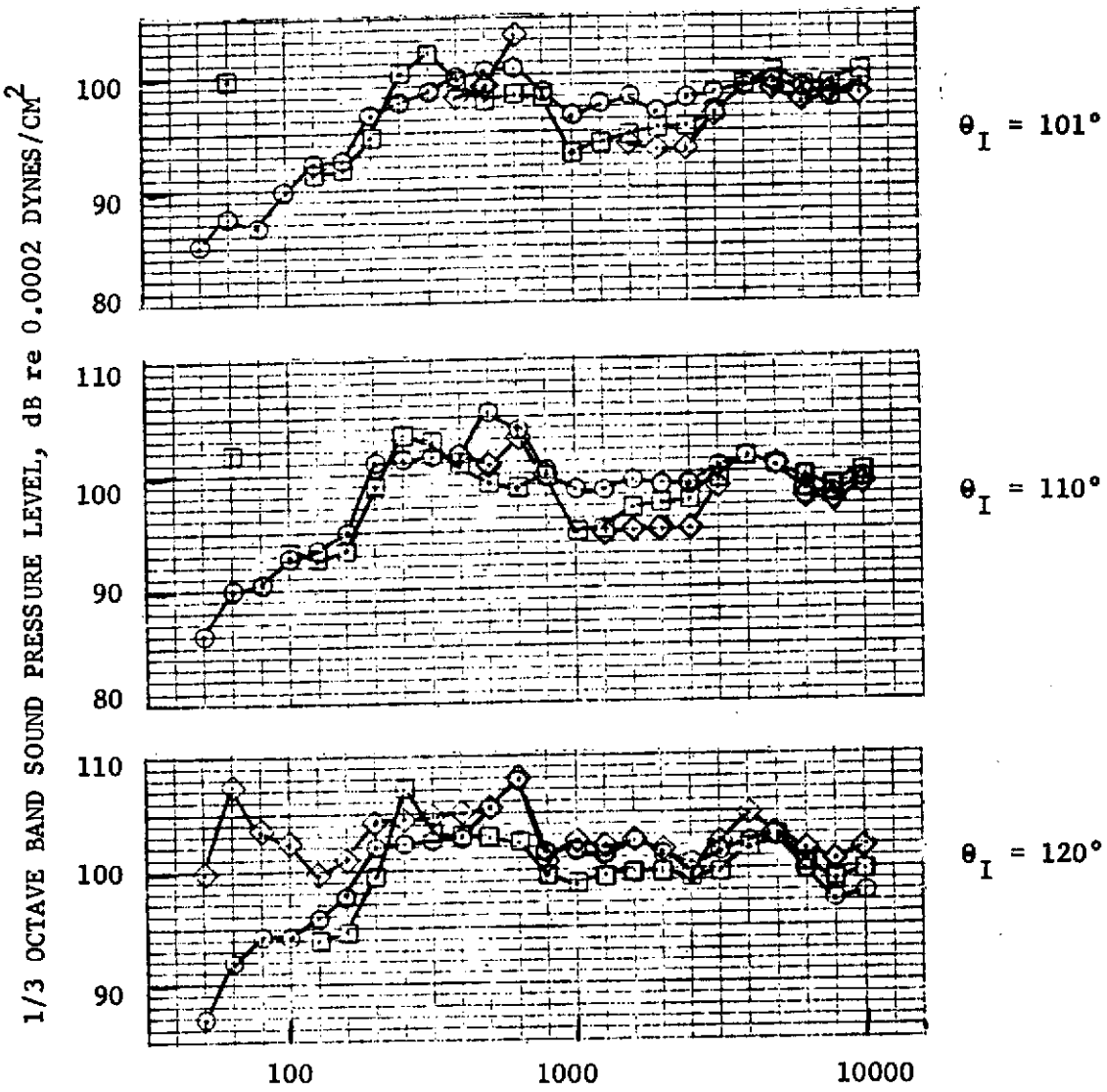

FIGURE 10.49 - ISOLATED NACELLE WIND TUNNEL TEST, 1/3 OCTAVE BAND SPECTRA, CONICAL EJECTOR NOZZLE

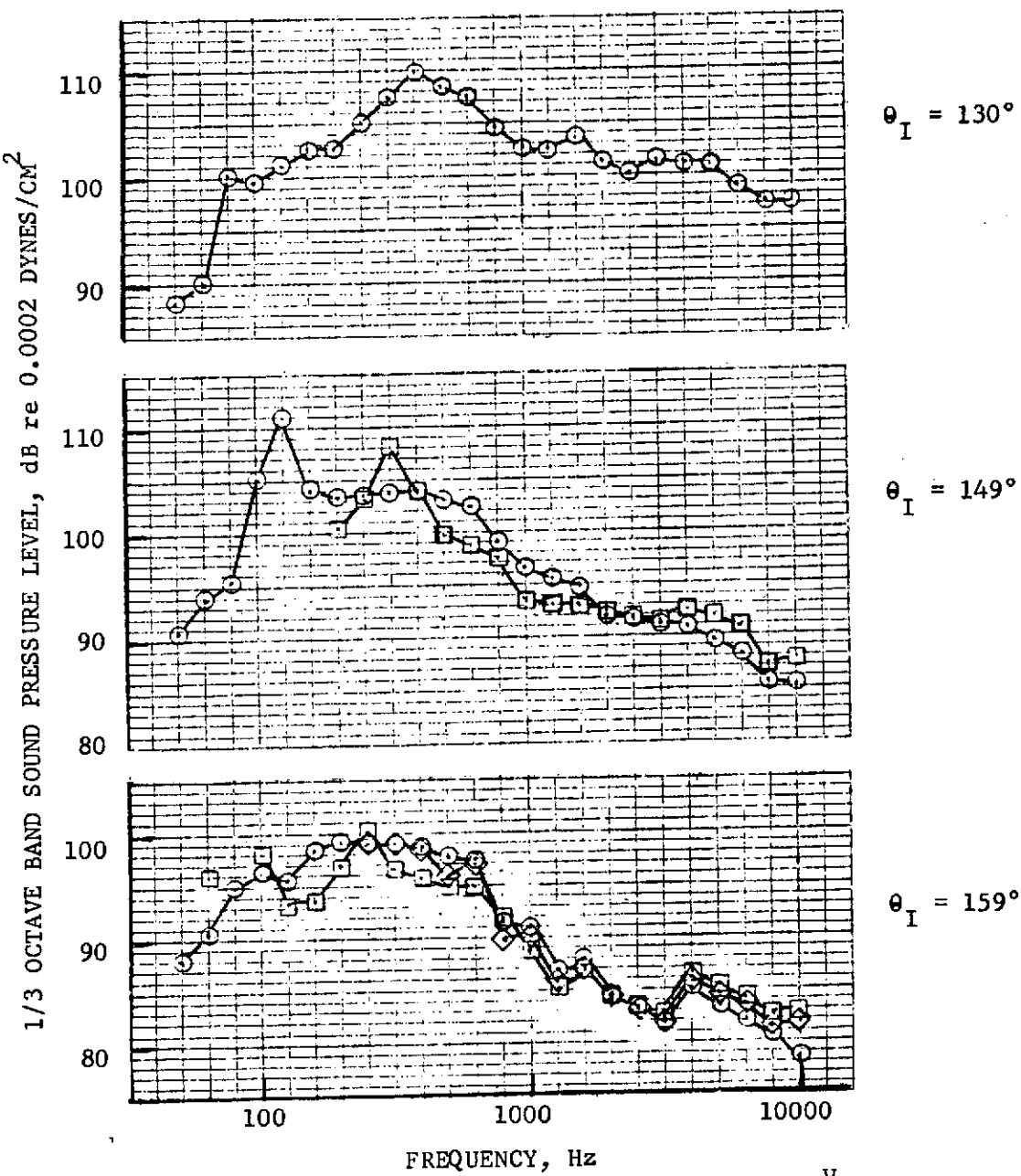

FIGURE 10.50 - ISOLATED NACELLE WIND TUNNEL TEST, 1/3 OCTAVE BAND SPECTRA, CONICAL EJECTOR NOZZLE

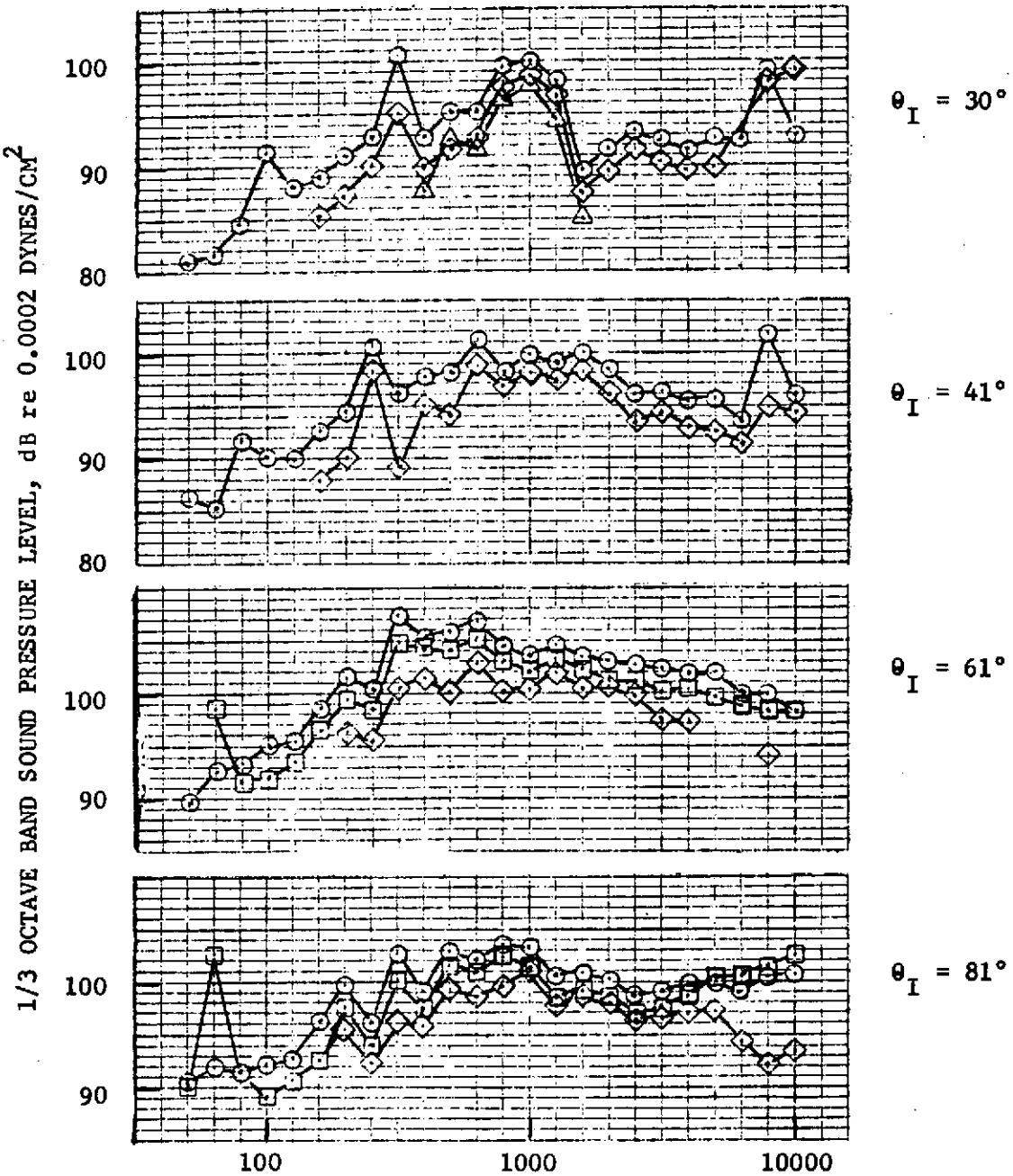

FIGURE 10.51 - ISOLATED NACELLE WIND TUNNEL TEST, 1/3 OCTAVE BAND SPECTRA, CONICAL EJECTOR NOZZLE

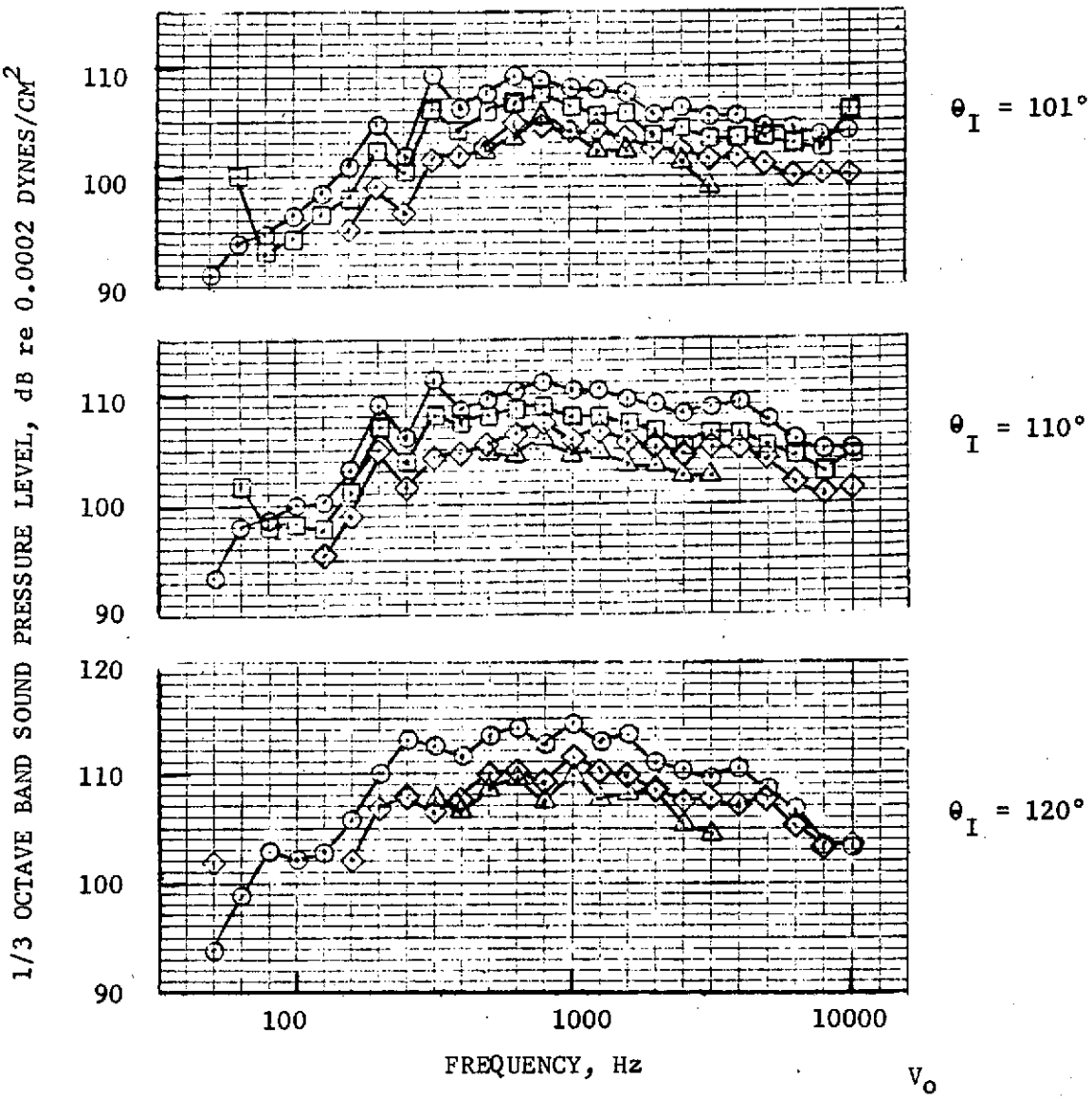

FIGURE 10.52 - ISOLATED NACELLE WIND TUNNEL TEST, 1/3 OCTAVE BAND SPECTRA, CONICAL EJECTOR NOZZLE

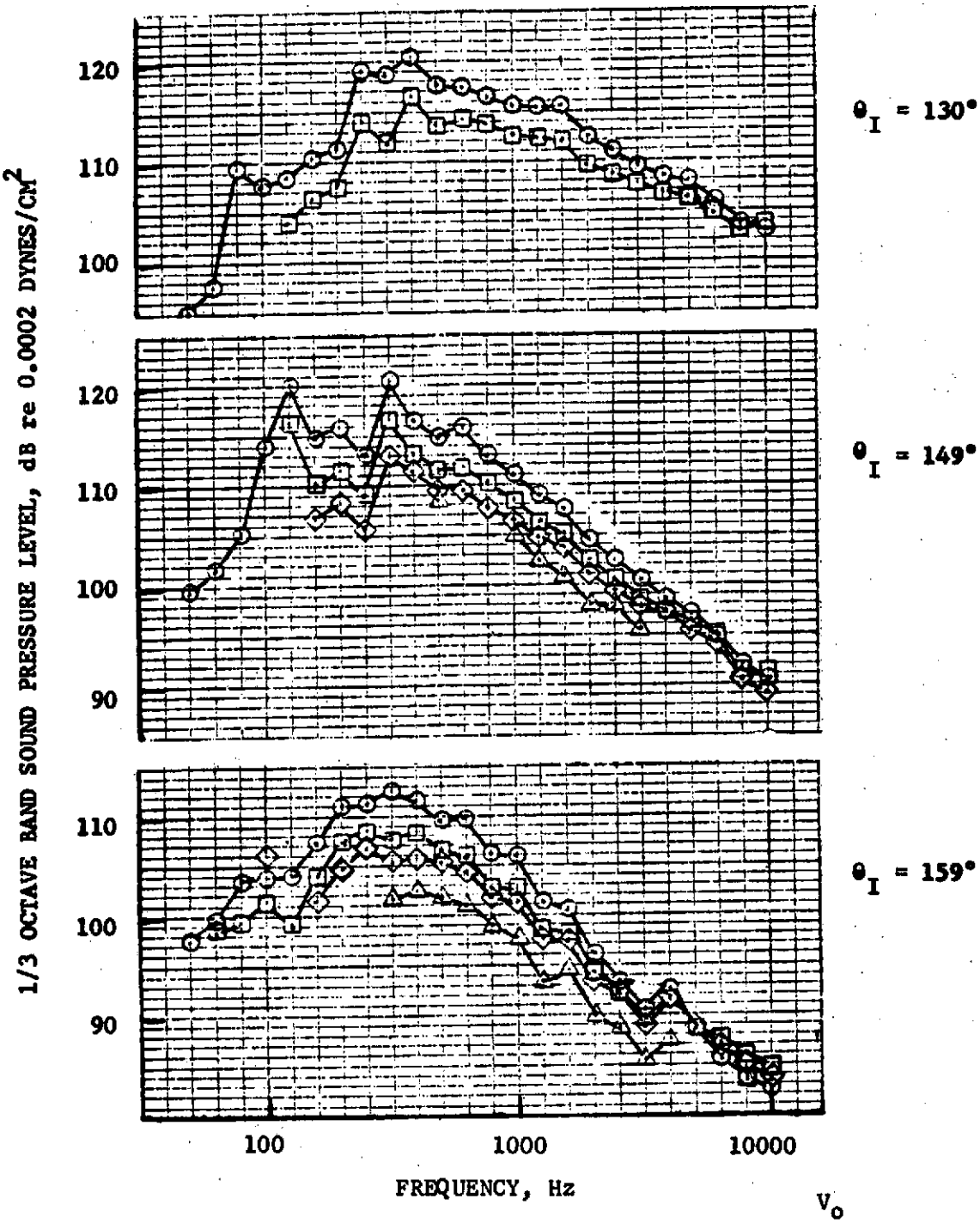

FIGURE 10.53 - ISOLATED NACELLE WIND TUNNEL TEST, 1/3 OCTAVE BAND SPECTRA, CONICAL EJECTOR NOZZLE

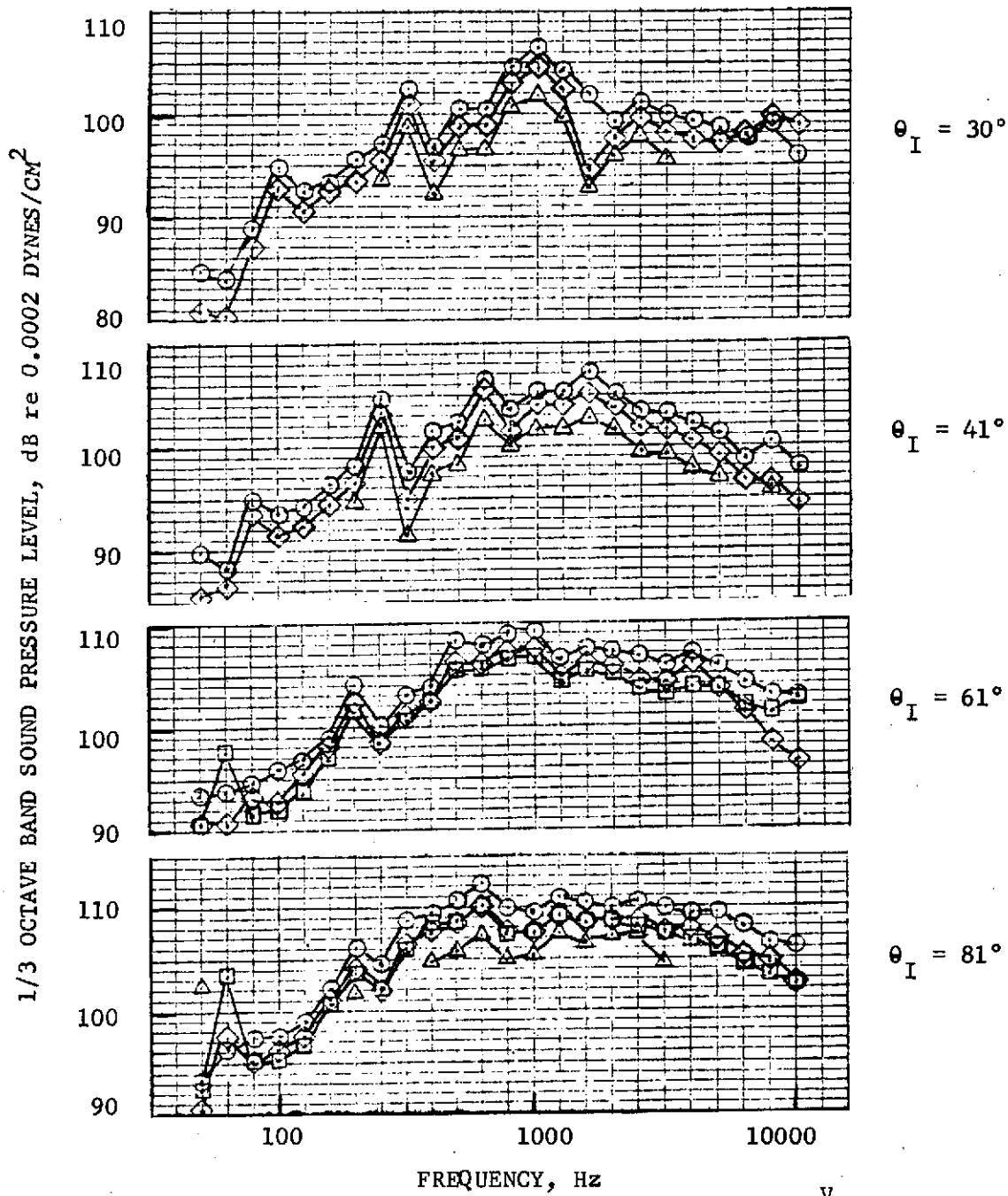

- CONICAL EJECTOR NOZZLE
- 18 FT. S.L. (5.49 M)
- V_j = 1900 FT/SEC (579 M/SEC)
- 59°F, 70% REL. HUM.

V_o	FT/SEC	M/SEC
○	0	0
□	150	45.7
◇	250	76.2
△	340	103.6

FIGURE 10.54 - ISOLATED NACELLE WIND TUNNEL TEST, 1/3 OCTAVE BAND SPECTRA, CONICAL EJECTOR NOZZLE

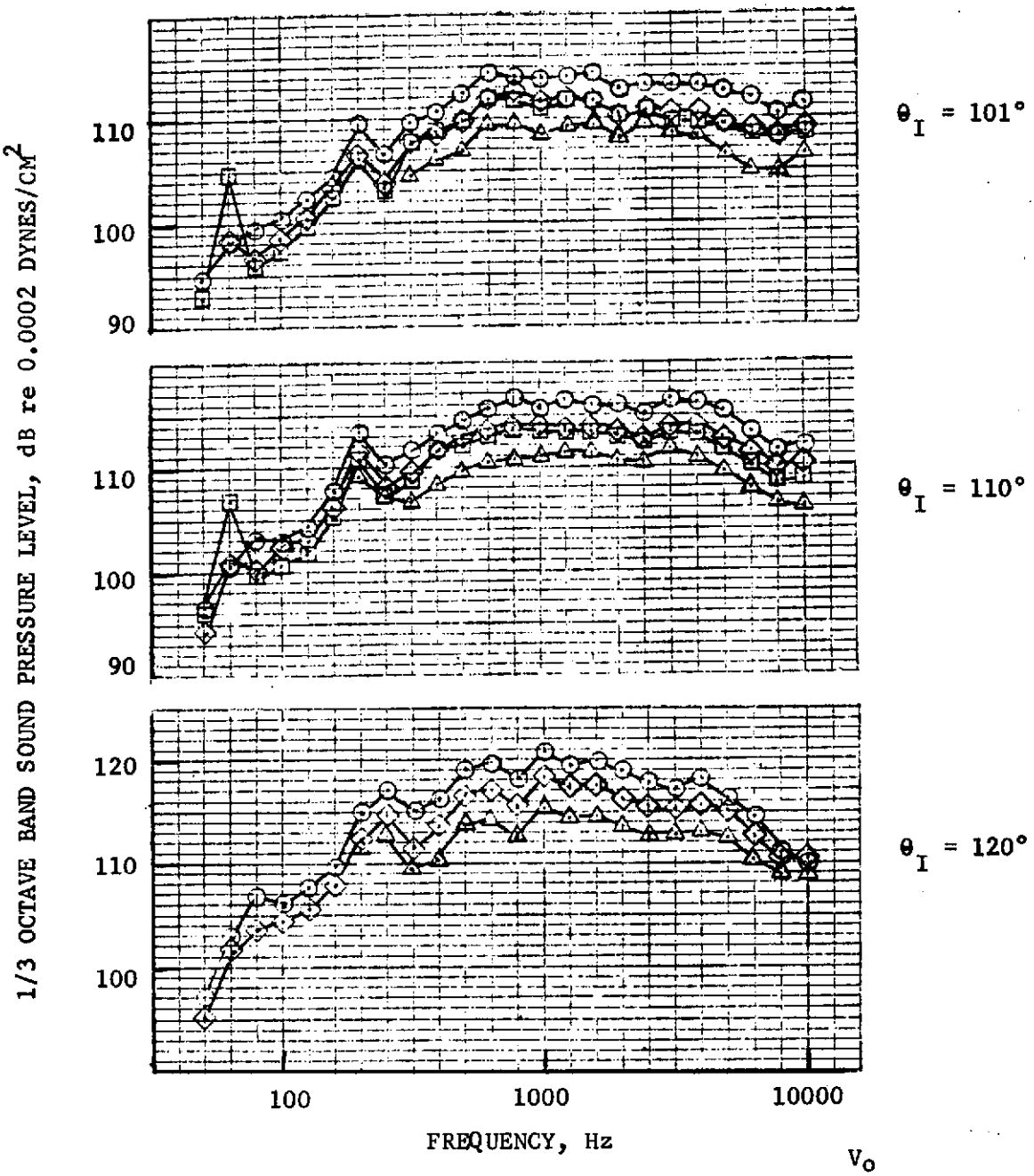

FIGURE 10.55 - ISOLATED NACELLE WIND TUNNEL TEST, 1/3 OCTAVE BAND SPECTRA, CONICAL EJECTOR NOZZLE

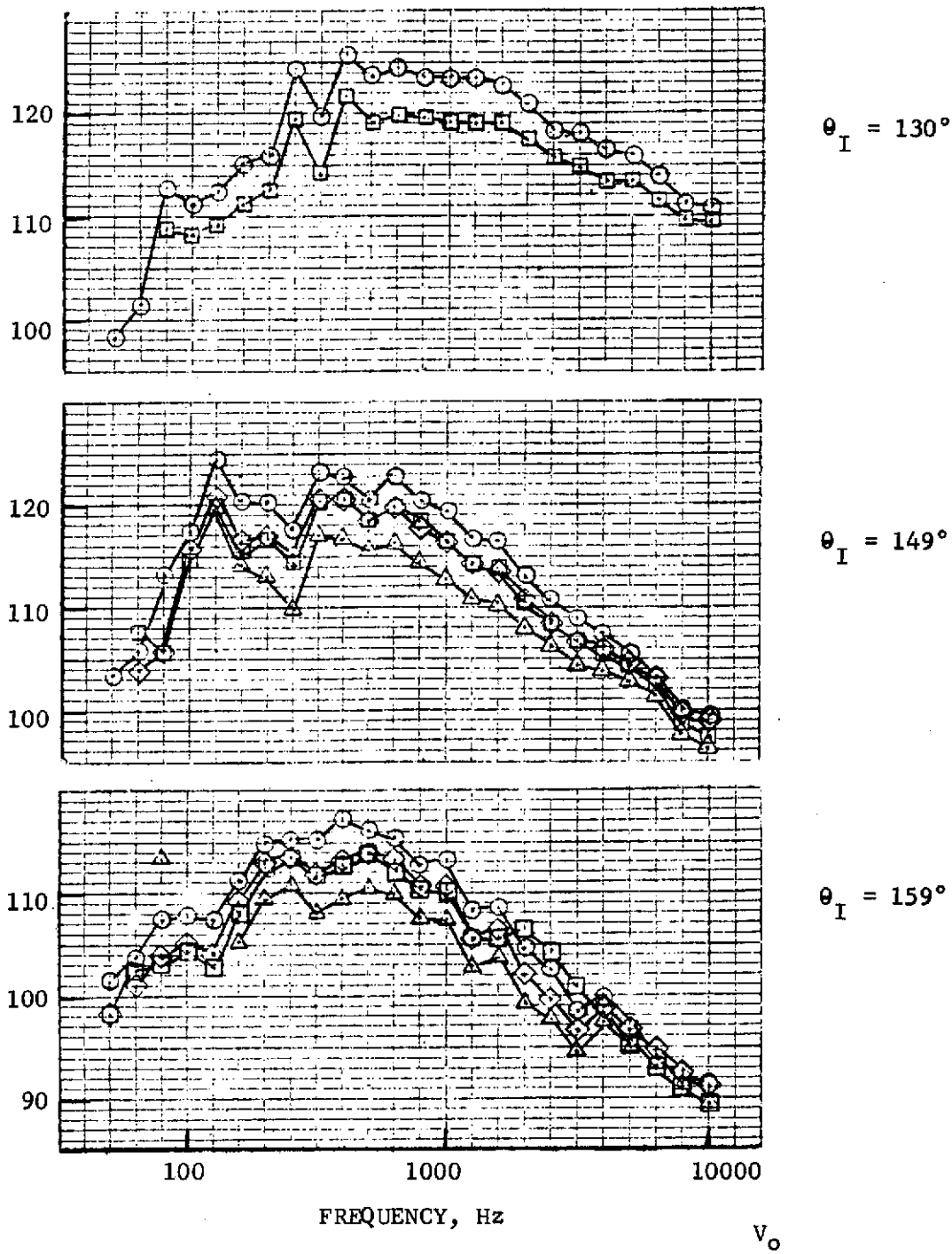

FIGURE 10.56 - ISOLATED NACELLE WIND TUNNEL TEST, 1/3 OCTAVE BAND SPECTRA, CONICAL EJECTOR NOZZLE

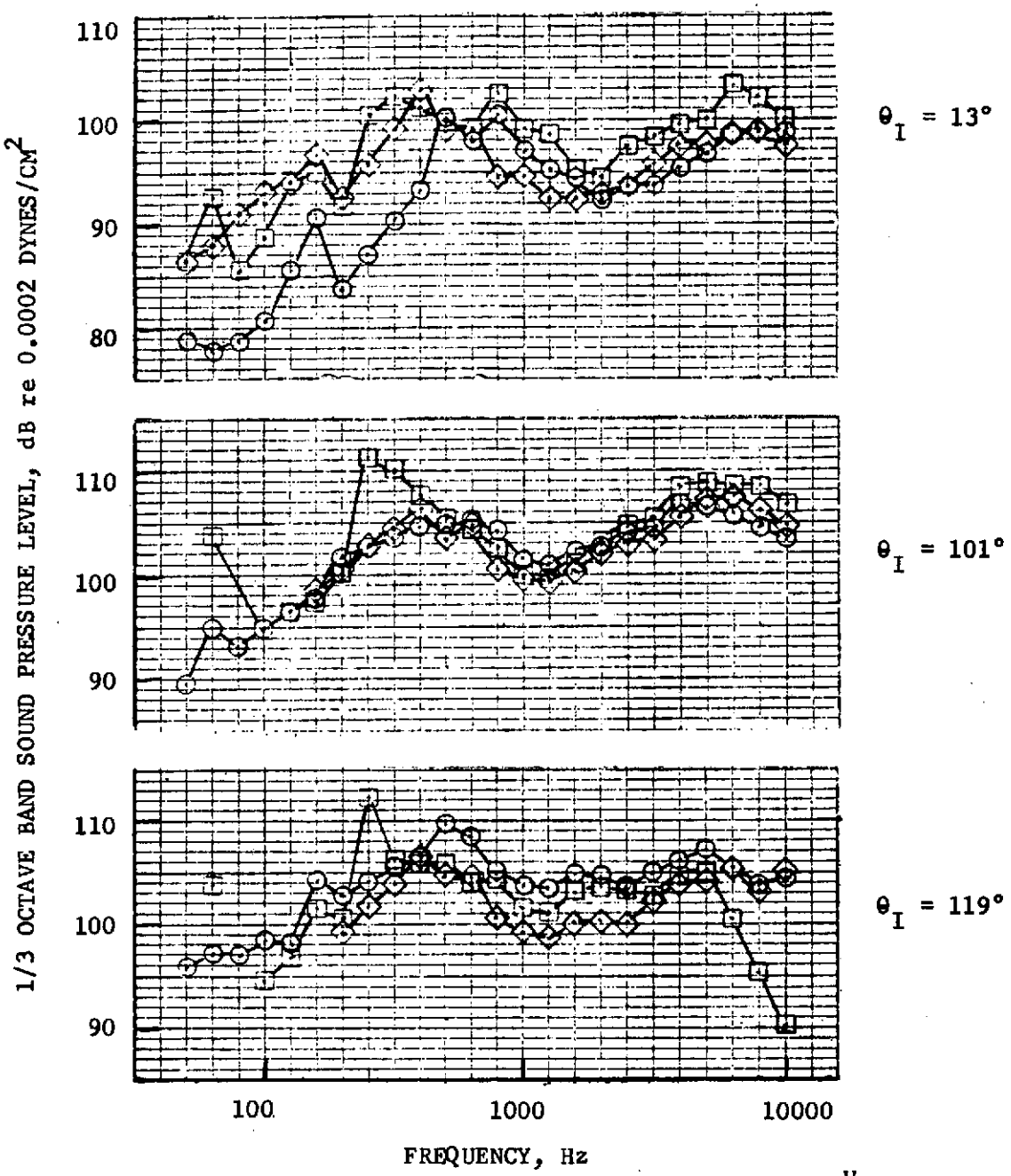

FIGURE 10.57 - ISOLATED NACELLE WIND TUNNEL TEST, 1/3 OCTAVE BAND SPECTRA, CONICAL EJECTOR NOZZLE

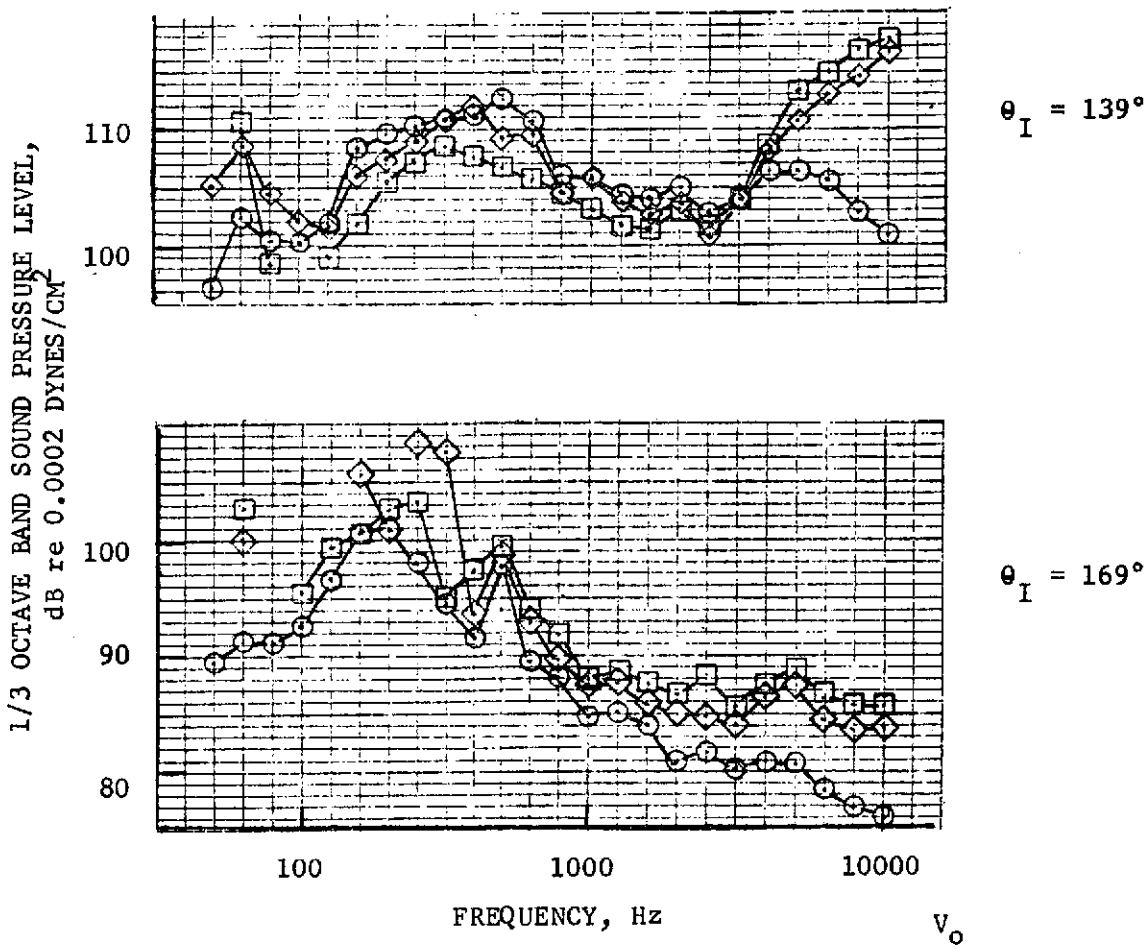

FIGURE 10.58 - ISOLATED NACELLE WIND TUNNEL TEST, 1/3 OCTAVE BAND SPECTRA, CONICAL EJECTOR NOZZLE

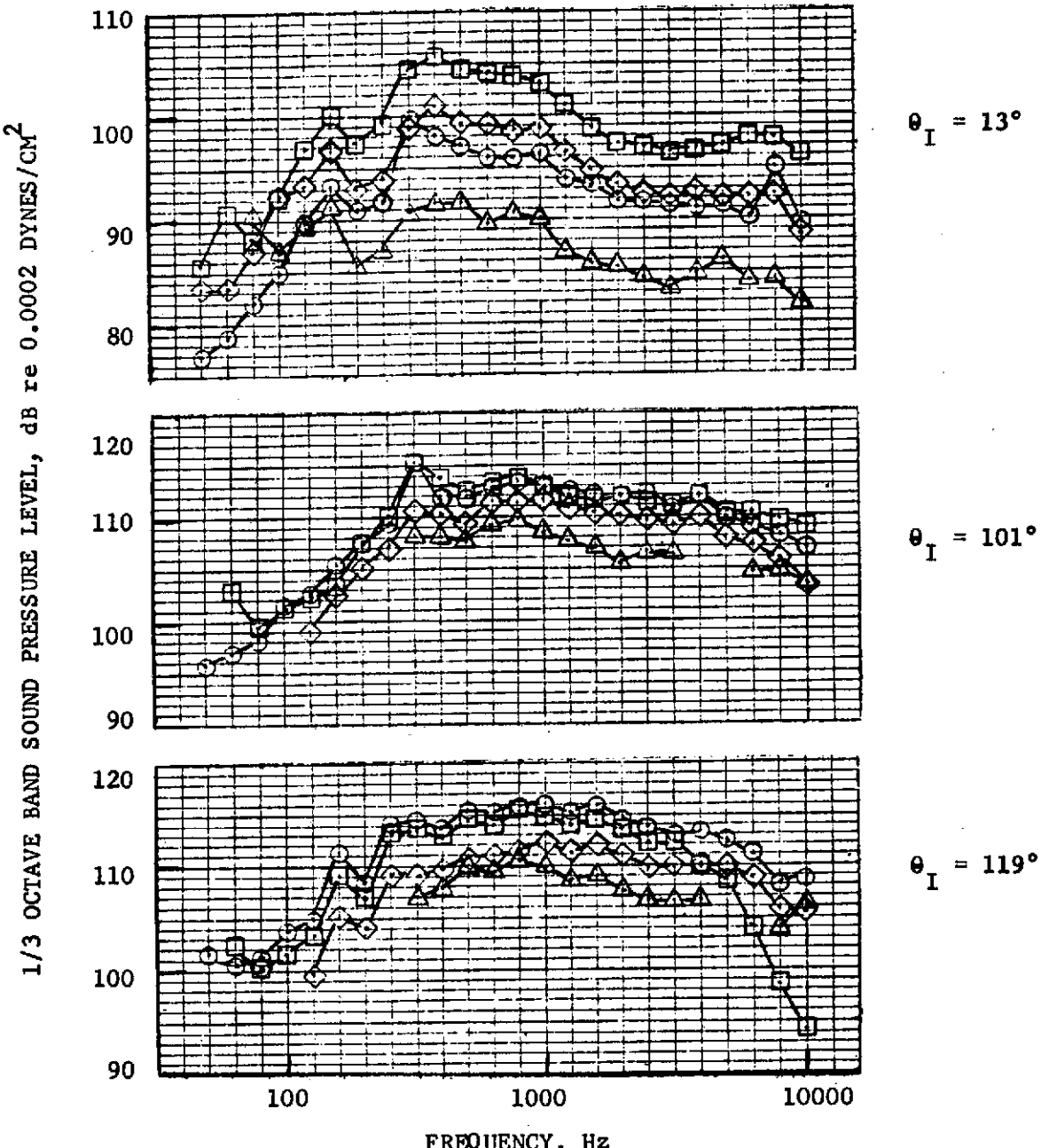

- CONICAL EJECTOR NOZZLE
- 13 FT. S.L. (3.96 M)
- V_j = 1475 FT/SEC (450 M/SEC)
- 59°F, 70% REL. HUM.

	V_o FT/SEC	V_o M/SEC
○	0	0
□	150	45.7
◇	250	76.2
△	340	103.6

FIGURE 10.59 - ISOLATED NACELLE WIND TUNNEL TEST, 1/3 OCTAVE BAND SPECTRA, CONICAL EJECTOR NOZZLE

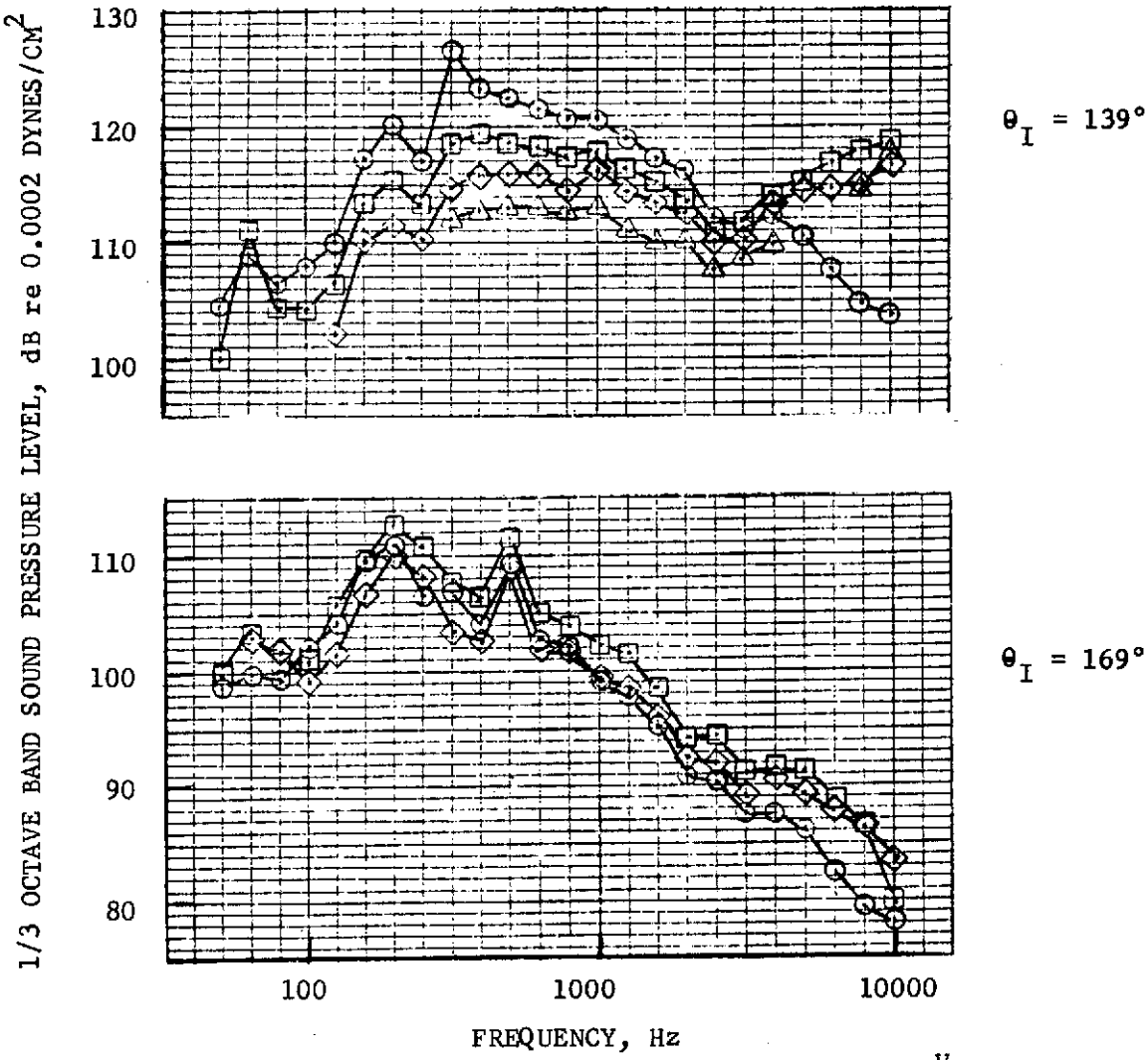

FIGURE 10.60 - ISOLATED NACELLE WIND TUNNEL TEST, 1/3 OCTAVE BAND SPECTRA, CONICAL EJECTOR NOZZLE

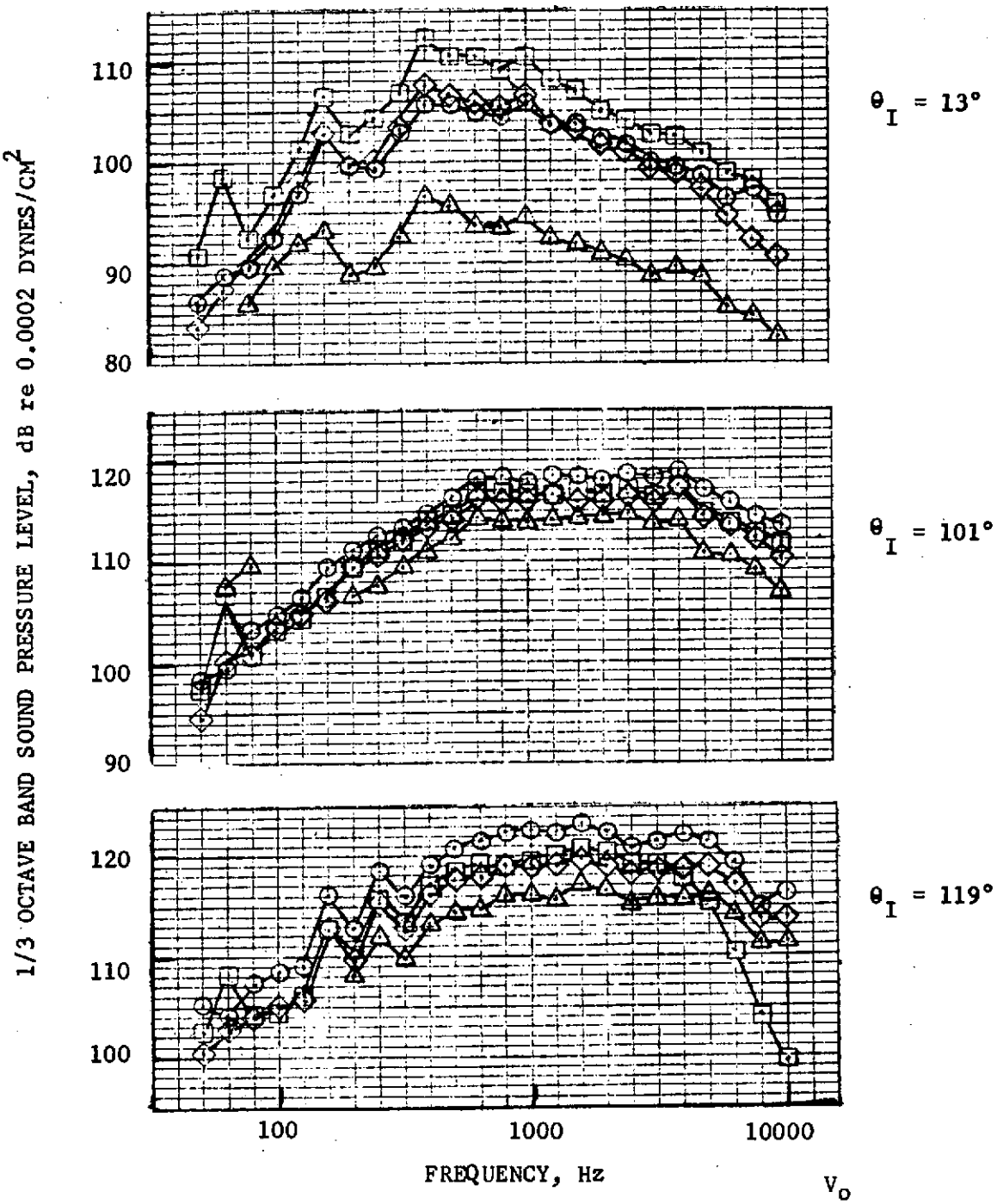

FIGURE 10.61 - ISOLATED NACELLE WIND TUNNEL TEST, 1/3 OCTAVE BAND SPECTRA, CONICAL EJECTOR NOZZLE

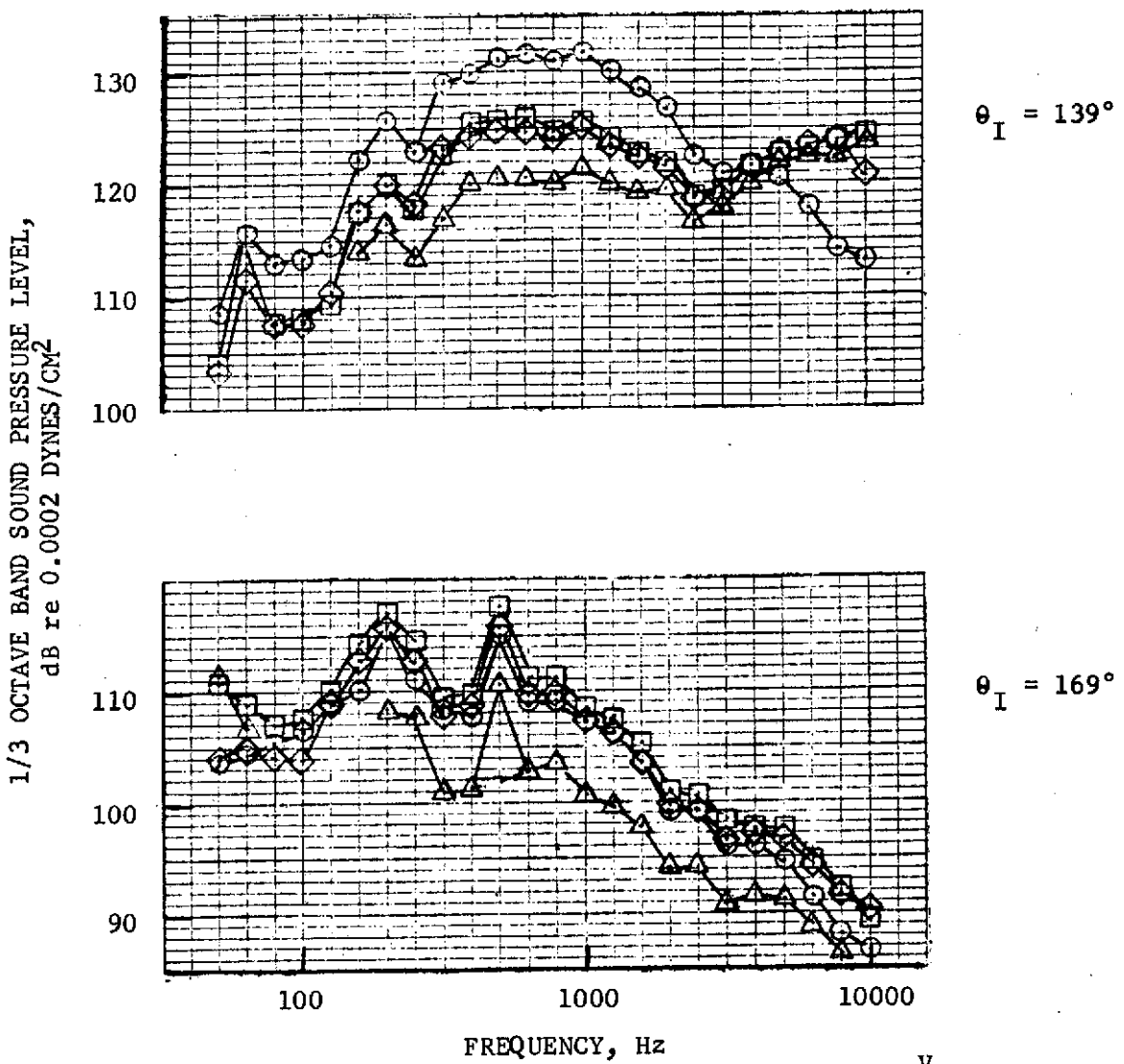

FIGURE 10.62 - ISOLATED NACELLE WIND TUNNEL TEST, 1/3 OCTAVE BAND SPECTRA, CONICAL EJECTOR NOZZLE

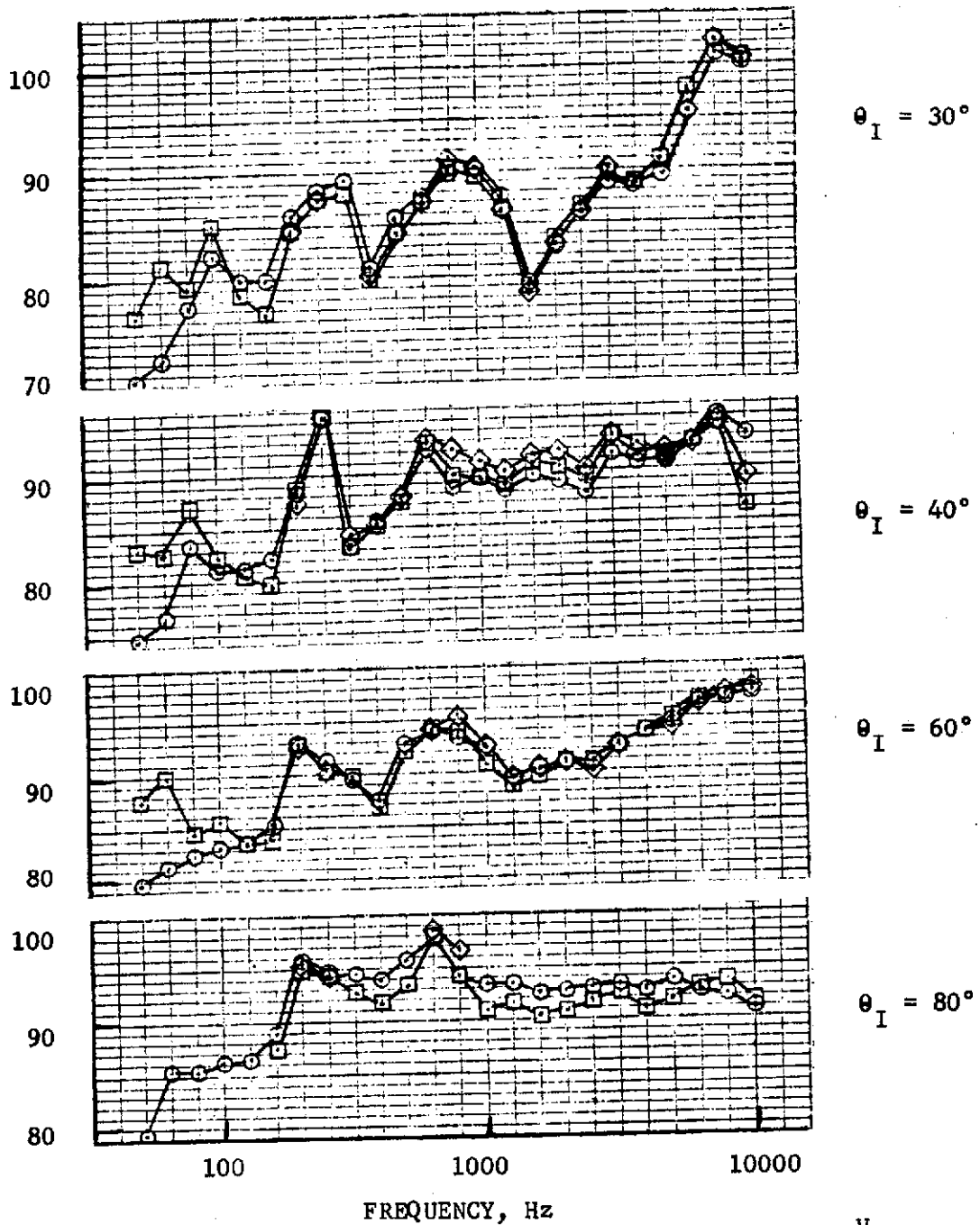

FIGURE 10.63 - ISOLATED NACELLE WIND TUNNEL TEST, 1/3 OCTAVE BAND SPECTRA, AIE NOZZLE

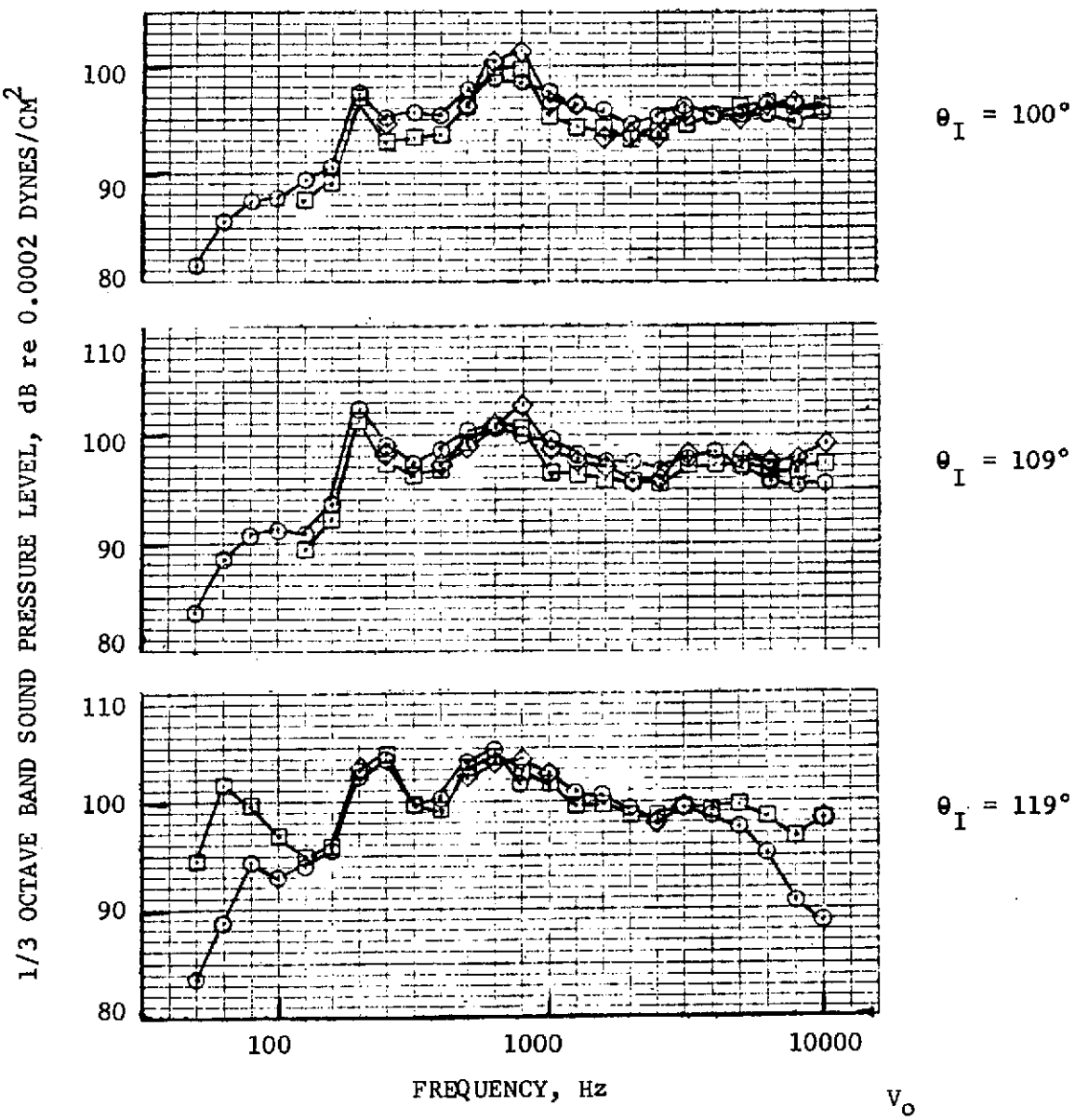

FIGURE 10.64 - ISOLATED NACELLE WIND TUNNEL TEST, 1/3 OCTAVE BAND SPECTRA, AIE NOZZLE

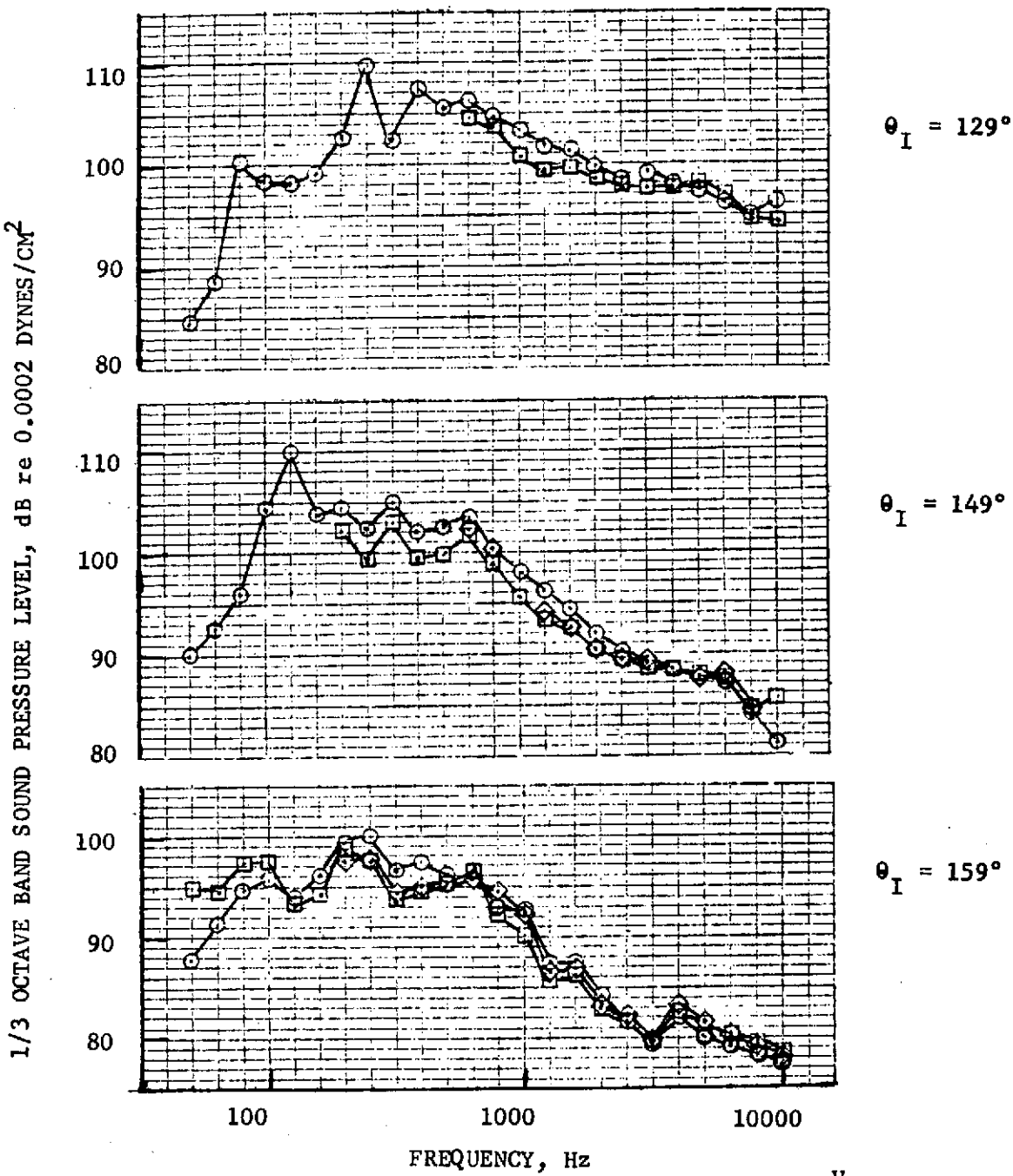

- AIE AUX NOZZLE
- 18 FT. S.L. (5.49 M)
- V_j = 1000 FT/SEC (305 M/SEC)
- 59°F, 70% REL. HUM.

	V_o FT/SEC	V_o M/SEC
○	0	0
□	150	45.7
◇	250	76.2
△	340	103.6

FIGURE 10.65 - ISOLATED NACELLE WIND TUNNEL TEST, 1/3 OCTAVE BAND SPECTRA, AIE NOZZLE

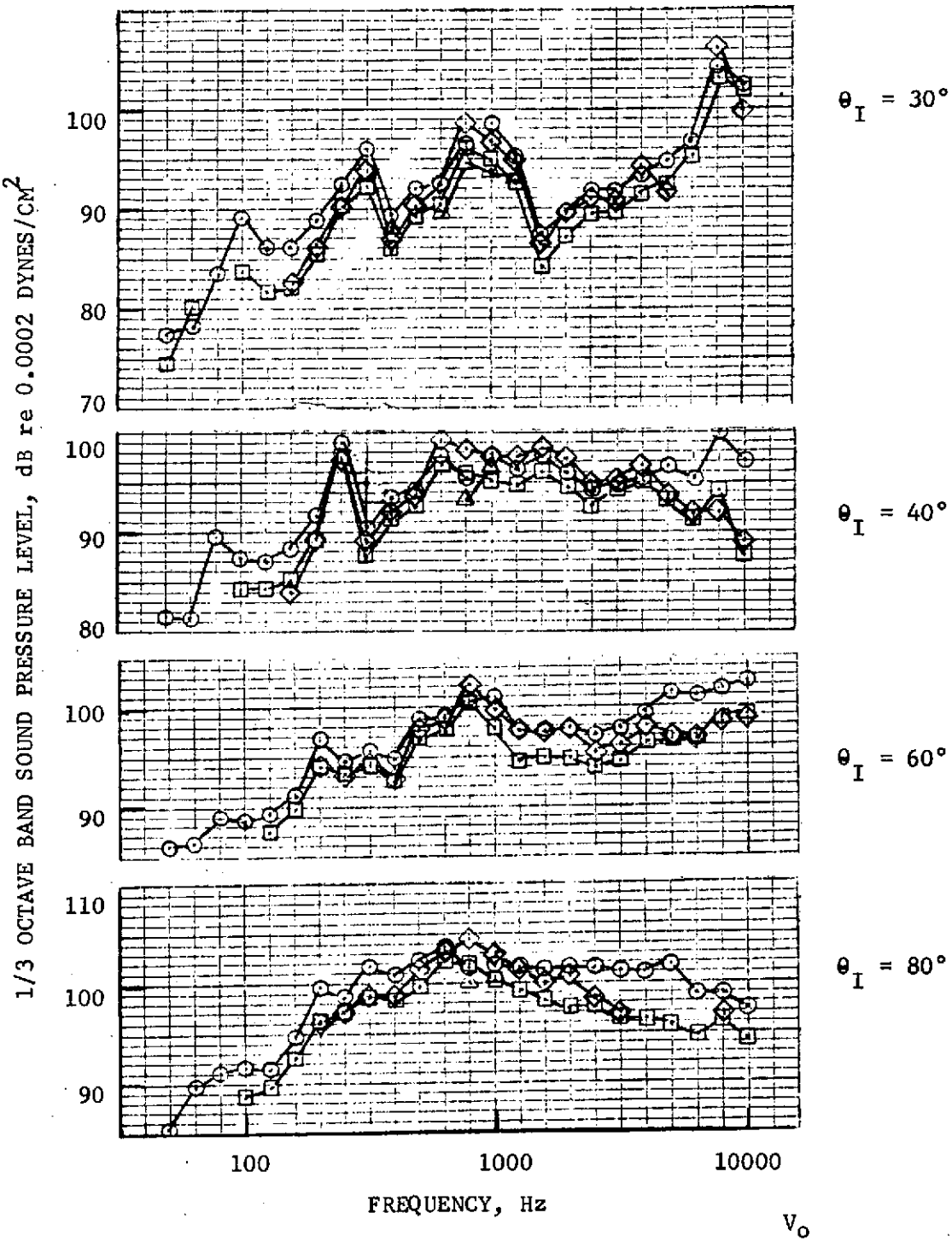

- AIE AUX NOZZLE
- 18 FT. S.L.(5.49 M)
- V_j = 1330 FT/SEC (405 M/SEC)
- 59°F, 70% REL. HUM.

V_o FT/SEC	V_o M/SEC
○ 0	0
□ 150	45.7
◇ 250	76.2
△ 340	103.6

FIGURE 10.66 - ISOLATED NACELLE WIND TUNNEL TEST, 1/3 OCTAVE BAND SPECTRA, AIE NOZZLE

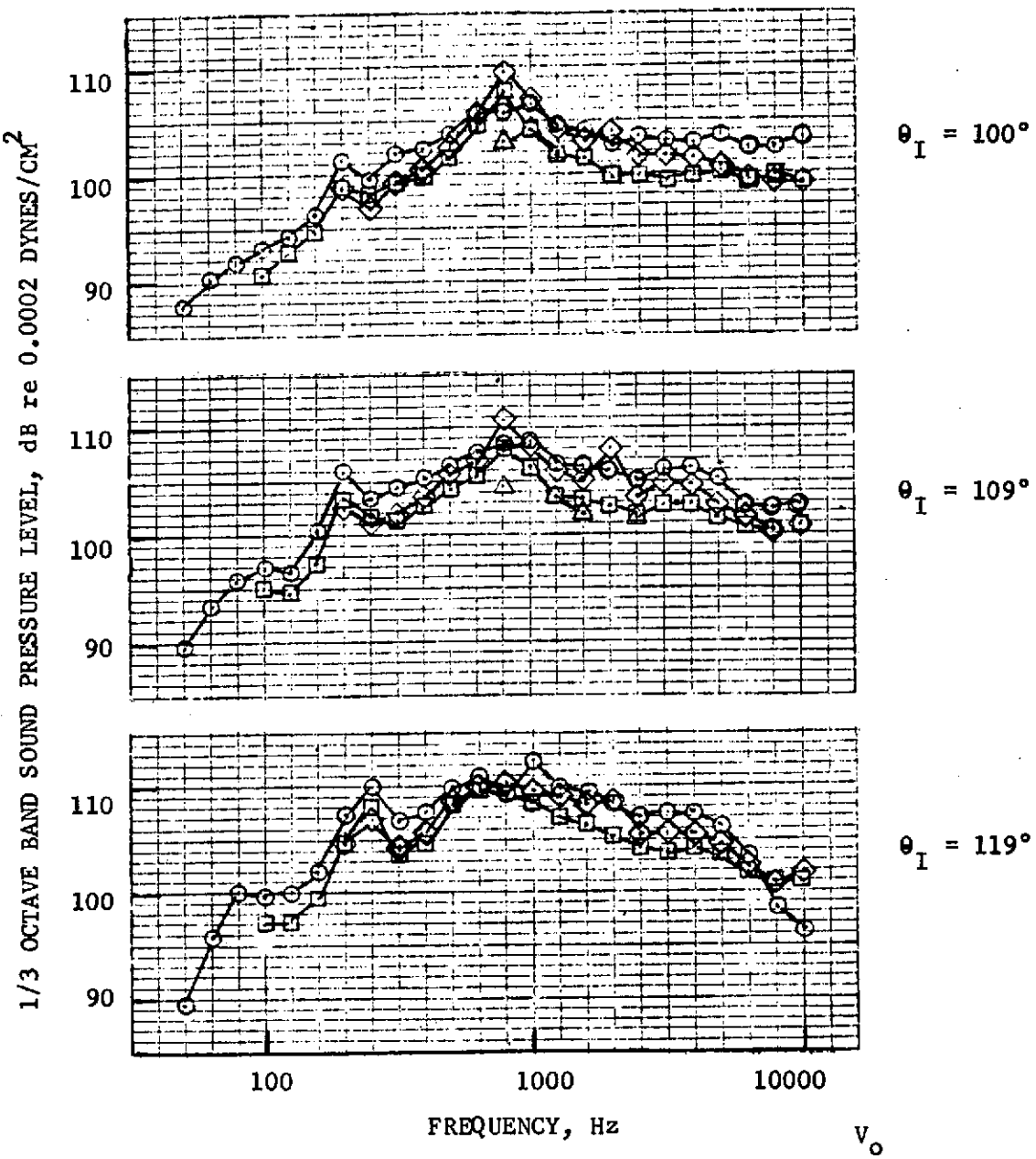

FIGURE 10.67 - ISOLATED NACELLE WIND TUNNEL TEST, 1/3 OCTAVE BAND SPECTRA, AIE NOZZLE

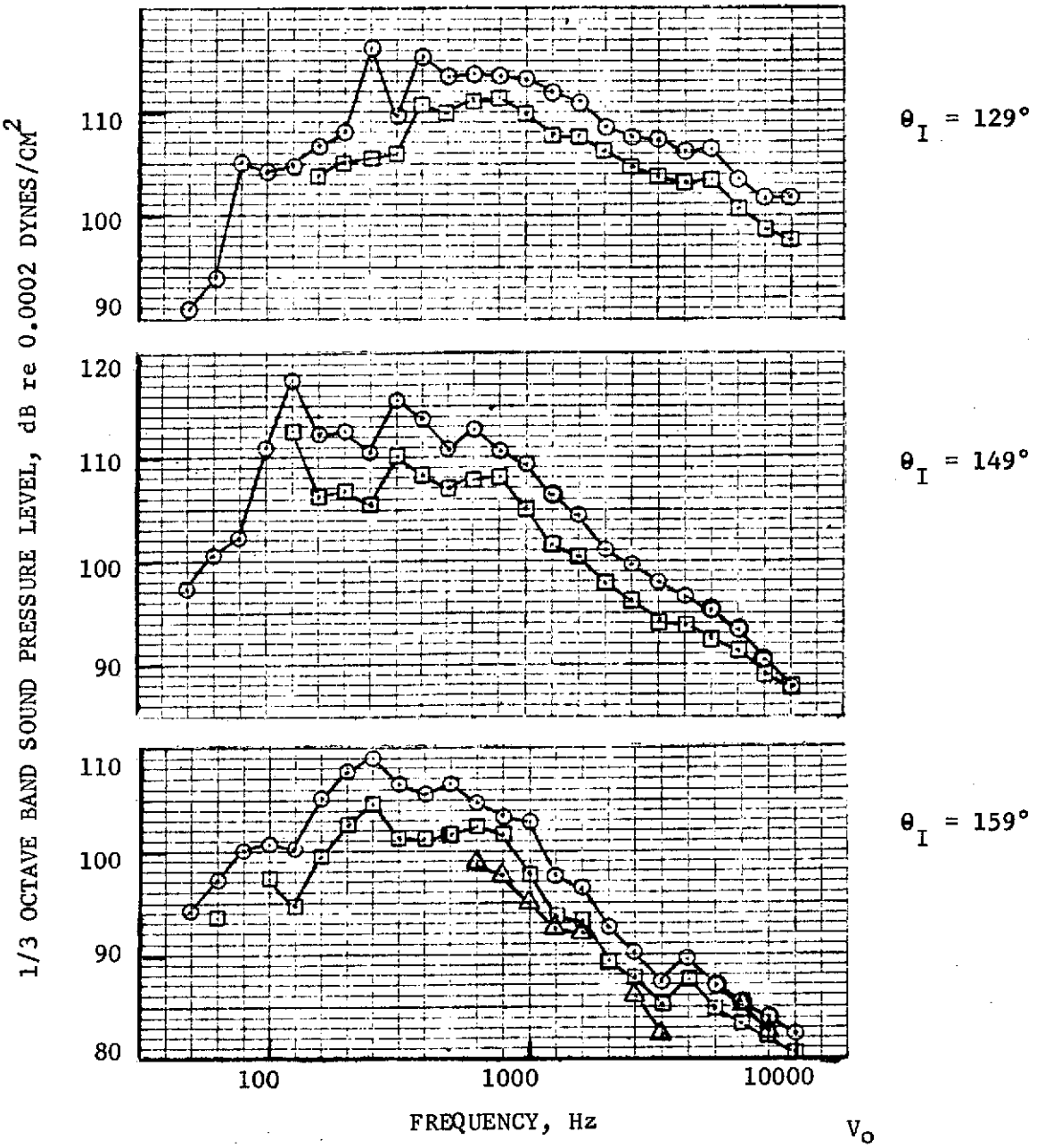

FIGURE 10.68 - ISOLATED NACELLE WIND TUNNEL TEST, 1/3 OCTAVE BAND SPECTRA, AIE NOZZLE

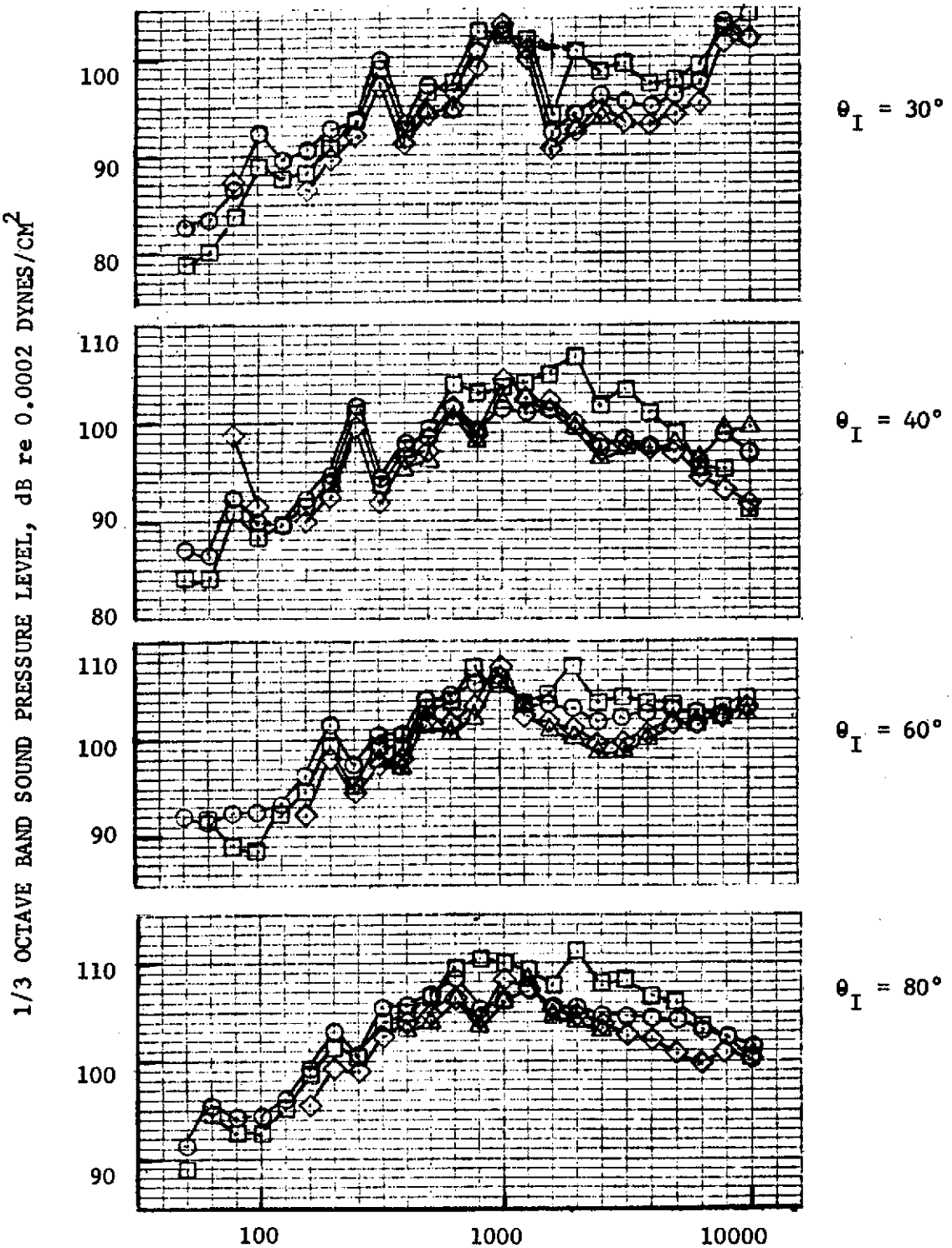

- AIE AUX NOZZLE
- 18 FT. S.L. (5.49 M)
- V_j = 1700 FT/SEC (518 M/SEC)
- 59°F, 70% REL. HUM.

V_o	FT/SEC	M/SEC
○	0	0
□	150	45.7
◇	250	76.2
△	340	103.6

FIGURE 10.69 - ISOLATED NACELLE WIND TUNNEL TEST, 1/3 OCTAVE BAND SPECTRA, AIE NOZZLE

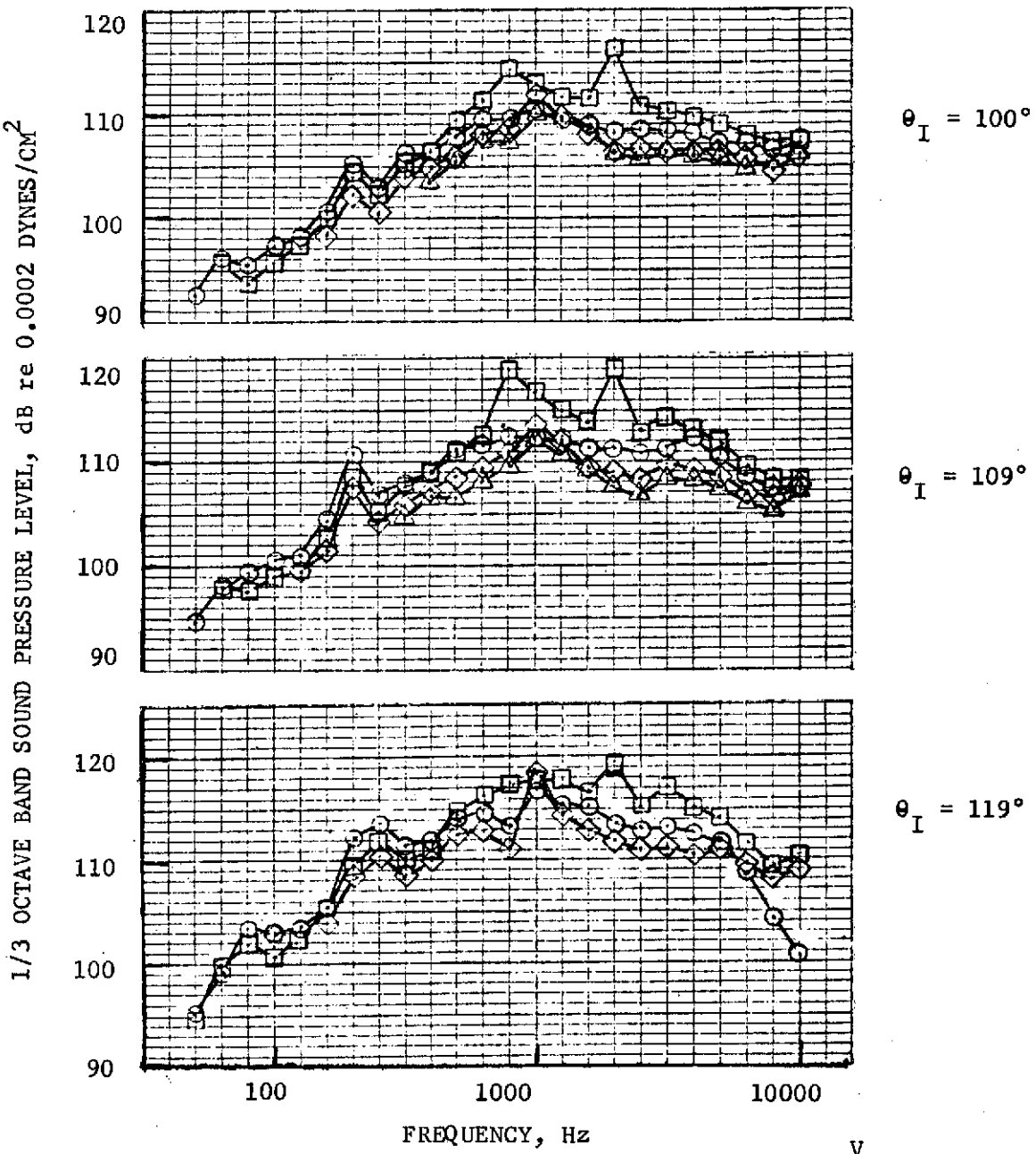

FIGURE 10.70 - ISOLATED NACELLE WIND TUNNEL TEST, 1/3 OCTAVE BAND SPECTRA, AIE NOZZLE

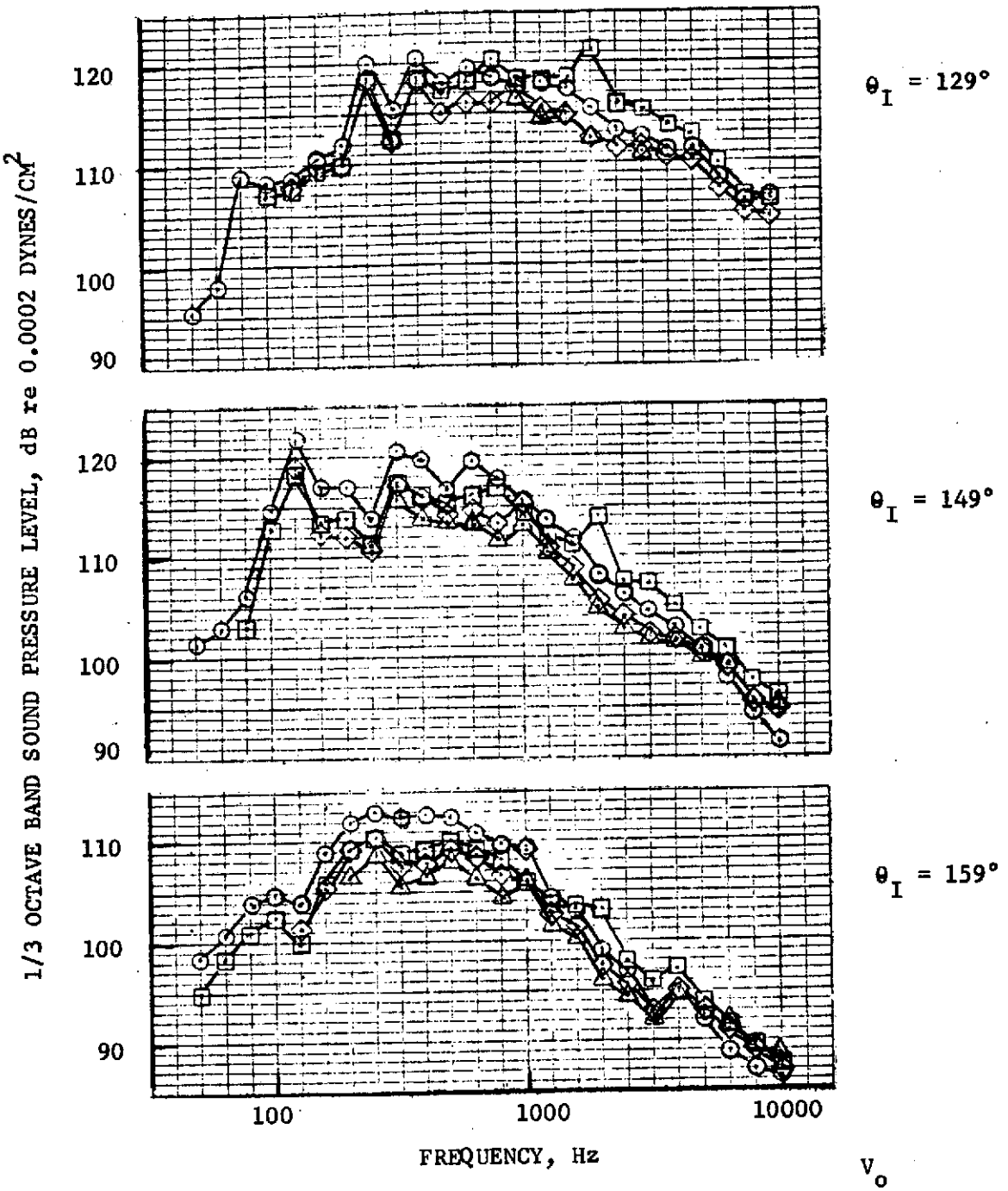

FIGURE 10.71 - ISOLATED NACELLE WIND TUNNEL TEST, 1/3 OCTAVE BAND SPECTRA, AIE NOZZLE

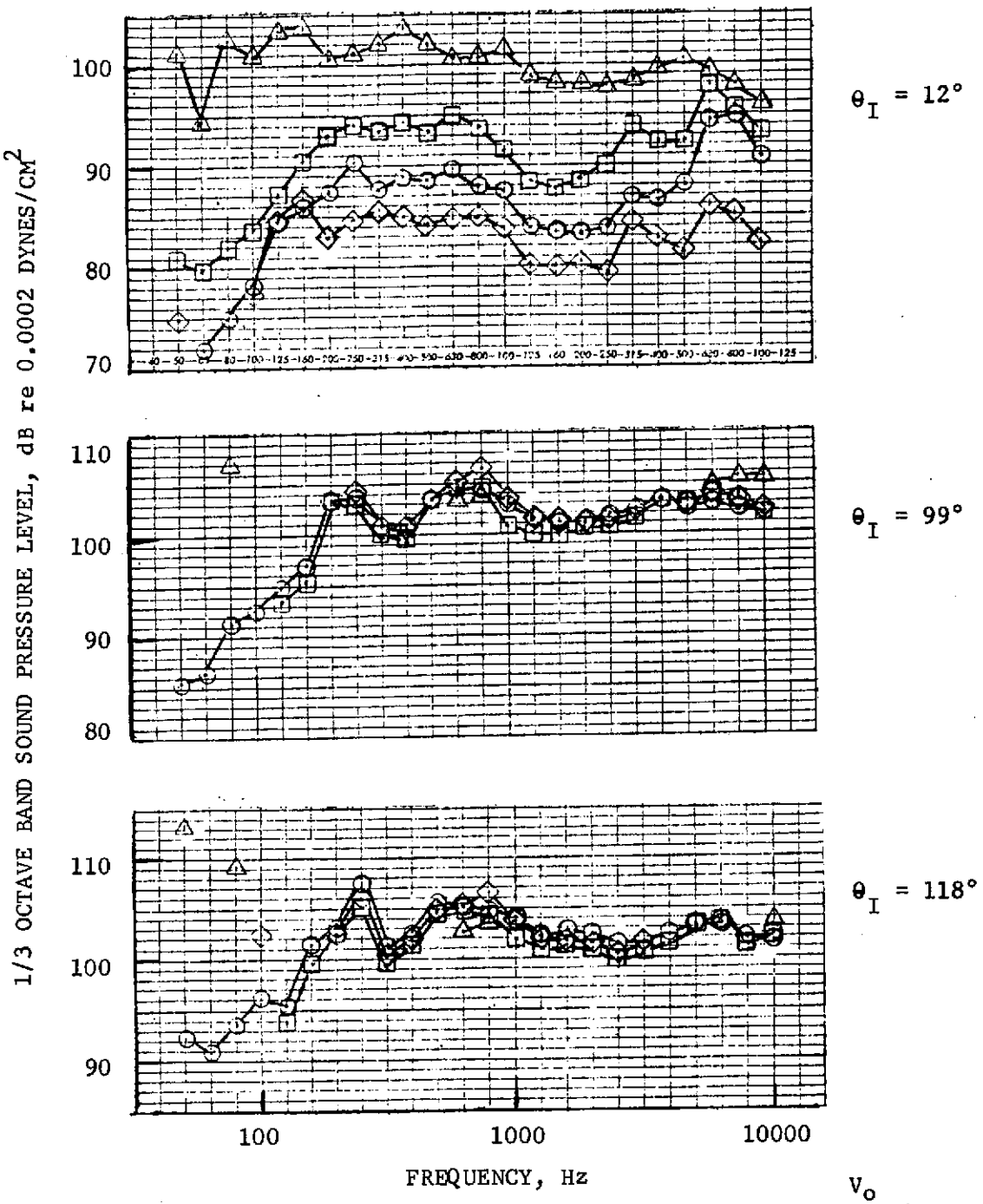

FIGURE 10.72 - ISOLATED NACELLE WIND TUNNEL TEST, 1/3 OCTAVE BAND SPECTRA, AIE NOZZLE

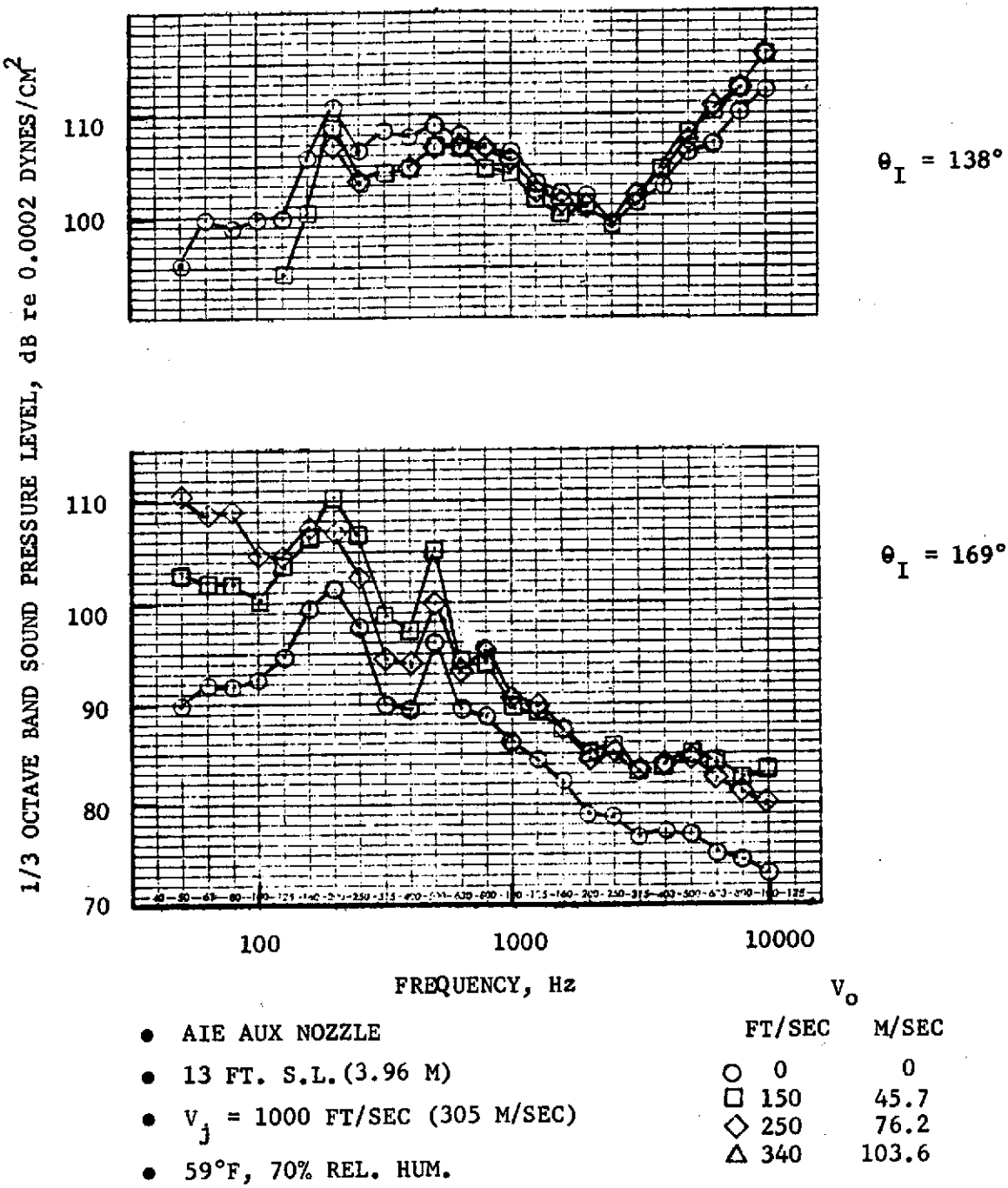

FIGURE 10.73 - ISOLATED NACELLE WIND TUNNEL TEST, 1/3 OCTAVE BAND SPECTRA, AIE NOZZLE

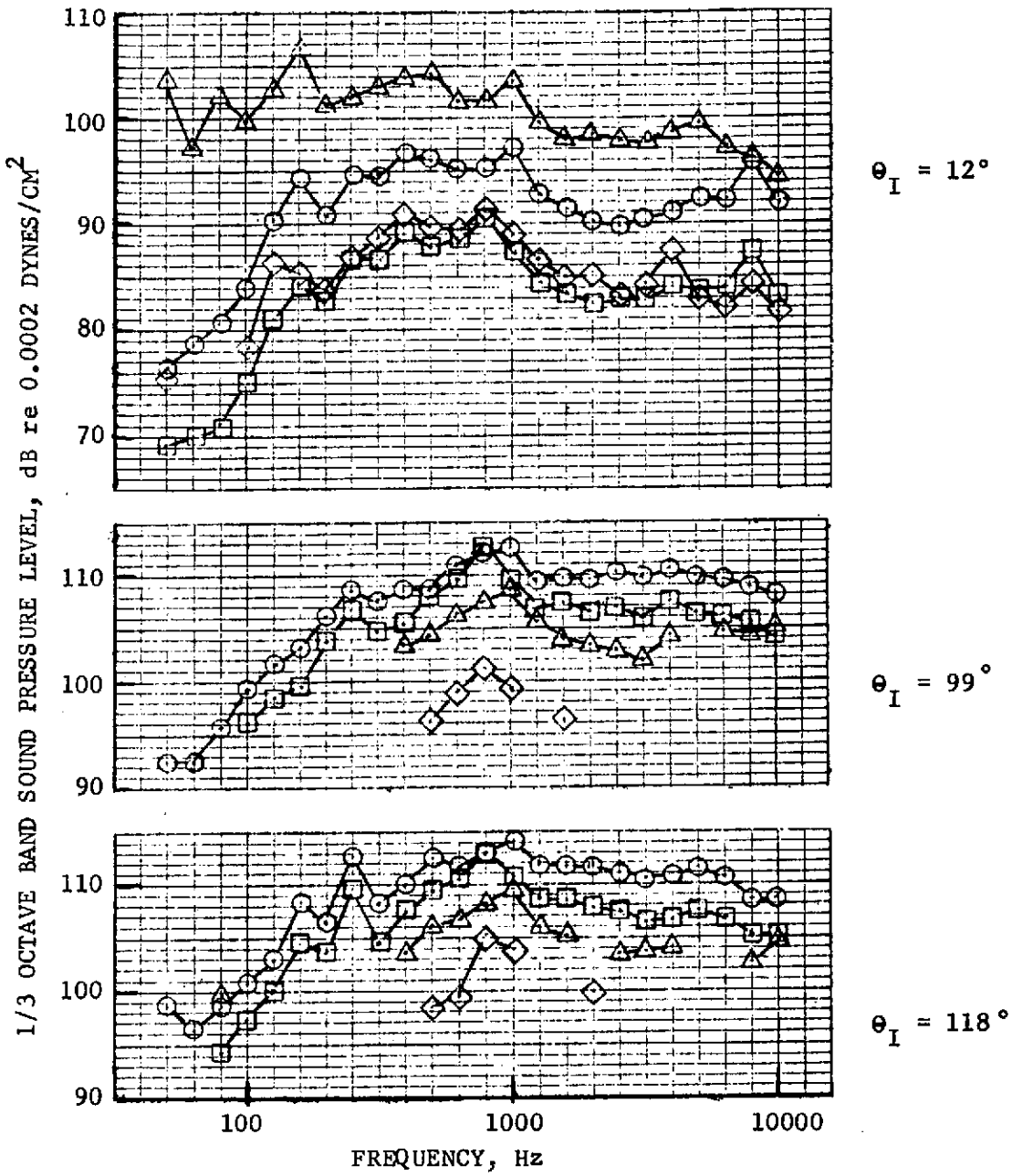

- AIE AUX NOZZLE
- 13 FT. S.L. (3.96 M)
- V_j = 1330 FT/SEC (405 M/SEC)
- 59°F, 70% REL. HUM.

	V_o FT/SEC	V_o M/SEC
○	0	0
□	150	45.7
◇	250	76.2
△	340	103.6

FIGURE 10.74 - ISOLATED NACELLE WIND TUNNEL TEST, 1/3 OCTAVE BAND SPECTRA, AIE NOZZLE

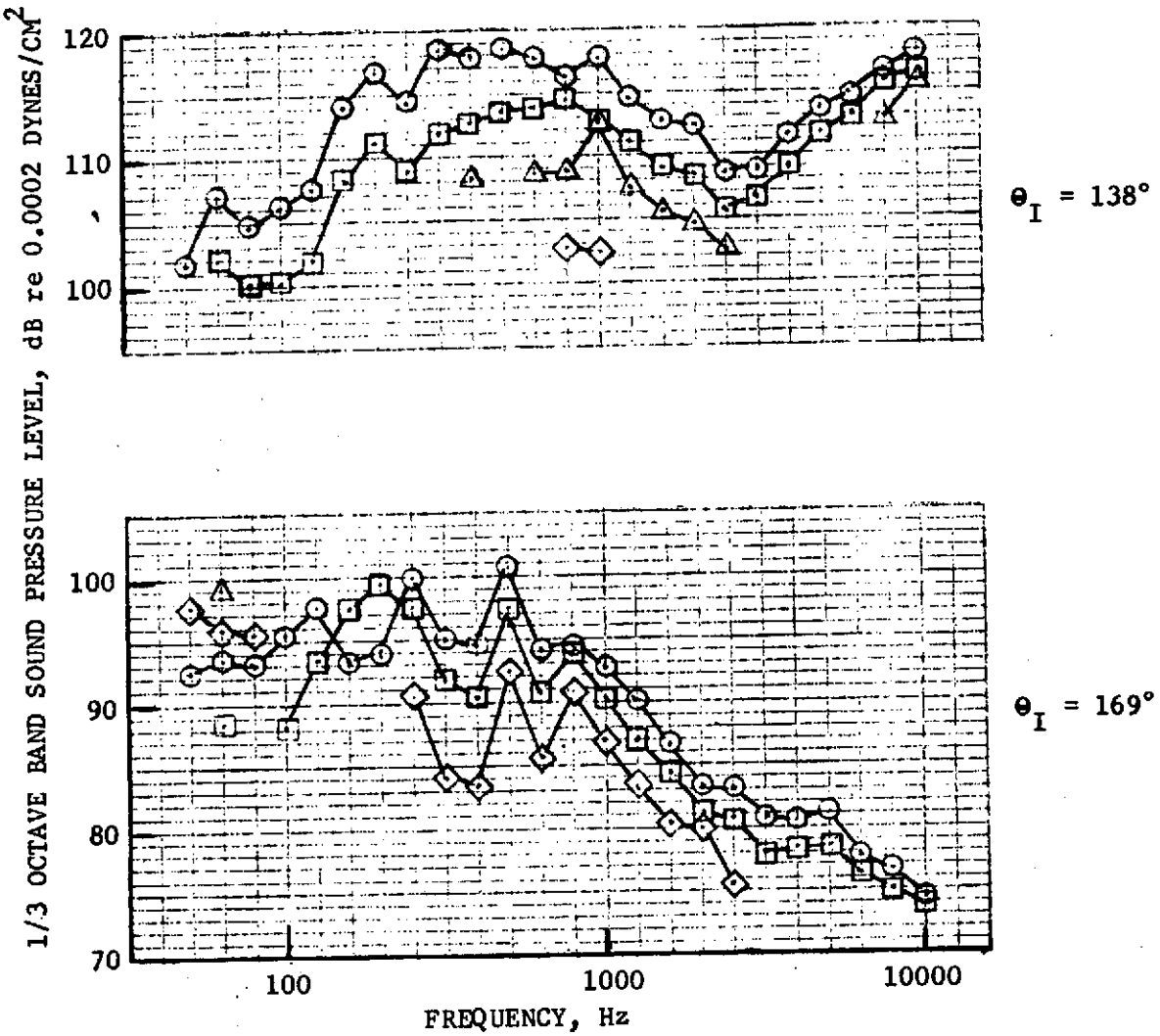

		V_o FT/SEC	V_o M/SEC
o AIE AUX NOZZLE			
o 13 FT. S.L. (3.96 M)	○	0	0
o V_j = 1330 FT/SEC (405 M/SEC)	□	150	45.7
o 59°F, 70% REL. HUM.	◇	250	76.2
	△	340	103.6

FIGURE 10.75 - ISOLATED NACELLE WIND TUNNEL TEST, 1/3 OCTAVE BAND SPECTRA, AIE NOZZLE

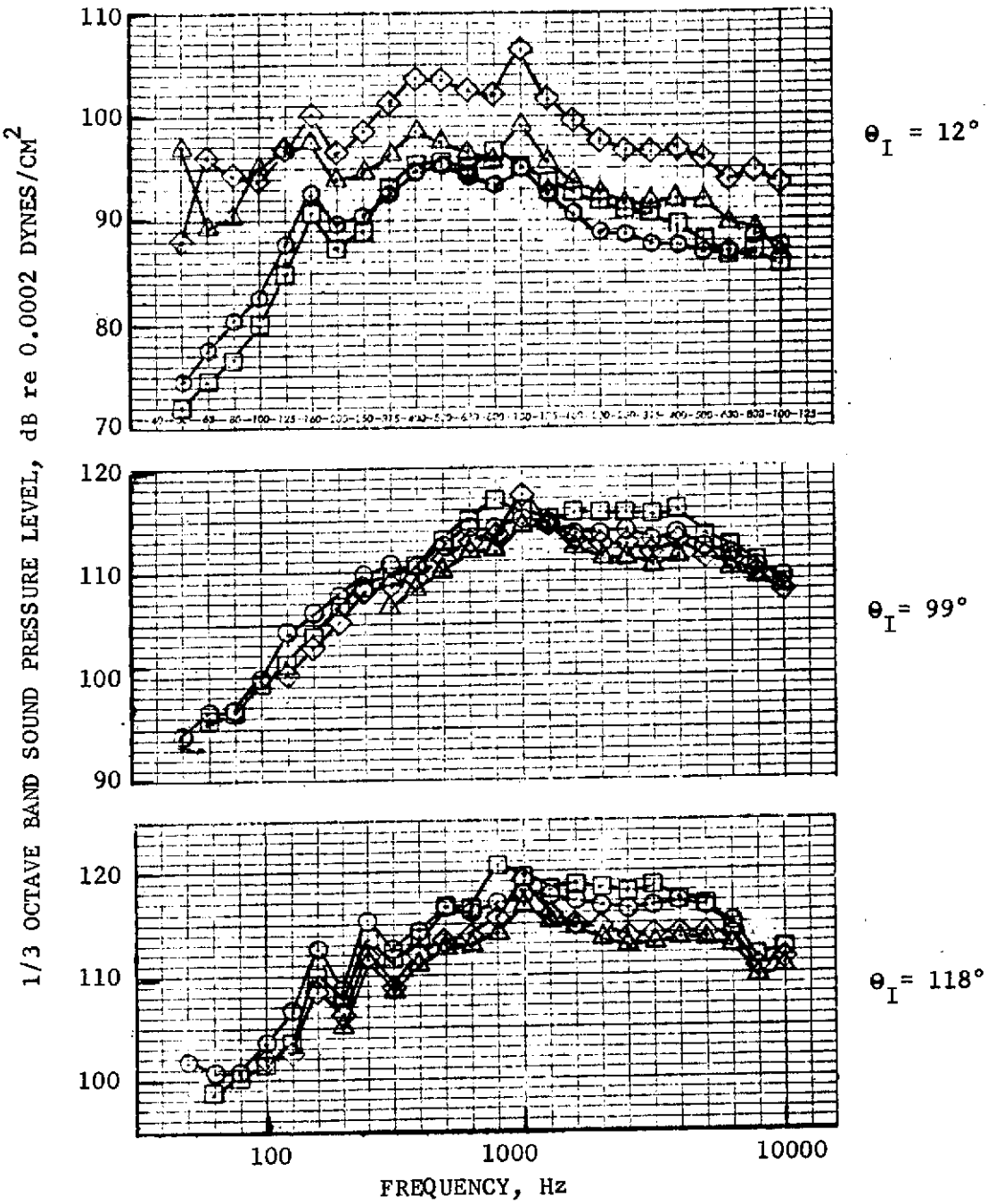

- AIE AUX NOZZLE
- 13 FT. S.L. (3.96 M)
- V_j = 1700 FT/SEC (518 M/SEC)
- 59°F, 70% REL. HUM.

V_o	FT/SEC	M/SEC
○	0	0
□	150	45.7
◇	250	76.2
△	340	103.6

FIGURE 10.76 - ISOLATED NACELLE WIND TUNNEL TEST, 1/3 OCTAVE BAND SPECTRA, AIE NOZZLE

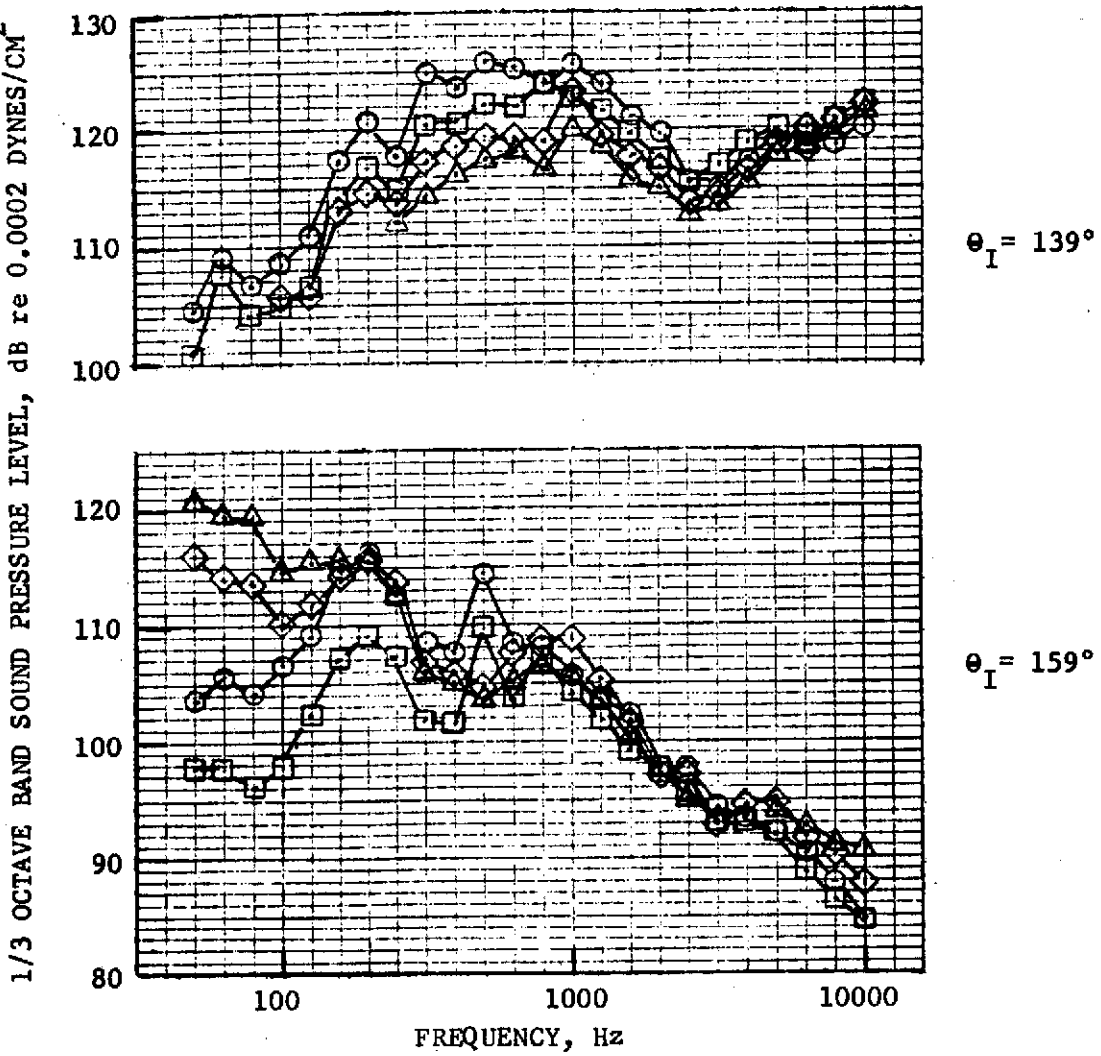

- AIE AUX NOZZLE
- 13 FT. S.L. (3.96 M)
- V_j= 1700 FT/SEC (518 M/SEC)
- 59°F, 70% REL. HUM.

	V_o FT/SEC	V_o M/SEC
○	0	0
□	150	45.7
◇	250	76.2
△	340	103.6

FIGURE 10.77 - ISOLATED NACELLE WIND TUNNEL TEST, 1/3 OCTAVE BAND SPECTRA, AIE NOZZLE

TABLE 10.4

ISOLATED NACELLE WIND TUNNEL TEST

EFFECT OF RELATIVE VELOCITY ON OASPL & PNdB FOR CONICAL EJECTOR AND AIE NOZZLE

V_j = 1235 FT/SEC (376 M/SEC)

ANGLE REF. TO INLET,	V_o		18 FT. SIDELINE (5.49M)						13 FT. SIDELINE (3.96M)					
			CONICAL		AIE		△dB SUPPRESSION*		CONICAL		AIE		△dB SUPPRESSION*	
DEGREES	FPS	MPS	OASPL	PNdB	OASPL	PNdB	OASPL	PNdB	OASPL	PNdB	OASPL	PNdB	OASPL	PNdB
100	0	0	116	128	114	126	2	2	122	134	121	134	1	0
	150	45.7	114	125	113	124	1	1	120	133	119	131	1	2
	250	76.2	112	121	112	122	0	-1	119	130	119	130	0	0
	300	103.6	-	-	-	-	-	-	-	-	-	-	-	-
130 - 140 (PEAK)	0	0	125	134	121	131	4	3	127	136	126	137	1	-1
	150	45.7	119	128	119	128	0	0	125	136	124	134	1	2
	250	76.2	-	-	-	-	-	-	124	134	123	134	1	0
	300	103.6	-	-	-	-	-	-	-	-	-	-	-	-
160	0	0	116	123	113	120	3	3	118	125	116	124	2	1
	150	45.7	112	119	110	117	2	2	117	125	114	122	3	3
	250	76.2	110	116	109	115	1	1	116	123	120	119	-4	4
	300	103.6	-	-	-	-	-	-	-	-	-	-	-	-

* SUPPRESSION OF AIE NOZZLE RELATIVE TO CONICAL EJECTOR NOZZLE

\- BACKGROUND NOISE LEVEL TOO GREAT TO OBTAIN JET NOISE SIGNATURE

TABLE 10.5

ISOLATED NACELLE WIND TUNNEL TEST

EFFECT OF RELATIVE VELOCITY ON OASPL & PNdB FOR CONICAL EJECTOR AND AIE NOZZLE

V_j = 1700 FT/SEC (518 M/SEC)

ANGLE REF. TO INLET,	V_o		18 FT. SIDELINE (5.49M)						13 FT. SIDELINE (3.96M)					
			CONICAL		AIE		Δ dB SUPPRESSION*		CONICAL		AIE		Δ dB SUPPRESSION*	
DEGREES	FPS	MPS	OASPL	PNdB	OASPL	PNdB	OASPL	PNdB	OASPL	PNdB	OASPL	PNdB	OASPL	PNdB
100	0	0	123	135	122	133	1	2	127	140	126	137	1	3
	150	45.7	120	133	123	136	-3	-3	125	139	127	140	-2	-1
	250	76.2	120	132	120	131	0	1	124	138	124	137	0	1
	300	103.6	117	129	119	130	-2	-1	122	135	123	134	-1	1
130 - 140 (PEAK)	0	0	132	141	125	139	7	2	137	146	135	144	2	2
	150	45.7	128	139	130	141	-2	-2	133	145	133	144	0	1
	250	76.2	-	-	127	137	-	-	133	144	131	143	2	1
	300	103.6	-	-	-	-	-	-	130	142	130	141	0	1
160	0	0	123	130	123	129	0	1	125	133	127	134	-2	-1
	150	45.7	120	128	119	128	1	0	125	135	122	134	3	1
	250	76.2	120	127	118	125	2	2	125	133	127	134	-2	-1
	300	103.6	117	124	116	123	1	1	120	127	128	130	-8	-3

* SUPPRESSION OF AIE NOZZLE RELATIVE TO CONICAL EJECTOR NOZZLE

\- BACKGROUND NOISE LEVEL TOO GREAT TO OBTAIN JET NOISE SIGNATURE

TABLE 10.6

ISOLATED NACELLE WIND TUNNEL TEST

1/3 OCTAVE BAND SOUND PRESSURE LEVELS

V_j = 1330 FT/SEC
(405 M/SEC)

ANGLE REF. TO INLET, DEGREES	V_o FT/SEC	V_o M/SEC	250 Hz						500 Hz						1000 Hz						4000 Hz					
			18' S.L. (5.49M)			13' S.L. (3.96M)			18' S.L. (5.49M)			13' S.L. (3.96M)			18' S.L. (5.49M)			13' S.L. (3.96M)			18' S.L. (5.49M)			13' S.L. (3.96M)		
			CON.	AIE	ΔdB SUPP.	CON.	AIE	ΔdB SUPP.	CON.	AIE	ΔdB SUPP.	CON.	AIE	ΔdB SUPP.	CON.	AIE	dB SUPP.	CON.	AIE	ΔdB SUPP.	CON.	AIE	ΔdB SUPP.	CON.	AIE	ΔdB SUPP.
100	0	0	99.0	99.5	-0.5	107.0	109.0	-2.0	104.5	104.0	0.5	109.0	109.0	0	105.0	106.5	-1.5	110.0	112.5	-2.5	102.5	103.0	-0.5	109.0	110.5	-1.5
	150	45.7	98.5	98.0	0.5	107.0	107.0	0	103.0	101.5	1.5	109.5	108.0	1.5	103.0	104.0	-1.0	110.0	110.0	0	100.5	100.0	0.5	109.0	107.5	1.5
	250	76.2	93.5	97.0	-3.5	104.0	-	-	100.0	102.5	-2.5	106.5	106.0	0.5	101.0	107.0	-6.0	108.5	109.0	-0.5	99.0	101.5	-2.5	107.0	104.5	2.5
	340	103.6	-	-	-	-	-	-	99.5	-	-	104.5	104.0	-0.5	101.0	104.0	-3.0	105.5	109.0	-3.5	-	-	-	-	-	-
120	0	0	111.0	110.0	1.0	111.5	108.0	3.5	110.5	110.0	0.5	112.5	112.5	0	112.0	113.0	-1.0	113.0	114.0	-1.0	107.0	107.5	-0.5	110.5	111.0	-0.5
	150	45.7	105.0	108.0	-3.0	110.0	110.0	0	-	108.0	-	111.5	109.5	2.0	-	108.5	-	112.0	111.0	1.0	-	104.5	-	107.0	106.5	0.5
	250	76.2	-	107.0	-	106.0	-	-	107.0	109.0	-2.0	108.0	109.0	-1.0	108.5	109.5	-1.0	109.0	114.0	-5.0	104.0	105.5	-1.5	107.0	-	-
	340	103.6	-	-	-	-	-	-	105.5	-	-	107.0	106.0	1.0	107.0	-	-	107.7	110.0	-3.0	-	-	-	103.5	104.0	-0.5
130	0	0	116.0	116.0	0				115.5	113.5	2.0				112.5	113.0	-0.5				105.0	106.0	-1.0			
	150	45.7	111.0	106.0	5.0				111.0	110.0	1.0				109.5	110.0	-0.5				104.0	103.0	1.0			
	250	76.2	-	-	-				-	-	-				-	-	-				-	-	-			
	340	103.6	-	-	-				-	-	-				-	-	-				-	-	-			
140	0	0				114.0	114.5	-0.5				119.5	118.5	1.0				118.0	117.5	0.5				107.5	111.5	-4.0
	150	45.7				110.0	109.0	1.0				115.5	114.0	1.5				115.0	113.0	2.0				112.0	109.0	3.0
	250	76.2				107.0	-	-				113.0	-	-				113.0	113.0	0				111.5	-	-
	340	103.6				-	-	-				110.0	-	-				110.0	112.5	-2.5				-	-	-

NOTE: SUPPRESSION IS RELATIVE TO CONICAL EJECTOR NOZZLE

- BACKGROUND NOISE LEVEL TOO GREAT TO OBTAIN JET NOISE SIGNATURE

TABLE 10.7

ISOLATED NACELLE WIND TUNNEL TEST

1/3 OCTAVE BAND SOUND PRESSURE LEVELS

V_j = 1700 FT/SEC
(518 M/SEC)

ANGLE REF. TO INLET, DEG.	V_o, FT/SEC	V_o, M/SEC	250 Hz						500 Hz						1000 Hz						4000 Hz					
			18' S.L.(5.49M)			13' S.L.(3.96M)			18' S.L.(5.49M)			13' S.L.(3.96M)			18' S.L.(5.49M)			13' S.L.(3.96M)			18' S.L.(5.49M)			13' S.L.(3.96M)		
			CON.	AIE	ΔdB SUPP.	CON.	AIE	ΔdB SUPP.	CON.	AIE	ΔdB SUPP.	CON.	AIE	ΔdB SUPP.	CON.	AIE	ΔdB SUPP.	CON.	AIE	ΔdB SUPP.	CON.	AIE	ΔdB SUPP.	CON.	AIE	ΔdB SUPP.
100	0	0	104.5	103.0	1.5	109.5	110.0	-0.5	110.5	107.5	3.0	113.5	112.5	1.0	111.5	110.5	1.0	114.5	115.0	-0.5	110.5	108.0	2.5	116.0	113.5	2.5
	150	45.7	100.5	102.0	-1.5	108.5	108.5	0	107.5	109.5	-2.0	112.0	113.0	-1.0	108.5	113.0	-4.5	113.5	116.0	-2.5	107.5	109.5	-2.0	114.5	116.0	-1.5
	250	76.2	101.5	100.5	1.0	107.5	108.5	-1.0	107.5	106.0	1.5	111.0	111.0	0	109.5	112.0	2.5	113.0	117.0	-4.0	108.5	106.5	2.0	114.5	113.0	1.5
	340	103.6	-	-	-	104.5	-	-	104.0	105.5	-1.5	109.5	110.0	-0.5	106.0	110.0	-4.0	111.0	114.5	-3.5	105.0	106.0	-1.0	111.0	111.5	-0.5
120	0	0	114.5	114.0	0.5	115.5	115.5	0	116.5	114.0	2.5	118.0	116.5	1.5	118.5	116.5	2.0	119.5	118.0	1.5	115.5	112.5	3.0	119.0	117.0	2.0
	150	45.7	-	112.0	-	113.0	113.5	-0.5	-	115.0	-	115.5	116.5	-1.0	-	118.0	-	116.5	119.5	-3.0	-	115.0	-	115.0	117.0	-2.0
	250	76.2	112.5	109.5	3.0	112.5	112.0	0.5	114.0	112.5	1.5	115.0	113.0	2.0	115.0	118.5	-3.5	116.0	119.0	-3.0	113.0	110.5	2.5	116.0	114.0	2.0
	340	103.6	110.0	-	-	109.0	111.5	-2.5	111.0	-	-	111.5	113.0	-1.5	112.5	-	-	113.0	117.0	-4.0	110.0	-	-	112.5	113.5	-1.0
130	0	0	122.0	120.0	2.0				121.5	118.0	3.5				121.0	117.5	3.5				114.0	111.5	2.5			
	150	45.7	117.0	118.5	-1.5				116.5	117.0	-0.5				116.5	118.5	-2.0				111.0	113.5	-2.5			
	250	76.2	-	118.5	-				-	115.0	-				-	117.5	-				-	110.5	-			
	340	103.6	-	-	-				-	-	-				-	116.5	-				-	-	-			
140	0	0				120.0	117.5	2.5				128.5	126.0	2.5				129.0	126.0	3.0				119.0	117.5	1.5
	150	45.7				115.0	115.0	0				123.0	122.0	1.0				122.5	123.0	-0.5				118.5	119.5	-1.0
	250	76.2				115.0	113.5	1.5				122.0	119.5	2.5				122.0	123.5	-1.5				118.5	116.5	2.0
	340	103.6				110.5	112.0	-1.5				117.5	117.0	0.5				118.5	120.0	-1.5				117.0	115.5	1.5

NOTE: SUPPRESSION IS RELATIVE TO CONICAL EJECTOR NOZZLE

- BACKGROUND NOISE LEVEL TOO GREAT TO OBTAIN JET NOISE SIGNATURE

10.1.3.2 Wing/Nacelle Wind Tunnel Test

The acoustsic data measured during the wing/nacelle wind tunnel test were analyzed and compared for the conical ejector nozzle and the 104 tube nozzle with and without an acoustically treated shroud. The data were measured using a 3.96 meter (13 foot) sideline microphone array in the NASA/ Ames 40 by 80 - Foot Wind Tunnel. The material is presented in the same manner as in Section 10.1.3.1.

Presented on Figure 10.78 are peak overall sound pressure levels as a function of jet velocity for three freestream velocities. These peaks occurred between 130-150 degrees, depending upon the nozzle. A comparison of how the freestream velocity affects the suppression characteristics of the 104 tube nozzle configurations relative to the conical nozzle is presented below:

V_j FPS (MPS)	V_o FPS, MPS	Conical	104 Tube w/o Shroud	104 Tube w/Shroud	Δ dB_1* Suppression	Δ dB_2** Suppression
1500 (457)	0,0	132	123	118.5	9	4.5
	170,51.8	129.5	121	117	8.5	4
	250,76.2	127	118	---	9	---
	300,91.4	124	116	112	8	4
2000 (610)	0,0	139	128	124	11	4
	170,51.8	137	126	121	11	5
	250,76.2	135	123	---	12	---
	300,91.4	135	122	116	13	6

*Suppression of 104 tube nozzle w/o shroud relative to conical nozzle.
**Suppression of 104 tube nozzle w/shroud relative to 104 tube nozzle w/o shroud.

From this table, the following results can be stated:

- For all nozzle configurations at both jet velocities, peak OASPL decreases as freestream velocity increases.
- The amount of suppression is essentially unaffected by forward flight speed.

- The 104 tube nozzle is most effective at the highest jet velocity. The average amount of suppression of the 104 tube nozzle without the shroud relative to the conical nozzle is 8.5 dB and 12 dB for jet velocities of 458 m/sec (1500 ft/sec) and 610 m/sec (2000 ft/sec), respectively.
- The acoustically treated shroud provided an additional 4-6 db of suppression depending on the jet velocity and was essentially unaffected by freestream velocity.

Presented on Figures 10.79 and 10.84 are the OASPL and PNL directivity patterns for the three configurations. As in the isolated nacelle wind tunnel test, several spectra are only defined by a limited number of one-third octave band SPL's at various microphone locations and engine power settings. This is because of the background noise at the high freestream velocities. To correct for this effect the same criteria that was used for the isolated nacelle wind tunnel test was instituted. To compliment the figures and further illustrate the effects of freestream velocity, Tables 10.8 and 10.9 are presented.

Summarized on these tables are the OASPL and PNL values at five acoustic angles. Using the figures and tables as a basis, the following conclusions may be drawn.

- The 104 tube nozzle without the acoustically treated shroud is most effective at the angle of peak noise generation. For example, at a jet velocity of 580 m/sec (1900 ft/sec) and on a basis of PNL, 12 dB suppression occurs at 147 degrees while only 5 dB suppression occurs at 101 degrees.
- The addition of the acoustically treated shroud causes an additional 6 dB suppression on the basis of PNL. This additional suppression is not a strong function of acoustic angle.
- As the freestream velocity increases, the amount of suppression remains essentially constant at all acoustic angles.

One irregularity that stands out in the directivity patterns is a high OASPL and PNL value that occurs at 90 degrees for the 104 tube nozzle without the shroud. This can be explained by considering the double peak phenomenon that occurs in the spectra plots of the 104 tube nozzle. One of the peaks occurs at low frequency and the other at high frequencies. At angles of other than 90 degrees, the one-third octave band sound pressure levels at the low frequencies were contaminated by the background noise and did not occur in the corrected spectra. At the 90 degree angle, the background noise did not contaminate the low frequency portion of the spectra to the extent required to delete them from the corrected spectra. Consequently, in this case, a large change was observed in the OASPL and PNL values.

This problem must be considered when analyzing the wind tunnel data. The problem is encountered at the select condition of high freestream velocity and low jet velocity as well as for high suppression nozzles. To assure that the trends predicted by the preceding analysis are valid, one-third octave band sound pressure spectra were also analyzed.

Presented on Figures 10.85 through 10.102 are the spectra for the three configurations. Note that all data presented have been corrected for background noise and reverberation effects.

To illustrate salient points, four representative frequencies were selected and tabulated in Table 10.10 for the three nozzles and two jet velocities. In studying the illustrations, note the following:

- The suppression level remains essentially constant as the freestream velocity increases.
- Maximum 1/3 OBSPL suppression occurs in the 500-1000 Hz bands.
- The addition of the acoustically treated shroud affects the high frequency portion of the spectra and has minimal effect on the low frequency portion of the spectra.
- For freestream velocities greater than 52 m/sec (170 ft/sec) the background noise masks the low frequency portion of the spectra even at a jet velocity of 580 m/sec (1900 ft/sec).

In summary, a reduction in the noise signature of a complex suppressor nozzle due to an increase in freestream velocity has been measured. The magnitude of the wind tunnel background noise has been shown to have a significant effect in determining at what freestream velocities this effect can be measured.

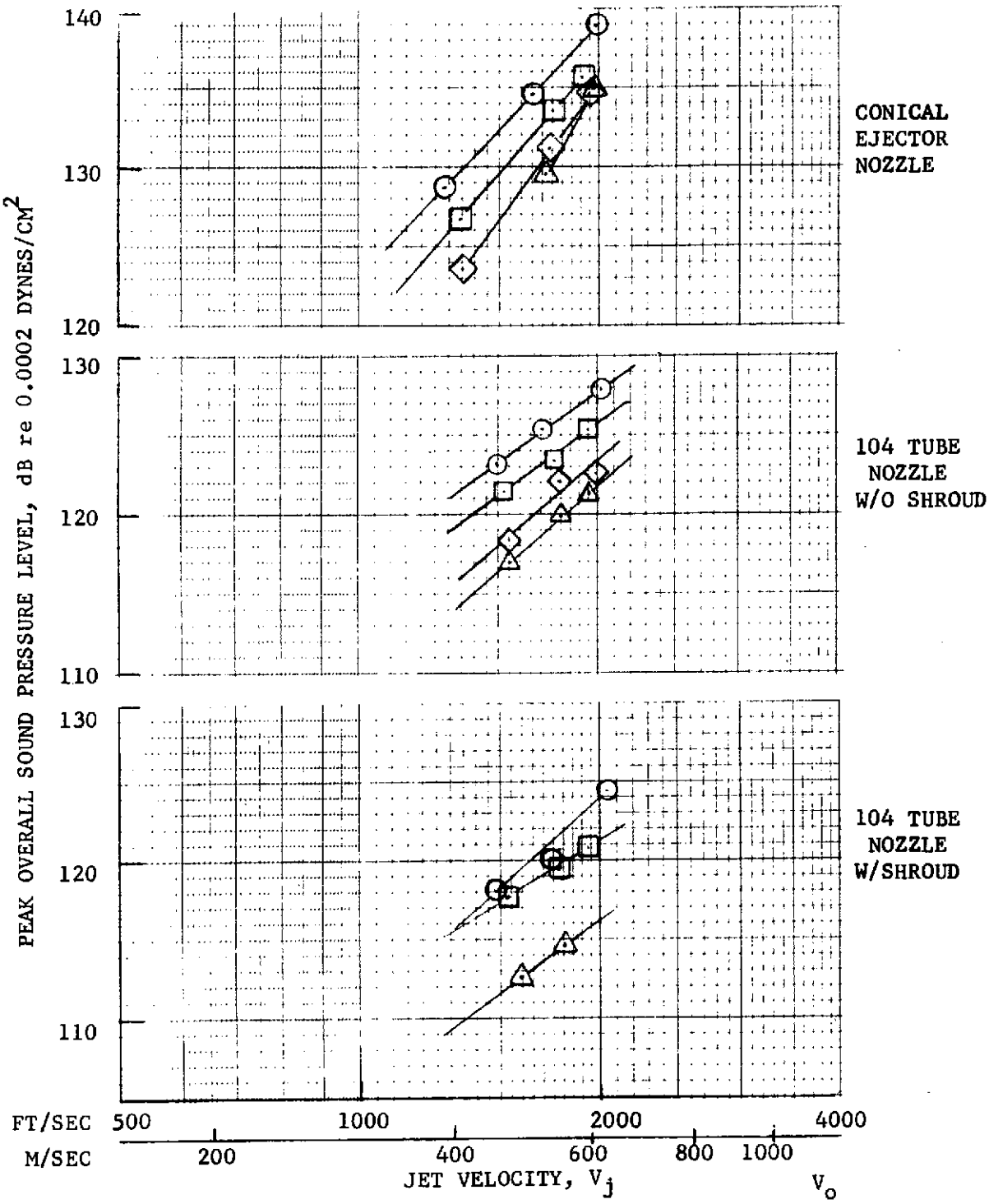

FIGURE 10.78 - WING NACELLE WIND TUNNEL TEST, PEAK OASPL VS V_J, CONICAL EJECTOR AND 104-TUBE NOZZLE WITH AND WITHOUT SHROUD

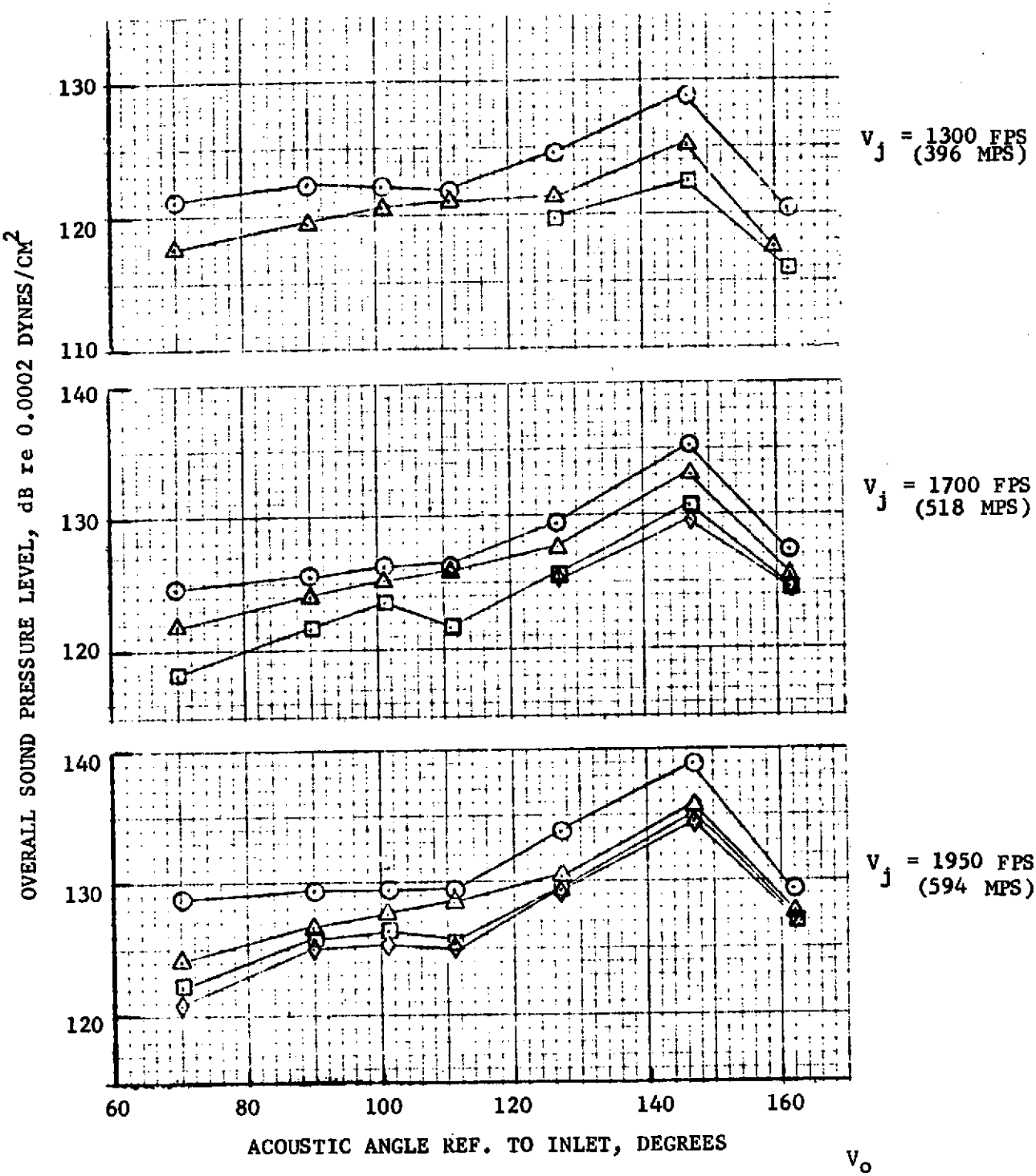

- CONICAL EJECTOR NOZZLE
- 13 FT. S.L. (3.96 M)
- 59°F, 70% REL. HUM.

V_o FT/SEC	V_o M/SEC
○ 0	0
△ 170	51.8
□ 250	76.2
◇ 300	91.4

FIGURE 10.79 - WING NACELLE WIND TUNNEL TEST, OASPL DIRECTIVITY, CONICAL EJECTOR NOZZLE

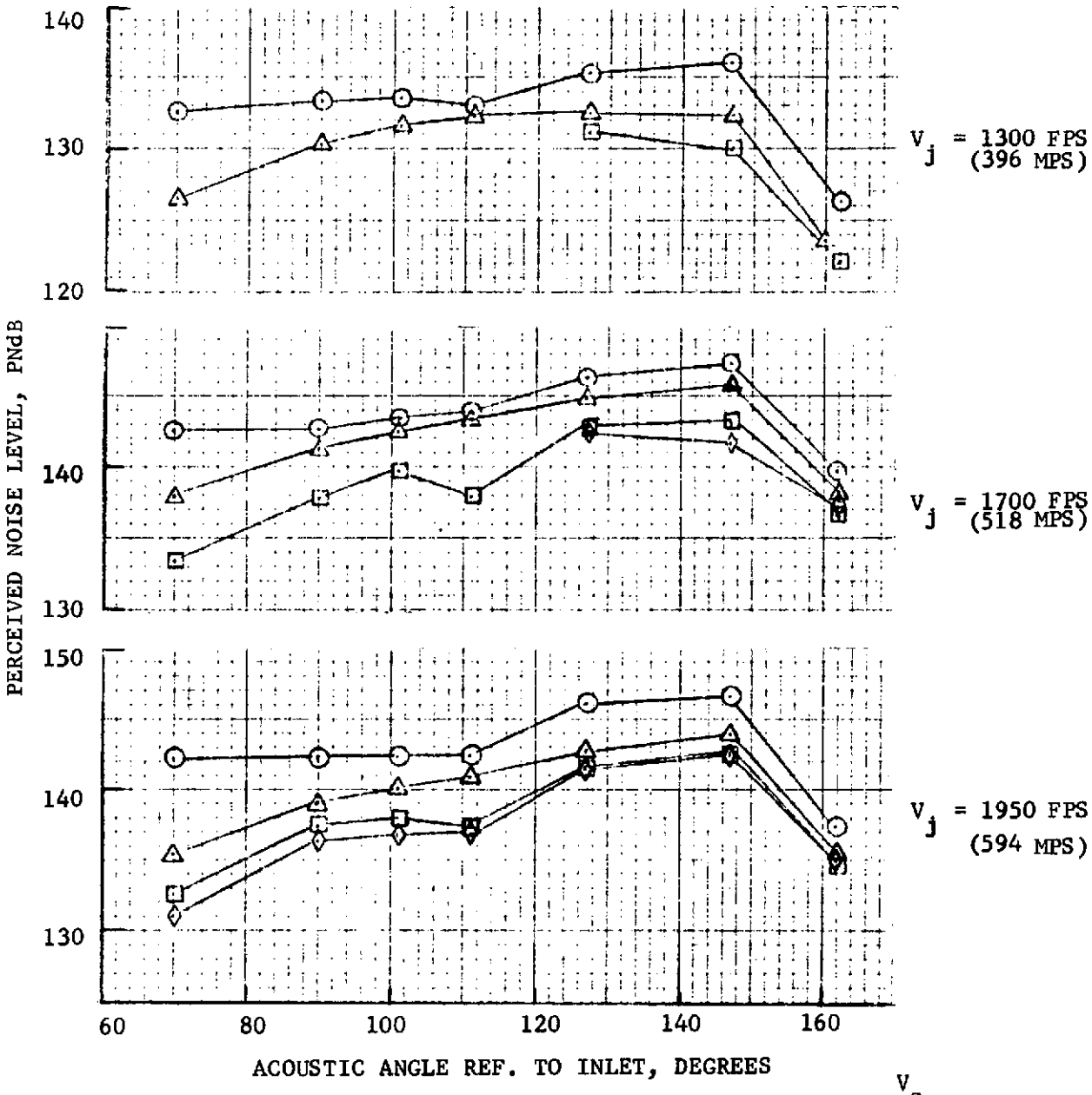

- CONICAL EJECTOR NOZZLE
- 13 FT. S.L. (3.96 M)
- 59°F, 70% REL. HUM.

	V_o FT/SEC	M/SEC
○	0	0
△	170	51.8
□	250	76.2
◊	300	91.4

FIGURE 10.80 - WING NACELLE WIND TUNNEL TEST, PNdB DIRECTIVITY, CONICAL EJECTOR NOZZLE

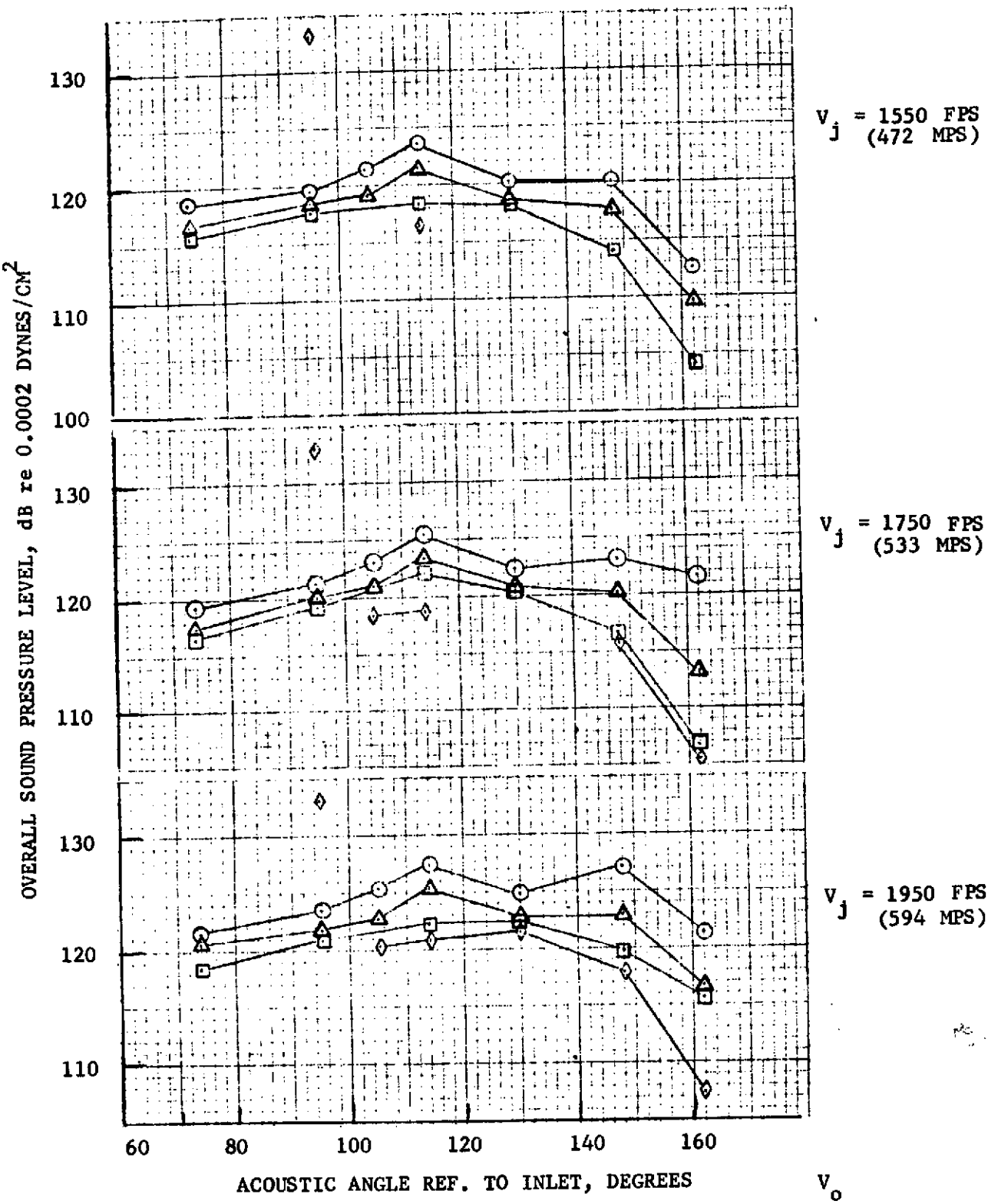

- 104 TUBE NOZZLE W/O SHROUD
- 13 FT. S.L. (3.96 M)
- 59°F, 70% REL. HUM.

V_o FT/SEC	M/SEC
○ 0	0
△ 170	51.8
□ 250	76.2
◊ 300	91.4

FIGURE 10.81 - WING NACELLE WIND TUNNEL TEST, OASPL DIRECTIVITY, 104-TUBE NOZZLE W/O SHROUD

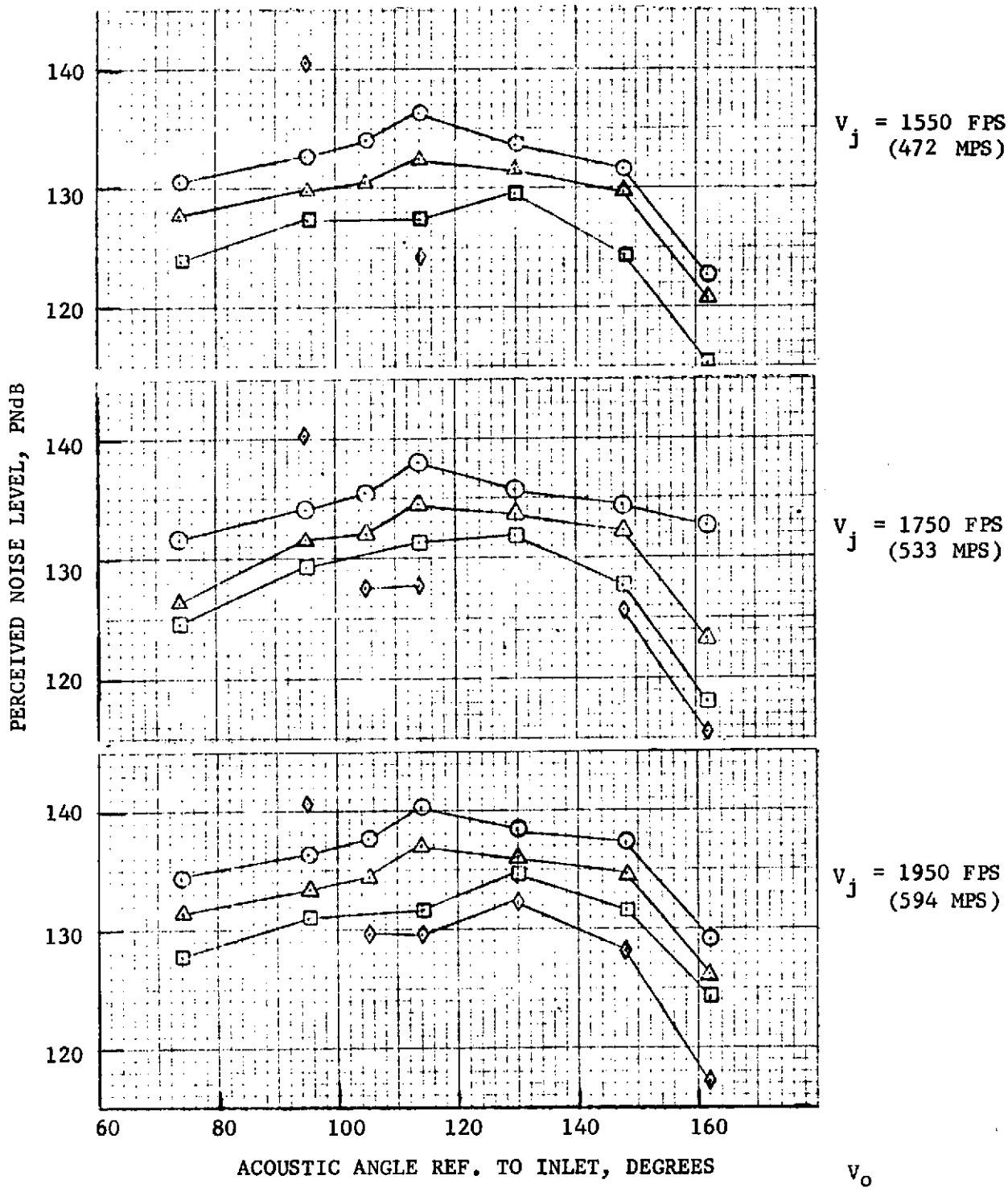

- 104 TUBE NOZZLE W/O SHROUD
- 13 FT. S.L. (3.96 M)
- 59°F, 70% REL. HUM.

FIGURE 10.82 - WING NACELLE WIND TUNNEL TEST, PNdB DIRECTIVITY, 104-TUBE NOZZLE W/O SHROUD

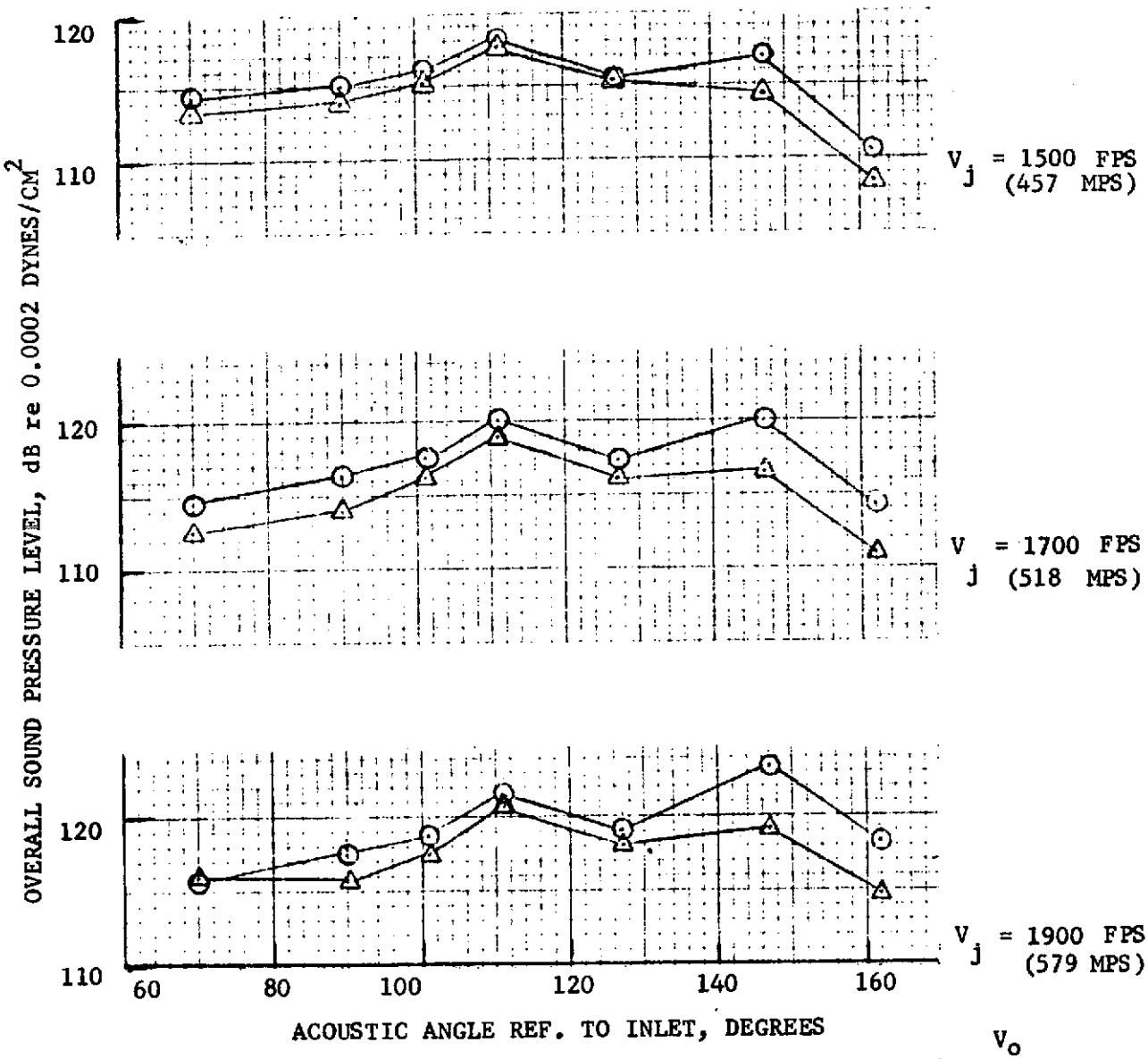

FIGURE 10.83 - WING NACELLE WIND TUNNEL TEST, OASPL DIRECTIVITY, 104-TUBE NOZZLE WITH SHROUD

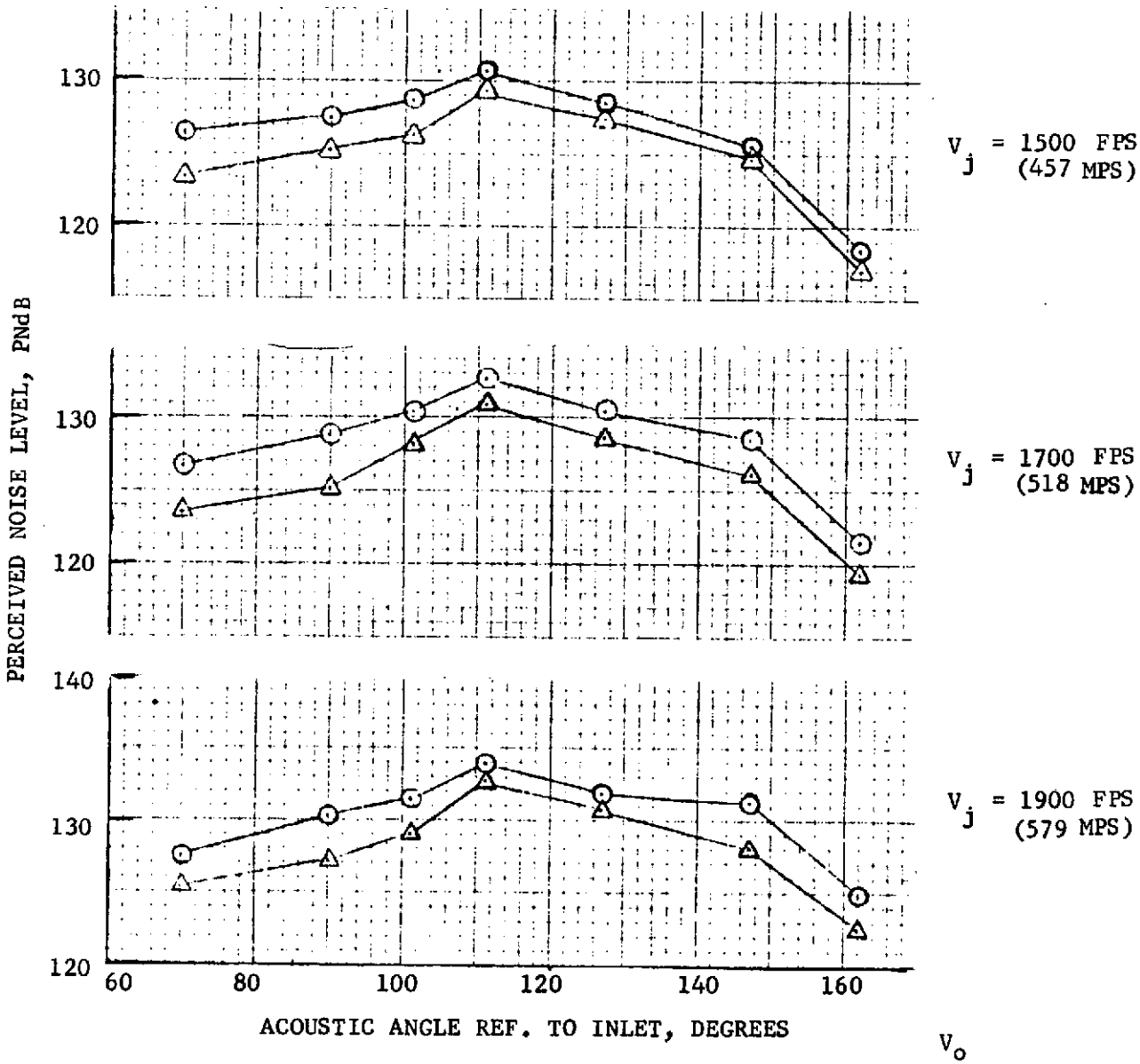

- 104 TUBE NOZZLE W/SHROUD
- 13 FT. S.L. (3.96 M)
- 59°F, 70% REL. HUM.

V_o	FT/SEC	M/SEC
○	0	0
△	170	51.8

FIGURE 10.84 - WING NACELLE WIND TUNNEL TEST, PNdB DIRECTIVITY, 104-TUBE NOZZLE WITH SHROUD

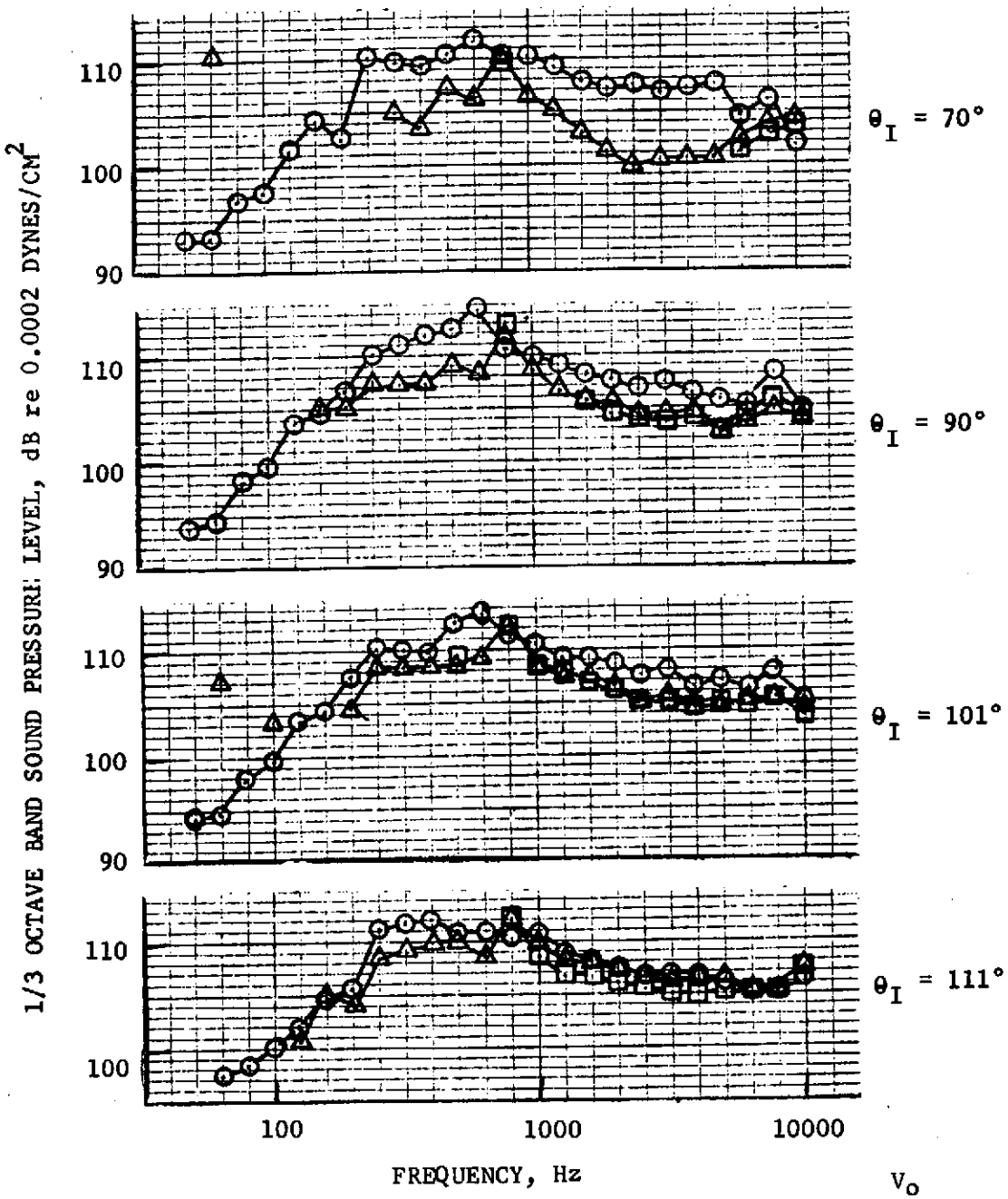

- CONICAL EJECTOR NOZZLE
- 13 FT. S.L. (3.96 M)
- V_j = 1300 FT/SEC (396 M/SEC)
- 59°F, 70% REL. HUM.

V_o	FT/SEC	M/SEC
○	0	0
△	170	51.8
□	250	76.2

FIGURE 10.85 - WING NACELLE WIND TUNNEL TEST, 1/3 OCTAVE BAND SPECTRA, CONICAL EJECTOR NOZZLE

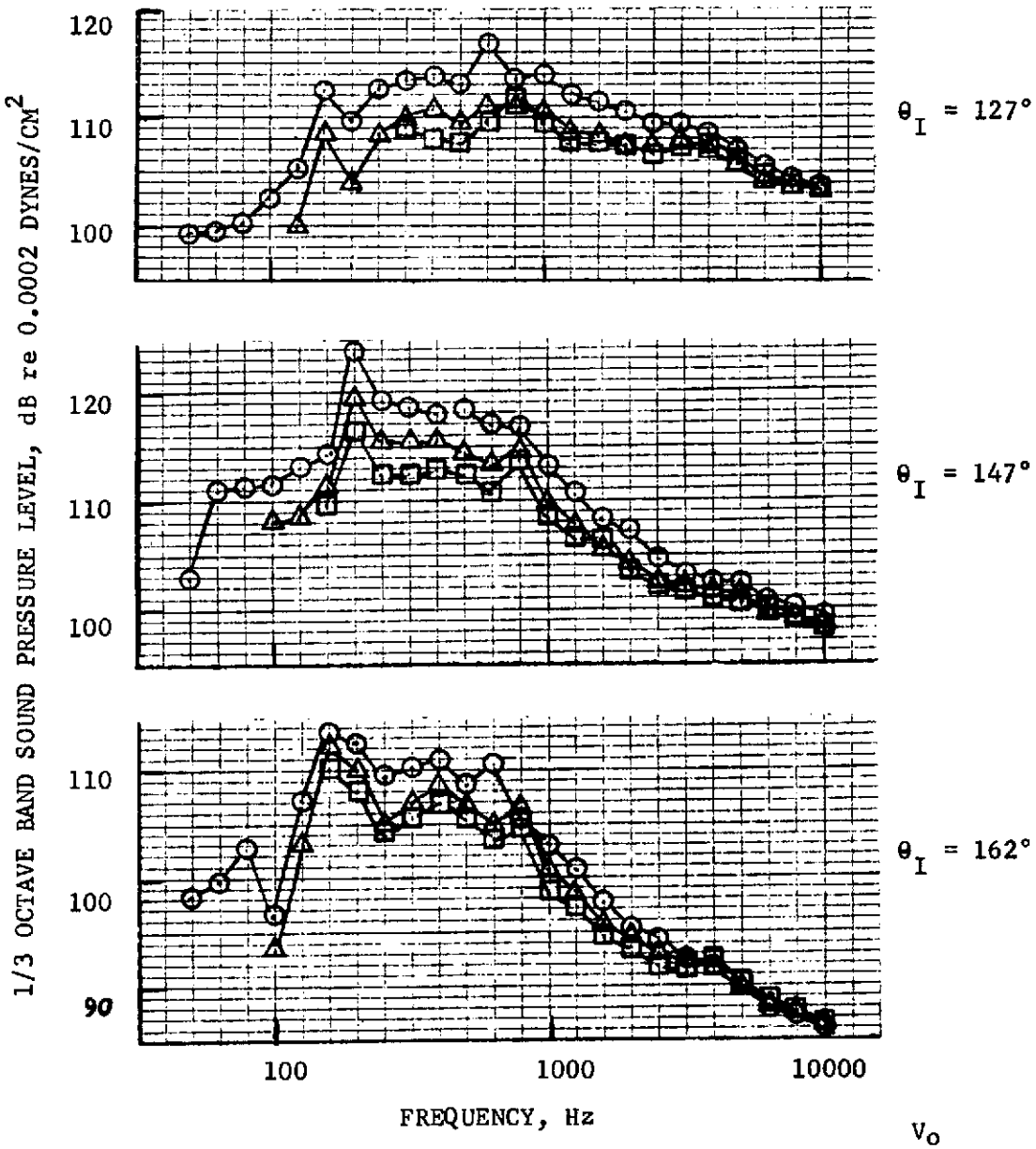

- CONICAL EJECTOR NOZZLE
- 13 FT. S.L. (3.96 M)
- V_j = 1300 FT/SEC (396 M/SEC)
- 59°F, 70% REL. HUM.

V_o	FT/SEC	M/SEC
○	0	0
△	170	51.8
□	250	76.2

FIGURE 10.86 - WING NACELLE WIND TUNNEL TEST, 1/3 OCTAVE BAND SPECTRA, CONICAL EJECTOR NOZZLE

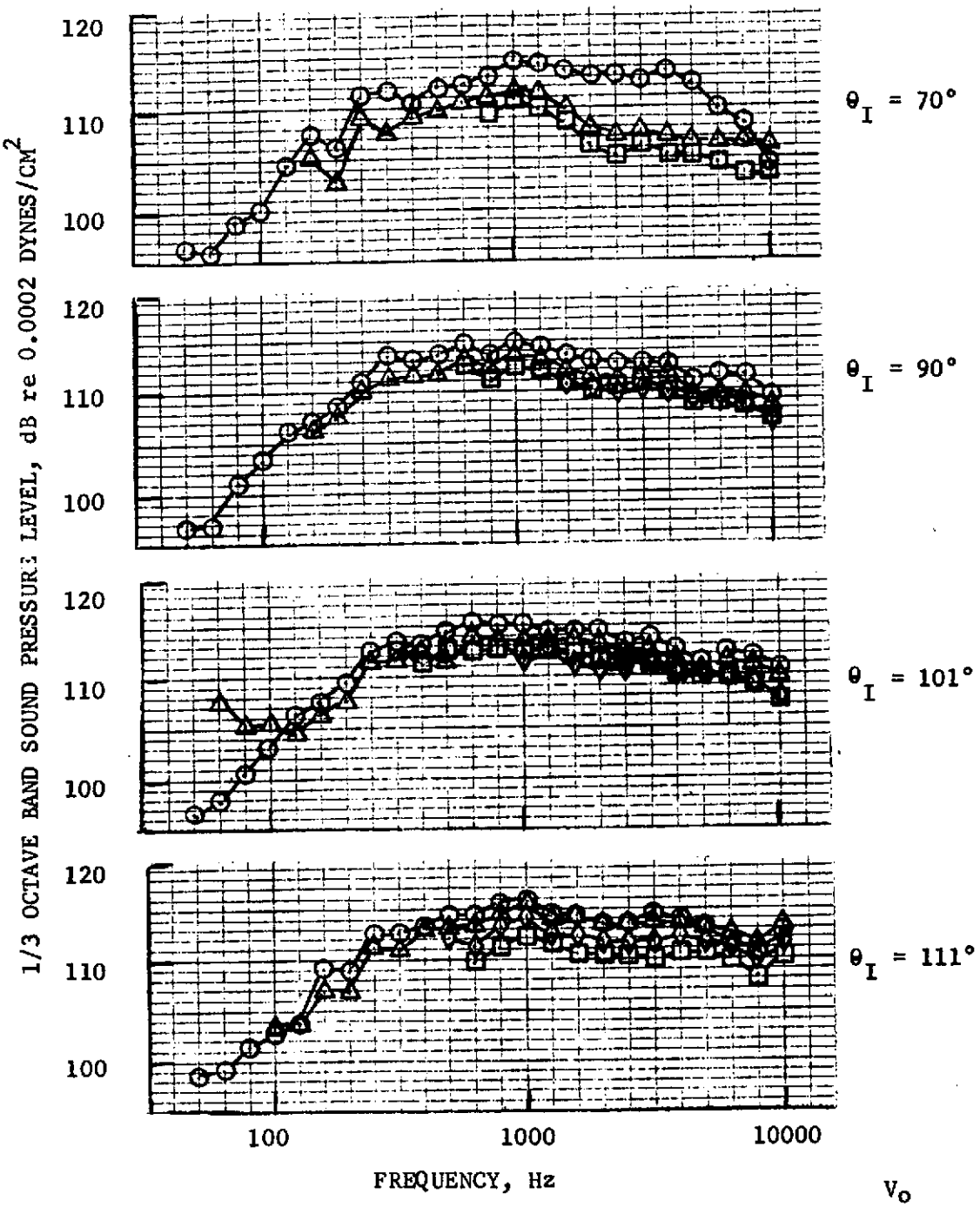

- CONICAL EJECTOR NOZZLE
- 13 FT. S.L. (3.96 M)
- V_j = 1700 FT/SEC (518 M/SEC)
- 59 °F, 70% REL. HUM.

	V_o FT/SEC	V_o M/SEC
○	0	0
△	170	51.8
□	250	76.2
◇	300	91.4

FIGURE 10.87 - WING NACELLE WIND TUNNEL TEST, 1/3 OCTAVE BAND SPECTRA, CONICAL EJECTOR NOZZLE

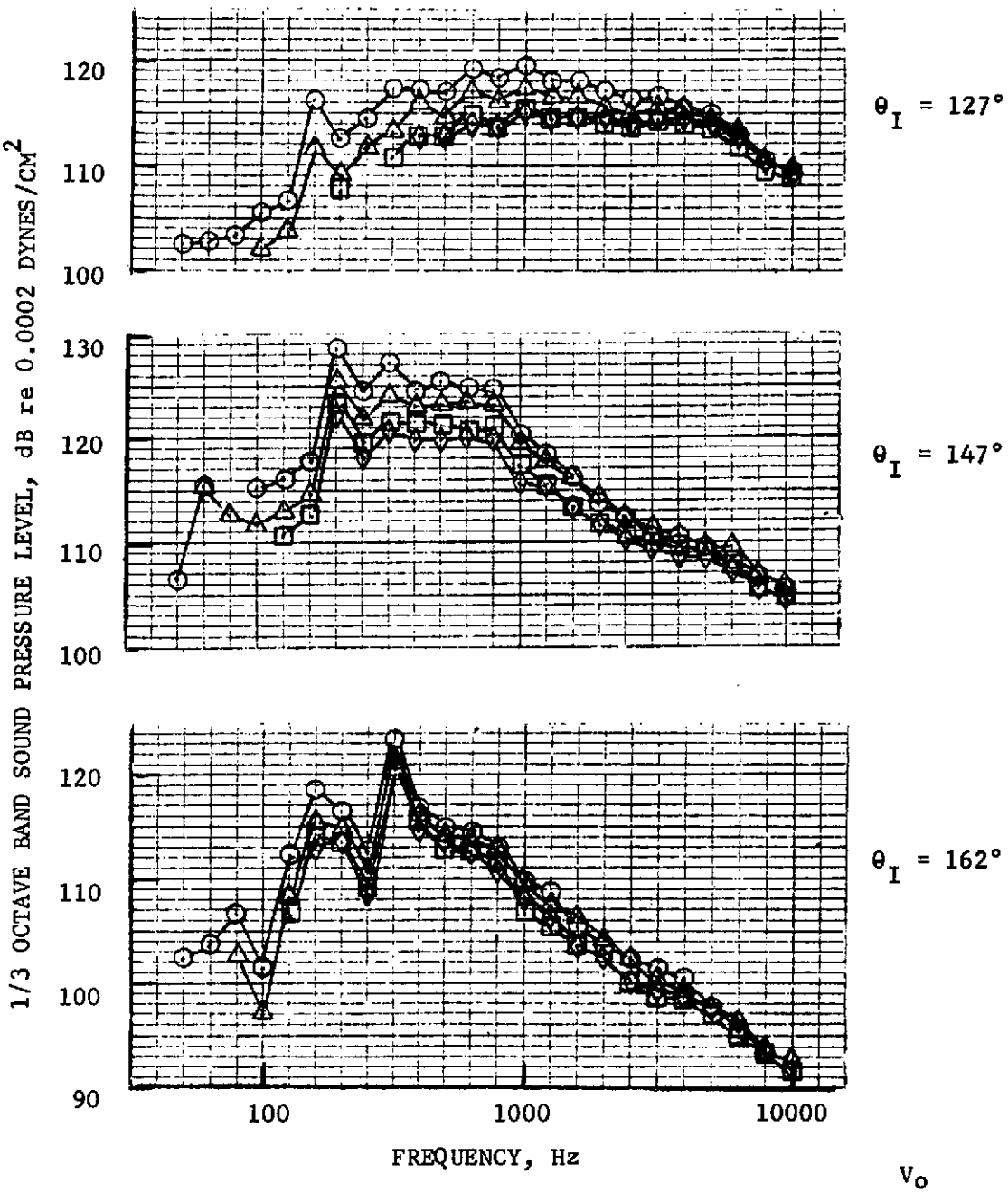

- CONICAL EJECTOR NOZZLE
- 13 FT. S.L. (3.96 M)
- V_j = 1700 FT/SEC (518 M/SEC)
- 59°F, 70% REL. HUM.

V_o	FT/SEC	M/SEC
○	0	0
△	170	51.8
□	250	76.2
◇	300	91.4

FIGURE 10.88 - WING NACELLE WIND TUNNEL TEST, 1/3 OCTAVE BAND SPECTRA, CONICAL EJECTOR NOZZLE

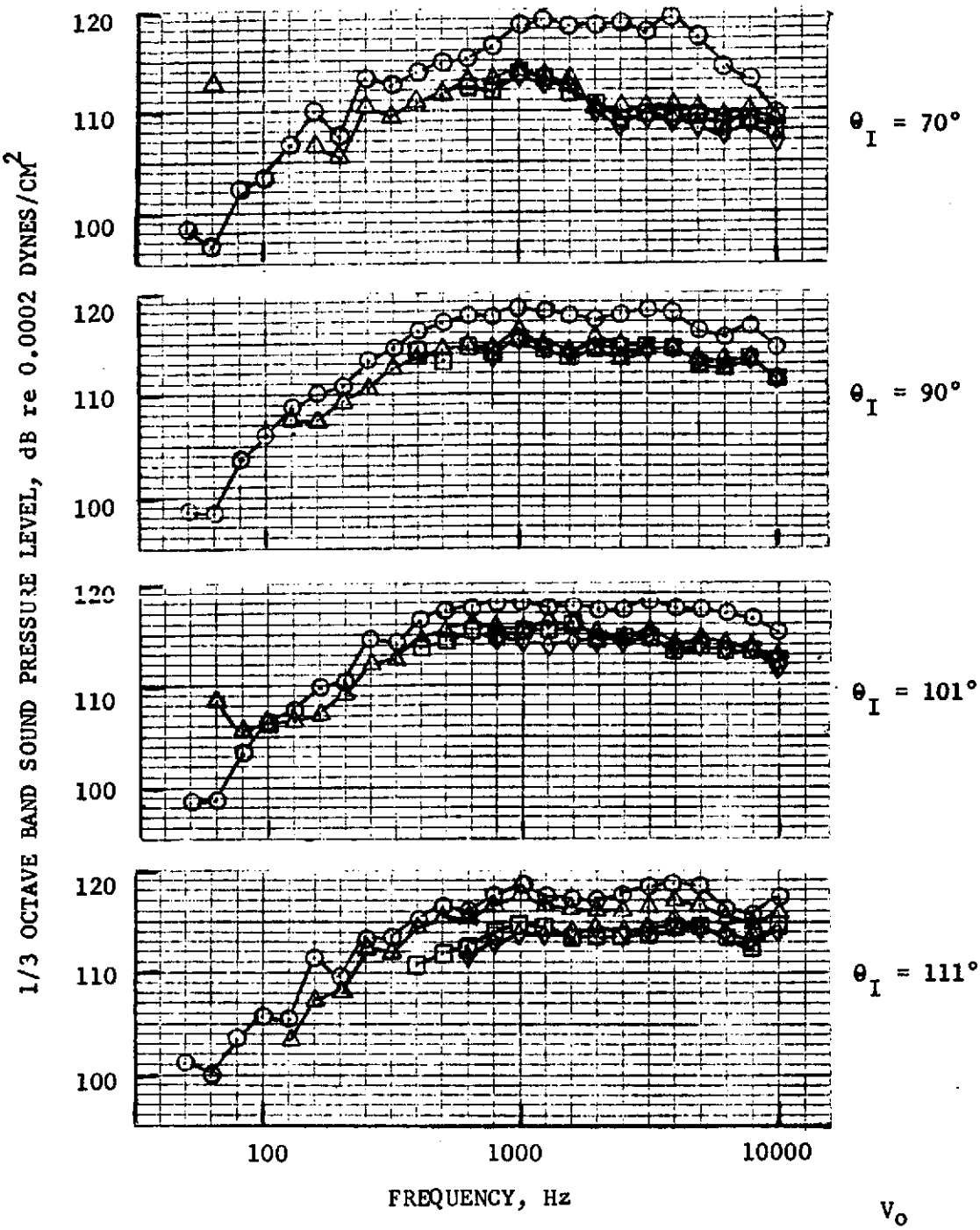

- CONICAL EJECTOR NOZZLE
- 13 FT. S.L. (3.96 M)
- V_j = 1950 FT/SEC (594 M/SEC)
- 59°F, 70% REL. HUM.

V_o	FT/SEC	M/SEC
○	0	0
△	170	51.8
□	250	76.2
◊	300	91.4

FIGURE 10.89 - WING NACELLE WIND TUNNEL TEST, 1/3 OCTAVE BAND SPECTRA, CONICAL EJECTOR NOZZLE

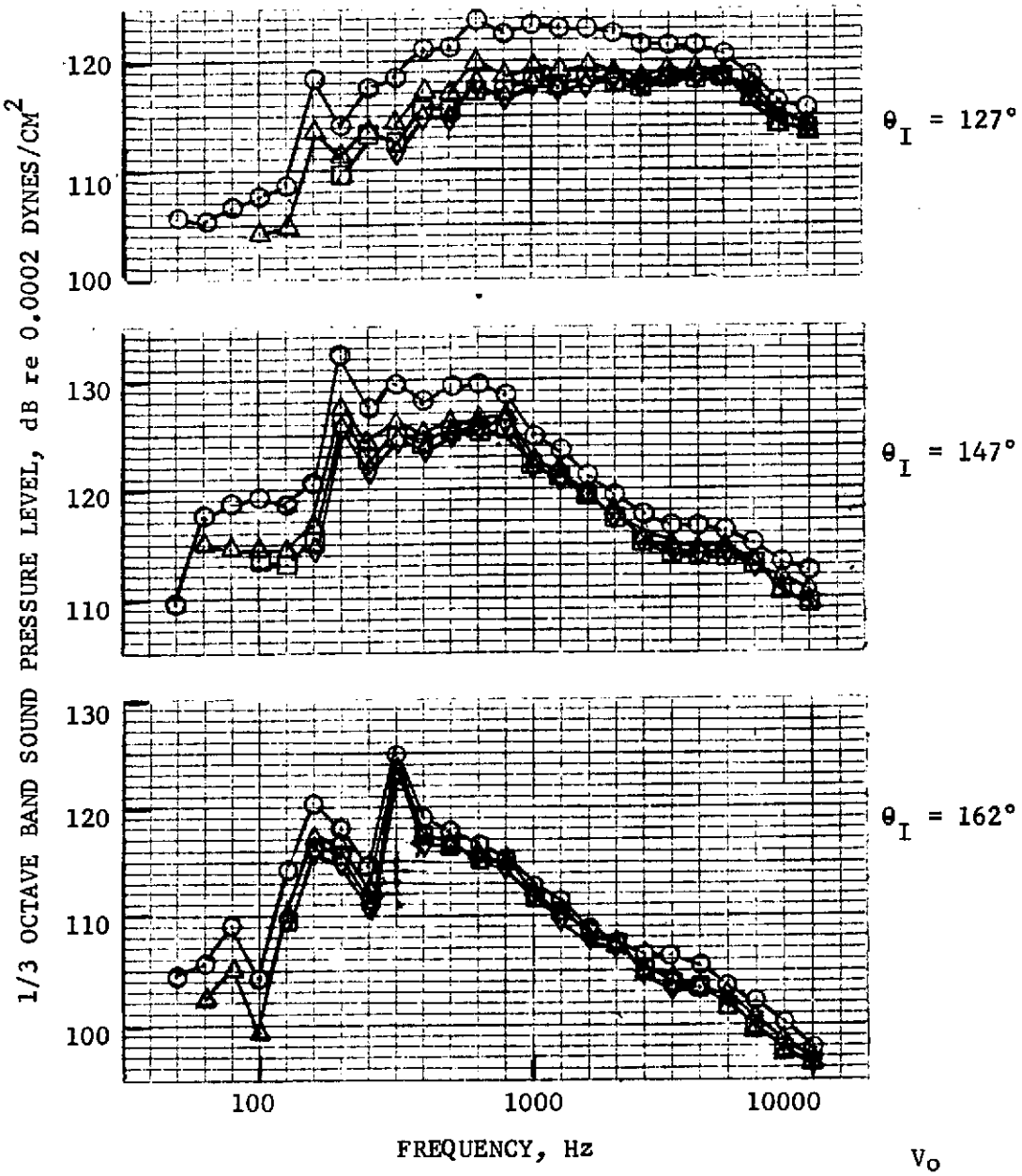

FIGURE 10.90 - WING NACELLE WIND TUNNEL TEST, 1/3 OCTAVE BAND SPECTRA, CONICAL EJECTOR NOZZLE

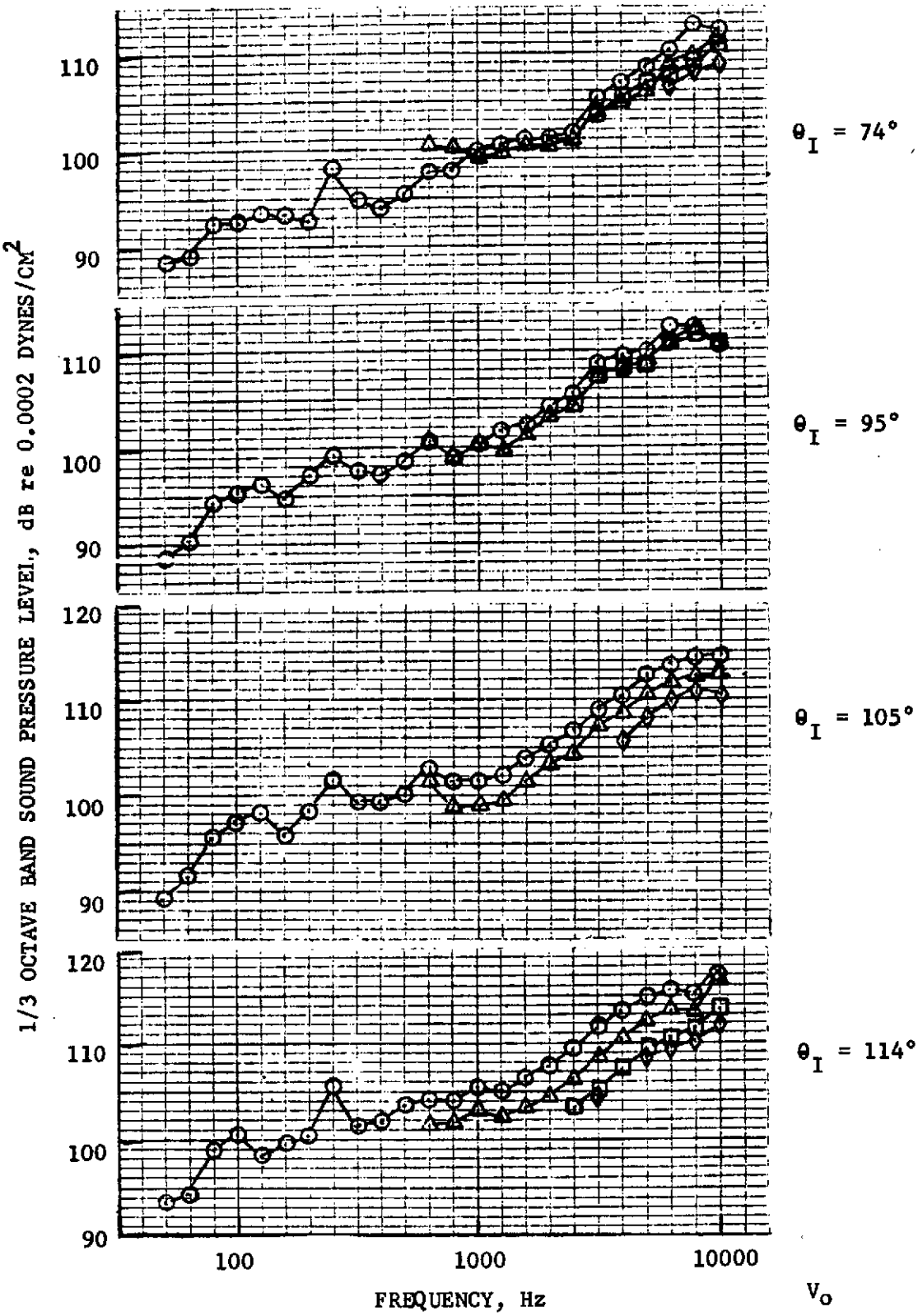

FIGURE 10.91 - WING NACELLE WIND TUNNEL TEST, 1/3 OCTAVE BAND SPECTRA, 104-TUBE NOZZLE W/O SHROUD

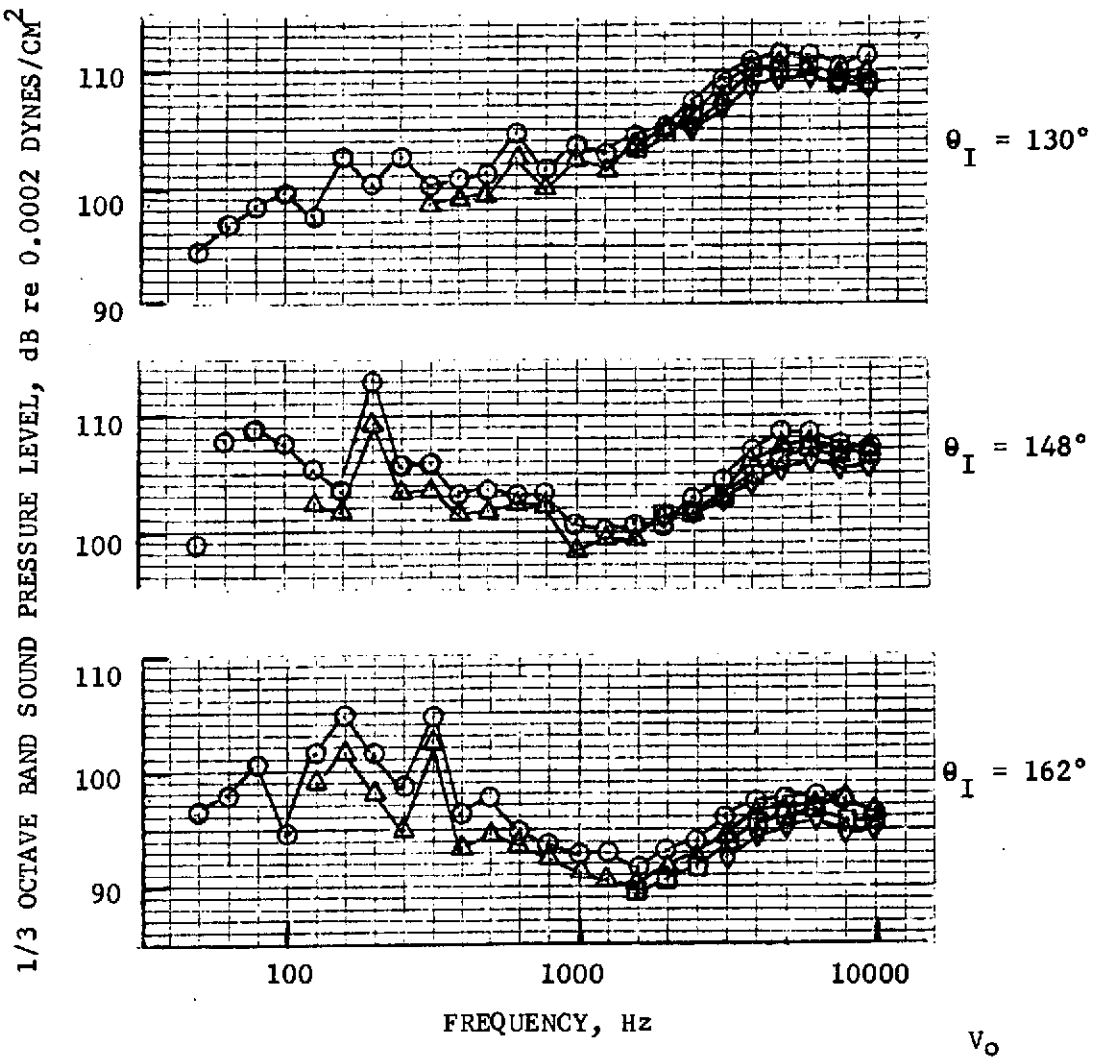

- 104 TUBE NOZZLE W/O SHROUD
- 13 FT. S.L. (3.96 M)
- V_j = 1550 FT/SEC (472 M/SEC)
- 59°F, 70% REL. HUM.

	V_o FT/SEC	V_o M/SEC
○	0	0
△	170	51.8
□	250	76.2
◇	305	93.0

FIGURE 10.92 - WING NACELLE WIND TUNNEL TEST, 1/3 OCTAVE BAND SPECTRA, 104-TUBE NOZZLE W/O SHROUD

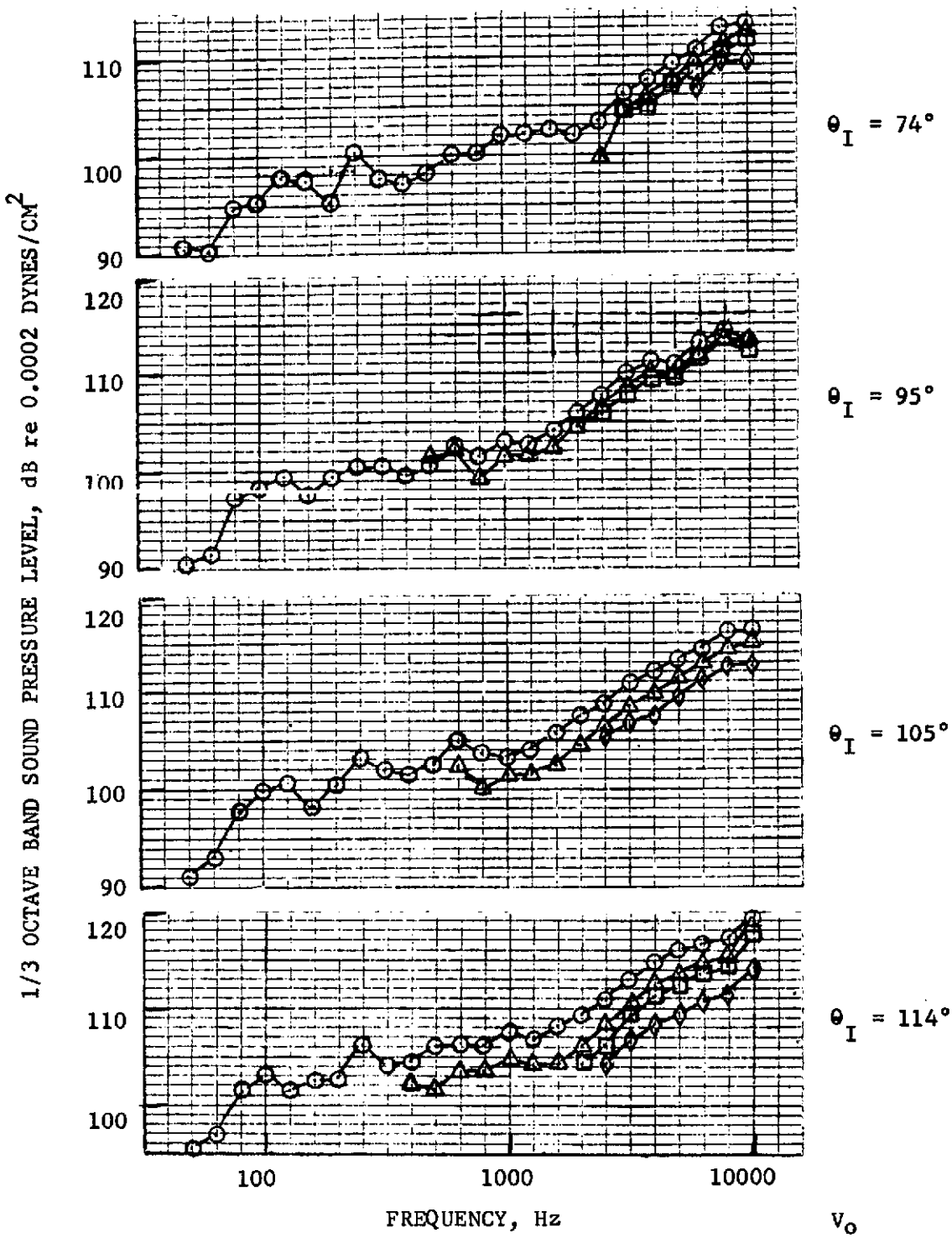

- 104 TUBE NOZZLE W/O SHROUD
- 13 FT. S.L. (3.96 M)
- V_j = 1750 FT/SEC (533 M/SEC)
- 59°F, 70% REL. HUM.

V_o	FT/SEC	M/SEC
○	0	0
△	170	51.8
□	250	76.2
◊	305	93.0

FIGURE 10.93 - WING NACELLE WIND TUNNEL TEST, 1/3 OCTAVE BAND SPECTRA, 104-TUBE NOZZLE W/O SHROUD

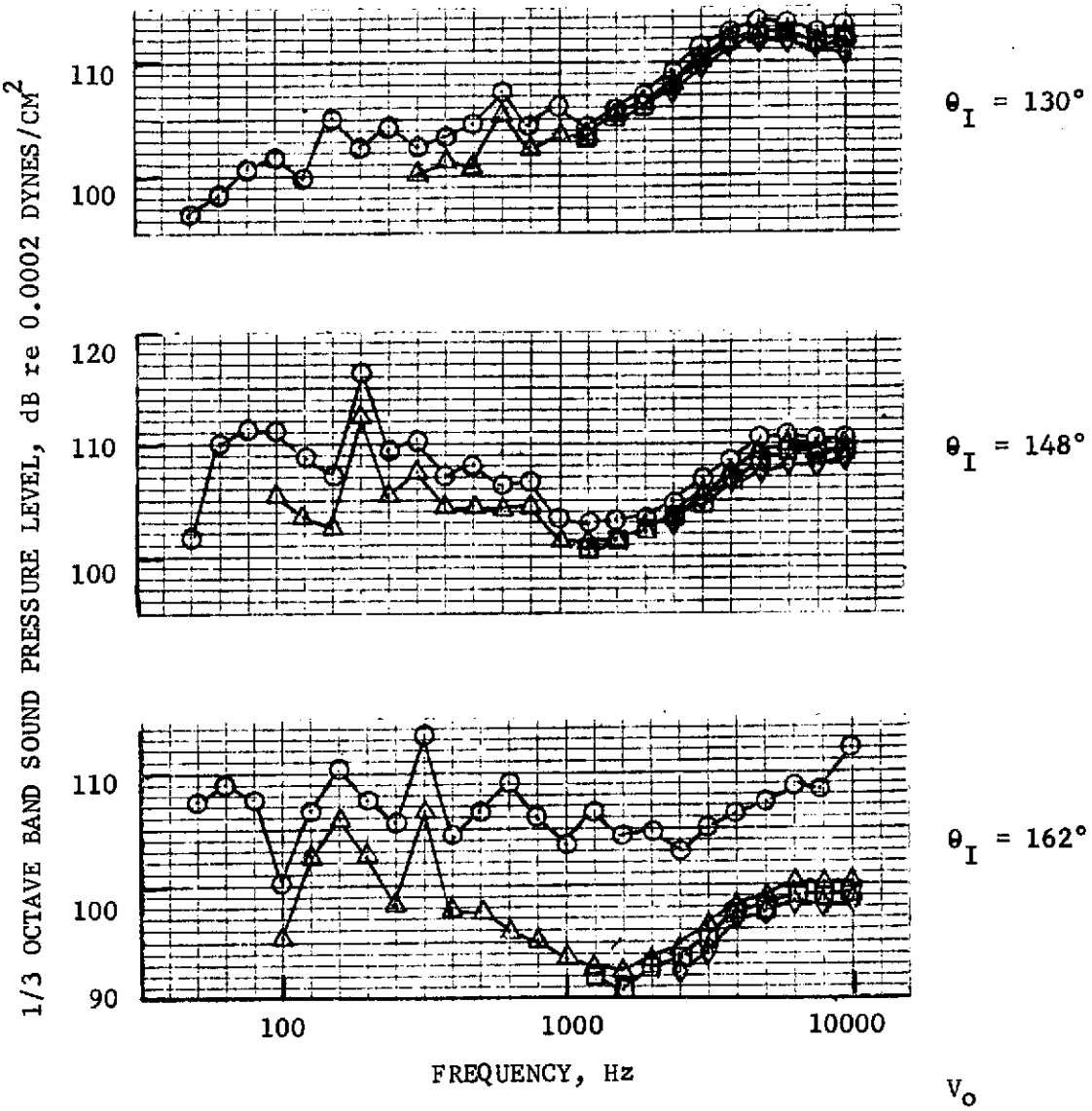

FIGURE 10.94 - WING NACELLE WIND TUNNEL TEST, 1/3 OCTAVE BAND SPECTRA, 104-TUBE NOZZLE W/O SHROUD

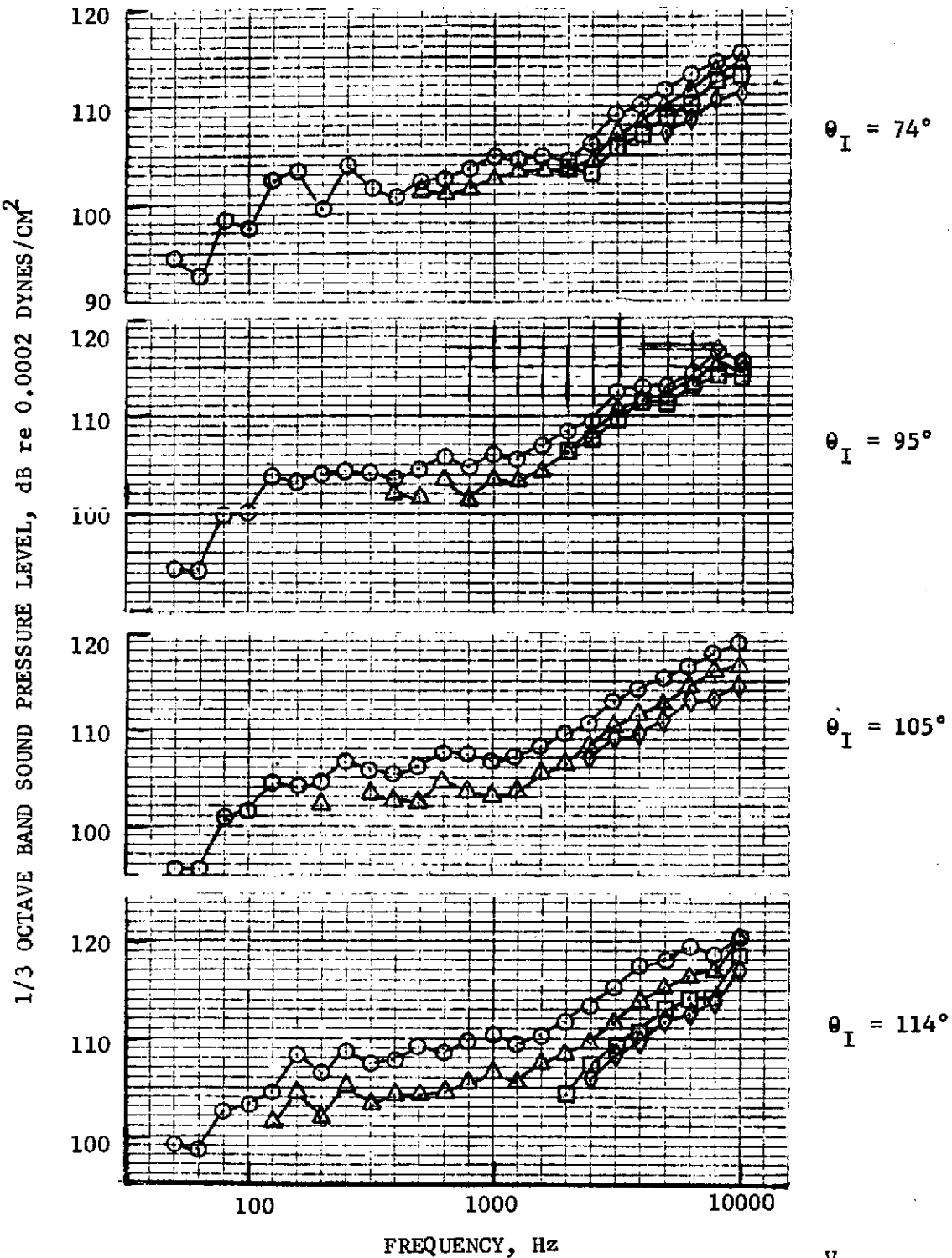

- 104 TUBE NOZZLE W/O SHROUD
- 13 FT. S.L. (3.96 M)
- V_j = 1950 FT/SEC (594 M/SEC)
- 59°F, 70% REL. HUM.

V_o FT/SEC	V_o M/SEC
○ 0	0
△ 170	51.8
□ 250	76.2
◇ 305	93.0

FIGURE 10.95 - WING NACELLE WIND TUNNEL TEST, 1/3 OCTAVE BAND SPECTRA, 104-TUBE NOZZLE W/O SHROUD

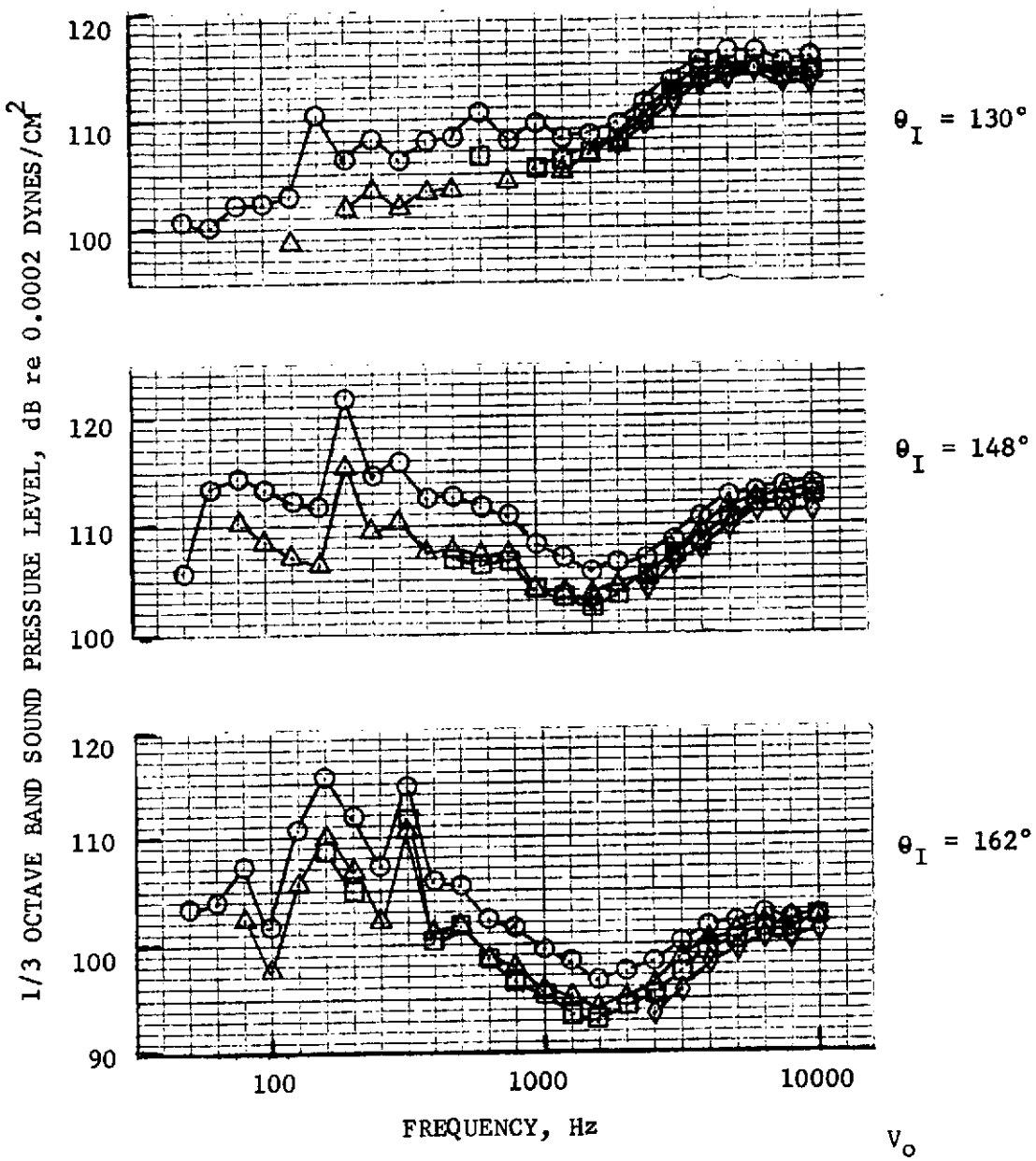

FIGURE 10.96 - WING NACELLE WIND TUNNEL TEST, 1/3 OCTAVE BAND SPECTRA, 104-TUBE NOZZLE W/O SHROUD

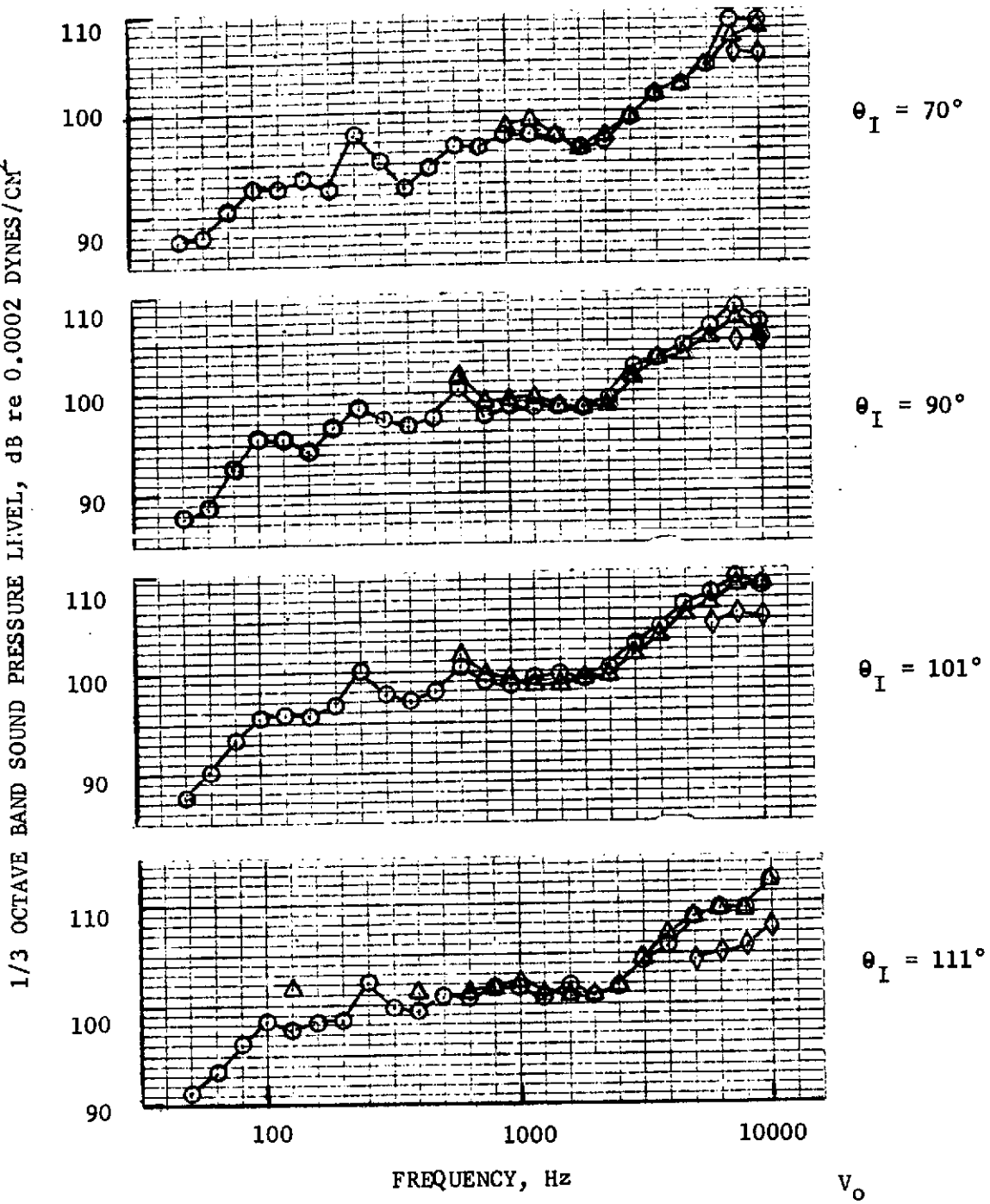

FIGURE 10.97 - WING NACELLE WIND TUNNEL TEST, 1/3 OCTAVE BAND SPECTRA, 104-TUBE NOZZLE WITH SHROUD

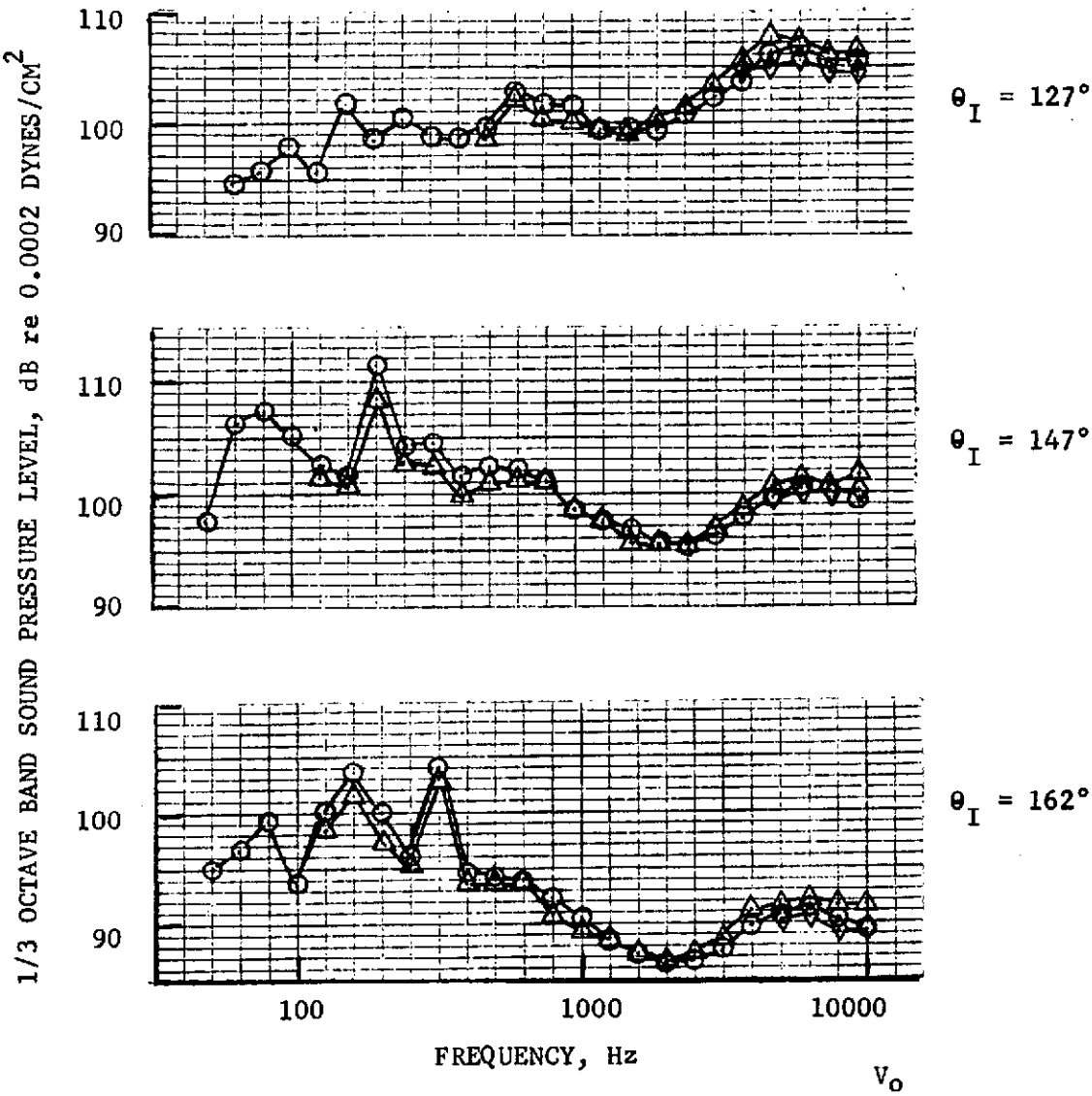

- 104 TUBE NOZZLE W/SHROUD
- 13 FT. S.L. (3.96 M)
- V_j = 1500 FT/SEC (457 M/SEC)
- 59°F, 70% REL. HUM.

V_o	FT/SEC	M/SEC
○	0	0
△	170	51.8
◊	305	93.0

FIGURE 10.98 - WING NACELLE WIND TUNNEL TEST, 1/3 OCTAVE BAND SPECTRA, 104-TUBE NOZZLE WITH SHROUD

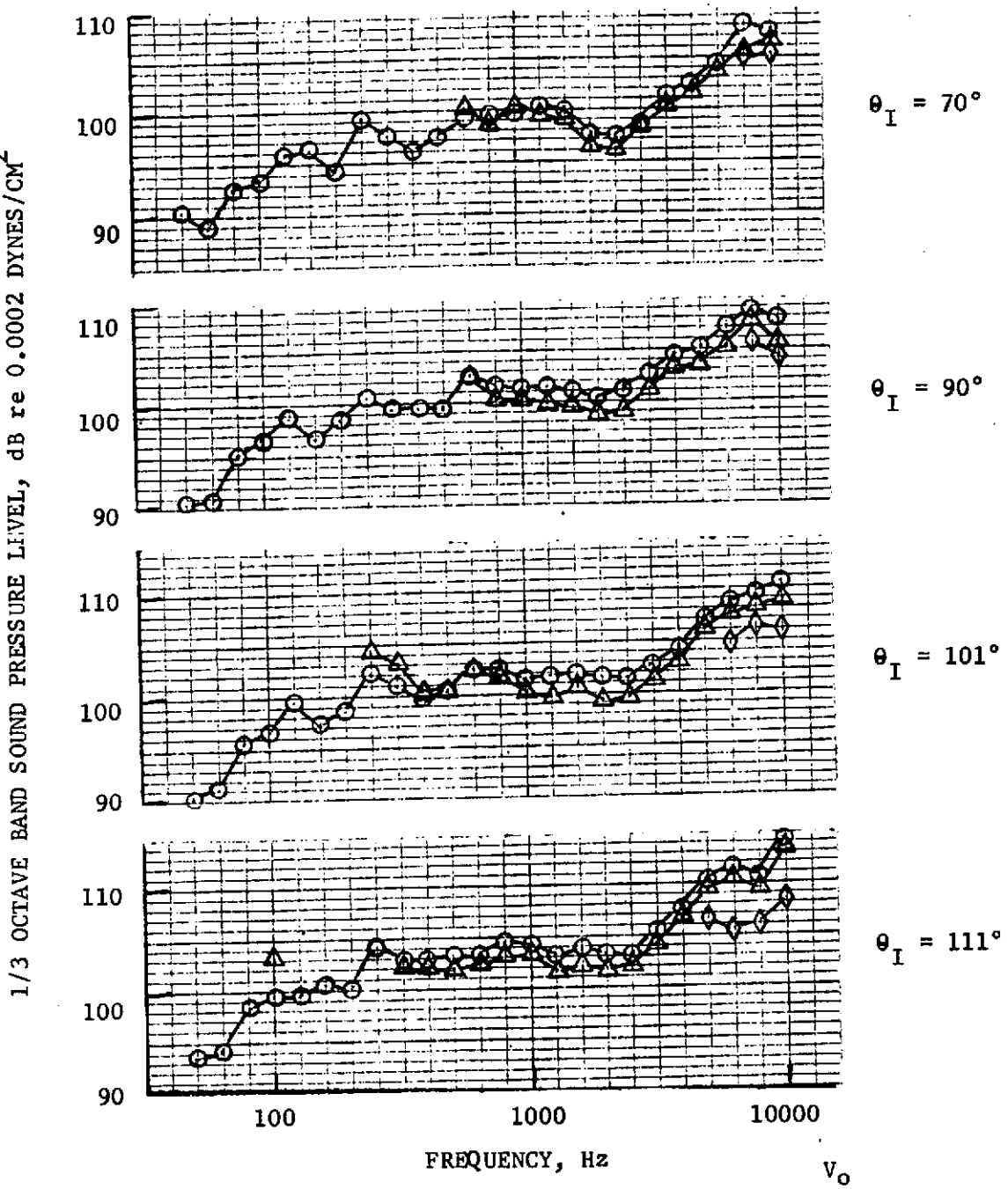

- 104 TUBE NOZZLE W/SHROUD
- 13 FT. S.L. (3.96 M)
- V_j = 1700 FT/SEC (518 M/SEC)
- 59°F, 70% REL. HUM.

FIGURE 10.99 - WING NACELLE WIND TUNNEL TEST, 1/3 OCTAVE BAND SPECTRA, 104-TUBE NOZZLE WITH SHROUD

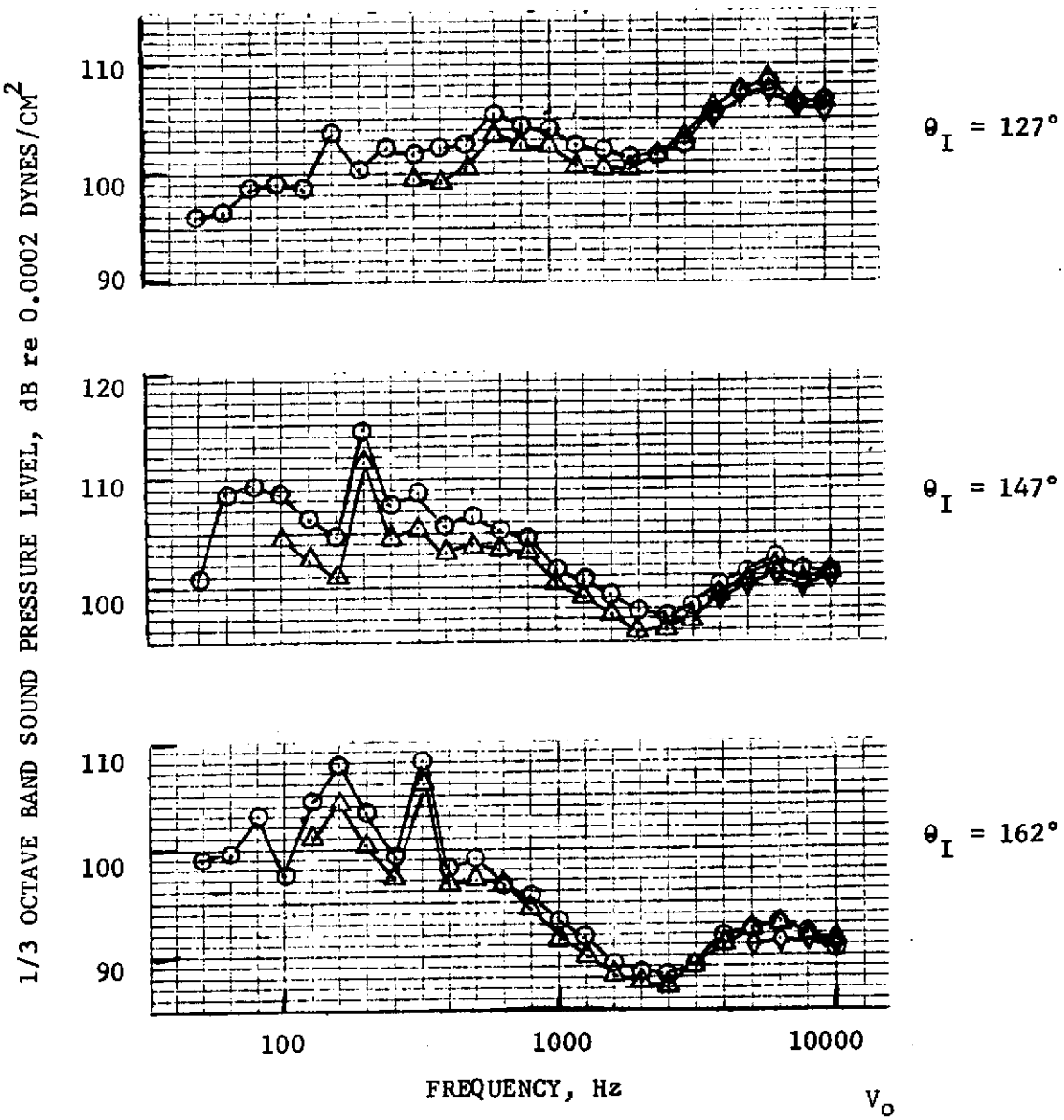

FIGURE 10.100- WING NACELLE WIND TUNNEL TEST, 1/3 OCTAVE BAND SPECTRA, 104-TUBE NOZZLE WITH SHROUD

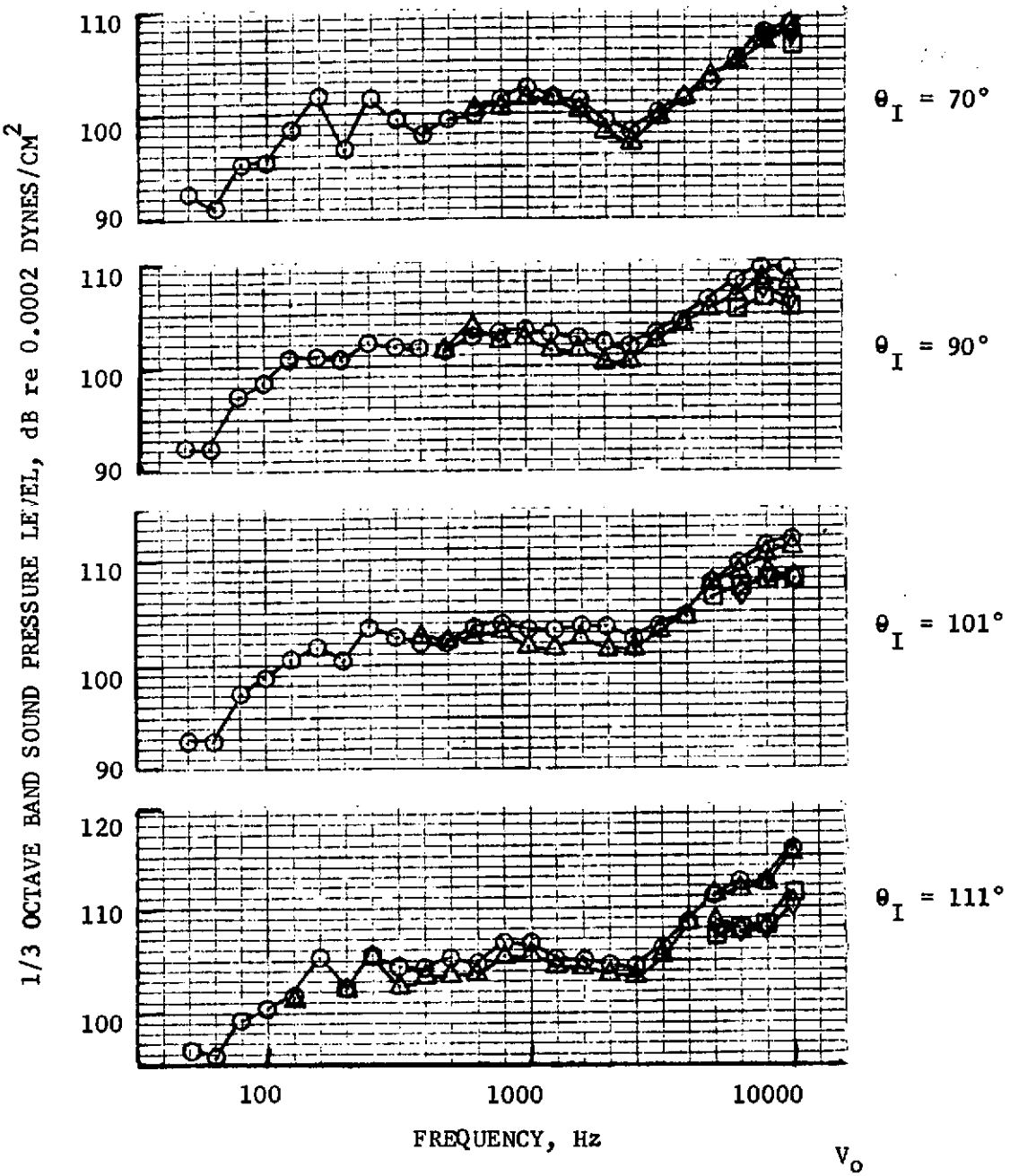

FIGURE 10.101- WING NACELLE WIND TUNNEL TEST, 1/3 OCTAVE BAND SPECTRA, 104-TUBE NOZZLE WITH SHROUD

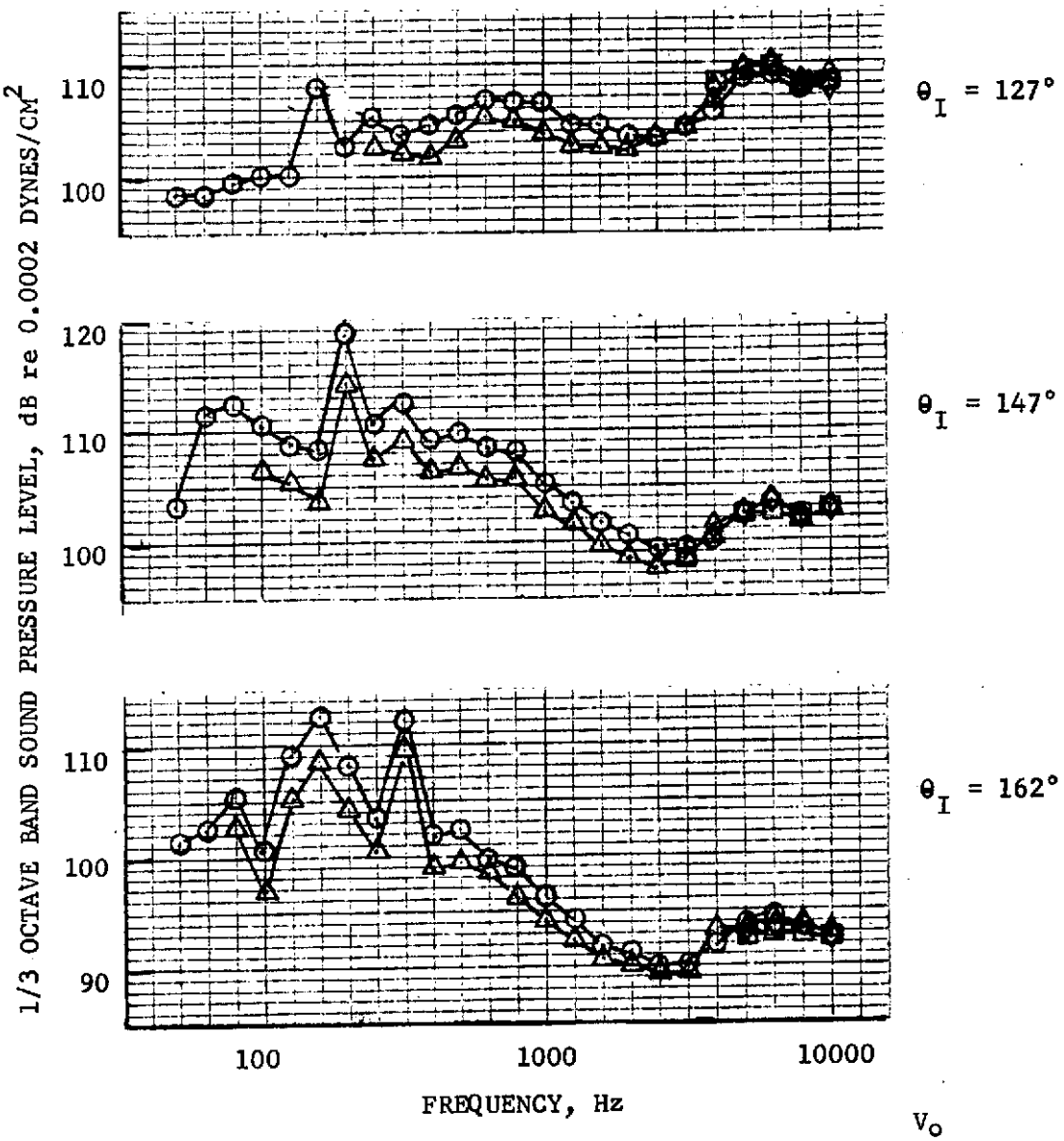

FIGURE 10.102- WING NACELLE WIND TUNNEL TEST, 1/3 OCTAVE BAND SPECTRA, 104-TUBE NOZZLE WITH SHROUD

TABLE 10.8

OASPL AND PNdB FOR WING NACELLE WIND TUNNEL TEST

13 FT. SIDELINE (3.96M)

V_J = 1700 FT/SEC (518 M/SEC)

θ_I	V_o FPS	V_o MPS	CONICAL OASPL	CONICAL PNdB	104-TUBE W/O SHROUD OASPL	104-TUBE W/O SHROUD PNdB	104-TUBE WITH SHROUD OASPL	104-TUBE WITH SHROUD PNdB	ΔdB SUPPRESSION* OASPL	ΔdB SUPPRESSION* PNdB	ΔdB SUPPRESSION** OASPL	ΔdB SUPPRESSION** PNdB
70°	0	0	124.5	137.5	119.5	131	115	126.5	5	6.5	4.5	4.5
	170	52	122	133	117.5	126	112.5	123.5	4.5	7	5	2.5
	250	76	118	128.5	117	125	-	-	1	3.5	-	-
	300	91	-	-	-	-	-	-	-	-	-	-
101°	0	0	126	138.5	123	135	118	130	3	3.5	5	5
	170	52	125	137.5	121	132	116	128	4	5.5	5	4
	250	76	123.5	135	-	130	-	-	-	5	-	-
	300	91	-	-	118.5	127.5	-	-	-	-	-	-
127°	0	0	129.5	141.5	122.5	135.5	117.5	130.5	7	6	5	5
	170	52	127.5	140	121	133.5	116	128.5	6.5	6.5	5	5
	250	76	125.5	138	120.5	132	-	-	5	6	-	-
	300	91	125.5	137.5	-	-	-	-	-	-	-	-
147°	0	0	135	142.5	123	134.5	120	128	12	8	3	6.5
	170	52	133	141	120	132.5	116.5	126	13	8.5	3.5	6.5
	250	76	131	138.5	116.5	128	-	-	14.5	10.5	-	-
	300	91	129.5	137	116	125.5	-	-	13.5	11.5	-	-
162°	0	0	128	135	121	133	114	121.5	7	2	7	11.5
	170	52	125.5	133	113	123	111	119.5	12.5	10	2	3.5
	250	76	124.5	132	107	118	-	-	17.5	14	-	-
	300	91	124.5	132	105	115.5	-	-	19.5	16.5	-	-

* Suppression of 104-tube nozzle without shroud relative to conical ejector nozzle.

** Suppression of 104-tube nozzle with shroud relative to 104-tube nozzle without shroud.

- Background noise level too great to obtain jet noise signature.

TABLE 10.9

OASPL AND PNdB FOR WING NACELLE WIND TUNNEL TEST

13 FT. SIDELINE (3.96M)

V_J = 1900 FT/SEC (580 M/SEC)

θ_I	V_o FPS	V_o MPS	CONICAL OASPL	CONICAL PNdB	104-TUBE W/O SHROUD OASPL	104-TUBE W/O SHROUD PNdB	104-TUBE WITH SHROUD OASPL	104-TUBE WITH SHROUD PNdB	ΔdB SUPPRESSION* OASPL	ΔdB SUPPRESSION* PNdB	ΔdB SUPPRESSION** OASPL	ΔdB SUPPRESSION** PNdB
70°	0	0	129	142	122	134.5	116	127.5	7	7.5	6	7
	170	52	124	135.5	120.5	131	116	125.5	3.5	4.5	4.5	5.5
	250	76	122.5	133	118	128	-	-	4.5	5	-	-
	300	91	121	131	-	-	-	-	-	-	-	-
101°	0	0	129.5	142.5	125.5	137.5	119	131	4	5	6.5	6.5
	170	52	128	140	123	134	117.5	129	5	6	5.5	5
	250	76	126.5	138	121.5	131	-	-	5	7	-	-
	300	91	125	136.5	120.5	130	-	-	4.5	6.5	-	-
127°	0	0	134	146	125	138	119	132	9	8	6	6
	170	52	130.5	143	123	136	118	131	7.5	7	5	5
	250	76	129.5	141.5	122.5	134.5	-	-	7	7	-	-
	300	91	129.5	141.5	121.5	132	-	-	8	9.5	-	-
147°	0	0	139	146.5	127	137	123	131	12	9.5	4	6
	170	52	139	144	123	135	119	128	16	9	4	7
	250	76	135	142.5	120	131.5	-	-	15	11	-	-
	300	91	135	142.5	118	128	-	-	17	14.5	-	-
162°	0	0	129.5	137.5	121.5	129	118	125	8	8.5	3.5	4
	170	52	128	135.5	117	126	115	123	11	9.5	2	3
	250	76	127	135	116	124	-	-	11	11	-	-
	300	91	127	135	108	117	-	-	19	18	-	-

* Suppression of 104-tube nozzle without shroud relative to conical ejector nozzle.

** Suppression of 104-tube nozzle with shroud relative to 104-tube nozzle without shroud.

\- Background noise level too great to obtain jet noise signature.

TABLE 10.10

1/3 OCTAVE BAND SOUND PRESSURE LEVELS FOR WING NACELLE WIND TUNNEL TEST - 13 FT. SIDELINE (3.96M)

V_j FPS (MPS)	θ_I	V_o FPS	V_o MPS	250 Hz CONICAL	250 Hz 104-TUBE W/O SHROUD	250 Hz 104-TUBE WITH SHROUD	250 Hz ΔdB_1*	250 Hz ΔdB_2**	500 Hz CONICAL	500 Hz 104-TUBE W/O SHROUD	500 Hz 104-TUBE WITH SHROUD	500 Hz ΔdB_1	500 Hz ΔdB_2	1000 Hz CONICAL	1000 Hz 104-TUBE W/O SHROUD	1000 Hz 104-TUBE WITH SHROUD	1000 Hz ΔdB_1	1000 Hz ΔdB_2	4000 Hz CONICAL	4000 Hz 104-TUBE W/O SHROUD	4000 Hz 104-TUBE WITH SHROUD	4000 Hz ΔdB_1	4000 Hz ΔdB_2
1700 (518)	100°	0	0	112.5	103	102	9.5	1	114.5	102.5	100.5	12	2	115	103	101	12	2	112.5	112	104.5	.5	7.5
		170	51.8	111.5	-	104.5	-	-	111.5	-	100.5	-	-	113.5	101.5	100.5	12	1	111.5	110	103	1.5	7
		250	76.2	-	-	-	-	-	112.5	-	-	-	-	112.5	-	-	-	-	110	-	-	-	-
		300	91.4	-	-	-	-	-	-	-	-	-	-	111.5	-	-	-	-	111	107.5	-	3.5	-
	127°	0	0	114.5	104.5	102	10	2.5	117	104.5	102.5	12.5	2	119.5	106	104	13.5	2	115.5	113	-	2.5	-
		170	51.8	111.5	-	-	-	-	114.5	101	100.5	13.5	.5	117.5	104	102.5	13.5	1.5	115.5	112.5	105	3	6.5
		250	76.2	111	-	-	-	-	112.5	-	-	-	-	115.5	-	-	-	-	114	112	105.5	2	6.5
		300	91.4	-	-	-	-	-	112.5	-	-	-	-	115	-	-	-	-	114.5	112	-	2.5	-
	147°	0	0	124.5	110	107.5	14.5	2.5	125.5	108	106.5	17.5	1.5	120	103.5	101.5	16.5	2	110.5	108.5	100	2	8.5
		170	51.8	122	105.5	104.5	16.5	1	123.5	104.5	104	19	.5	119.5	101.5	100.5	18	1	110.5	107.5	99	3	8.5
		250	76.2	119.5	-	-	-	-	121	-	-	-	-	117.5	-	-	-	-	109.5	107	-	2.5	-
		300	91.4	118	-	-	-	-	120	-	-	-	-	115.5	-	-	-	-	109.5	107	99	1.5	8
1900 (580)	100°	0	0	114.5	106.5	104	8	2.5	117	106	102.5	11	3.5	118	106.5	103	11.5	3.5	117.5	114	104.5	3.5	9.5
		170	51.8	112	-	-	-	-	115.5	102.5	102.5	13	0	115.5	103	101.5	12.5	2.5	114.5	111.5	104.5	3	7
		250	76.2	-	-	-	-	-	115.5	-	-	-	-	115.5	-	-	-	-	113.5	-	-	-	-
		300	91.4	-	-	-	-	-	114.5	-	-	-	-	114.5	-	-	-	-	114	109.5	-	4.5	-
	127°	0	0	117.5	108	105.5	9.5	2.5	121	108	105.5	13	2.5	123.5	109.5	106	14	3.5	121.5	115	106	6.5	9
		170	51.8	113.5	103.5	102.5	10	1	117	103.5	103	13.5	.5	119.5	106	103.5	13.5	2.5	-	115	106.5	-	8.5
		250	76.2	113.5	-	-	-	-	115.5	-	-	-	-	118.5	105.5	-	13	-	118.5	114.5	107	4	7.5
		300	91.4	-	-	-	-	-	115	-	-	-	-	118	-	-	-	-	118.5	114	107	4.5	7
	147°	0	0	127.5	114.5	110.5	13	4	129.5	112.5	110	17	2.5	125	108	105	17	3	117	110.5	100	6.5	10.5
		170	51.8	124	109.5	107	14.5	2.5	126.5	107.5	106.5	19	1	122.5	104	103	18.5	1	115	109.5	100	5.5	9.5
		250	76.2	123	-	-	-	-	125.5	107	-	18.5	-	122.5	104	-	18.5	-	114	108	100	6	8
		300	91.4	121.5	-	-	-	-	125.5	-	-	-	-	122.5	-	-	-	-	114	108	101	6	7

* ΔdB_1 is suppression of 104-tube nozzle without shroud relative to conical ejector nozzle.

** ΔdB_2 is suppression of 104-tube nozzle with shroud relative to 104-tube nozzle without shroud.

- Background noise level too great to obtain jet noise signature.

10.2 Outdoor Static Acoustic Data

10.2.1 Isolated Nacelle Static Test

Four nozzle configurations were evaluated during the "Outdoor Static Isolated Nacelle Test Series." The nozzles were the conical ejector nozzle, auxiliary inlet ejector (AIE) nozzle, 32 spoke nozzle and the 104 tube nozzle with and without an acoustically treated shroud. The jet noise signature of each nozzle was monitored over the velocity range defined on Table 9.1. The data were then analyzed on the following basis.

- Compare each configuration on the basis of OAPWL over the velocity range evaluated to determine the jet noise suppression characteristic of each nozzle using the conical ejector nozzle as the baseline.
- Present the one-third octave band power spectra for each configuration at various jet velocities.
- Compare each of the configurations on the basis of peak OASPL and PNdB to determine nozzle suppression characteristics on the basis of these parameters.
- Determine changes in directivity patterns on the basis of OASPL and PNdB for the conical ejector nozzle and the 104 tube nozzle with and without the acoustically treated shroud for the range of jet velocities evaluated.
- Determine changes in spectra characteristics at several acoustic angles for the range of jet velocities evaluated.

Presented on Figures 10.104 and 10.105 are the one-third octave band sound power level spectra for the four configurations. The spectra representing the conical ejector nozzle at a jet velocity of 580 m/sec (1900 ft/sec) peaks at a frequency of 630 Hz at a level of 162 dB. In contrast, the 104 tube nozzle has a power level spectra that has two distinct peak regions. The first peak occurs at 125 Hz and is representative of the fully merged region of the jet. The second peak occurs at the 6300 Hz and represents the noise produced by each individual tube element before merging. This hypothesis is supported

by comparing the spectra of the 104 tube nozzle without the acoustically treated shroud to the power level spectra with the shroud. These spectra are presented on Figures 10.105. Note that the peak level for the high velocity condition at 6300 Hz shows a drop of 5 dB when the shroud is added. In comparing this 104 tube nozzle with the conical nozzle, 12 dB suppression is observed on the basis of sound pressure level at the peak frequency. In contrast, a less complex suppressor such as the AIE nozzle exhibits a power level spectra very similar to that of the conical nozzle.

Presented on Figure 10.106 are graphs of peak OASPL and PNL as a function of exhaust jet velocity for the 5 configurations tested. Comparisons were made with the data corrected to standard day conditions 288° K (59° F), 70% R.H. and extrapolated to a 61 meter (200 foot) sideline. The conical ejector nozzle has a peak OASPL of 118 dB for a jet velocity of 610 m/sec (2000 ft/sec) and 102 dB for a jet velocity of 305 m/sec (1000 ft/sec). The AIE nozzle causes an increase in OASPL of 4 dB (after extrapolation) at a jet velocity of 610 m/sec (2000 ft/sec) and causes 7 dB suppression at 305 m/sec (1000 ft/sec). The velocity at which the AIE nozzle is no longer an effective suppressor is 518 m/sec (1700 ft/sec). The 32-spoke nozzle and 104 tube nozzle have suppression levels of 8 dB and 12 dB, respectively, at 610 m/sec (2000 ft/sec), and 13 dB and 15 dB, respectively, at 305 m/sec (1000 ft/sec). The addition of a shroud to the 104 tube nozzle increases suppression by 2 to 3 dB for the velocity range evaluated. The conical ejector nozzle has a peak PNL of 125 dB for a jet velocity of 610 m/sec (2000 ft/sec) and 110 dB for a jet velocity of 305 m/sec (1000 ft/sec). The AIE nozzle causes an increase in PNL of 6 dB (after extrapolation) for a jet velocity of 610 m/sec (2000 ft/sec) and decreases PNL by 8 dB at 305 m/sec (1000 ft/sec). The velocity at which the AIE nozzle no longer causes suppression on a PNL basis is approximately 305 m/sec (1650 ft/sec). The 32-spoke and 104 tube nozzles yield PNL suppression levels of 8 dB and 11 dB, respectively, at 610 m/sec (2000 ft/sec), and 8 dB and 10 dB, respectively, at 305 m/sec (1000 ft/sec). The addition of a shroud to the 104 tube nozzle increases suppression by 7 dB at 610 m/sec (2000 ft/sec) and 3.5 dB at 305 m/sec (1000 ft/sec). The additional decrease in PNL, compared to OASPL, is due to the effectivness of the shroud suppressing the high frequency portion of the spectra which is where noy weighting is largest.

Figures 10.107 through 10.109 show overall sound pressure level (OASPL) and perceived noise level (PNL) as a function of acoustic angle, referenced to inlet, for the conical ejector nozzle and 104 tube nozzle with and without shroud. All data was corrected to a 288° K (59° F), 70% R.H. standard say and extrapolated to a 61 meter (200 foot) sideline. For the conical ejector nozzle, the peak OASPL's for all jet velocities greater than 305 m/sec (1000 ft/sec) occur at acoustic angles between 130 and 140 degrees. For jet velocities of 305 and 610 m/sec (1000 and 2000 ft/sec), the peak OASPL's are 106 and 118 dB, respectively. The 104 tube nozzle without shroud has peak OASPL's occurring at approximately 120 degrees. This 104 tube nozzle provides 13 dB suppression on the basis of peak OASPL for jet velocities over 305 m/sec (1000 ft/sec). In the forward quadrant at angles of 20 degrees through 80 degrees, the 104 tube nozzle provides suppression of about 7 dB. The addition of an acoustically treated shroud to the 104 tube nozzle provides an additional increase in suppression of 2 or 3 dB for acoustic angles between 40 to 160 degrees for all power settings. Comparing the configurations on the basis of perceived noise level (PNL), Figure 10.107 shows that for jet velocities of 580 and 411 m/sec (1900 and 1350 ft/sec), the peak PNL's for the conical ejector nozzle are 127 and 117 dB, respectively. Except for the highest power setting, the peak PNL angles have shifted 10° to 20° towards the forward quadrant compared to the peak OASPL angles. For jet velocities of 580 and 411 m/sec (1900 and 1350 ft/sec), the 104 tube nozzle provided suppression of 10 and 5 dB, respectively, on the basis of peak PNL. In the forward quadrant at angles of 40 through 80 degrees, the 104 tube nozzle suppresses PNL by 5-7 and 3-5 dB for jet velocities of 580 and 411 m/sec (1900 and 1350 ft/sec), respectively. Adding an acoustically treated shroud to the 104 tube nozzle provided additional suppression of peak PNL by 4 and 3 dB for jet velocities of 580 and 411 m/sec (1900 and 1350 ft/sec), respectively. Suppression with the shroud does occur for all angles greater than 40 degrees and at all power settings. The general trend is an increase in suppression from 1 dB at 40 degrees to 6 dB at 140 and 150 degrees for all power settings. The suppression then drops off between acoustic angles of 150 and 170 degrees.

Presented on Figures 10.110 through 10.121 are the one-third octave band sound pressure level spectra for the conical ejector nozzle and 104 tube nozzle with and without an acoustically treated shroud. The spectra presented are for acoustic angles ranging from 20° through 160°. All data were corrected to a 288° K (59° F), 70% R.H. standard day and extrapolated to a 61 meter (200 foot) sideline. In analyzing the data, several trends have become apparent and may be summarized as follows:

- At a jet velocity of 584 m/sec (1915 ft/sec) the conical ejector nozzle spectra peaks at a frequency of 400 Hz at the peak noise angle of 130° to the inlet. If a peak strouhal number of .22 was assumed, the predicted peak frequency would be 315 Hz.
- The 104 tube nozzle without shroud causes a marked change in shape of the frequency spectra which is illustrated on Figures 10.114 through 10.117. This "double humped" spectra is characteristic of multi-element nozzles.
- Comparing the conical ejector and 104 tube nozzle at a jet velocity of 600 m/sec (1970 ft/sec) indicates that the 104 tube nozzle causes substantial low frequency suppression. For example, at a frequency of 160 Hz, 13 dB suppression is observed.
- Adding an acoustically treated shroud to the 104 tube nozzle provides additional suppression in the high frequency portion of the spectra. For example, the 104 tube nozzle without shroud has a maximum sound pressure level of 88 dB at 5000 Hz for an acoustic angle of 140 degrees and a jet velocity of 600 m/sec (1970 ft/sec). The addition of the shroud decreases the level by 15 dB for equivalent conditions.

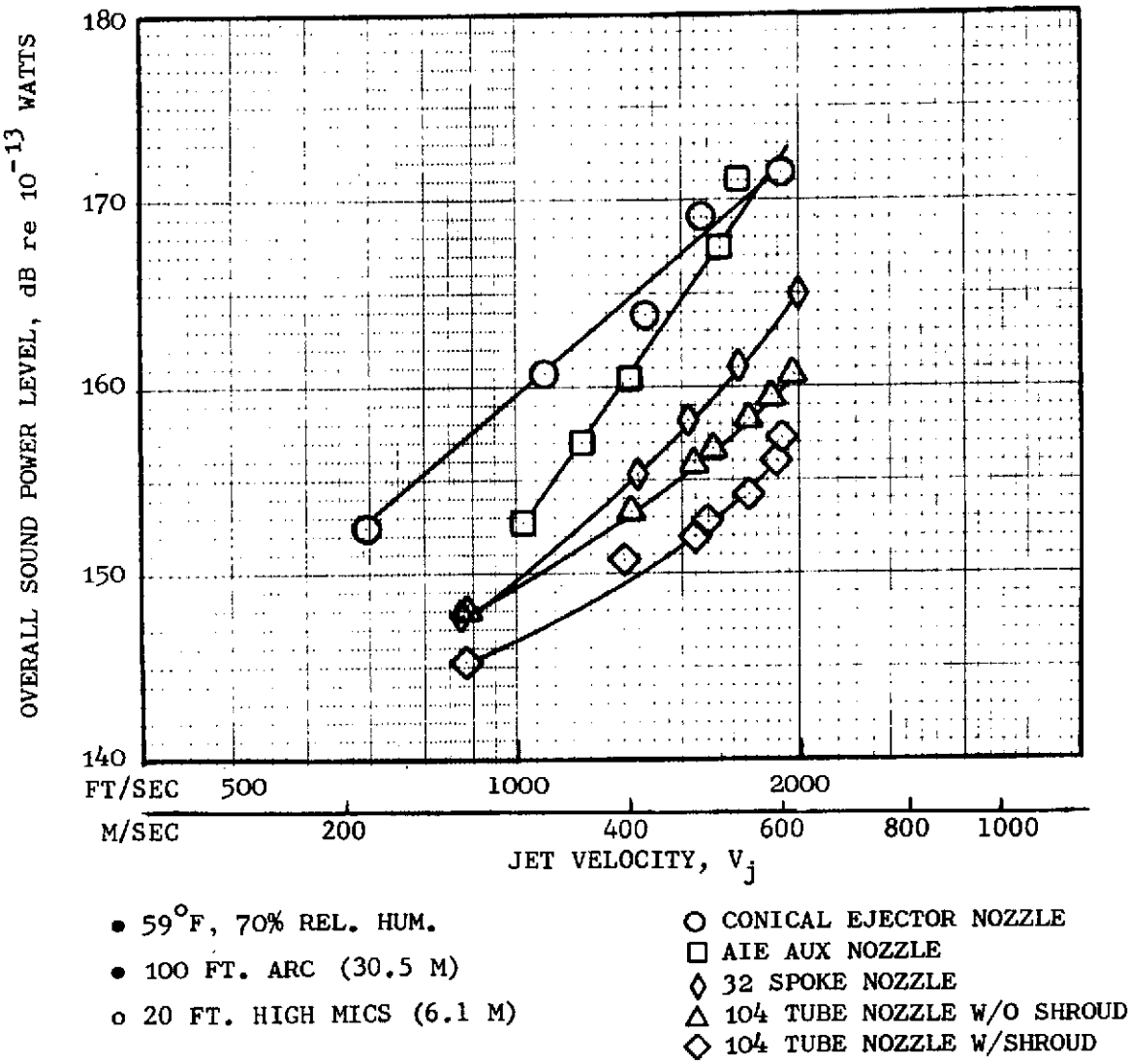

FIGURE 10.103- ISOLATED NACELLE OUTDOOR STATIC TEST, OAPWL Vs V_J

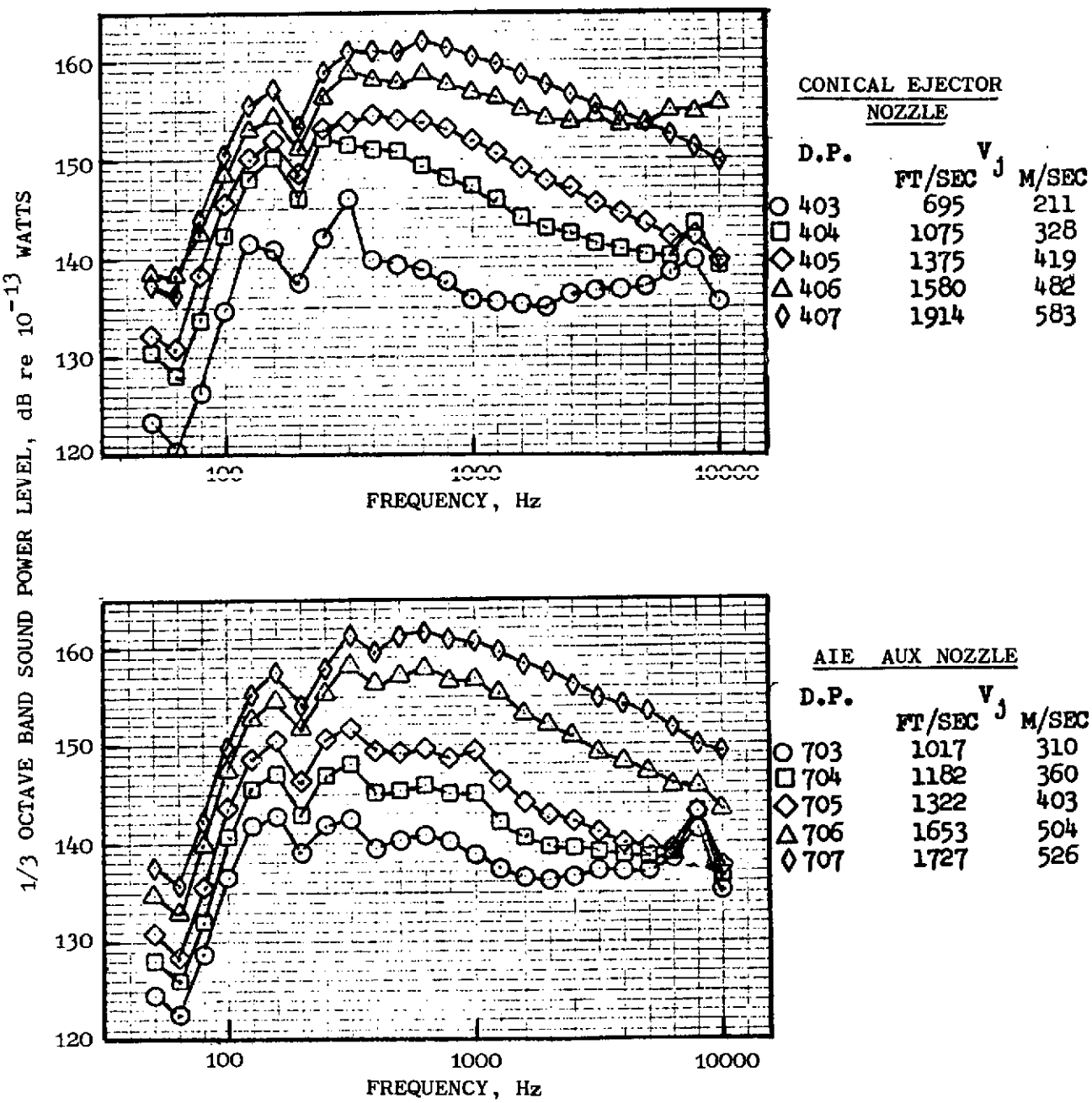

FIGURE 10.104- ISOLATED NACELLE OUTDOOR STATIC TEST, 1/3 OCTAVE BAND POWER SPECTRA, CONICAL EJECTOR AND AIE NOZZLES

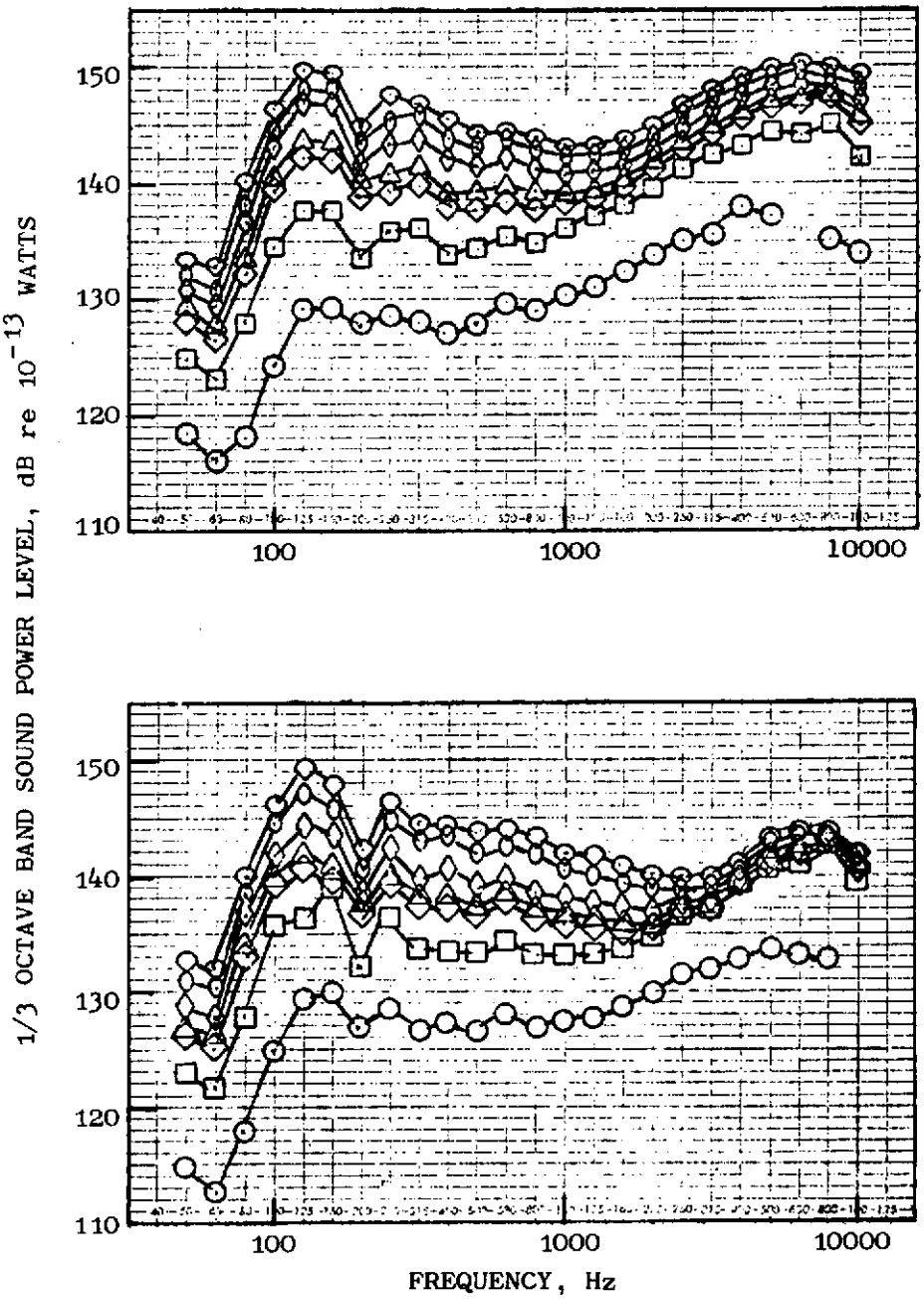

104 TUBE NOZZLE W/O SHROUD

D.P.	V_j FT/SEC	V_j M/SEC
○ 1402	888	271
□ 1403	1325	404
◇ 1404	1545	471
△ 1405	1618	493
◊ 1406	1763	537
0 1407	1872	571
◇ 1408	1968	600

104 TUBE NOZZLE W/SHROUD

D.P.	V_j FT/SEC	V_j M/SEC
○ 1002	858	262
□ 1003	1305	398
◇ 1004	1548	472
△ 1005	1604	489
◊ 1006	1770	539
0 1007	1896	578
◇ 1008	1914	583

- 59°F, 70% REL. HUM.
- 100 FT. ARC (30.5 M)
- o 20 FT. HIGH MICS (6.1 M)

FIGURE 10.105- ISOLATED NACELLE OUTDOOR STATIC TEST, 1/3 OCTAVE BAND POWER SPECTRA, 104-TUBE NOZZLE WITH AND W/O SHROUD

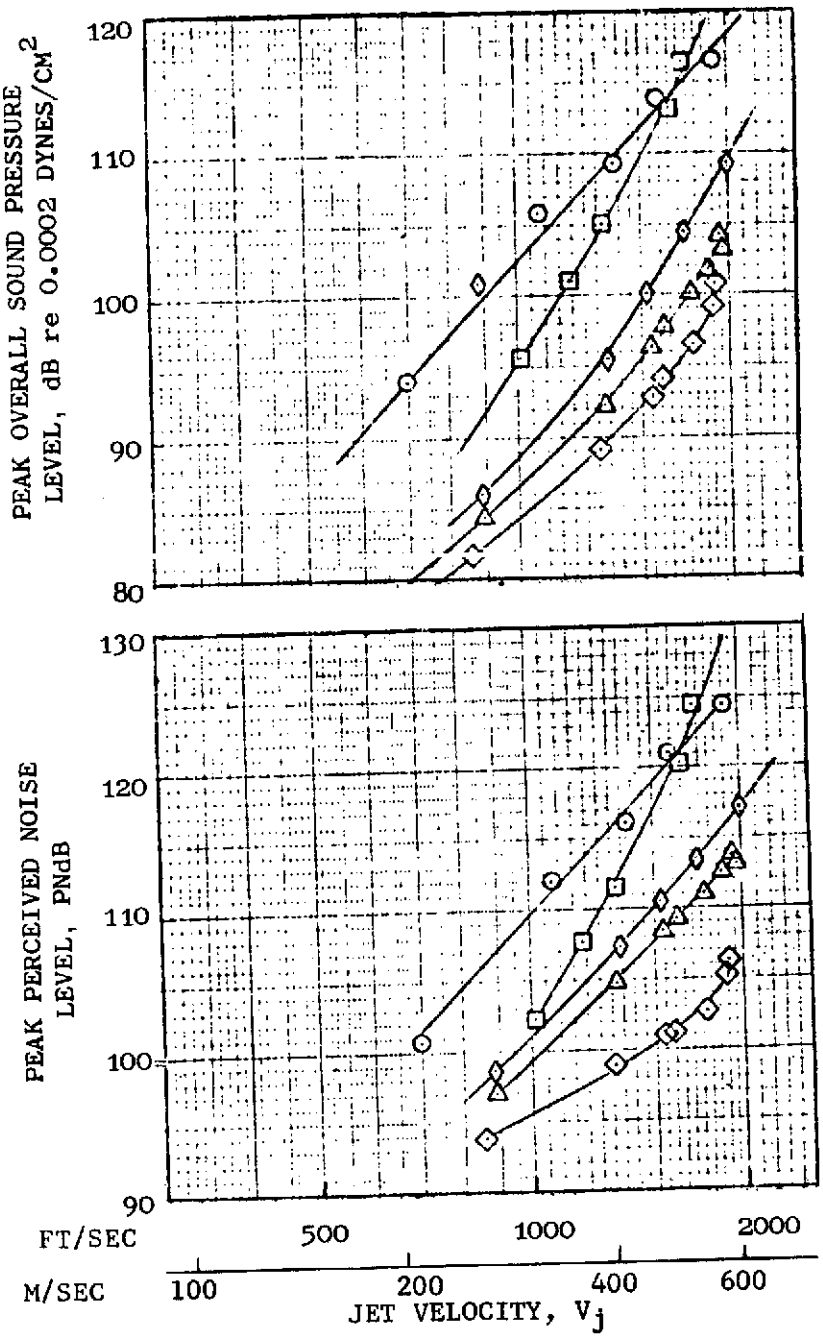

- o 59°F, 70% REL. HUM.
- o 200 FT. S.L. (61 M)
- o 20 FT. HIGH MICS (6.1 M)
- o θ_I = 110 - 140 DEGREES

- ○ CONICAL EJECTOR NOZZLE
- □ AIE AUX NOZZLE
- ◇ 104 TUBE NOZZLE W/SHROUD
- △ 104 TUBE NOZZLE W/O SHROUD
- ◊ 32 SPOKE NOZZLE

FIGURE 10.106- ISOLATED NACELLE OUTDOOR STATIC TEST, PEAK OASPL AND PNdB Vs V_J

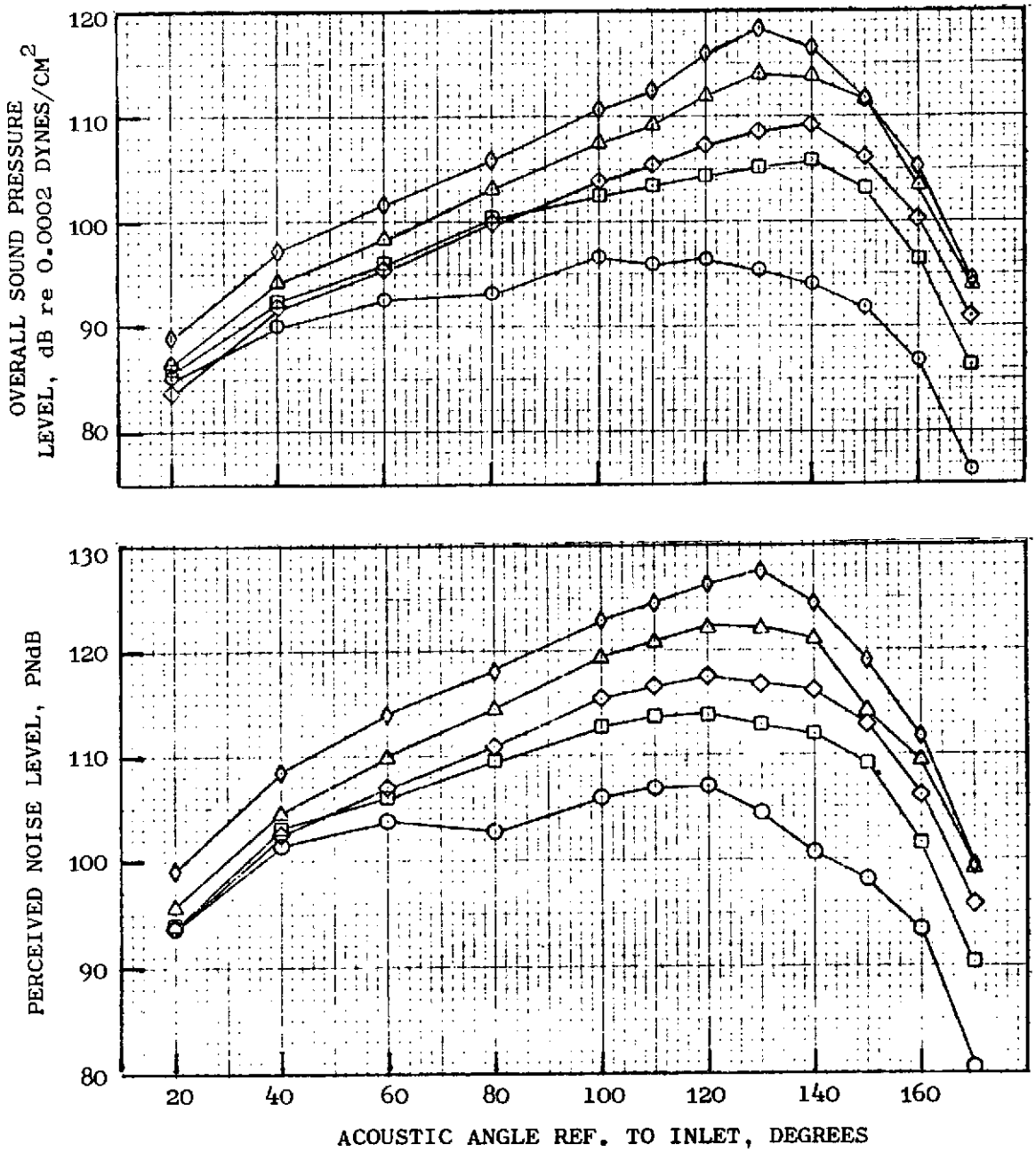

FIGURE 10.107- ISOLATED NACELLE OUTDOOR STATIC TEST, OASPL AND PNdB DIRECTIVITY, CONICAL EJECTOR NOZZLE

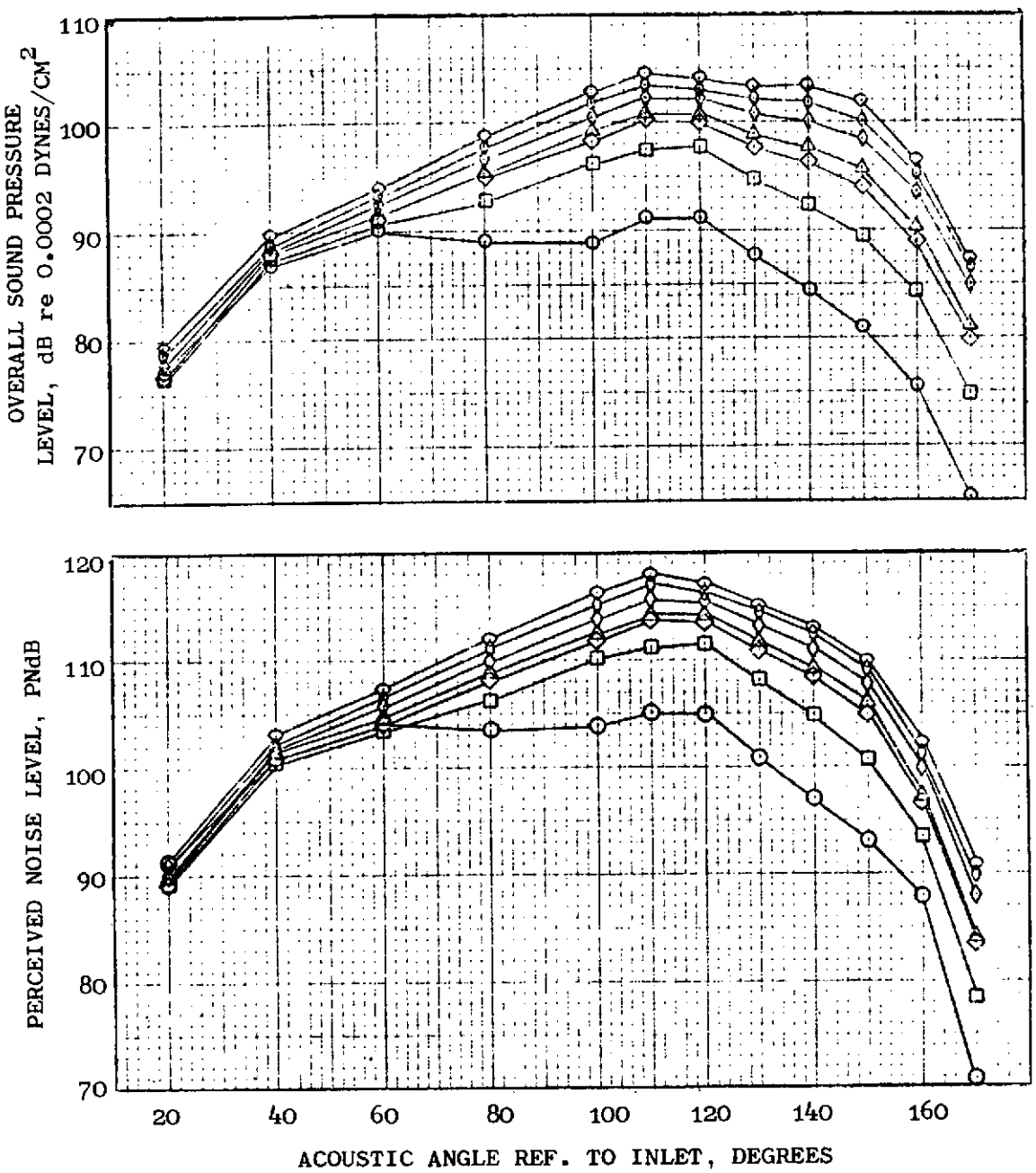

FIGURE 10.108- ISOLATED NACELLE OUTDOOR STATIC TEST, OASPL AND PNdB DIRECTIVITY, 104-TUBE NOZZLE WITHOUT SHROUD

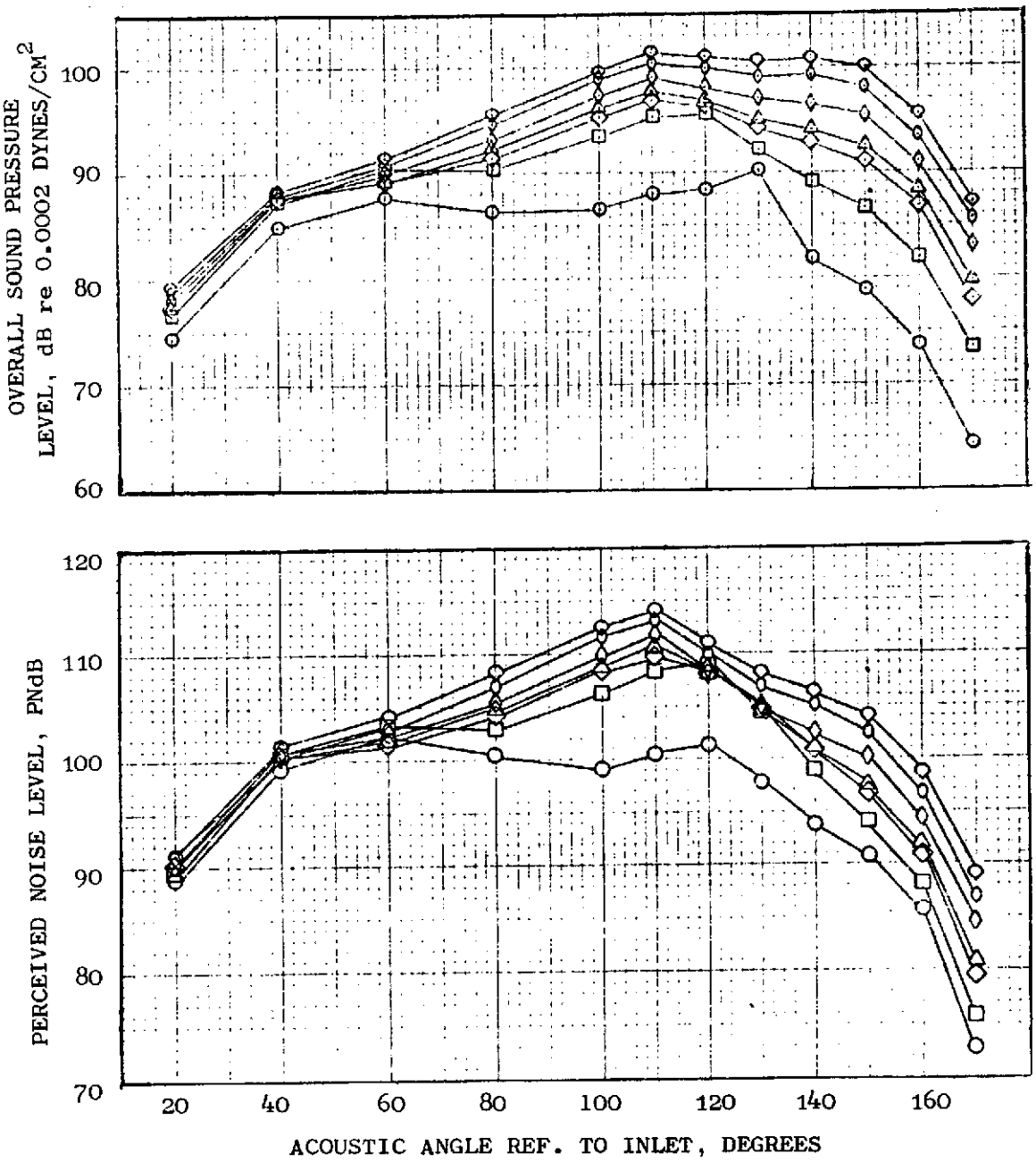

- 104 TUBE NOZZLE W/SHROUD
- 59°F, 70% REL. HUM.
- 200 FT. S.L. (61 M)
- o 20 FT. HIGH MICS (6.1 M)

D.P.	V_j FT/SEC	V_j M/SEC
○ 1002	858	262
□ 1003	1305	398
◇ 1004	1548	472
△ 1005	1604	489
◊ 1006	1770	539
◊ 1007	1896	578
◇ 1008	1914	583

FIGURE 10.109- ISOLATED NACELLE OUTDOOR STATIC TEST, OASPL AND PNdB DIRECTIVITY, 104-TUBE NOZZLE WITH SHROUD

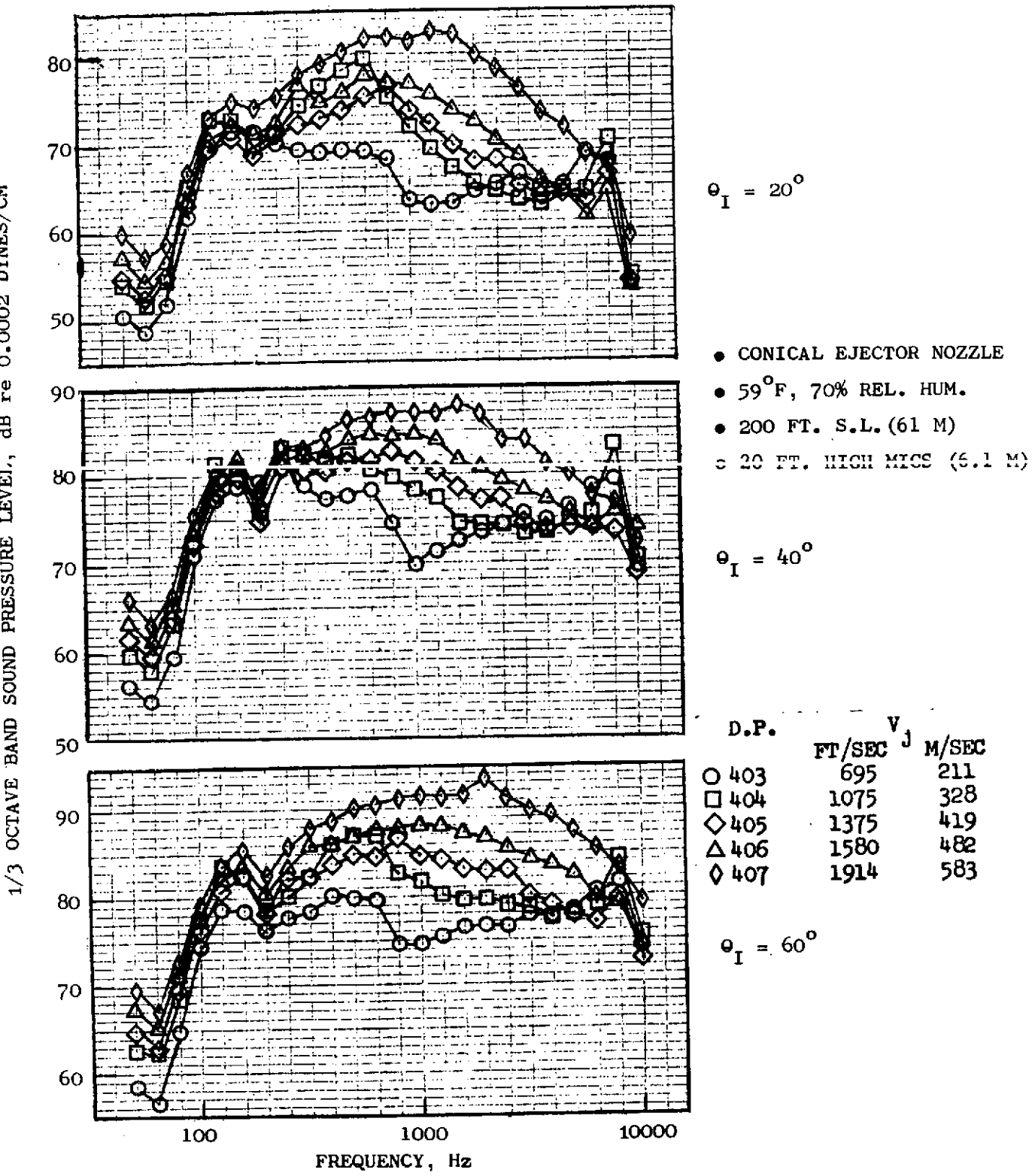

FIGURE 10.110- ISOLATED NACELLE OUTDOOR STATIC TEST, 1/3 OCTAVE BAND SPECTRA, CONICAL EJECTOR NOZZLE

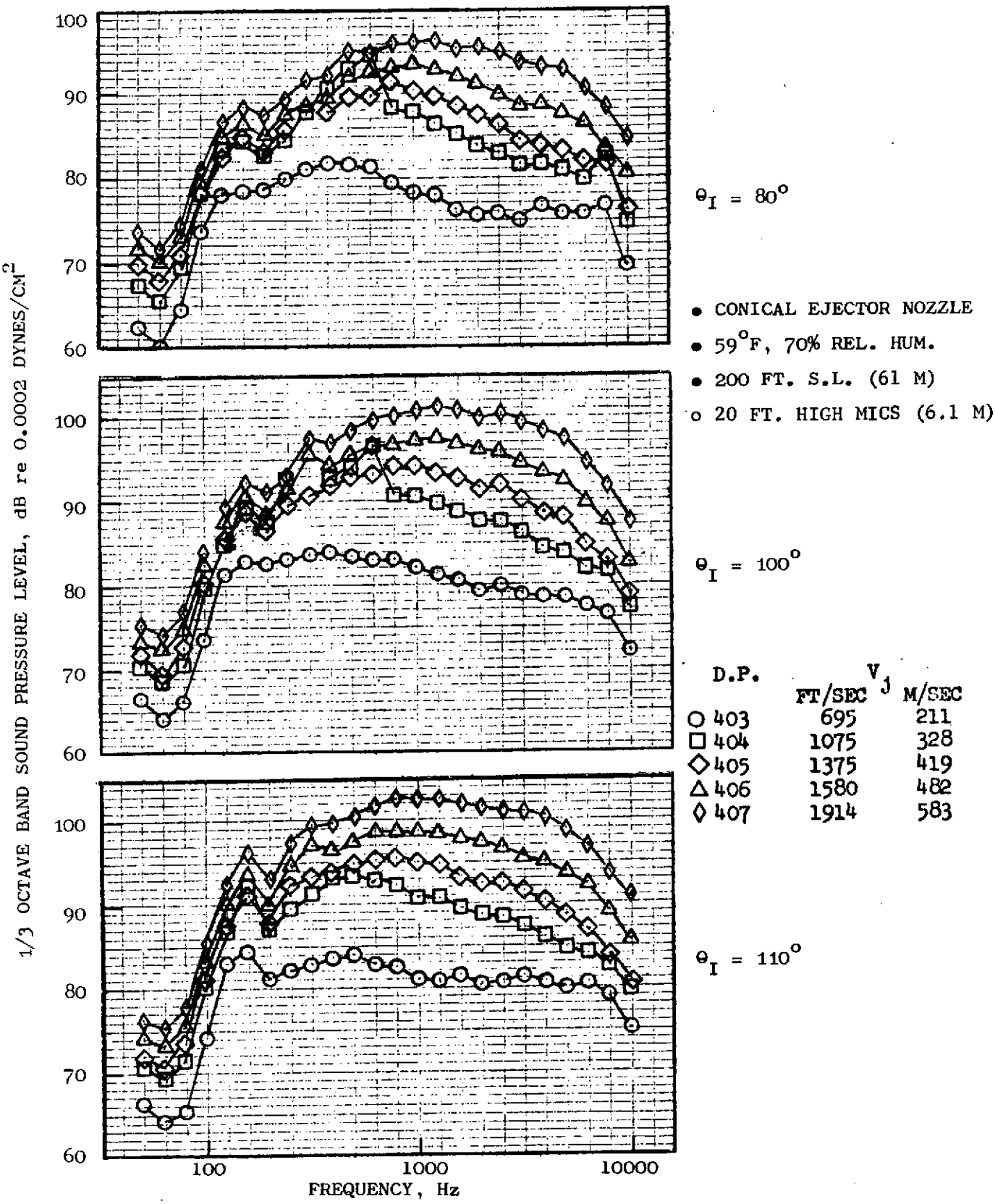

FIGURE 10.111- ISOLATED NACELLE OUTDOOR STATIC TEST, 1/3 OCTAVE BAND SPECTRA, CONICAL EJECTOR NOZZLE

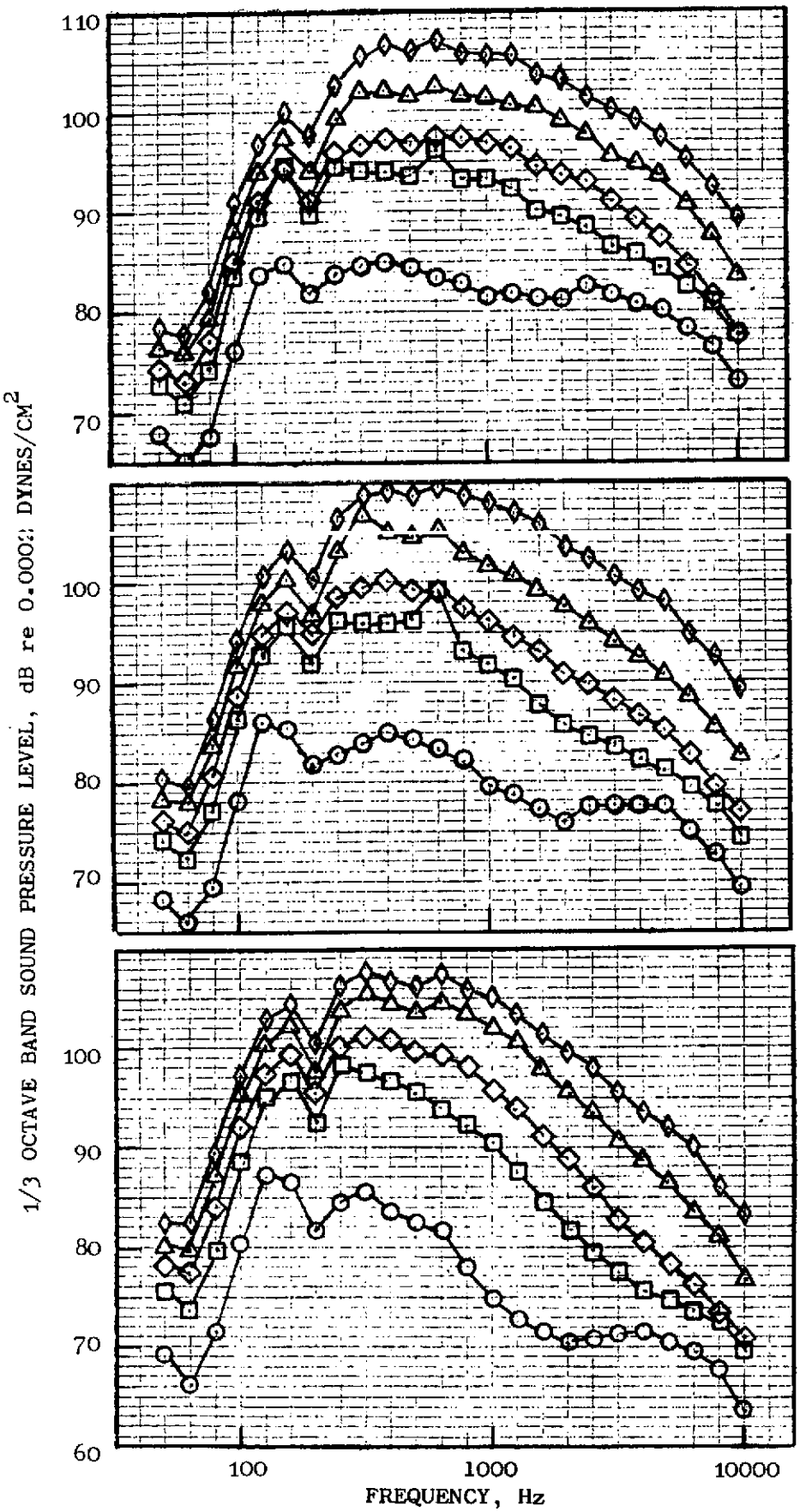

FIGURE 10.112- ISOLATED NACELLE OUTDOOR STATIC TEST, 1/3 OCTAVE BAND SPECTRA, CONICAL EJECTOR NOZZLE

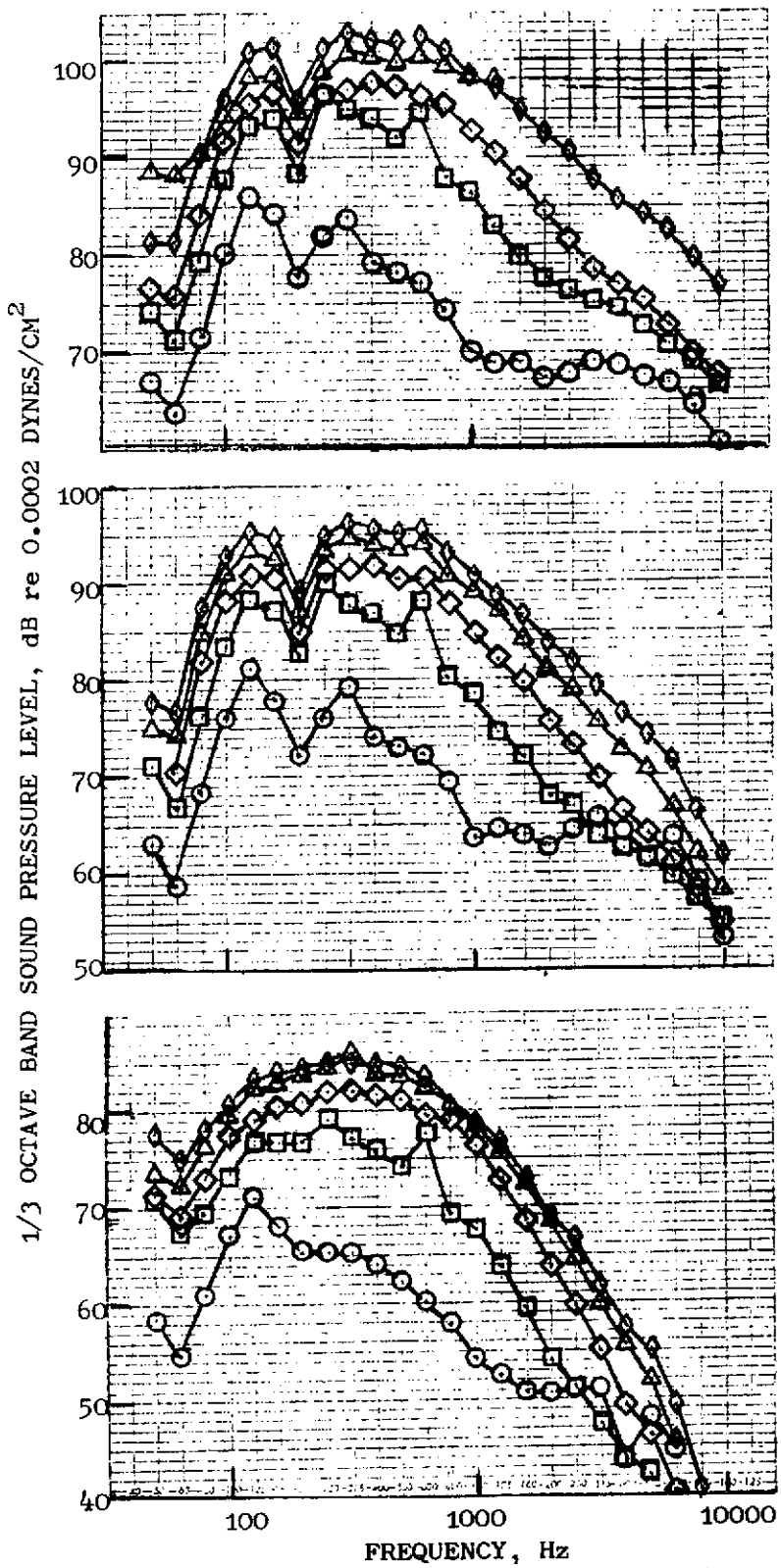

$\theta_I = 150^\circ$

$\theta_I = 160^\circ$

$\theta_I = 170^\circ$

- CONICAL EJECTOR NOZZLE
- 59°F, 70% REL. HUM.
- 200 FT. S.L. (61 M)
- o 20 FT. HIGH MICS (6.1 M)

D.P.	V_J FT/SEC	V_J M/SEC
○ 403	695	211
□ 404	1075	328
◇ 405	1375	419
△ 406	1580	482
◊ 407	1914	583

FIGURE 10.113- ISOLATED NACELLE OUTDOOR STATIC TEST, 1/3 OCTAVE BAND SPECTRA, CONICAL EJECTOR NOZZLE

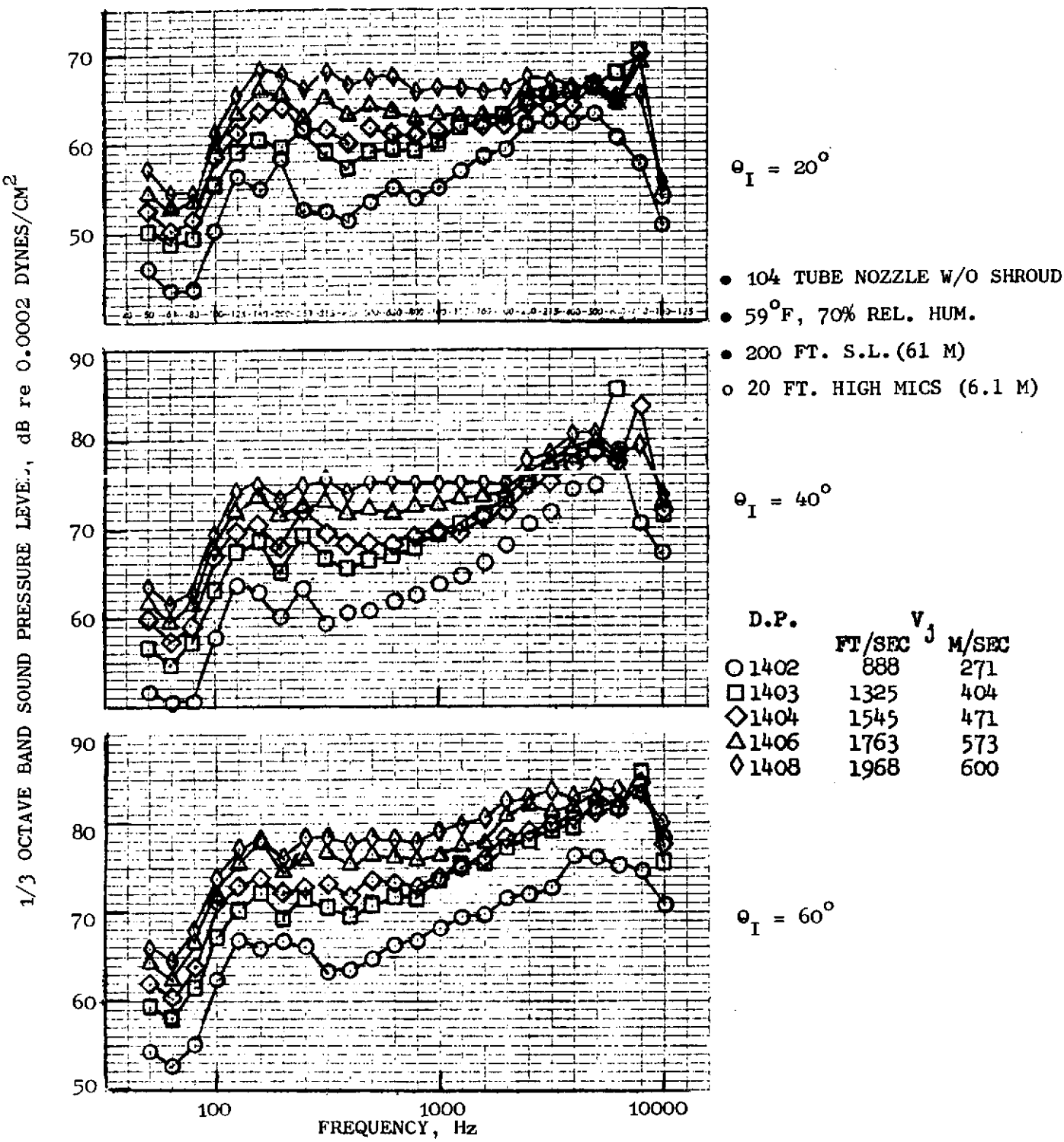

FIGURE 10.114- ISOLATED NACELLE OUTDOOR STATIC TEST, 1/3 OCTAVE BAND SPECTRA, 104-TUBE NOZZLE WITHOUT SHROUD

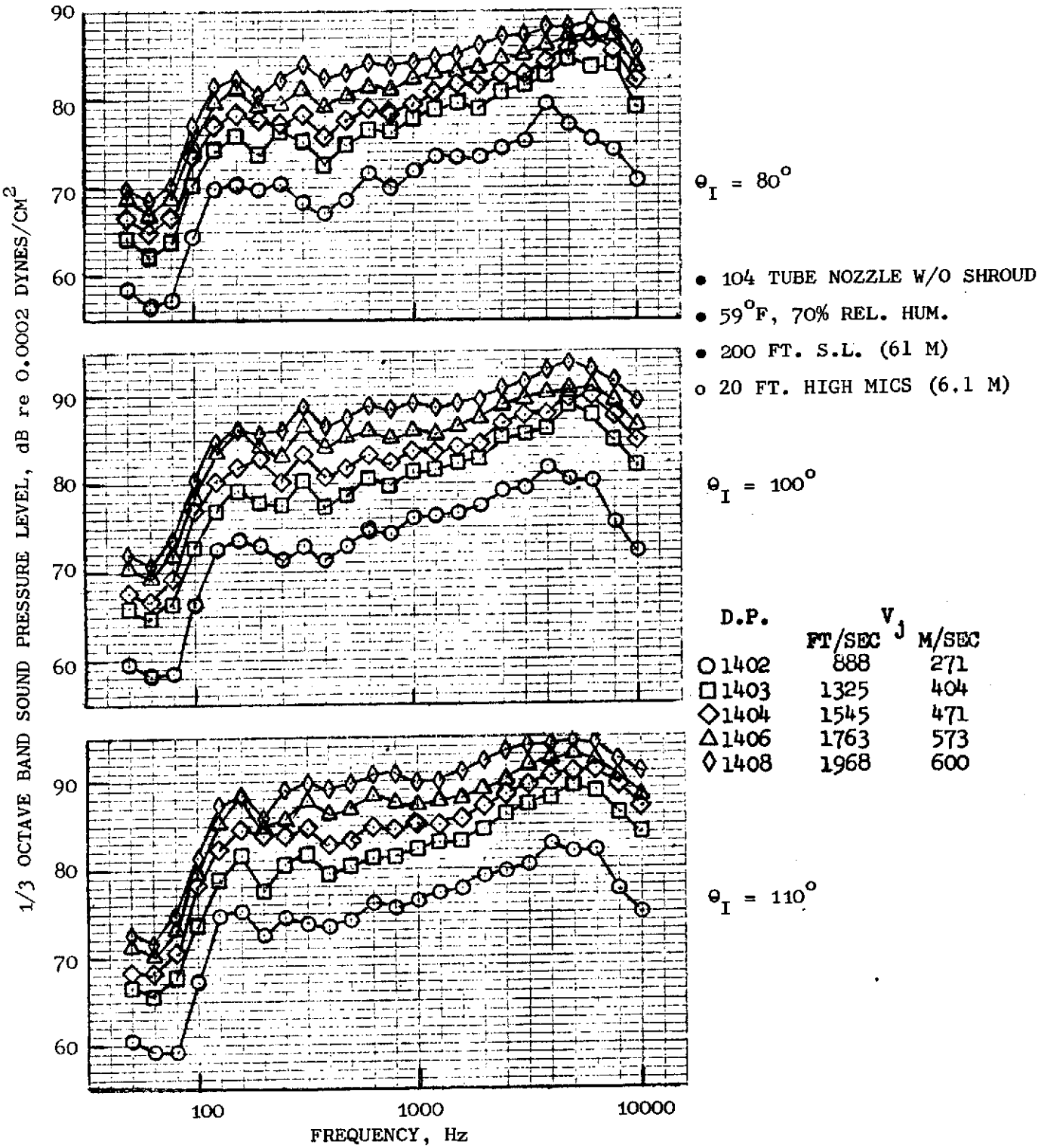

FIGURE 10.115- ISOLATED NACELLE OUTDOOR STATIC TEST, 1/3 OCTAVE BAND SPECTRA, 104-TUBE NOZZLE WITHOUT SHROUD

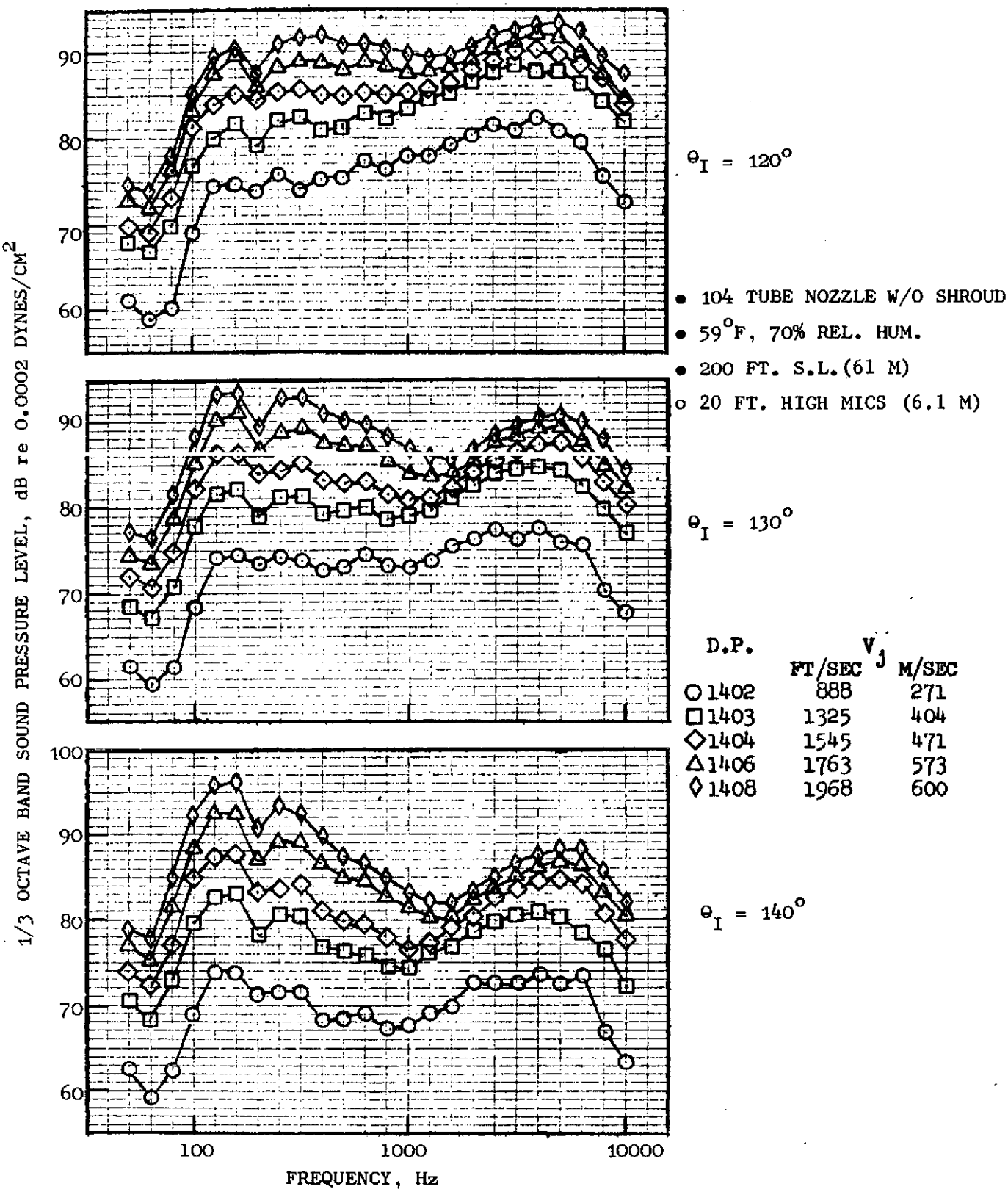

FIGURE 10.116- ISOLATED NACELLE OUTDOOR STATIC TEST, 1/3 OCTAVE BAND SPECTRA, 104-TUBE NOZZLE WITHOUT SHROUD

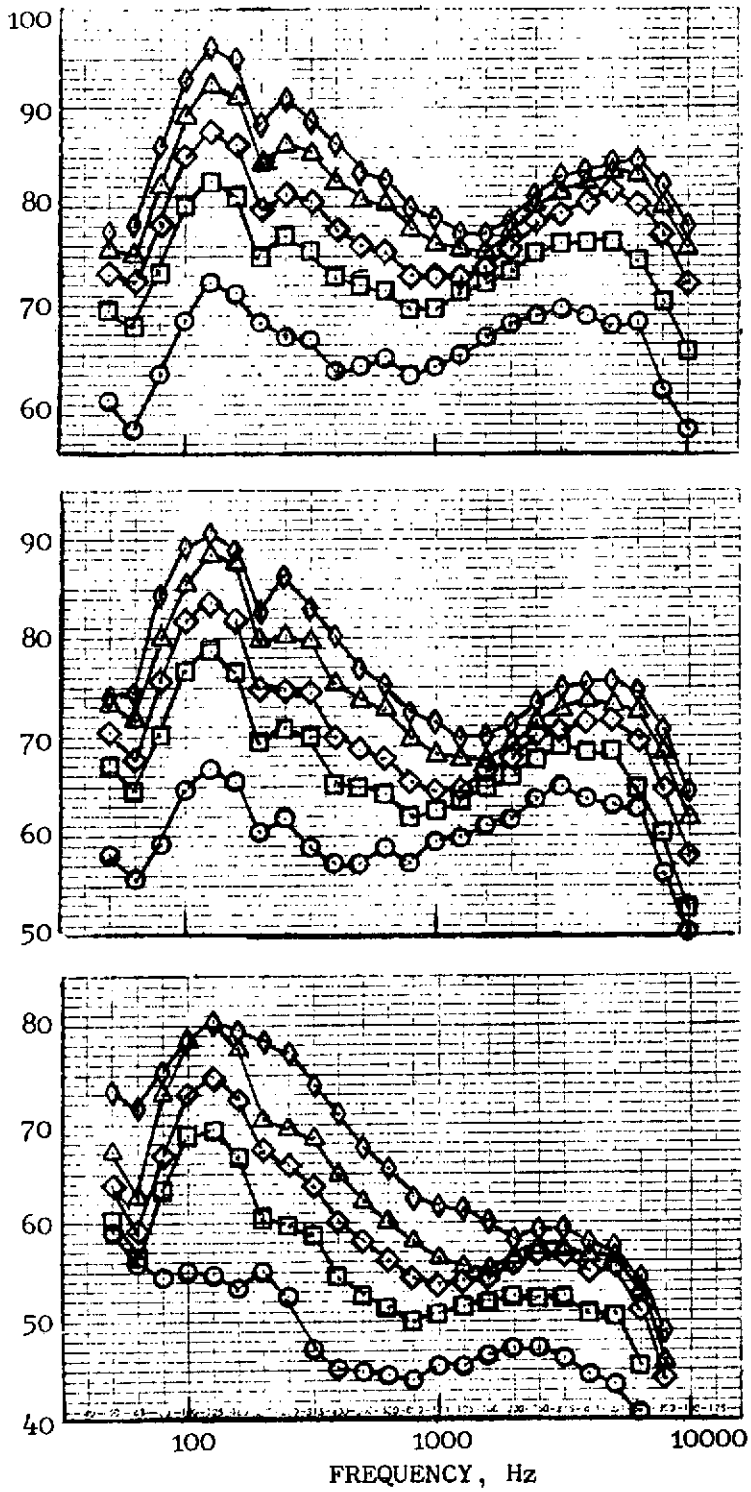

θ_I = 150°

θ_I = 160°

θ_I = 170°

- 104 TUBE NOZZLE W/O SHROUD
- 59°F, 70% REL. HUM.
- 200 FT. S.L. (61 M)
- o 20 FT. HIGH MICS (6.1 M)

D.P.	V_j FT/SEC	V_j M/SEC
○ 1402	888	271
□ 1403	1325	404
◇ 1404	1545	471
△ 1406	1763	573
◊ 1408	1968	600

FIGURE 10.117- ISOLATED NACELLE OUTDOOR STATIC TEST, 1/3 OCTAVE BAND SPECTRA, 104-TUBE NOZZLE WITHOUT SHROUD

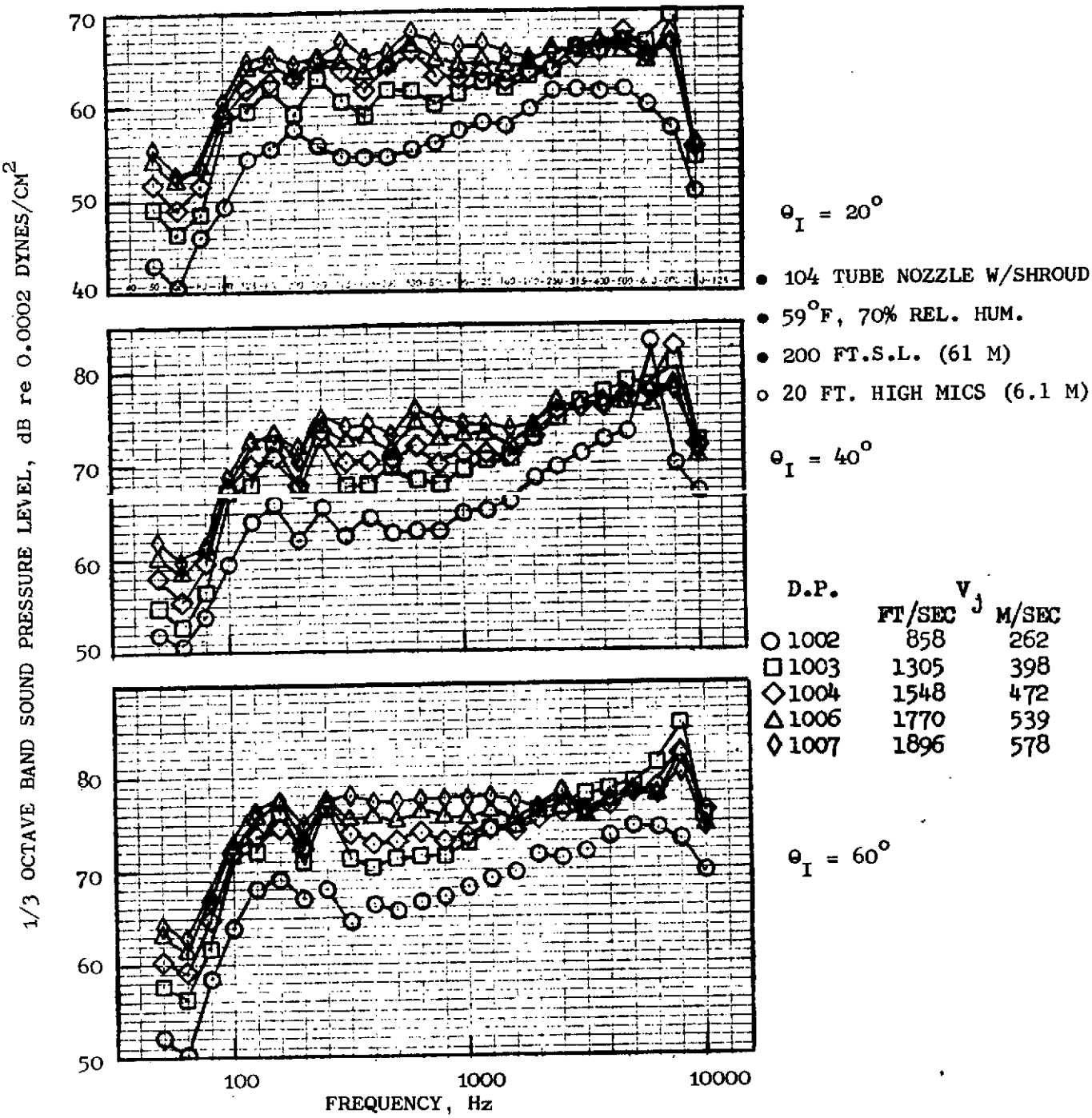

FIGURE 10.118- ISOLATED NACELLE OUTDOOR STATIC TEST, 1/3 OCTAVE BAND SPECTRA, 104-TUBE NOZZLE WITH SHROUD

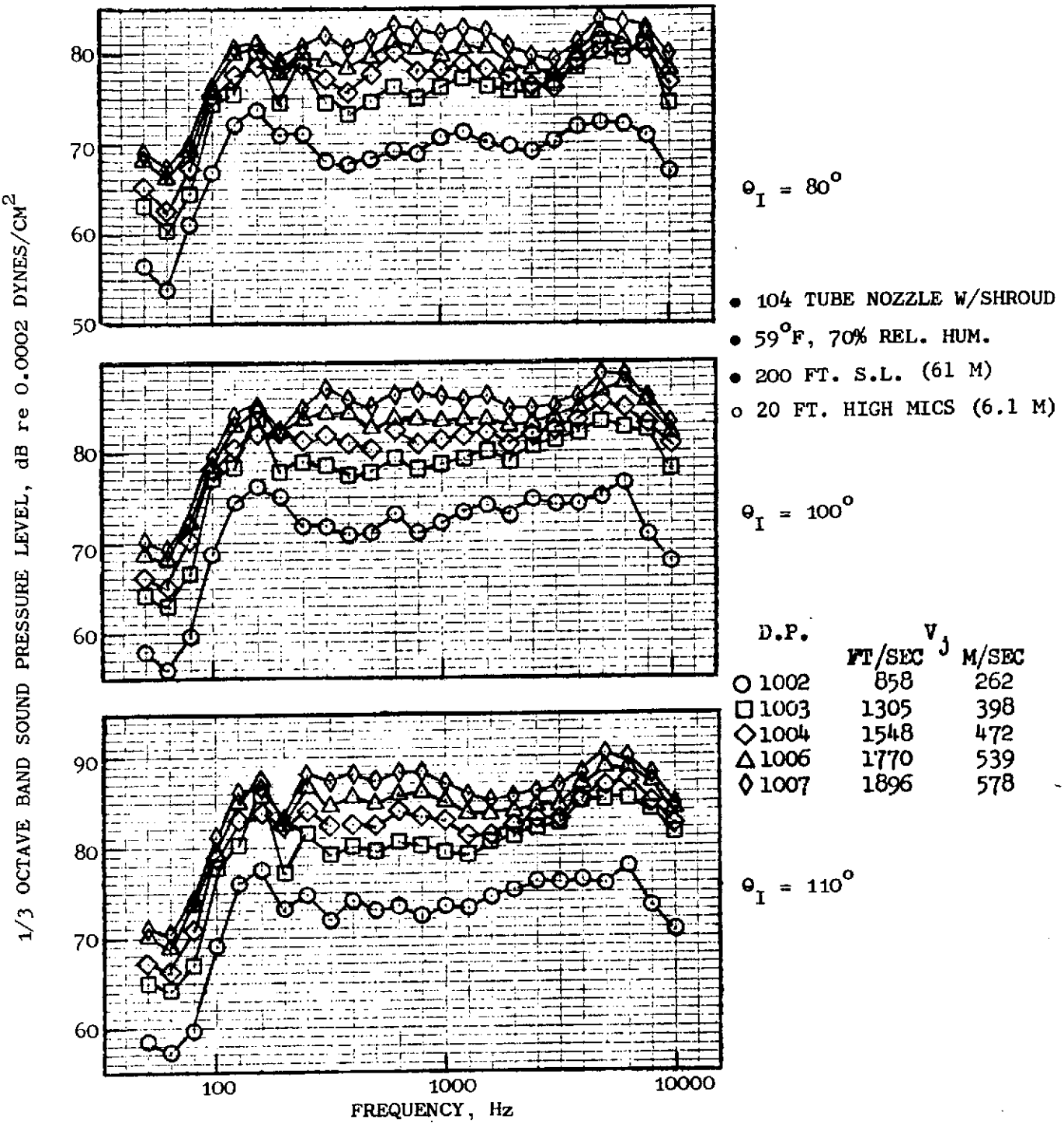

FIGURE 10.119- ISOLATED NACELLE OUTDOOR STATIC TEST, 1/3 OCTAVE BAND SPECTRA, 104-TUBE NOZZLE WITH SHROUD

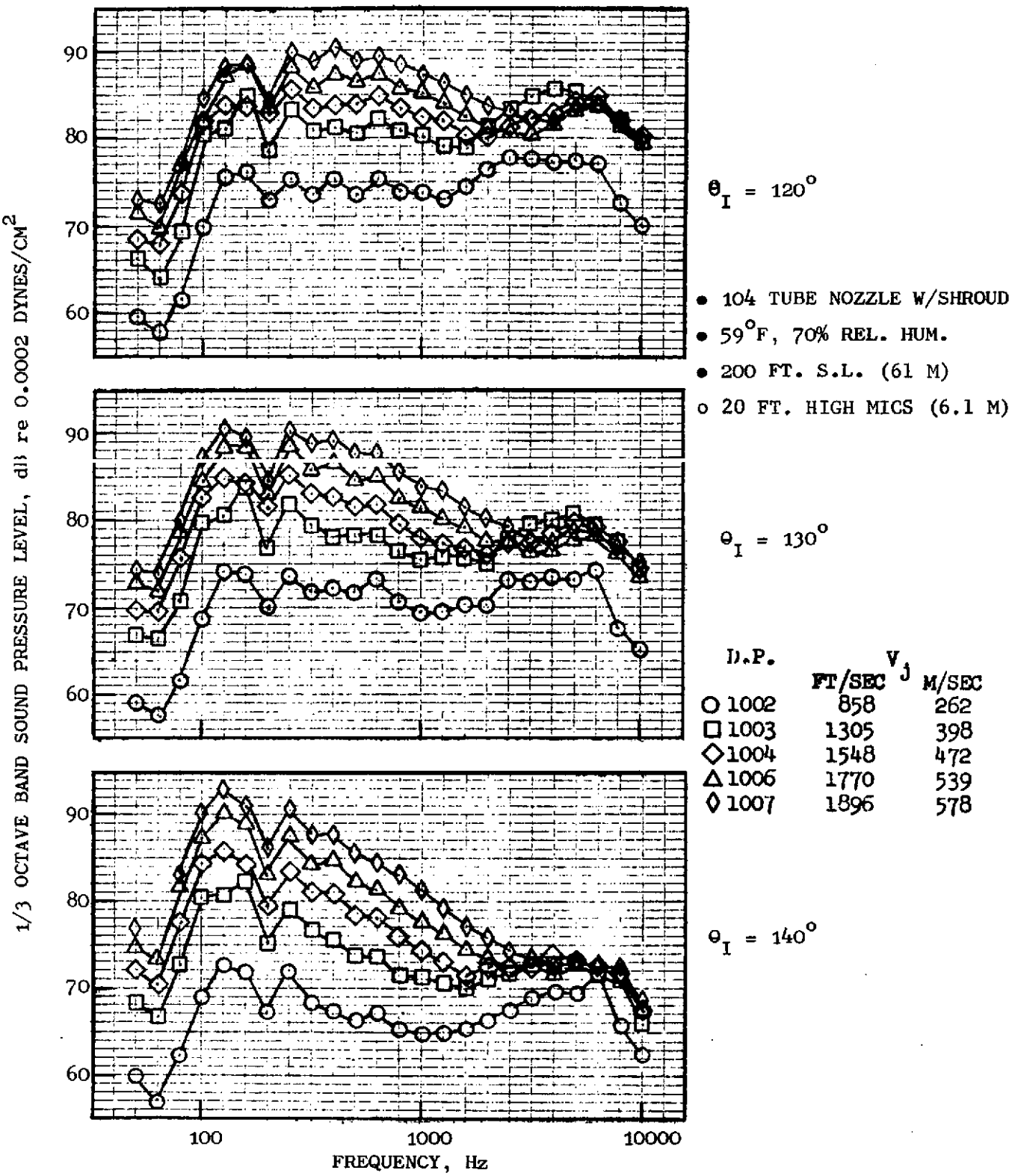

FIGURE 10.120- ISOLATED NACELLE OUTDOOR STATIC TEST, 1/3 OCTAVE BAND SPECTRA, 104-TUBE NOZZLE WITH SHROUD

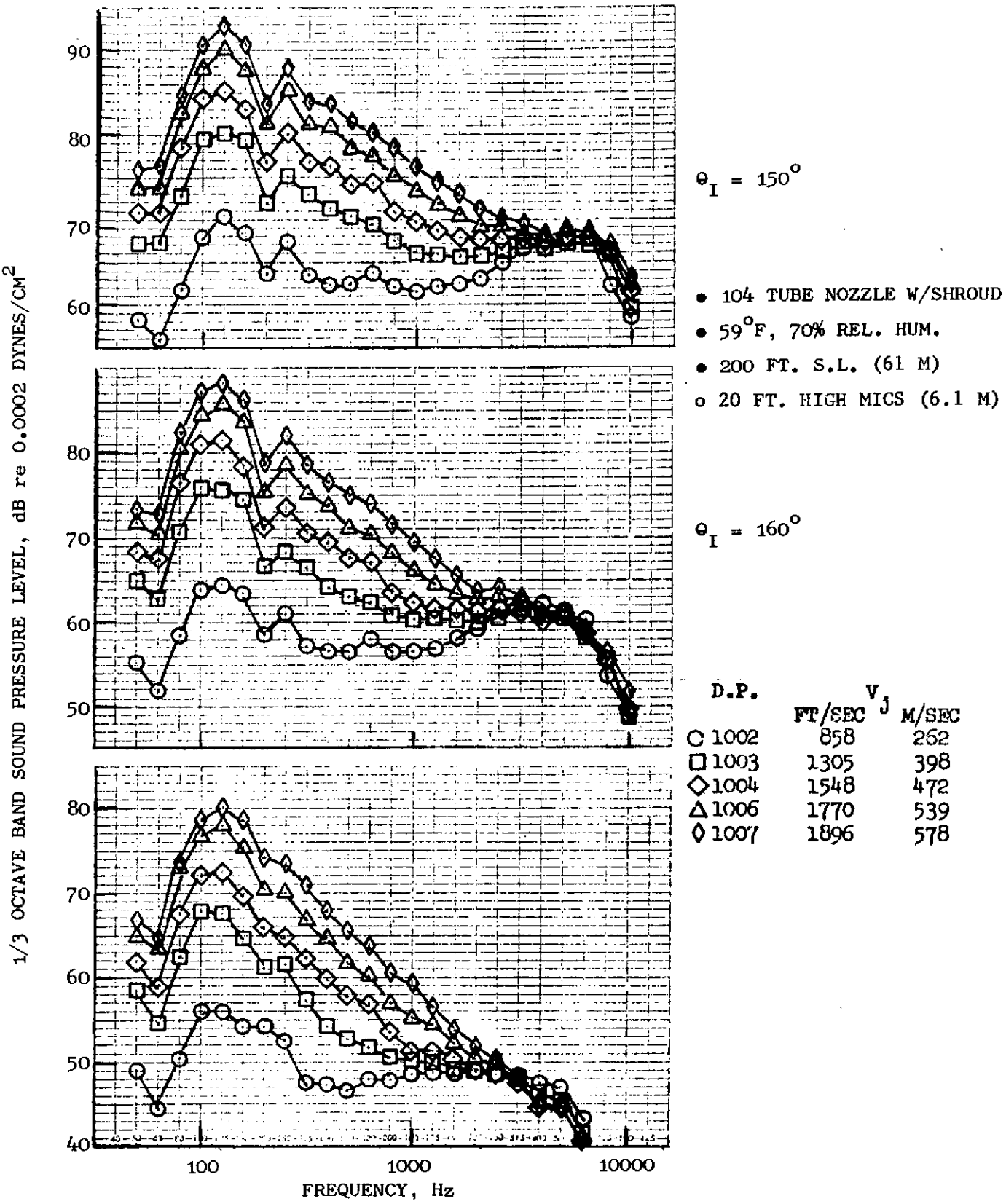

FIGURE 10.121- ISOLATED NACELLE OUTDOOR STATIC TEST, 1/3 OCTAVE BAND SPECTRA, 104-TUBE NOZZLE WITH SHROUD

10.2.2 Wing/Nacelle Static Test

Three nozzle configurations were evaluated during the "Outdoor Static Wing/Nacelle Test Series." The nozzles were the conical ejector nozzle and the 104 tube nozzle with and without an acoustically treated shroud. The jet noise signature of each nozzle was monitored over the velocity range defined on Table 9.5. The material is presented in the same manner as Section 10.2.1.

Presented on Figure 10.122 are the overall sound power level characteristics for each configuration evaluated. Using the conical nozzle as the reference configuration, the following trends are observed.

- The 104 tube nozzle yields 5 dB suppression at a low jet velocity of 305 m/sec (1000 ft/sec) and 11 dB suppression at 610 m/sec (2000 ft/sec).
- Adding an acoustically treated shroud to the 104 tube nozzle yields an additional 3 dB suppression over the velocity range.

Presented on Figure 10.123 are the one-third octave band sound power level spectra for the three configurations. The spectra representing the conical ejector nozzle at a jet velocity of 594 m/sec (1950 ft/sec) peaks at a frequency of 630 Hz at a level of 162 dB. In contrast, the 104 tube nozzle has a power level spectra that has two distinct peak regions. The first peak occurs at 125 Hz and represents the fully merged region of the jet. The second peak occurs at 6300 Hz and represents the noise produced by each individual tube element before merging. As in the isolated nacelle outdoor static test, this hypothesis is supported by comparing the spectra of the 104 tube nozzle without the acoustically treated shroud to the power level spectra with the shroud. The peak level for the high velocity condition at 6300 Hz shows a drop of 5 dB when the shroud is added, the same that was noted in the isolated nacelle test. In comparing the 104 tube nozzle with the conical nozzle, 11 dB suppression is observed on the basis of sound power level at the peak frequency.

Presented on Figure 10.124 are graphs of peak OASPL and PNL as a function of exhaust jet velocity for the three configurations tested. Comparisons were made with the data corrected to standard day conditions 288° K (59° F), 70% R.H. and extrapolated to a 61 meter (200 foot) sideline. The conical ejector nozzle has a peak OASPL of 118 dB for a jet velocity of 610 m/sec (2000 ft/sec) and 100

dB for a jet velocity of 305 m/sec (1000 ft/sec). The 104 tube nozzle has a suppression level of 14 dB over the velocity range evaluated. The addition of a shroud to the 104 tube nozzle increases suppression by 3 and 2 dB at jet velocities of 305 and 610 m/sec (1000 and 2000 ft/sec), respectively. The conical ejector nozzle had a peak PNL of 127 dB for a jet velocity of 610 m/sec (2000 ft/sec) and 107 dB for a jet velocity of 305 m/sec (1000 ft/sec). The 104 tube nozzle has 7 and 12 dB of peak PNdB suppression at jet velocities of 305 and 610 m/sec (1000 and 2000 ft/sec), respectively. The addition of a shroud to the 104 tube nozzle yields additional suppression of 3 and 7 dB for jet velocities of 305 and 610 m/sec (1000 and 2000 ft/sec), respectively. The explanation for the additional decrease in PNL compared to OASPL is the same as given in Section 10.2.1, i.e., the shroud suppresses the high frequency portion of the spectra where the noy weighting is largest.

Figures 10.125 through 10.127 show overall sound pressure level (OASPL) and perceived noise level (PNL) as a function of acoustic angle, referenced to inlet, for the conical ejector nozzle and 104 tube nozzle with and without shroud. All data were corrected to a 288° K (59° F), 70% R.H. standard day and extrapolated to a 61 meter (200 foot) sideline. For the conical ejector nozzle, the peak OASPL's for all jet velocities tested occur at acoustic angles between 130 and 140 degrees. For jet velocities of approximately 396 and 610 m/sec (1300 and 2000 ft/sec), the peak OASPL's are 107 and 117 dB, respectively. The 104 tube nozzle has peak OASPL's at 120 degrees. At jet velocities of 396 and 610 m/sec (1300 and 2000 ft/sec), this nozzle suppresses 9 and 12 dB, respectively. In the forward quadrant at angles of 20-80 degrees, the 104 tube nozzle suppresses 8 dB for a jet velocity of 610 m/sec (2000 ft/sec) and 6.5 dB for a jet velocity of 396 m/sec (1300 ft/sec). The addition of an acoustically treated shroud to the 104 tube nozzle causes an additional increase in suppression of 2 to 4 dB for acoustic angles between 40 and 160 degrees for all power settings. Comparing the configurations on the basis of perceived noise level (PNL), Figure 10.125 shows that for jet velocities of about 594 and 396 m/sec (1950 and 1300 ft/sec), the peak PNL's for the conical ejector nozzle are 127 and 115 dB, respectively. The 104 tube nozzle provides 4 dB suppression at 396 m/sec (1300 ft/sec) and 9 dB suppression at 594 m/sec (1950 ft/sec) on the basis of peak PNL. In the forward quadrant at angles of

40 through 80 degrees, the 104 tube nozzle suppresses PNL by 3-5 and 5-7 dB for jet velocities of 396 and 594 m/sec (1300 and 1950 ft/sec), respectively. For the 104 tube nozzle, peak PNL's occur at the same angles as peak OASPL's. Adding an acoustically treated shroud to the 104 tube nozzle yields additional suppression of peak PNL by 5 and 3 dB for jet velocities of 594 and 396 m/sec (1950 and 1300 ft/sec), respectively. Suppression with the shroud does occur for all angles greater than 40 degrees and at all power settings. Peak suppression is 7 dB for all power settings at 140 degrees.

Presented on Figures 10.128 through 10.136 are the 1/3 octave band sound pressure level spectra for the conical ejector nozzle and 104 tube nozzle with and without an acoustically treated shroud. The spectra presented are for acoustic angles ranging from 40 to 150 degrees. All data were corrected to a 288° K (59° F), 70% R.H. standard day and extrapolated to a 61 meter (200 foot) sideline. In analyzing the data, the same spectra trends that occurred for the isolated nacelle test in the previous section became apparent for the nozzle configurations in this test. They may be summarized as follows:

- At a jet velocity of 595 m/sec (1954 ft/sec), the conical ejector nozzle spectra peaks at a frequency of 400 Hz at the peak noise angle of 140 degrees to the inlet.
- The 104 tube nozzle without shroud causes a marked change in shape of the frequency spectra which is illustrated on Figures 10.131 through 10.133. This "double humped" spectra is characteristic of multi-element nozzles.
- Comparing the conical ejector and 104 tube nozzle at a jet velocity of about 610 m/sec (2000 ft/sec) indicates that the 104 tube nozzle provides a suppression of 13 dB on the basis of peak 1/3 octave band SPL.
- Adding an acoustically treated shroud to the 104 tube nozzle causes additional suppression in the high frequency portion of the spectra. For example, at a jet velocity of about 610 m/sec (2000 ft/sec) and angle of 140 degrees, the shroud yields an additional 15 dB of suppression at 6300 Hz.

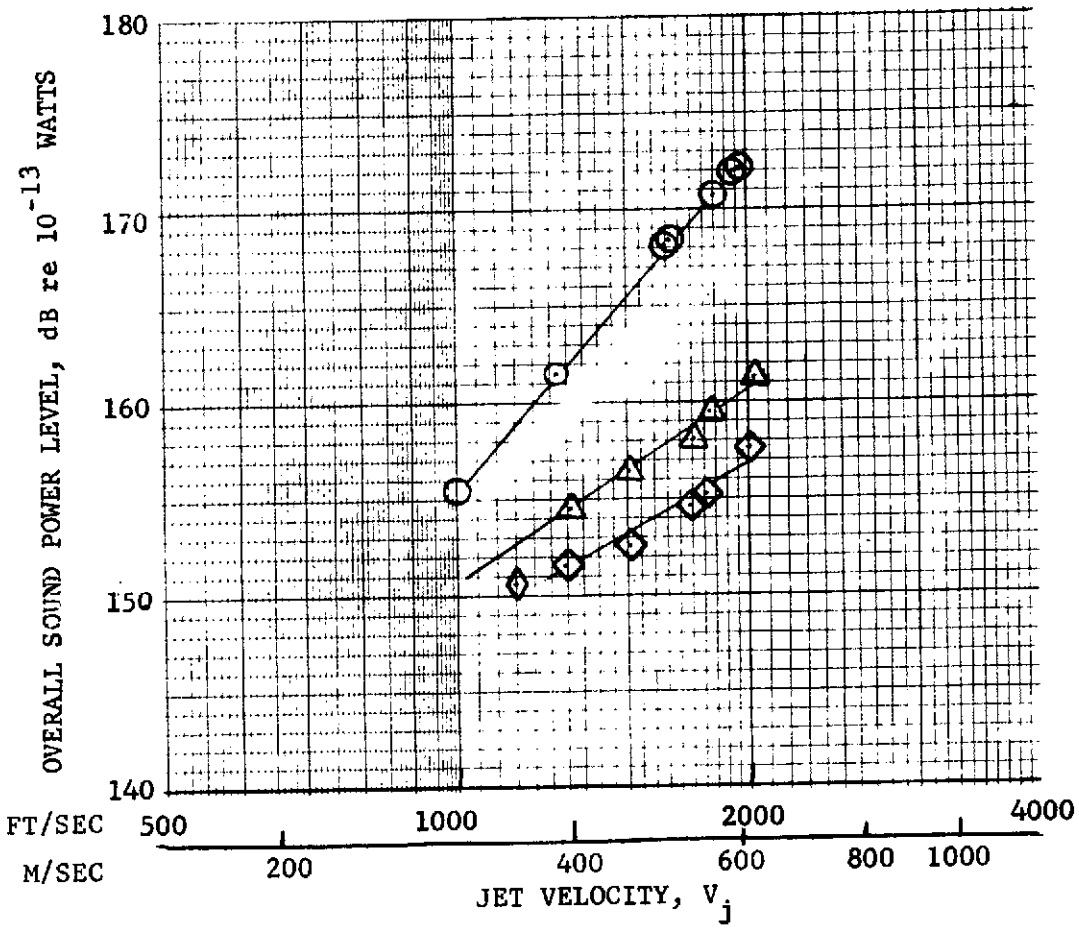

- ● 59°F, 70% REL. HUM.
- ● 100 FT. ARC (30.5 M)
- o 20 FT. HIGH MICS (6.1 M)

- O CONICAL NOZZLE W/BELLMOUTH
- △ 104 TUBE NOZZLE W/O SHROUD
- ◇ 104 TUBE NOZZLE W/SHROUD

FIGURE 10.122 - WING NACELLE OUTDOOR STATIC TEST, OAPWL Vs V_J

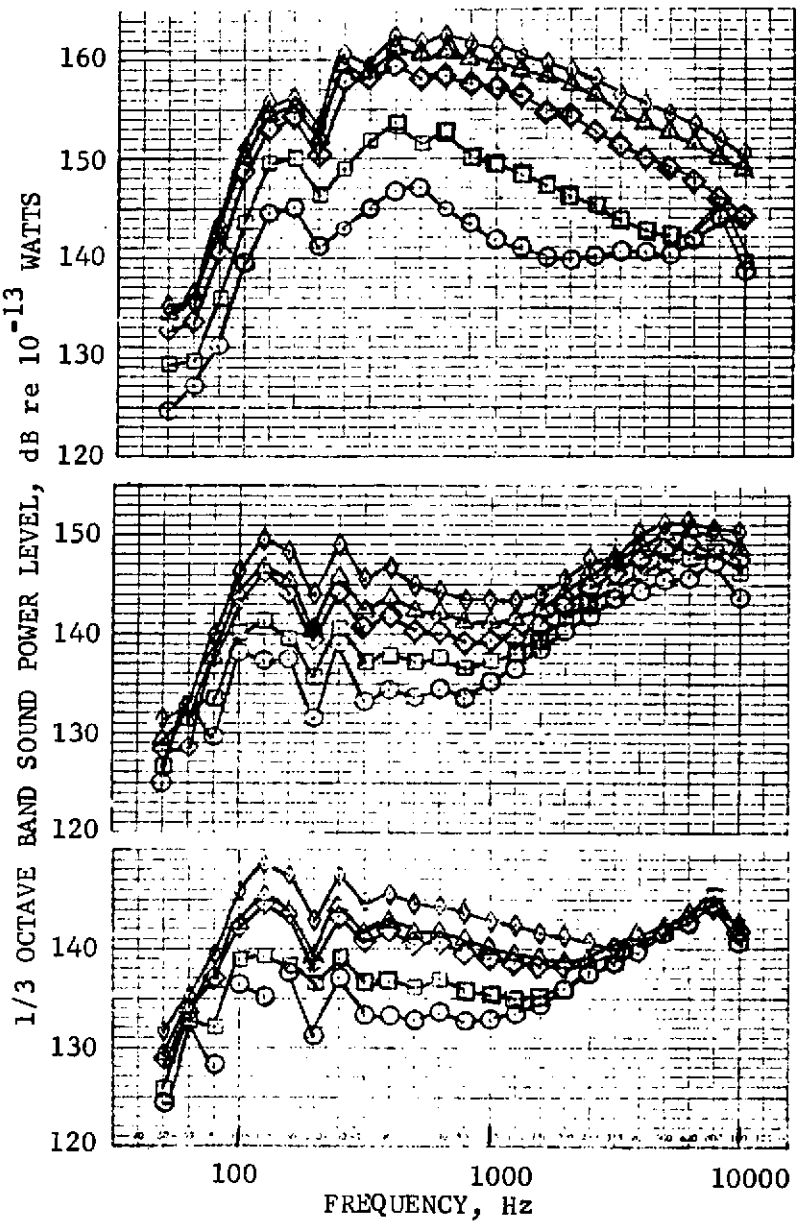

CONICAL NOZZLE W/BELLMOUTH

D.P.	V_j FT/SEC	V_j M/SEC
○ 1207	1006	307
□ 1206	1270	387
◇ 1205	1665	507
△ 1203	1850	564
◊ 1208	1954	596

104 TUBE NOZZLE W/O SHROUD

D.P.	V_j FT/SEC	V_j M/SEC
○ 602	1314	401
□ 603	1506	459
◇ 604	1755	535
△ 605	1823	556
◊ 606	2019	615

104 TUBE NOZZLE W/SHROUD

D.P.	V_j FT/SEC	V_j M/SEC
○ 302	1292	394
□ 303	1507	459
◇ 304	1741	531
△ 305	1810	552
◊ 306	2008	612

- 59°F, 70% REL. HUM.
- 100 FT. ARC (30.5 M)
- 20 FT. HIGH MICS (6.1 M)

FIGURE 10.123 - WING NACELLE OUTDOOR STATIC TEST, 1/3 OCTAVE BAND POWER SPECTRA

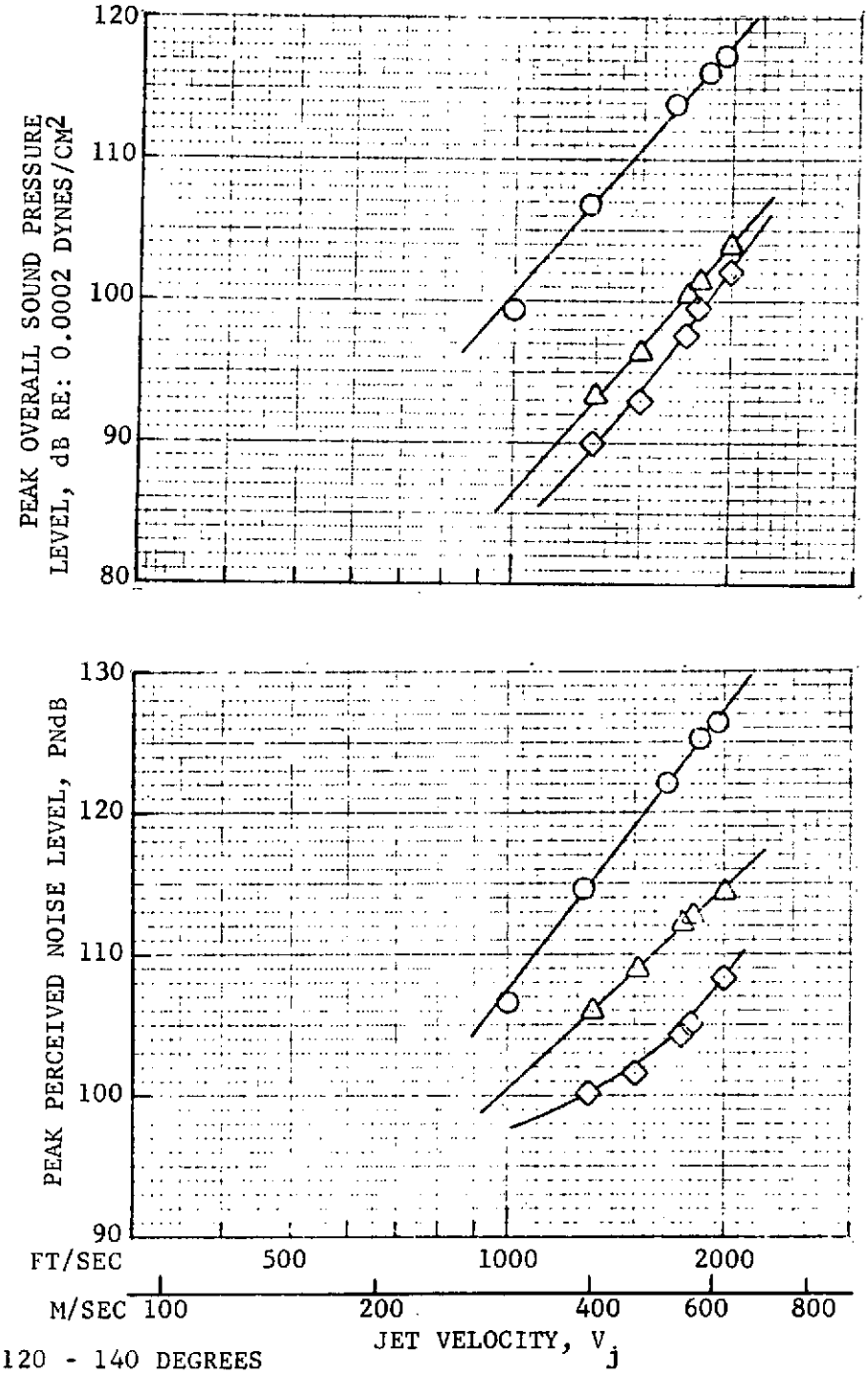

- o θ_I = 120 - 140 DEGREES
- o 59°F, 70% REL. HUM.
- o 200 FT. S.L. (61 M)
- o 20 FT. HIGH MICS (6.1 M)

- O CONICAL NOZZLE W/BELLMOUTH
- △ 104 TUBE NOZZLE W/O SHROUD
- ◇ 104 TUBE NOZZLE W/SHROUD

FIGURE 10.124 - WING NACELLE OUTDOOR STATIC TEST, PEAK OASPL AND PNdB Vs V_j

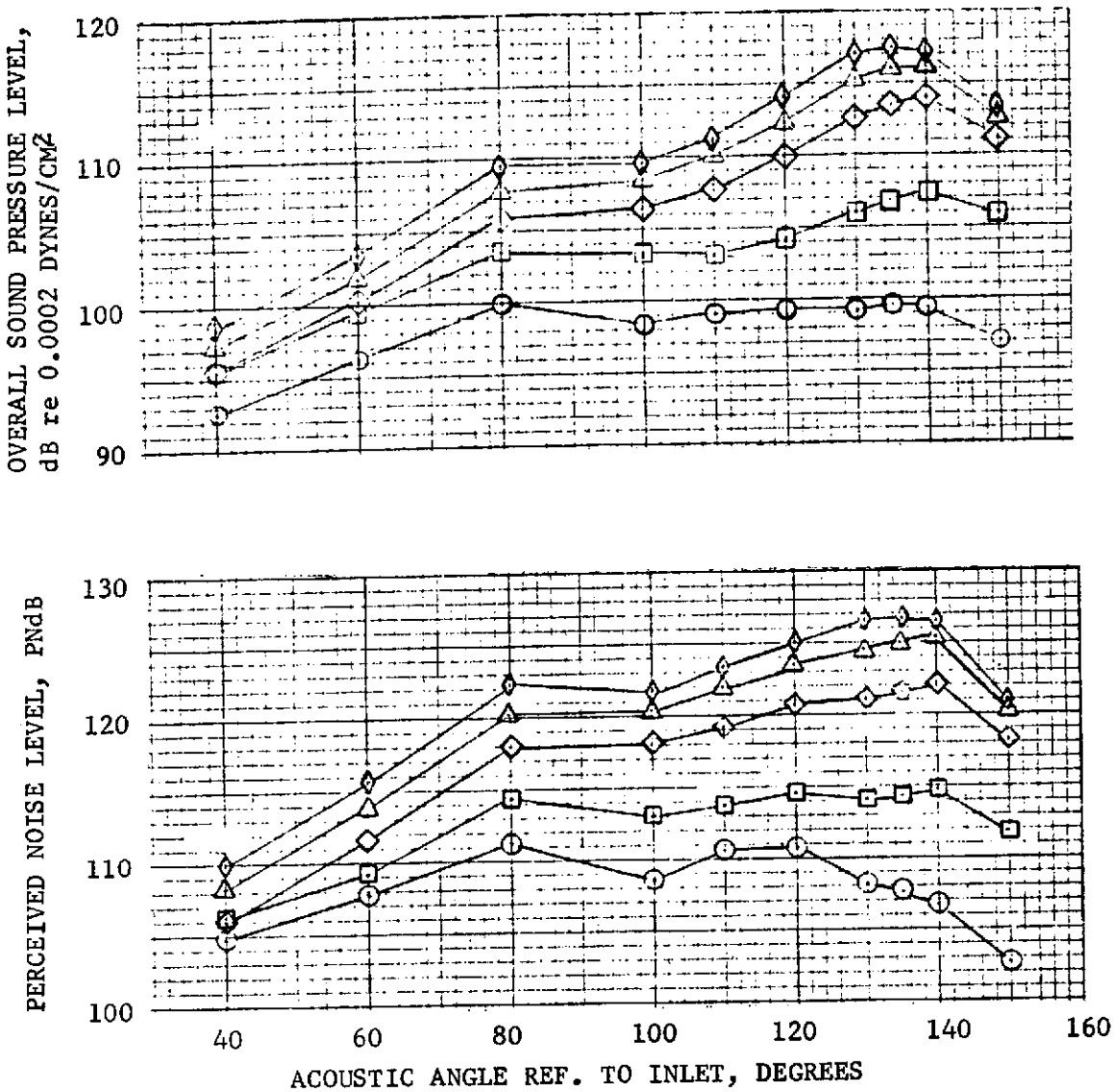

- ● CONICAL NOZZLE
- ● 59°F, 70% REL. HUM.
- ● 200 FT. S.L. (61 M)
- o 20 FT. HIGH MICS (6.1 M)

D.P.	V_j FT/SEC	V_j M/SEC
○ 1207	1006	307
□ 1206	1270	387
◇ 1205	1665	507
△ 1203	1850	564
◊ 1208	1954	596

FIGURE 10.125 - WING NACELLE OUTDOOR STATIC TEST, OASPL AND PNdB DIRECTIVITY, CONICAL EJECTOR NOZZLE

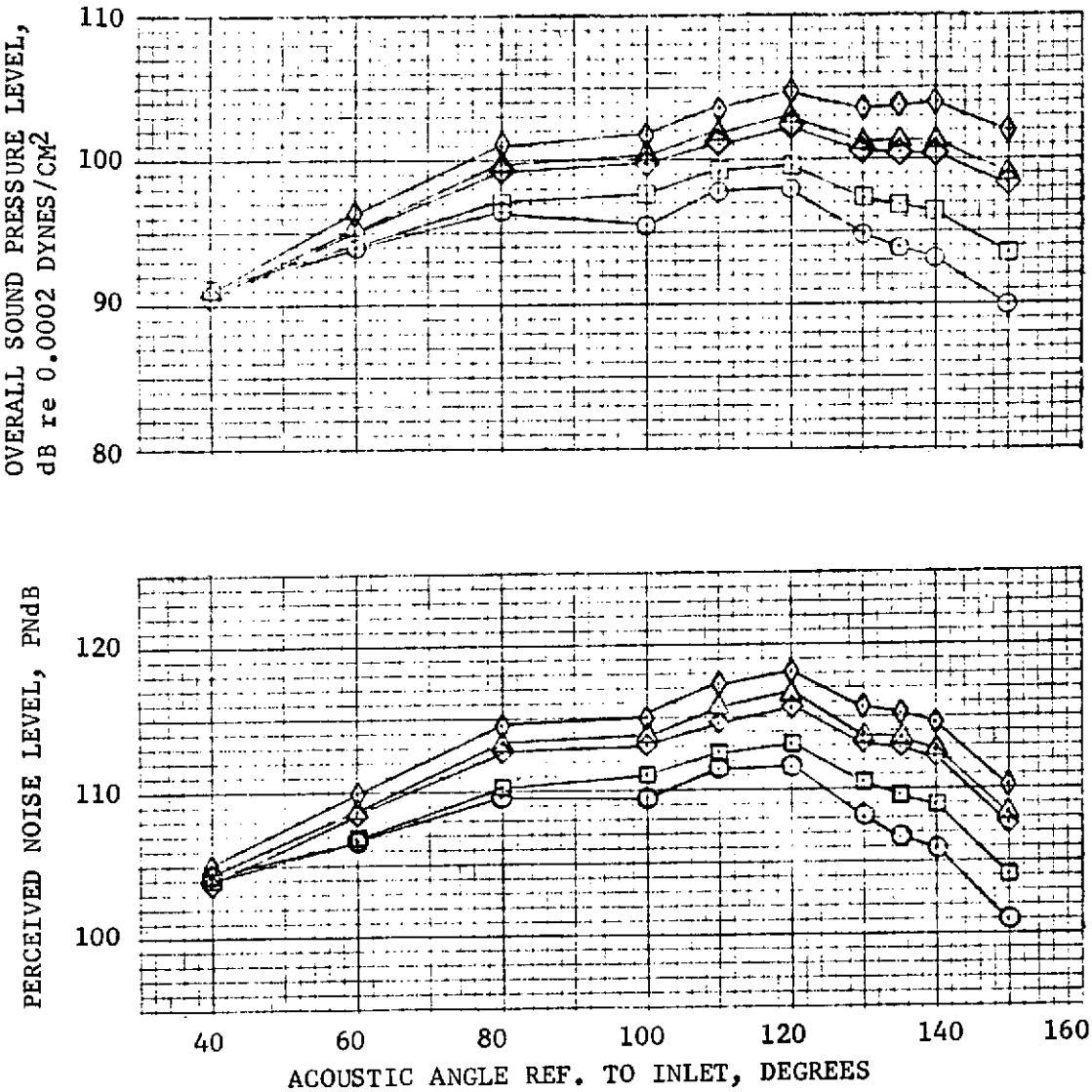

- 104 TUBE NOZZLE W/O SHROUD
- 59°F, 70% REL. HUM.
- 200 FT. S.L. (61 M)
- o 20 FT. HIGH MICS (6.1 M)

D.P.	V_j FT/SEC	V_j M/SEC
○ 602	1314	401
□ 603	1506	459
◇ 604	1755	535
△ 605	1823	556
◊ 606	2019	615

FIGURE 10.126 - WING NACELLE OUTDOOR STATIC TEST, OASPL AND PNdB DIRECTIVITY, 104-TUBE NOZZLE W/O SHROUD

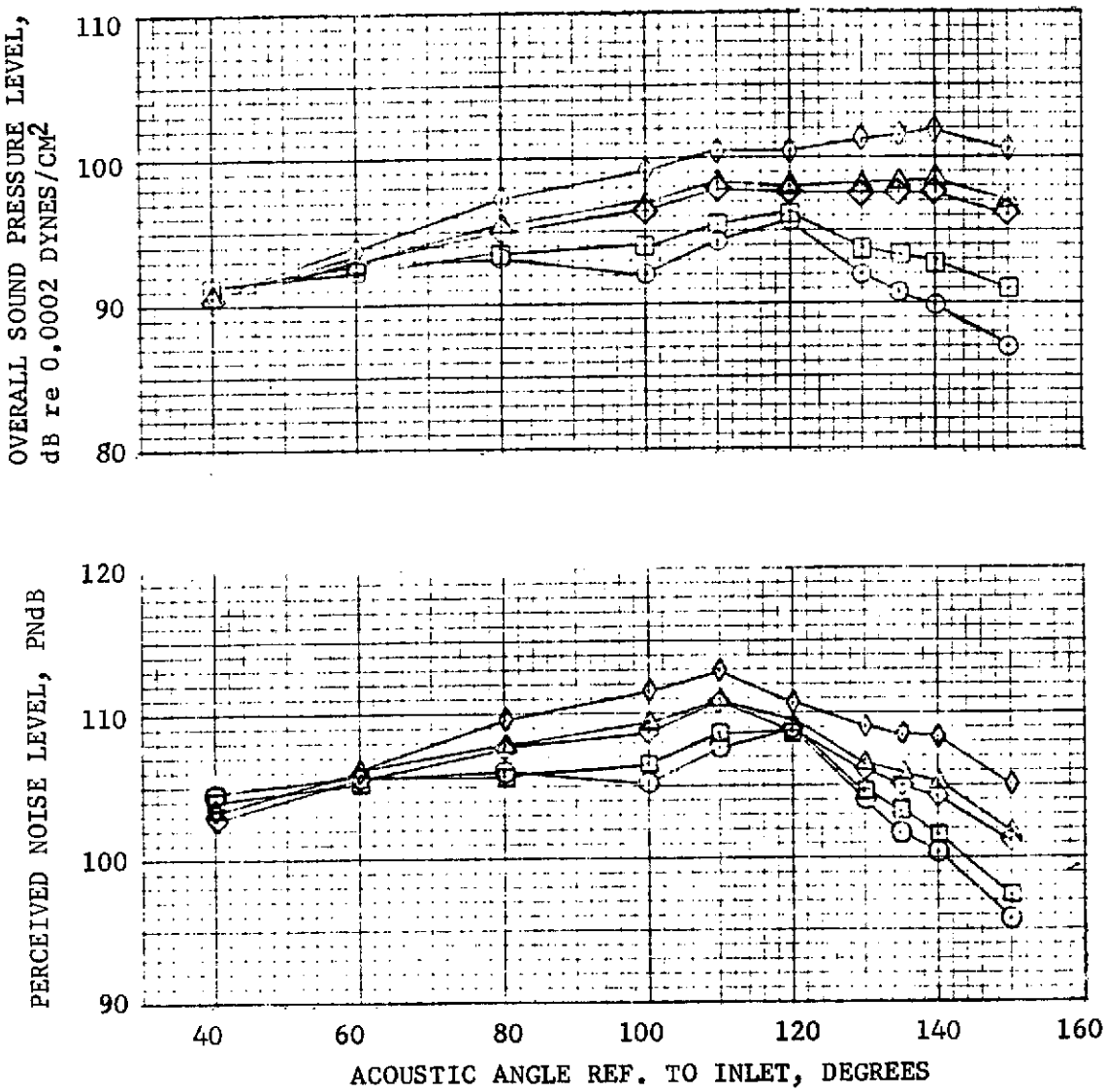

- 104 TUBE NOZZLE W/SHROUD
- 59°F, 70% REL. HUM.
- 200 FT. S.L. (61 M)
- o 20 FT. HIGH MICS (6.1 M)

D.P.	V_j FT/SEC	V_j M/SEC
○ 302	1292	394
□ 303	1507	459
◇ 304	1741	531
△ 305	1810	552
◊ 306	2008	612

FIGURE 10.127 - WING NACELLE OUTDOOR STATIC TEST, OASPL AND PNdB DIRECTIVITY, 104-TUBE NOZZLE WITH SHROUD

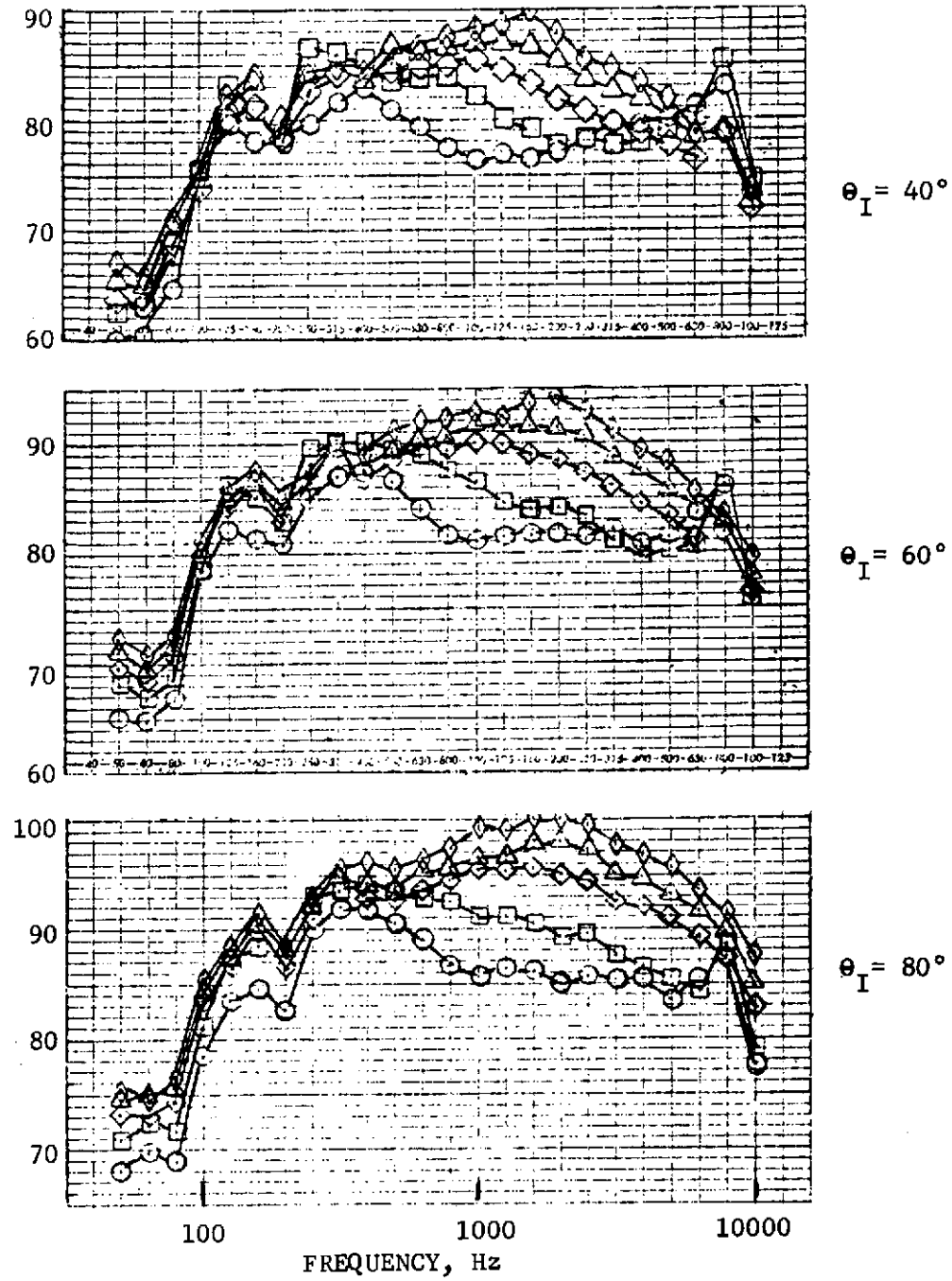

- CONICAL NOZZLE W/BELLMOUTH
- 59°F, 70% REL. HUM.
- 200 FT. S.L. (61 M)
- o 20 FT. HIGH MICS (6.1 M)

D.P.	V_j FT/SEC	V_j M/SEC
○ 1207	1006	307
□ 1206	1270	387
◇ 1205	1665	507
△ 1203	1850	564
◊ 1208	1954	596

FIGURE 10.128 - WING NACELLE OUTDOOR STATIC TEST, 1/3 OCTAVE BAND SPECTRA, CONICAL EJECTOR NOZZLE

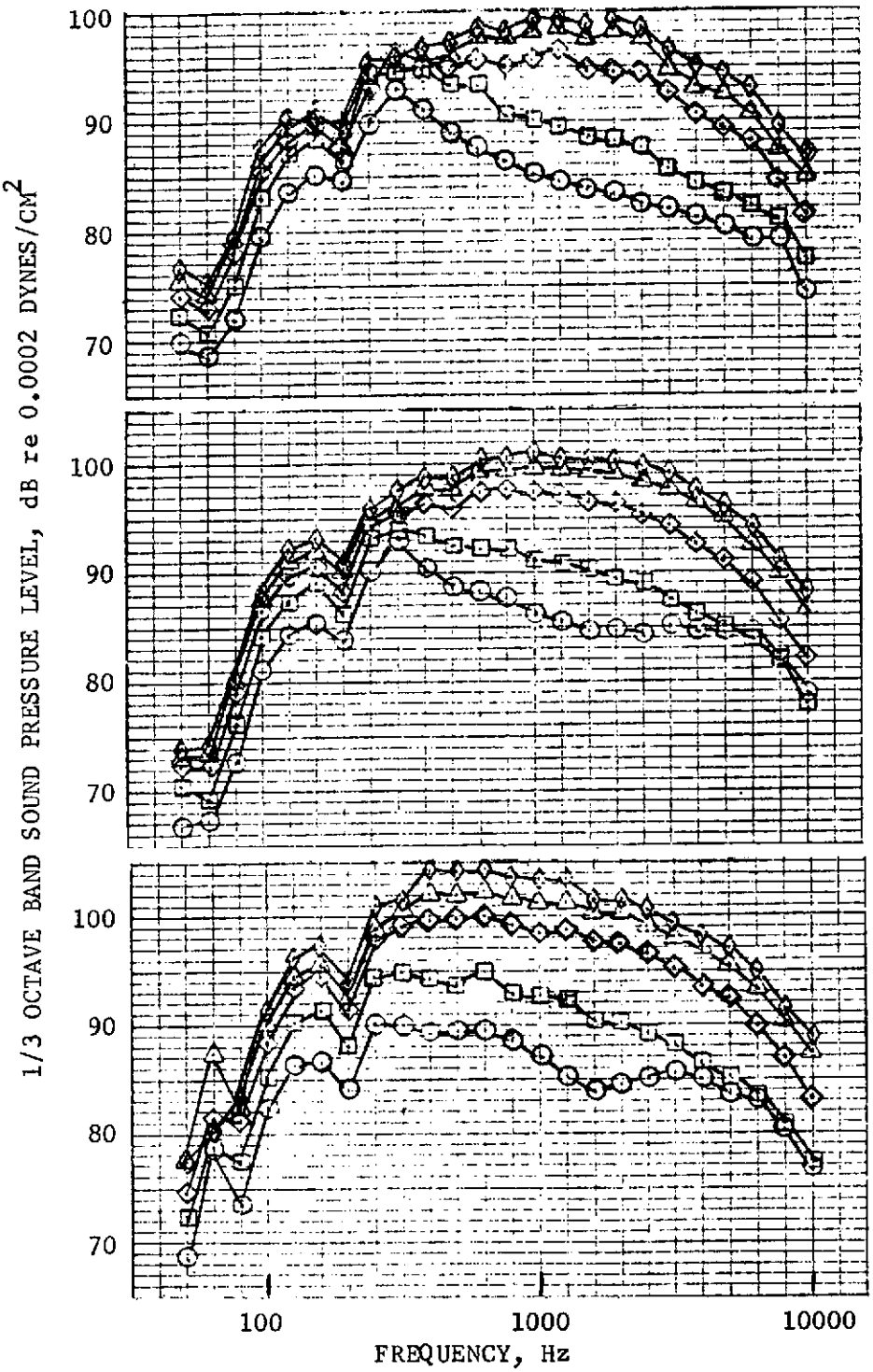

- CONICAL NOZZLE W/BELLMOUTH
- 59°F, 70% REL. HUM.
- 200 FT. S.L. (61 M)
- o 20 FT. HIGH MICS (6.1 M)

D.P.	V_j FT/SEC	V_j M/SEC
○ 1207	1006	307
□ 1206	1270	387
◇ 1205	1665	507
△ 1203	1850	564
◊ 1208	1954	596

FIGURE 10.129 - WING NACELLE OUTDOOR STATIC TEST, 1/3 OCTAVE BAND SPECTRA, CONICAL EJECTOR NOZZLE

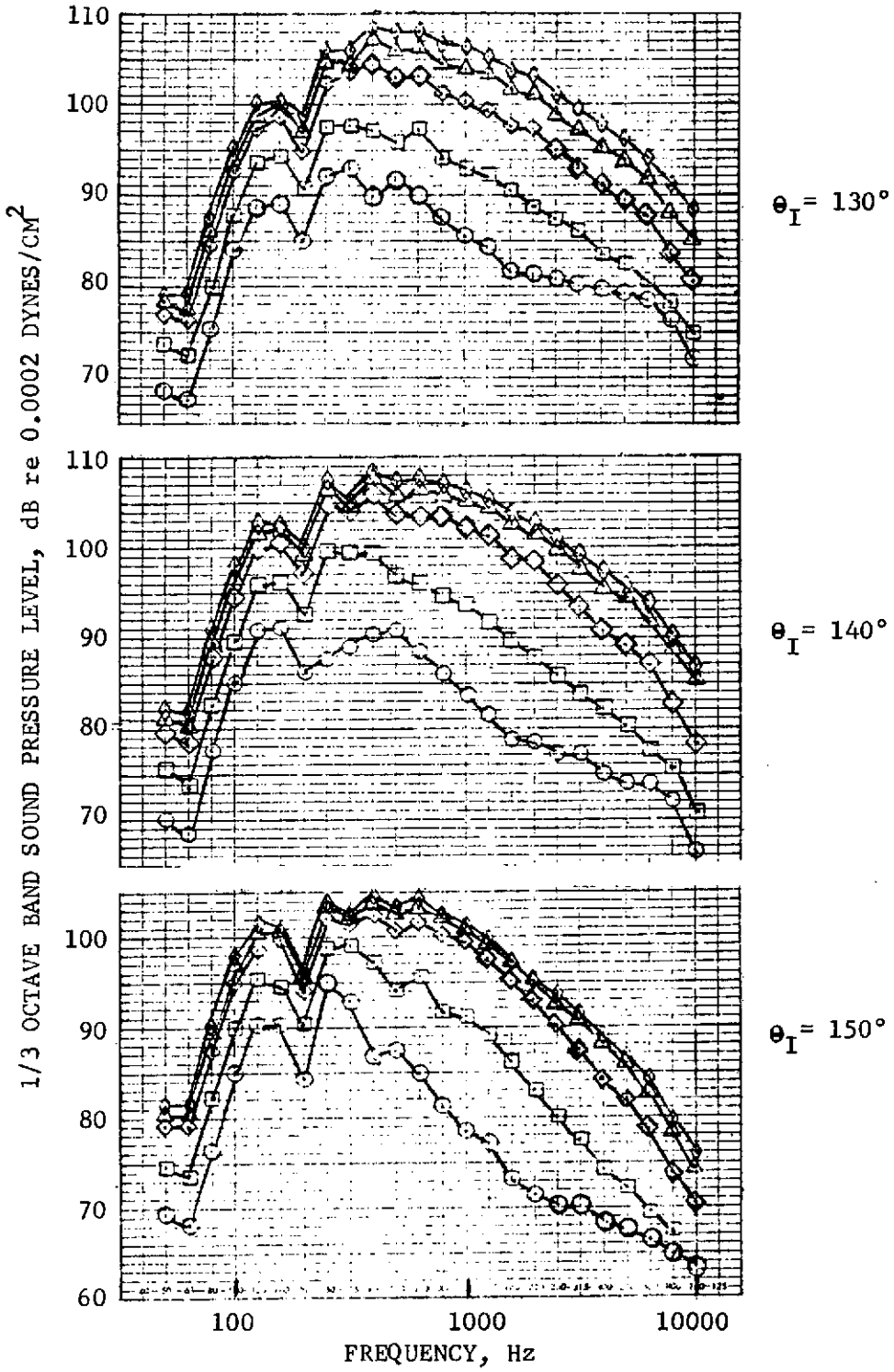

- CONICAL NOZZLE W/BELLMOUTH
- 59°F, 70% REL. HUM.
- 200 FT. S.L. (61 M)
- o 20 FT. HIGH MICS (6.1 M)

D.P.	V_j FT/SEC	V_j M/SEC
○ 1207	1006	307
□ 1206	1270	387
◇ 1205	1665	507
△ 1203	1850	564
◊ 1208	1954	596

FIGURE 10.130 - WING NACELLE OUTDOOR STATIC TEST, 1/3 OCTAVE BAND SPECTRA, CONICAL EJECTOR NOZZLE

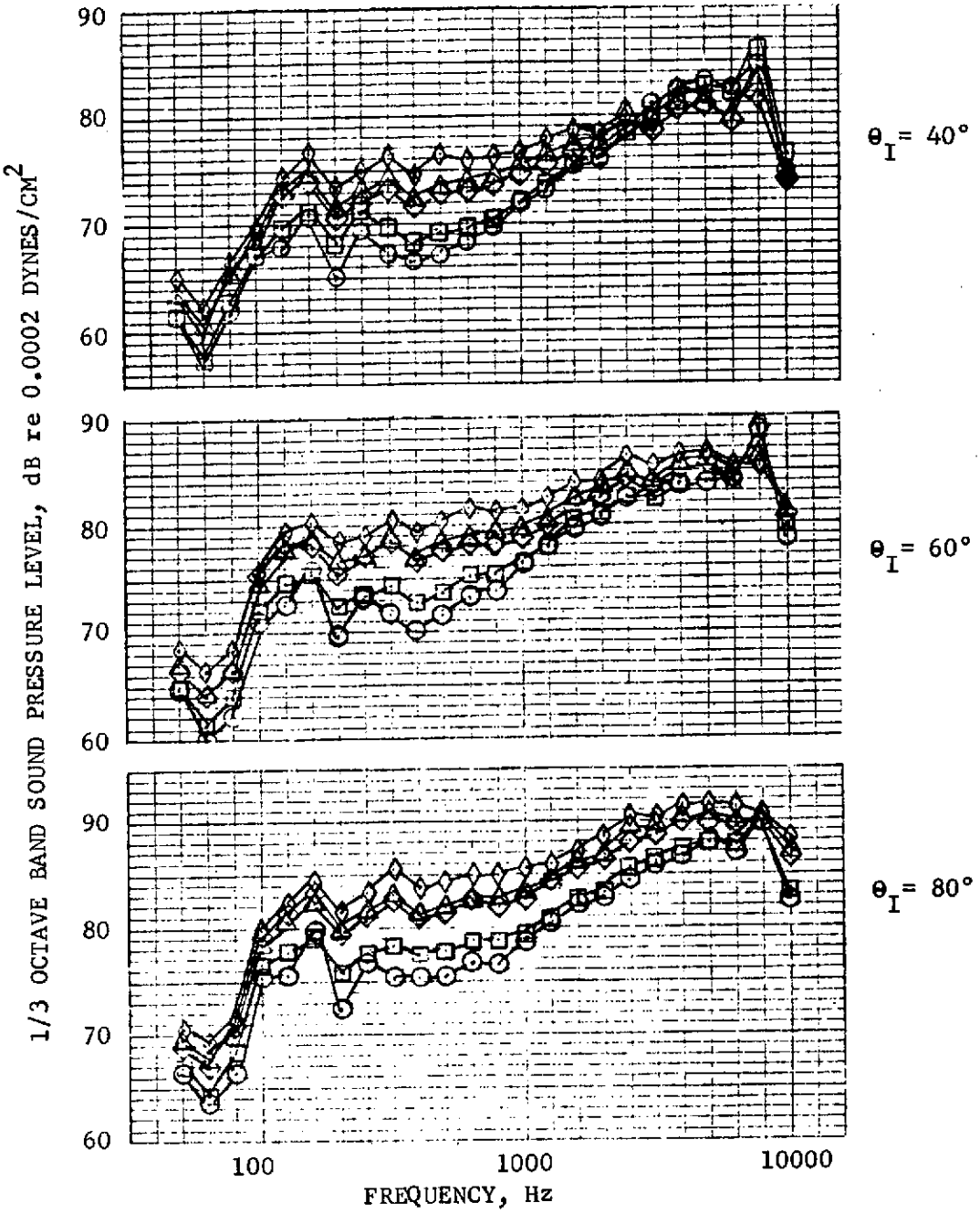

- 104 TUBE NOZZLE W/O SHROUD
- 59°F, 70% REL. HUM.
- 200 FT. S.L. (61 M)
- o 20 FT. HIGH MICS (6.1 M)

D.P.	V_j FT/SEC	V_j M/SEC
○ 602	1314	401
□ 603	1506	459
◇ 604	1755	535
△ 605	1823	556
◊ 606	2019	615

FIGURE 10.131 - WING NACELLE OUTDOOR STATIC TEST, 1/3 OCTAVE BAND SPECTRA, 104-TUBE NOZZLE WITHOUT SHROUD

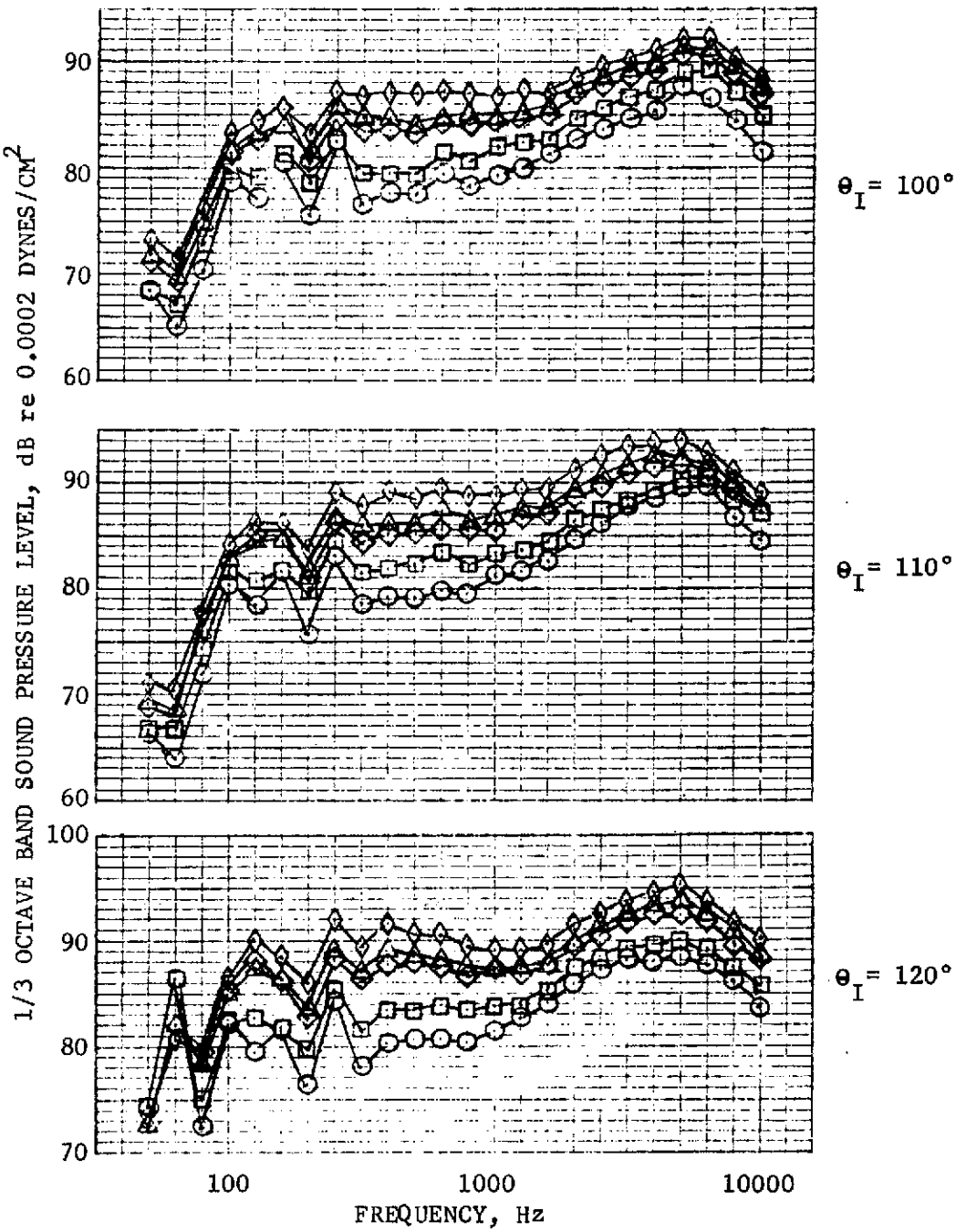

- 104 TUBE NOZZLE W/O SHROUD
- 59°F, 70% REL. HUM.
- 200 FT. S.L. (61 M)
- o 20 FT. HIGH MICS (6.1 M)

D.P.	V_j FT/SEC	V_j M/SEC
○ 602	1314	401
□ 603	1506	459
◇ 604	1755	535
△ 605	1823	556
◊ 606	2019	615

FIGURE 10.132 - WING NACELLE OUTDOOR STATIC TEST, 1/3 OCTAVE BAND SPECTRA, 104-TUBE NOZZLE WITHOUT SHROUD

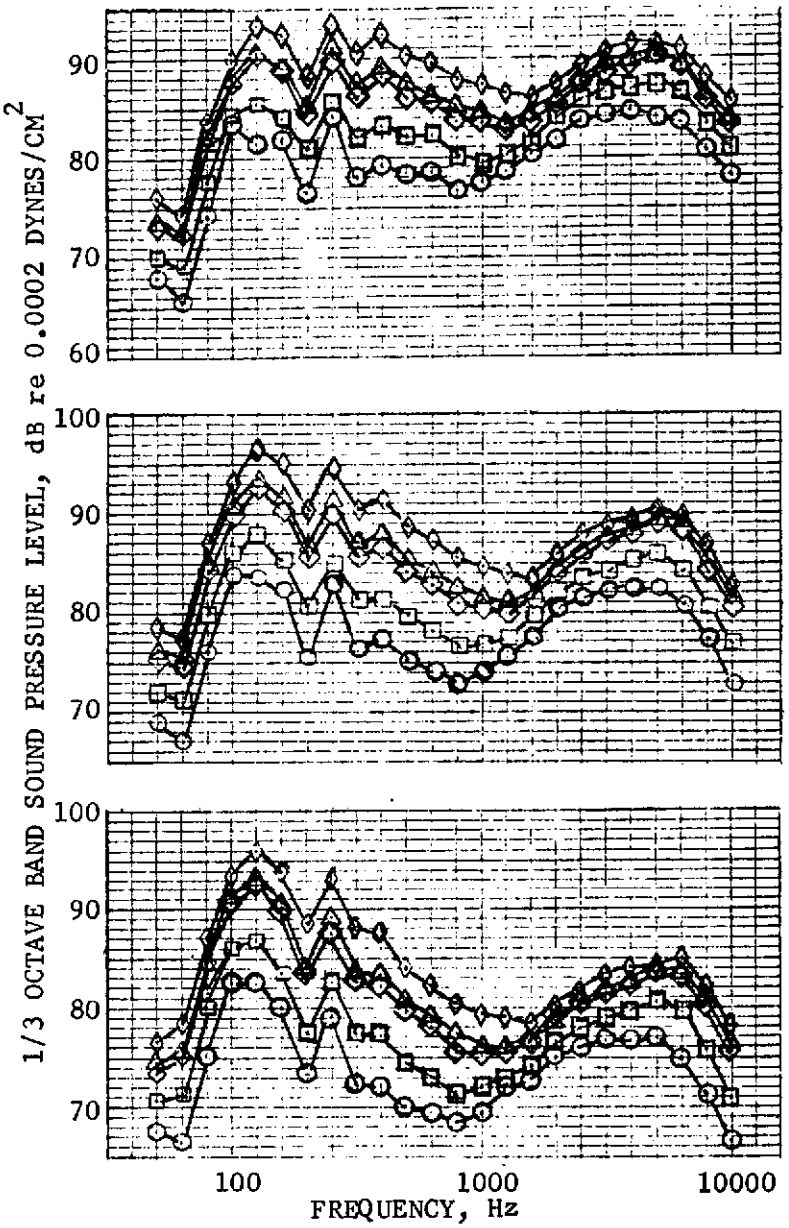

- 104 TUBE NOZZLE W/O SHROUD
- 59°F, 70% REL. HUM.
- 200 FT. S.L. (61 M)
- o 20 FT. HIGH MICS (6.1 M)

D.P.	V_j FT/SEC	V_j M/SEC
○ 602	1314	401
□ 603	1506	459
◇ 604	1755	535
△ 605	1823	556
◊ 606	2019	615

FIGURE 10.133 - WING NACELLE OUTDOOR STATIC TEST, 1/3 OCTAVE BAND SPECTRA, 104-TUBE NOZZLE WITHOUT SHROUD

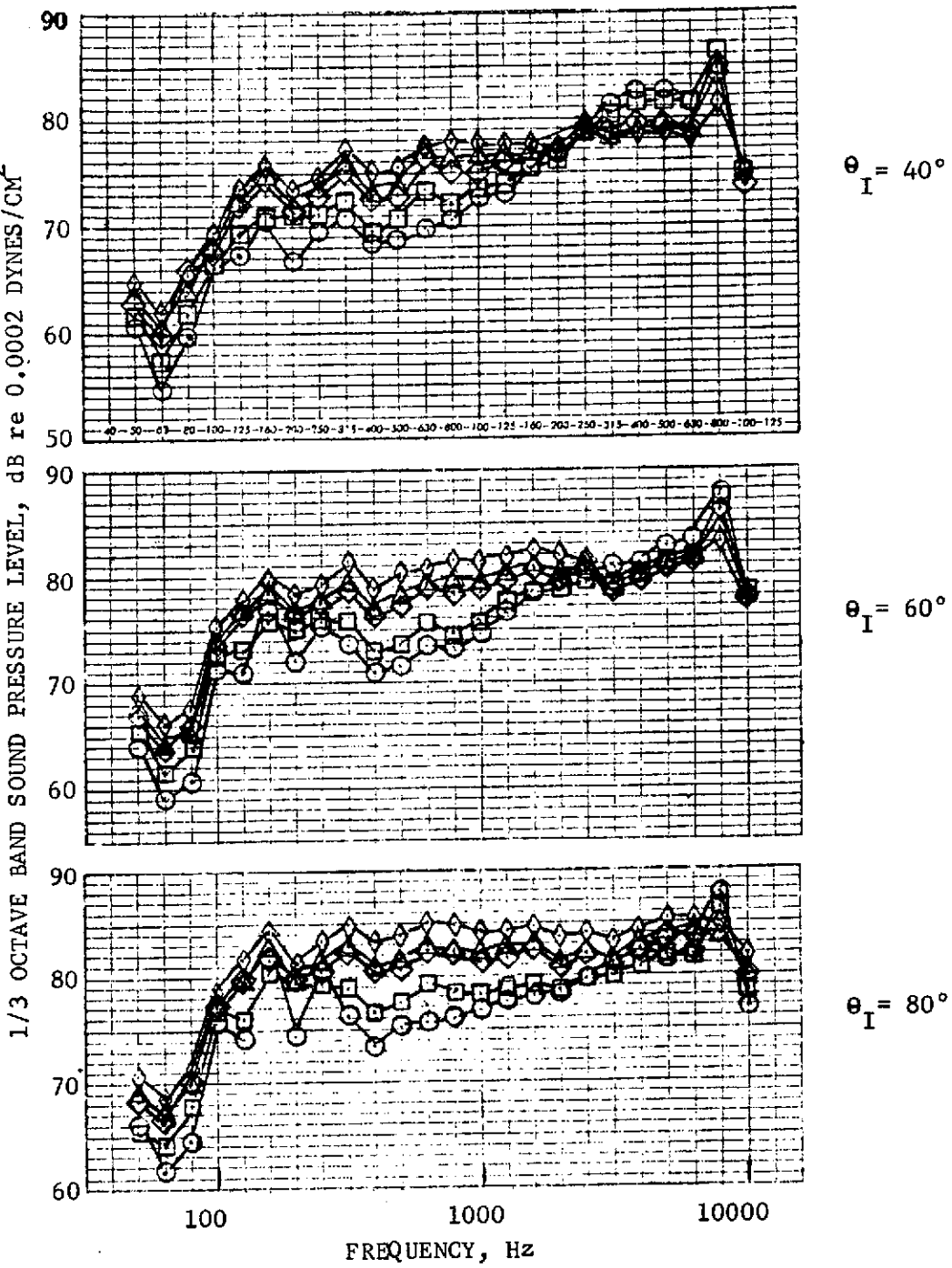

		V_j	
• 104 TUBE NOZZLE W/SHROUD	D.P.	FT/SEC	M/SEC
• 59°F, 70% REL. HUM.	○ 302	1292	394
• 200 FT. S.L. (61 M)	□ 303	1507	459
o 20 FT. HIGH MICS (6.1 M)	◇ 304	1741	531
	△ 305	1810	552
	◊ 306	2008	612

FIGURE 10.134 - WING NACELLE OUTDOOR STATIC TEST, 1/3 OCTAVE BAND SPECTRA, 104-TUBE NOZZLE WITH SHROUD

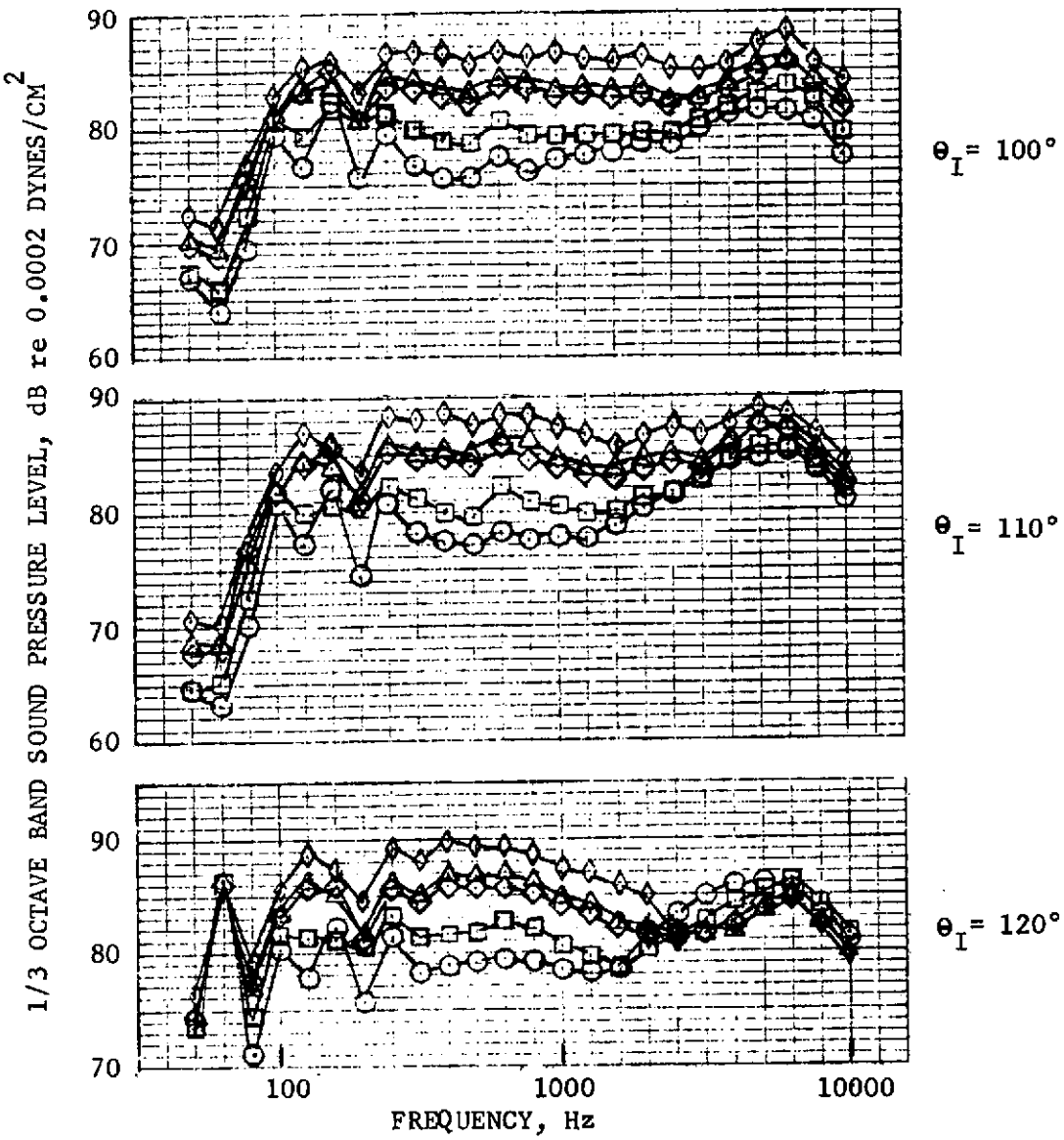

	D.P.	V_j FT/SEC	V_j M/SEC
● 104 TUBE NOZZLE W/SHROUD			
● 59°F, 70% REL. HUM.	○ 302	1292	394
● 200 FT. S.L. (61 M)	□ 303	1507	459
	◇ 304	1741	531
o 20 FT. HIGH MICS (6.1 M)	△ 305	1810	552
	◊ 306	2008	612

FIGURE 10.135 - WING NACELLE OUTDOOR STATIC TEST, 1/3 OCTAVE BAND SPECTRA, 104-TUBE NOZZLE WITH SHROUD

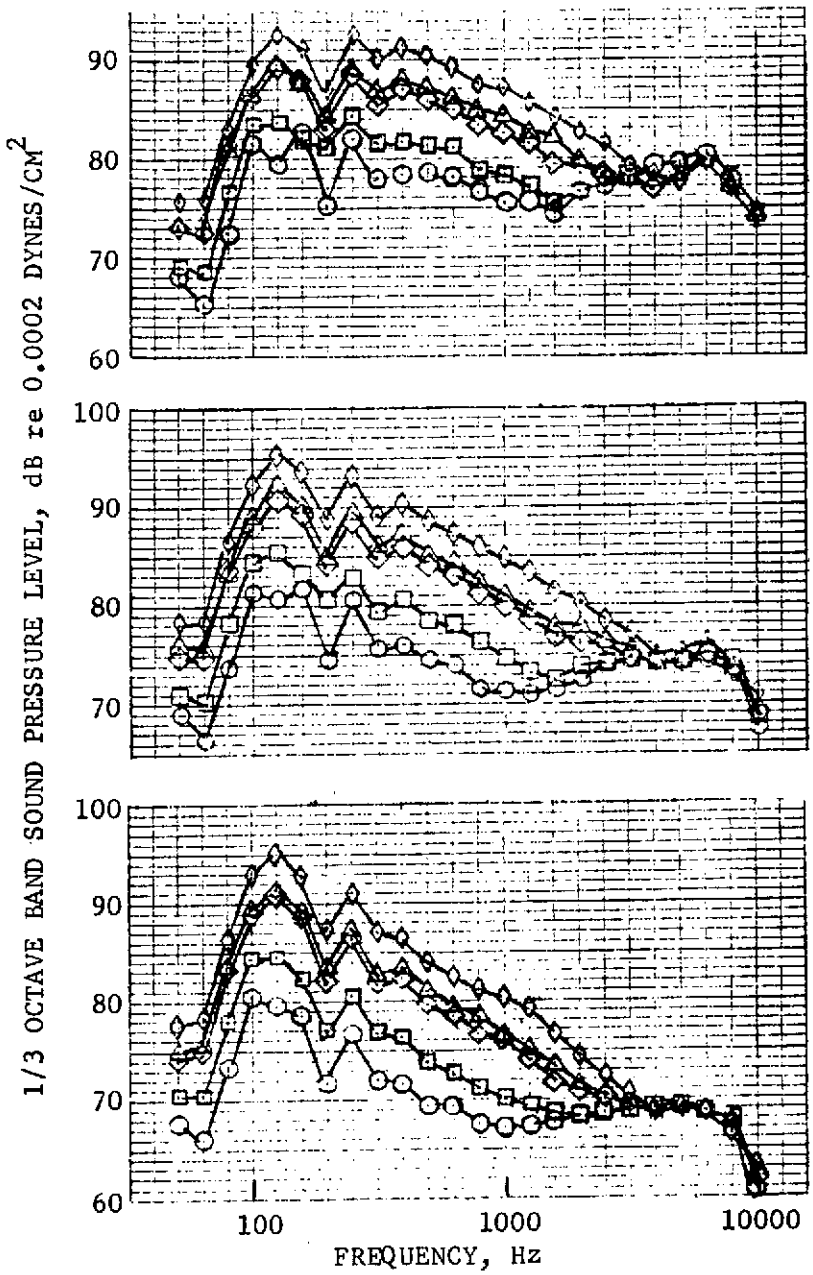

- 104 TUBE NOZZLE W/SHROUD
- 59°F, 70% REL. HUM.
- 200 FT. S.L. (61 M)
- o 20 FT. HIGH MICS (6.1 M)

D.P.	V_j FT/SEC	V_j M/SEC
○ 302	1292	394
□ 303	1507	459
◇ 304	1741	531
△ 305	1810	552
◊ 306	2008	612

FIGURE 10.136 - WING NACELLE OUTDOOR STATIC TEST, 1/3 OCTAVE BAND SPECTRA, 104-TUBE NOZZLE WITH SHROUD

11.0 ANALYTICAL STUDIES

Presented in this section are the methodology used and predictions for noise generation for the Conical Ejector Nozzle and 104 Tube Nozzle Noise generation. Predictions are compared with measured values for both static and inflight cases. Recommendations for improvements are also given.

11.1 Conical Ejector Nozzle - Static and Inflight Noise Prediction

General Electric has a technique to compute aerodynamic properties of a complex geometry exhaust nozzle. This is an extremely powerful analytical tool in that it can compute aerodynamic parameters of an exhaust nozzle for any arbitrary configuration. On the basis of the above aerodynamic parameters, acoustic power and spectrum for the conical nozzle are computed. However, the program in its present form can only be used to obtain order of magnitudes and trends in acoustic power of complex nozzles.

Paragraph 11.1.1 describes the basic principles of the prediction program. Then comparison between the prediction and measured values are made in paragraph 11.1.2. Recommendations for improvements are also made.

11.1.1 Prediction Program

The program computes aero-acoustic properties of complex nozzle geometry suppressors on the basis of superposition of momentum flux distribution. Then, aerodynamic parameters, computed from the above procedure, are substituted into an acoustic power equation. The logic flow chart is shown on Table 11.1. It is apparent from Table 11.1 that the present program consists of three sub programs and a master program AERODYNAMIC, which computes aerodynamic parameters of the jet exhaust nozzle. The auxiliary program ACOUSTIC computes flyby effect by using sub-routines NOISE 1 and NOISE 2. ACOUSTIC uses Kendall's acoustic model (Ref. 11.1). In the following paragraphs, the basic principles of the above procedures will be described.

Aerodynamic Parameter Calculation

Reichardt (Ref. 11.2) found from measurements in regions of free turbulence that an analogy exists between the processes of turbulent and molecular transfer. From these measurements, Reichardt introduced an inductive theory of free turbulence, in which he assumed that the mean velocity profiles can be represented by a normal distribution. From the momentum equation in the axial direction,

$$\frac{\partial \overline{\rho u^2}}{\partial x} + \frac{1}{r} \frac{\partial}{\partial r} (r\overline{\rho uv}) = 0 \tag{1}$$

An empirical relation between Reynolds stress and momentum flux is assumed as follows:

$$\overline{\rho uv} = - \Lambda (x) \frac{\partial}{\partial r} (\overline{\rho u^2}) \tag{2}$$

Substituting 2) into 1),

$$\frac{\partial}{\partial x} (\overline{\rho u^2}) = \Lambda (x) \frac{1}{r} \frac{\partial}{\partial r} (r \frac{\partial \overline{\rho u^2}}{\partial r}) \tag{3}$$

This is the fundamental equation of Reichardt which describes the distribution of momentum in free turbulence. It is a generalized heat conduction equation and the solution takes the form of,

$$\overline{\rho u^2} = C_1 + \frac{C_2}{b^2} \exp \left[- \left(\frac{r}{b}\right)^2 \right] \tag{4}$$

where:

C_1, C_2 = constants

b (x) = mixing zone half width

Equation (3) is a linear partial differential equation in $\overline{\rho u^2}$, thus the principle of superposition of momentum flux is applicable. This fact is extremely powerful in that the above processes enable one to compute aerodynamic properties of complex geometry suppressors.

Now taking the space derivative of equation (4) in the axial (x) and radial (r) directions, and substituting into equation (3) and solving for $\Lambda(x)$, we obtain,

$$\Lambda(x) = \frac{b}{2}\frac{db}{dx} \tag{5}$$

Then equation (4) can be written as

$$\overline{\rho u^2} = \frac{k}{b^2} \exp\left[-\left(\frac{r}{b}\right)^2\right] \tag{6}$$

The constant K can be determined as follows:

Conservation of momentum states that from equation (1),

$$\frac{\partial}{\partial x}\left[2\pi r dr\ (\overline{\rho u^2})\right] + 2\pi\frac{\partial}{\partial r}(\rho uvr)dr = 0 \tag{7}$$

Integrating the above with respect to r and recognizing that v vanishes in the limits,

$$\int_0^\infty (\overline{\rho u^2})\ 2\pi r dr = (\rho u^2)_e\ A_e \tag{8}$$

where

A_e = jet exit area

$(\rho u^2)_e$ = jet exit momentum flux

Next substitute (4) into (8), specifying $C_1 = 0$ and solving for C_2,

$$C_2 = (\rho u^2)_e\ A_e\ /\pi \tag{9}$$

Substituting equation (9) into (4),

$$\overline{\rho u^2} = \frac{(\rho u^2)_e\ A_e}{\pi b^2} \exp\left[-\left(\frac{r}{b}\right)^2\right] \tag{10}$$

Comparing equations (10) and (6), it can be seen that $K = (\rho u^2)_e\ A_e\ /\pi$.

Thus the momentum distribution in a jet can be determined knowing its exit condition and the characteristic length scale b (x).

Equation (10) can be extended for arbitrary nozzle exit configurations with the following assumptions.

1. The diffusion of momentum from a point source into a region of the same fluid is described by equation (10); and

2. The momentum from individual point sources of finite source area may be superimposed to give the momentum distribution from the entire source area.

Under these assumptions, the momentum distribution in a jet issuing from an arbitrary nozzle exit cross section can be represented by the integral

$$\overline{\rho u^2}\ (x,y,z) = \frac{1}{\pi b^2} \iint_{A_e} (\overline{\rho u^2})_e \exp\left[-\left(\frac{r}{b}\right)^2\right] dy'dz' \qquad (11)$$

where

$$r^2 = (Y-Y')^2 + (Z-Z')^2$$

and the (Y', Z') coordinate system defines the jet exit plane as illustrated in Figure 11.1. The turbulent shear stress τ can be written as

$$\tau = \overline{\rho u'v'} \cong \overline{\rho uv} = -\frac{b}{2}\frac{db}{dx}\frac{\partial \overline{\rho u^2}}{\partial r} \qquad (12)$$

This equation is valid for quasi-incompressible turbulence in a flow with a negligible radial component of velocity.

Characteristic width of the mixing zone

The turbulent mixing process is represented by b(x) in the present analysis.

$$b(x) = f(M_j, T_j, \frac{u'}{u_j}) \tag{13}$$

where,

M_j : jet Mach number

T_j : jet temperature

$\frac{u'}{u_j}$: initial turbulence level

For the case of a jet issuing into a moving stream (the in-flight case), the b(x) decreases as the external to jet stream ratio (u_s/u_j) increases. The relation among M_j, T_j and u_s/u_j and b(x) is shown in Figure 11.2

Models for calculating sound power spectrum

Jet noise may be regarded as sound generated by distributed sources in the jet flow field. Different parts of the jet may generate sound at different frequency bands.

Two assumptions are made in computing radiated power spectrum.

1. The sound power W generated by a slice of jet can be expressed in terms of local flow properties as

$$\frac{dw}{dx} = K \int_a (\text{source function})\ da \tag{14}$$

2. The typical frequency generated by a slice of jet is a function of axial location

$$f = f(x) \tag{15}$$

and the sound power spectrum can be obtained from

$$\frac{dw}{df} = \frac{dw}{dx}\frac{dx}{df} \tag{16}$$

Several models for the source function and the frequency distribution are programmed. However, Kendall's turbulent stress model is used here. The source function for the Kendall's model is:

$$\text{Source function} = \frac{\rho^2 u^3}{\rho_o c_o^5 \ell} \left(\frac{\tau}{\bar{\rho}}\right)^{5/2} \tag{17}$$

and the frequency distribution is given by

$$f = 2.2 \frac{u_c}{x} \tag{18}$$

where u_c is the local eddy convection velocity.

Model for calculation of sound pressure spectrum

The directivity function $F(\theta)$ in the mean square sound pressure expression is

$$p^2 (r, \theta, f) = (\text{source function}) \cdot F(\theta) \tag{19}$$

and $F(\theta)$ is assumed to take the form

$$F(\theta) = \begin{cases} F_1(\theta) & \theta > \theta_{max} \\ F_2(\theta) & \theta \leqslant \theta_{max} \end{cases} \tag{20}$$

where

$$F_1(\theta) = \left\{ [1 - M_c \text{ Cos } (2\theta_{max} - \theta)]^2 + q^2 \right\}^{-5/2} \tag{21}$$

$$F_2(\theta) = \left\{ (1 - M_c \text{ Cos } \theta)^2 + q^2 \right\} \tag{22}$$

where

$$q = w1/C_o = \alpha M_c$$

The function F2(θ) is the Lighthill's convection factor which correlates well with experimental data for overall sound pressures at positions with angles smaller than the peak angle θ max from the inlet.

In the present calculation, it is assumed that

$$\theta_{max} = \begin{cases} 160° & T_j = T_{amb} \\ 130° & T_j > T_{amb} \end{cases} \tag{23}$$

Since the sound power can be obtained by integration

$$\bar{w}\ (f) = \int_o^\pi \frac{\overline{p^2(r,\theta,f)}}{\rho_e a_e} 2\pi r^2 \sin\theta\ d\theta \tag{24}$$

the source function in equation (19) can be written as

$$(\text{source function}) = \frac{\rho_e\ a_e\ w\ (f)}{2\pi r^2 \int_o^\pi \sin\theta\ F(\theta) d\theta} \tag{25}$$

therefore

$$\overline{p^2}\ (r,\theta,f) = \frac{\rho_e\ a_e\ w\ (f)\ F(\theta)}{2\pi r^2 \int_o^\pi \sin\theta\, F(\theta) d\theta} \tag{26}$$

This equation relates the sound pressure spectrum and the sound power spectrum. In the present calculation, M_c is taken as .6 u_e/A_o and $q = \alpha M_c$, with α = .3 for cold jets and α = 0.5 for hot jets. The integral $\int_o^\pi \sin\theta F(\theta) d\theta$ was evaluated numerically.

Flyover Jet Noise

For the radiation sound field of a jet in flight, the mean square sound pressure and the frequency observed at a stationary farfield point are modified by a factor.

$$1 / (1 - M_o \cos\theta)$$

Therefore

$$\overline{p^2}_{fly}\ (r,\theta,f) = \overline{p^2}\ (r,\theta,f) / (1 - M_o \cos\theta) \tag{27}$$

and

$$f_{fly} = f / (1 - M_o \cos\theta) \tag{28}$$

The forward motion of the aircraft also affects the turbulent mixing process of the jet exhaust stream with the ambient air and modifies the sound power output. This process is controlled by the parameter b.

11.1.2 Comparison of Theoretical and Experimental Results

In the following paragraphs, comparison of aforementioned prediction and the experimental results will be made. The first part describes the static model and the second part describes the inflight model. Isolated Nacelle - wind tunnel data were used in both cases.

11.1.2.1 Static Model

Two cases of isolated nacelle - wind tunnel data were selected for no wind tunnel velocity. The jet velocities were 595 m/sec, (1953 ft/sec) and 381 m/sec, (1250 ft/sec). They are representative of high and low engine power settings.

Figure 11.3 shows a comparison of low power setting data (V_j = 381 m/sec, 1250 ft/sec) and the predicted values. On the basis of 1/3 OB PWL, Kendall's predicted values are slightly below the measured values.

Figure 11.4 shows a comparison of high power setting data (V_j = 595 m/sec, 1953 ft/sec) and the predicted values. The agreement between prediction and data is excellent. Therefore, it is generally considered that the prediction program for the static ease works for a wide range of jet exhaust velocities.

11.1.2.2 Inflight Model

Next, the jet noise signature of the nozzles were measured at various freestream velocities to investigate changes in source strength. Figure 11.5 shows a comparison of medium power setting (V_j = 404 m/sec, 1326 ft/sec) data and prediction at medium wind tunnel velocity (V_o = 76 m/sec, 249 ft/sec). On the basis of 1/3 OB PWL, the agreement between data and the prediction is excellent.

Figure 11.6 and Figure 11.7 are wind on ($V_o \sim 100$ m/sec, 330 ft/sec) cases of Figure 11.3 and Figure 11.4, respectively. In Figure 11.6 the dotted line is the static prediction of Figure 11.3. Note the decrease in PWL due to the addition of external flow. Due to the low jet velocity, 381 m/sec, 1250 ft/sec), the jet noise was below the facility noise and, therefore, no data is presented for comparison with the prediction. Presented in Figure 11.7 are similar comparisons between the static and wind on ($V_o \sim 100$ m/sec, 330 ft/sec) cases for the high engine power setting. The dotted line is the static spectrum of Figure 11.4

Slight discrepancies are seen between the prediction and the data. However, a marked source reduction has been achieved by the addition of the freestream velocity.

Therefore, on the basis of total power level, the prediction program has been demonstrated to show valid trends for a wide range of jet exhaust velocities and freestream velocities.

Investigation of directivity pattern will be made next. Figures 11.8 to 11.12 show the SPL distribution at 100° to 160° (angles measured from the inlet) for a jet velocity of 99 m/sec, (326 ft/sec). Figures 11.8 to 11.10 show that for $\theta > \theta$ max, equation (21) underpredicts the low frequency peak (200 Hz - 1 KHZ) and over predicts the higher frequency (1 KHZ and above) portion of the spectra. Equations (20) and (23) do not include refraction effects which may be one of the possible causes of the discrepancies between the data and the predictions.

Figures 11.13 to 11.17 show directivity patterns for the high jet velocity case. Comparison of data and the predicted values for this case also indicate that the equations (20), (21) and (23) need further development. The factor $q = w\ell/C_o$ may require more rigorous treatment to correctly account for all the mechanisms causing the generation of jet noise.

11.2 104 Tube Nozzle - Static and Inflight Noise Predictions

In order to predict the noise levels of the 104 tube nozzle, a semi-empirical prediction procedure was used. This model is described in detail in Reference 11.3. The assumptions in the model may be stated as follows:

- Noise generated by individual tube conical jet flow is determined by the nozzle discharge conditions.
- This noise is radiated only from that length of the individual jets before adjacent jet flow coalesce. The length is determined by an empirical modification of the spreading angle of single isolated jets.
- Self-shielding of noise from the inner tubes occurs.
- Noise generated by the merged flow from individual tubes is determined by the flow conditions existing at the merging location, assuming an equivalent larger diameter conical nozzle.
- Noise for the multi-tube suppressors is the sum of that from the individual tubes and from the merged flow.

Using this procedure, predictions were made statically and inflight. Presented on Figure 11.18 are comparisons between the predicted and measured data on the basis of peak OASPL and PNL. The agreement between the measured data and the predictions is excellent on the basis of OASPL. However, the predictions are four to five dB lower than the measured data on the basis of PNL. The reason for the PNL difference at low velocity can be explained by examining the spectra presented on Figure 11.19. At the high velocity condition, the second peak of the spectra is closely approximated by using the procedure. However, at the low velocity condition, the second peak is underpredicted. This region has an extremely high noy weighting and therefore results in a much lower PNL value.

To assess the effect of flight, the predicted spectra were corrected for an implicit pressure change by assuming a $V - V_o$ correction in the source generation term. Then to account for the motion of the source relative to the ovserver, dynamic and Droppler corrections were added. The dynamic and Doppler corrections are presented on Figure 11.20. The data measured in the wind tunnel at the various freestream velocities already accounts for the implicit change in the acoustic pressure and only has to be corrected for dynamic and Doppler effects.

The comparison between the measured data and predictions are presented on Figures 11.21 thru 11.24. The comparisons are presented on the basis of peak OASPL and PNL. The agreement at the low freestream velocity of 52 m/sec, (170 ft/sec) is within 3 dB for the velocity range studied. However, the agreement on the basis of PNL has a maximum difference between the measured and predicted spectra of 8 dB for a jet velocity of 465 m/sec, (1527 ft/sec). This difference may be explained by examining the spectra presented on Figure 11.23. At the high velocity condition, the predicted and measured spectra are generally in good agreement. In contrast, at the low velocity of 465 m/sec, (1527 ft/sec), the predicted spectra is much lower in the high frequency portion of the spectra. This is a high noy weighting region and, therefore, the difference on the basis of PNL would be larger than on the basis of OASPL. For a freestream velocity of 76 m/sec, (250 ft/sec) the trends are the same as the lower freestream velocity. However, only the high frequency portion of the measured spectra are available for comparison.

The large difference between the measured and predicted spectra in the high frequency region at the low jet velocity conditions may be due to the fact that the semi-empirical model used assumes that the outer tube annulus shields the noise generated by the inner tubes. This shielding phenomenon is assumed to be independent of jet velocity. However, the data presented in reference 11.4 indicate that the amount of shielding decreases as jet velocity decrease. This is a possible reason for the poor agreement between the measured and predicted results at the low jet velocity. This phenomenon of shielding in multi-element nozzles is currently the subject of both theoretical and experimental studies. As the result of these efforts become available, the prediction procedure will be revised to represent the correct physical phenomenon.

11.3 Summary

In summary, Reichardt's prediction program in its present form can compute aerodynamic parameters of a complex geometry nozzle. However, the aerodynamic model numerical computation procedures are not very efficient for multi-element suppressor nozzles with many (> 30) elements. The present program predicts acoustic behavior of a conical nozzle reasonably well on the basis of OAPWL and power level spectra. The relative velocity effect is predicted and appears to fit the data well. A semi-empirical procedure for the 104 tube nozzle demonstrated its capability to predict peak OASPL and spectrum. However, the directivity trends need to be updated to reflect the results of more recent experimental and theoretical studies. This work is currently in progress.

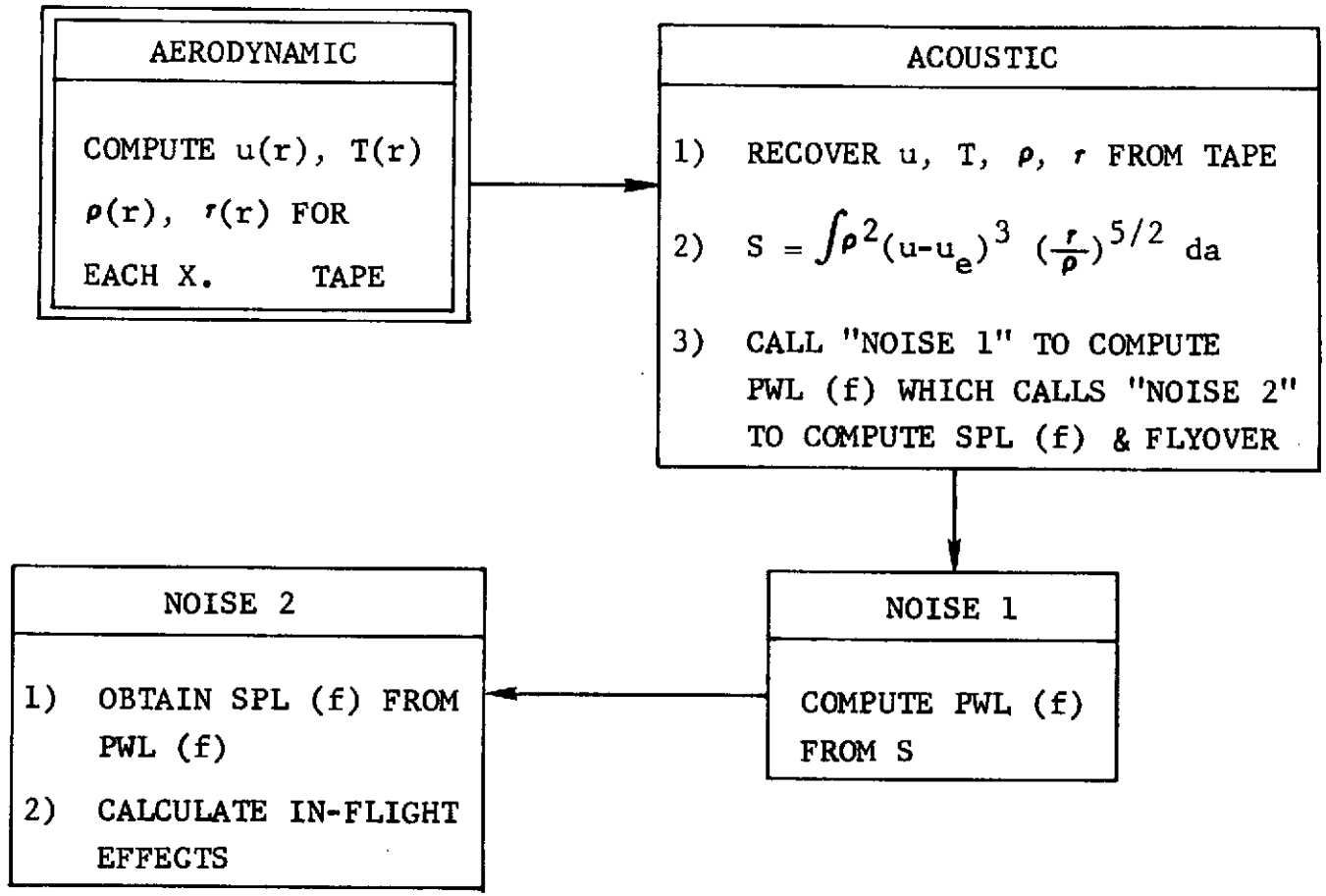

TABLE 11.1

AERODYNAMIC AND ACOUSTIC PARAMETER PREDICTION PROGRAM BLOCK DIAGRAM.

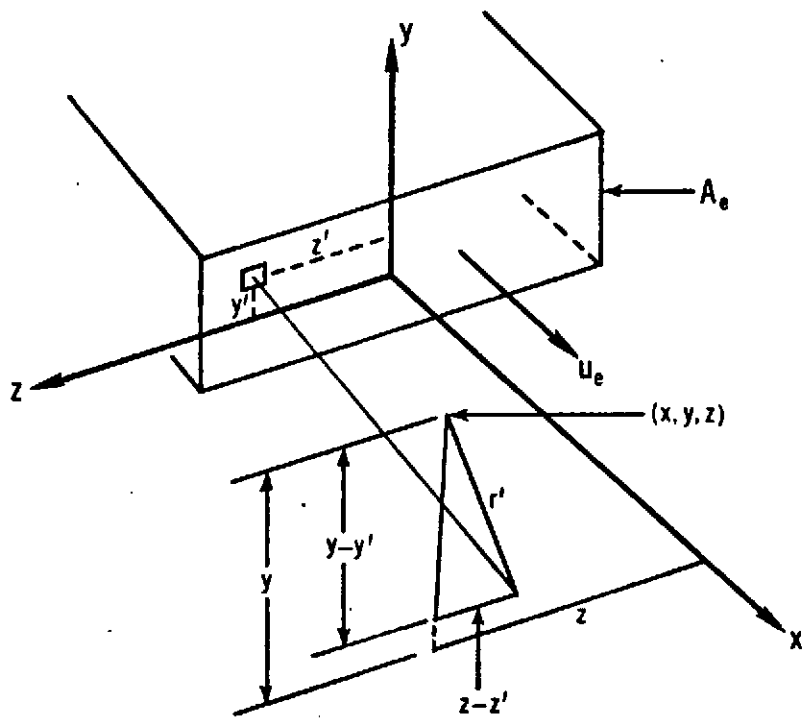

FIGURE 11.1 - AERODYNAMIC COORDINATE SYSTEMS

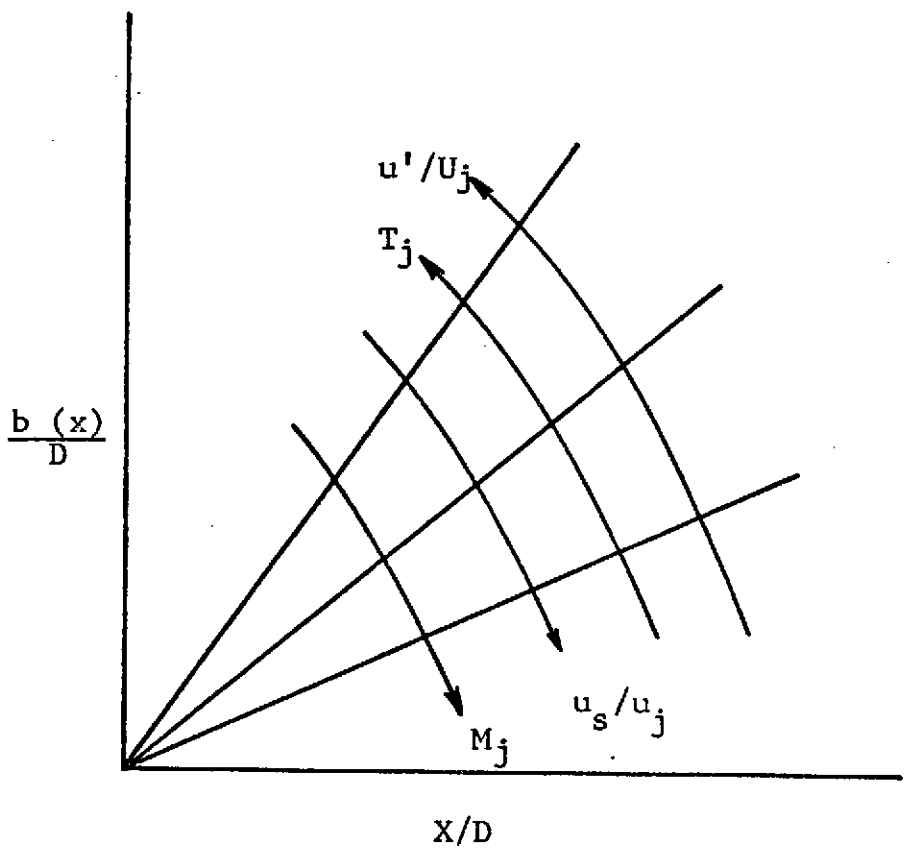

FIGURE 11.2 - FUNCTIONAL DEPENDENCE OF THE SPREADING PARAMETER b (x)

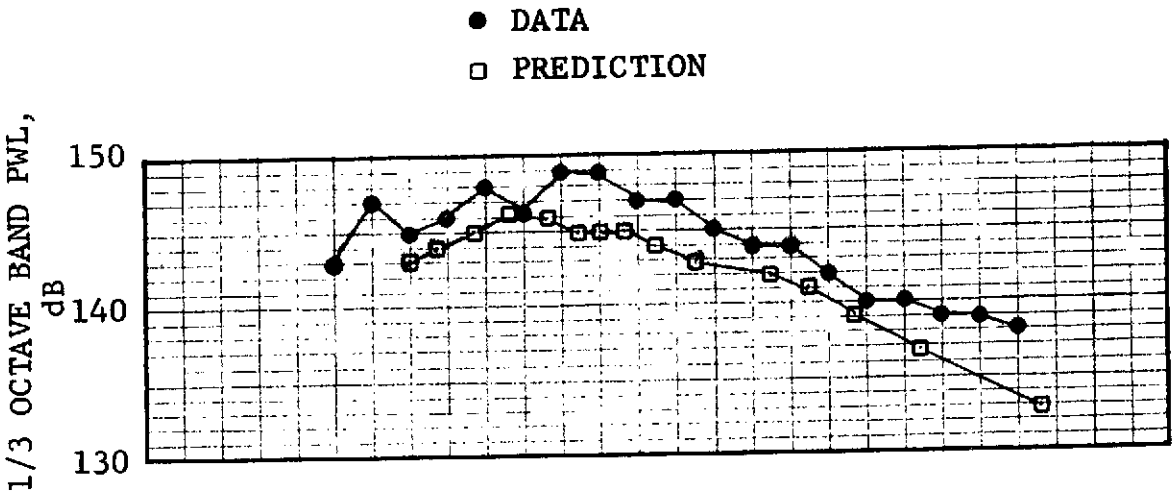

FIGURE 11.3 - ISOLATED NACELLE WIND TUNNEL TEST
$V_o = 0$ $V_j = 1250$ FT/SEC (381 M/SEC)

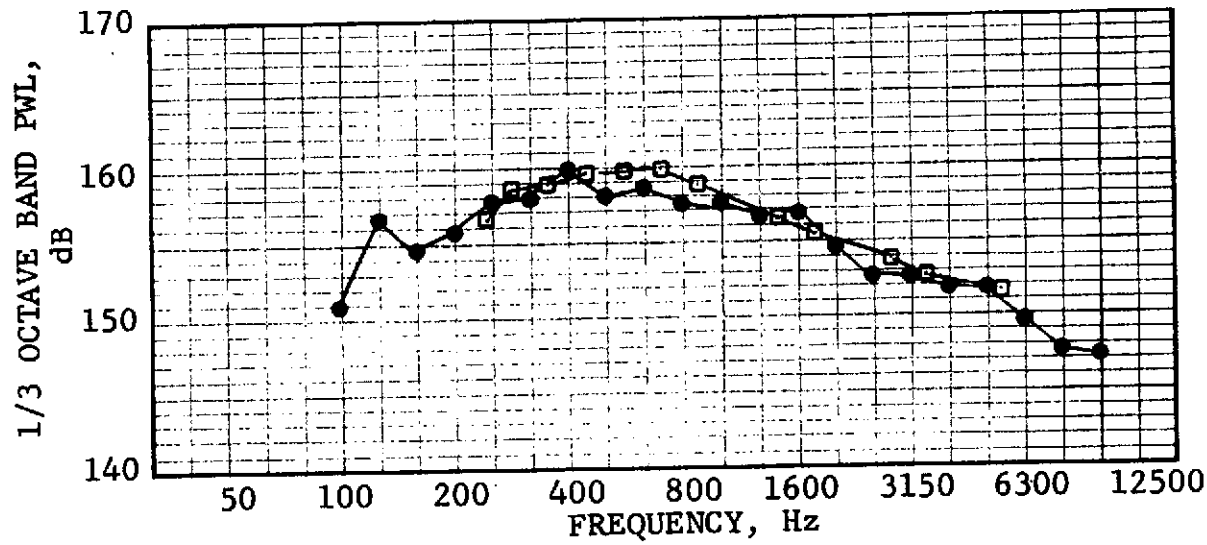

FIGURE 11.4 - ISOLATED NACELLE WIND TUNNEL TEST
$V_o = 0$ $V_j = 1953$ FT/SEC (595 M/SEC)

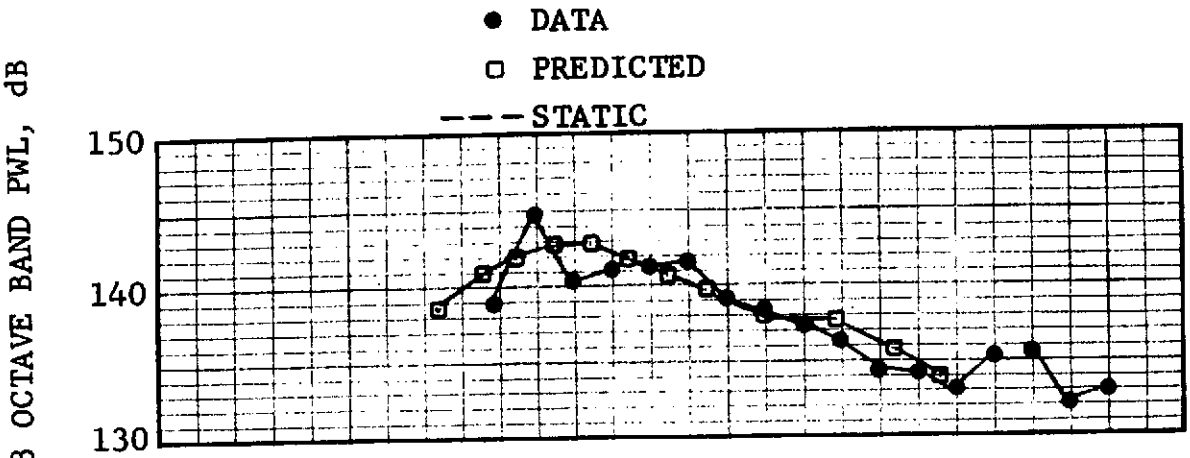

FIGURE 11.5 - ISOLATED NACELLE WIND TUNNEL TEST
V_o = 249 FT/SEC (75.9 M/SEC)
V_j = 1326 FT/SEC (404 M/SEC)

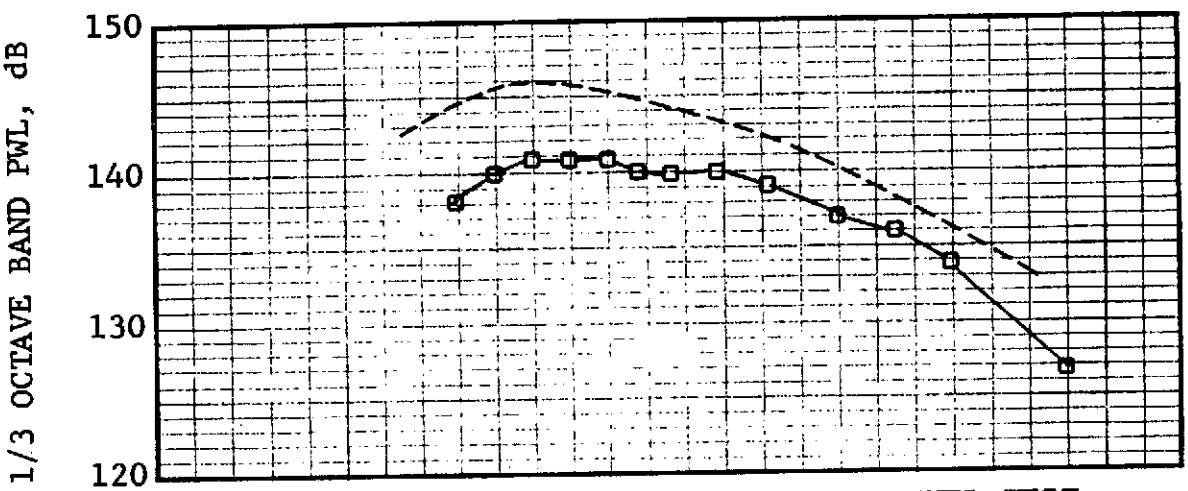

FIGURE 11.6 - ISOLATED NACELLE WIND TUNNEL TEST
V_o = 330 FT/SEC (101 M/SEC)
V_j = 1250 FT/SEC (381 M/SEC)

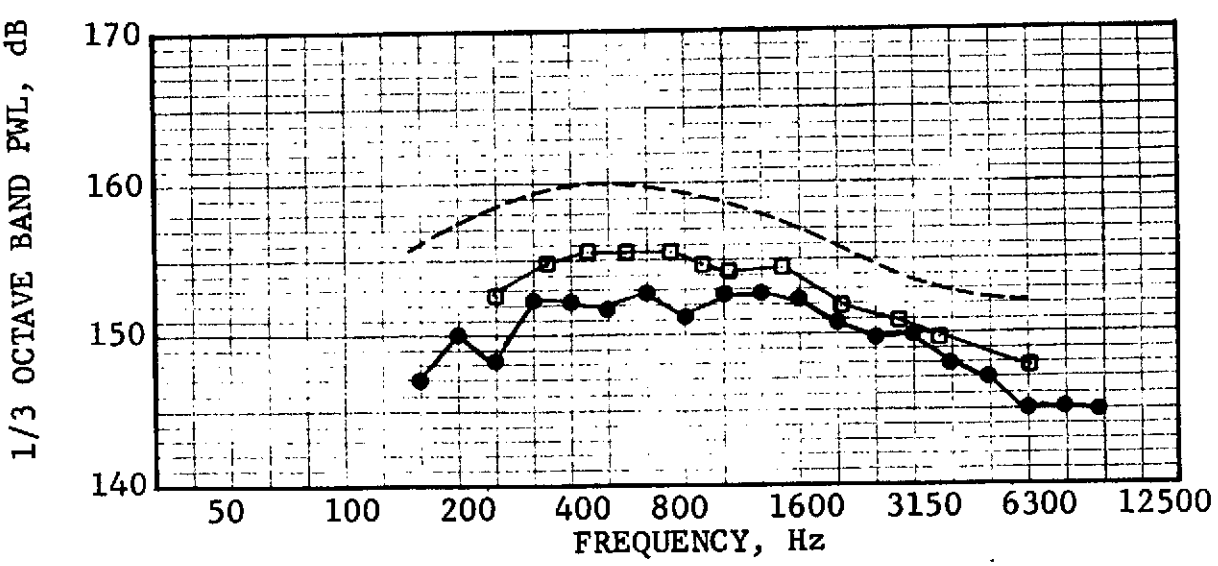

FIGURE 11.7 - ISOLATED NACELLE WIND TUNNEL TEST
V_o = 330 FT/SEC (101 M/SEC)
V_j = 1975 FT/SEC (602 M/SEC)

● DATA

□ PREDICTED

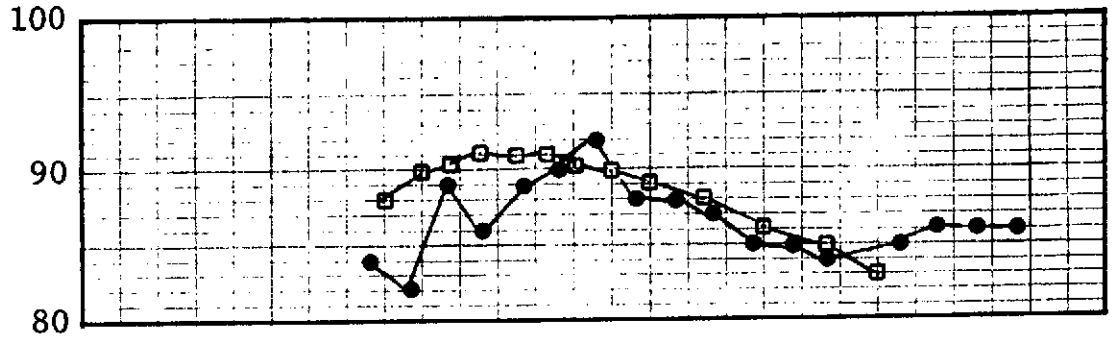

FIGURE 11.8 - ISOLATED NACELLE WIND TUNNEL TEST
V_∞ = 249 FT/SEC (75.9 M/SEC)
V_j^o = 1326 FT/SEC (404 M/SEC)
θ^j = 100° 100 FT. ARC (30.5M)

1/3 OCTAVE BAND SPL, dB

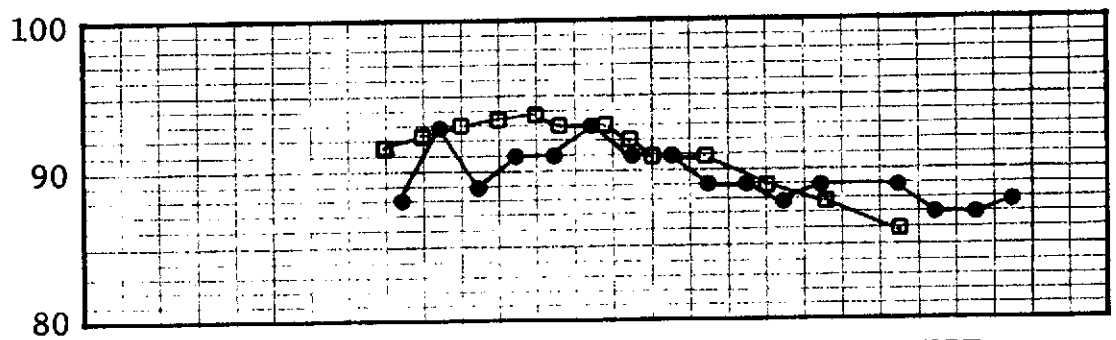

FIGURE 11.9 - ISOLATED NACELLE WIND TUNNEL TEST
V_∞ = 249 FT/SEC (75.9 M/SEC)
V_j^o = 1326 FT/SEC (404 M/SEC)
θ^j = 110° 100 FT. ARC (30.5M)

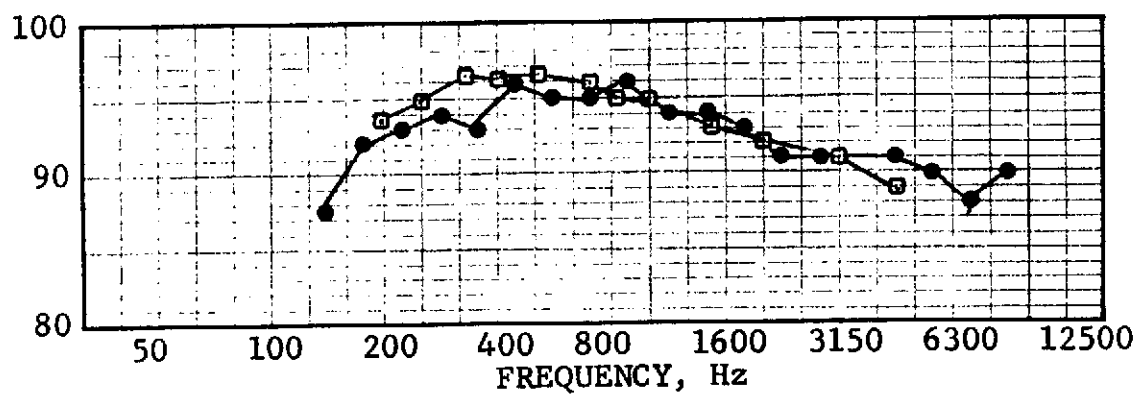

FIGURE 11.10 - ISOLATED NACELLE WIND TUNNEL TEST
V_∞ = 249 FT/SEC (75.9 M/SEC)
V_j^o = 1326 FT/SEC (404 M/SEC)
θ^j = 120° 100 FT. ARC (30.5M)

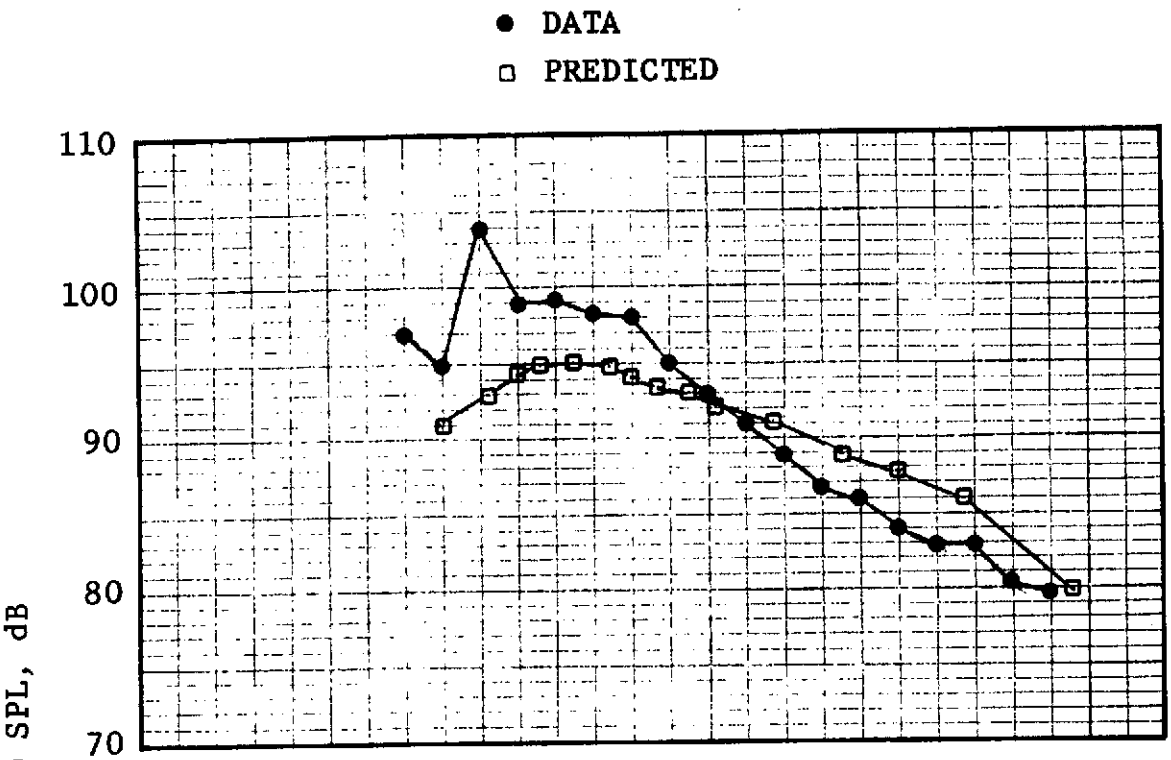

FIGURE 11.11 - ISOLATED NACELLE WIND TUNNEL TEST
V_∞ = 249 FT/SEC (75.9 M/SEC)
V_j^o = 1326 FT/SEC (404 M/SEC)
θ = 150° L00 FT. ARC (30.5M)

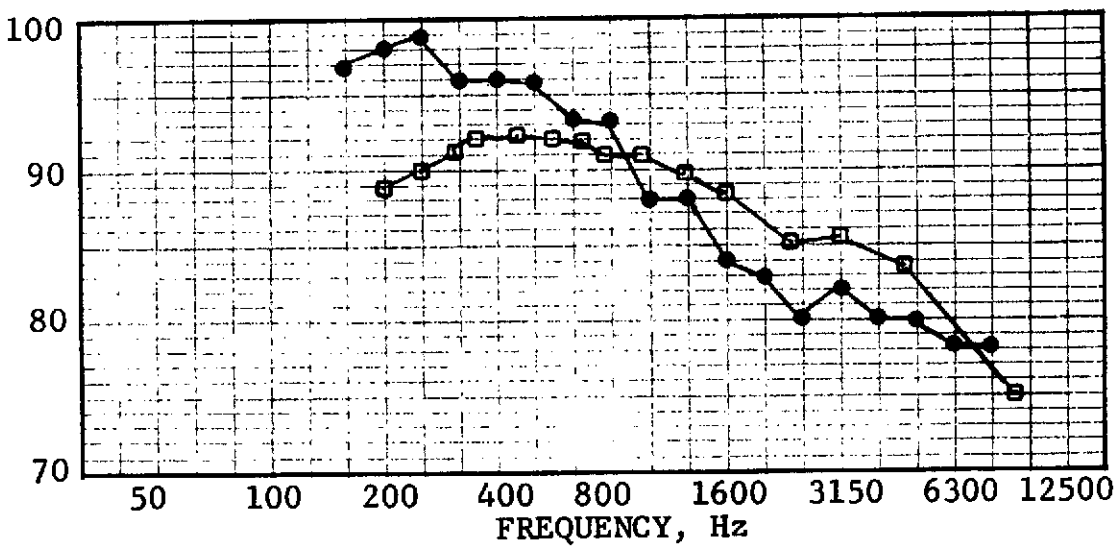

FIGURE 11.12 - ISOLATED NACELLE WIND TUNNEL TEST
V_∞ = 249 FT/SEC (75.9 M/SEC)
V_j^o = 1326 FT/SEC (404 M/SEC)
θ = 160° 100 FT. ARC (30.5M)

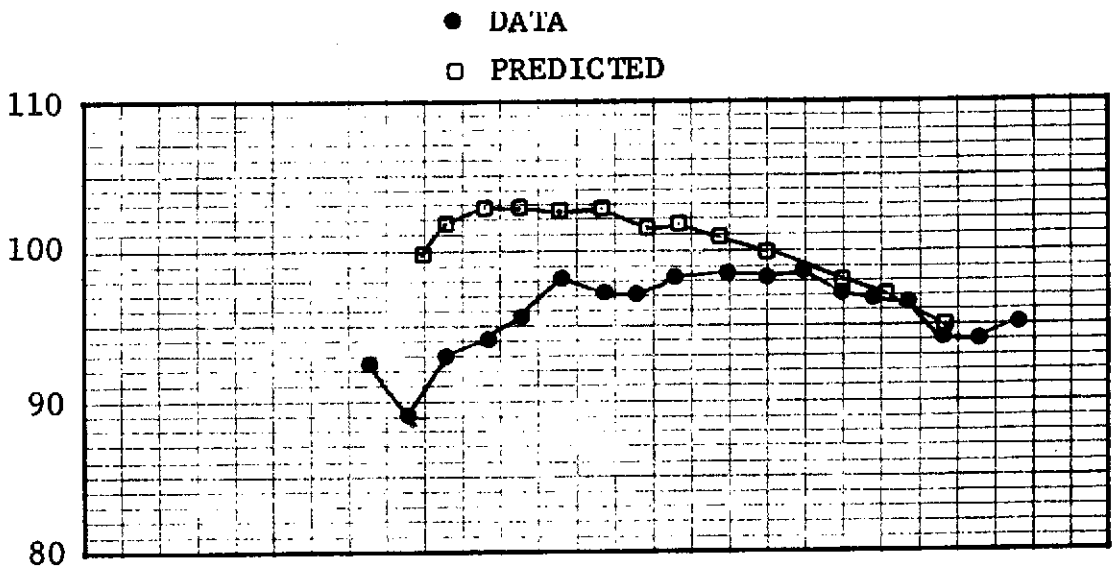

FIGURE 11.13 - ISOLATED NACELLE WIND TUNNEL TEST
V_∞ = 328 FT/SEC (100 M/SEC)
V_j^o = 1975 FT/SEC (602 M/SEC)
θ = 100° 100 FT. ARC (30.5M)

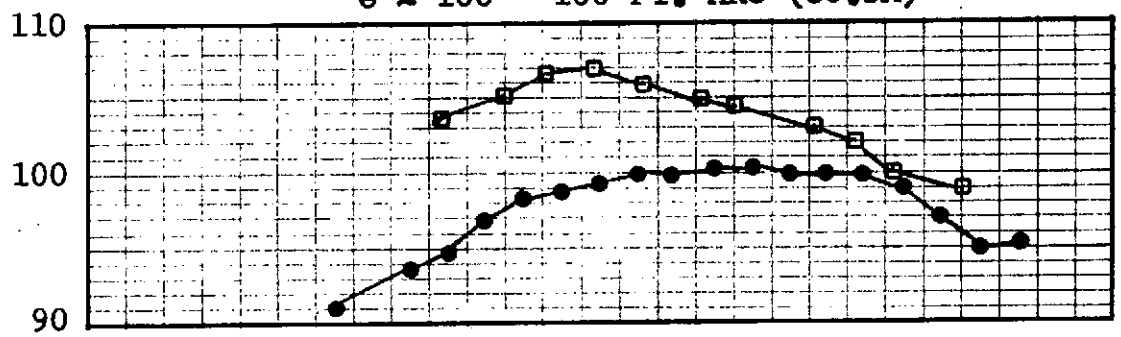

FIGURE 11.14 - ISOLATED NACELLE WIND TUNNEL TEST
V_∞ = 328 FT/SEC (100 M/SEC)
V_j^o = 1975 FT/SEC (602 M/SEC)
θ = 110° 100 FT. ARC (30.5M)

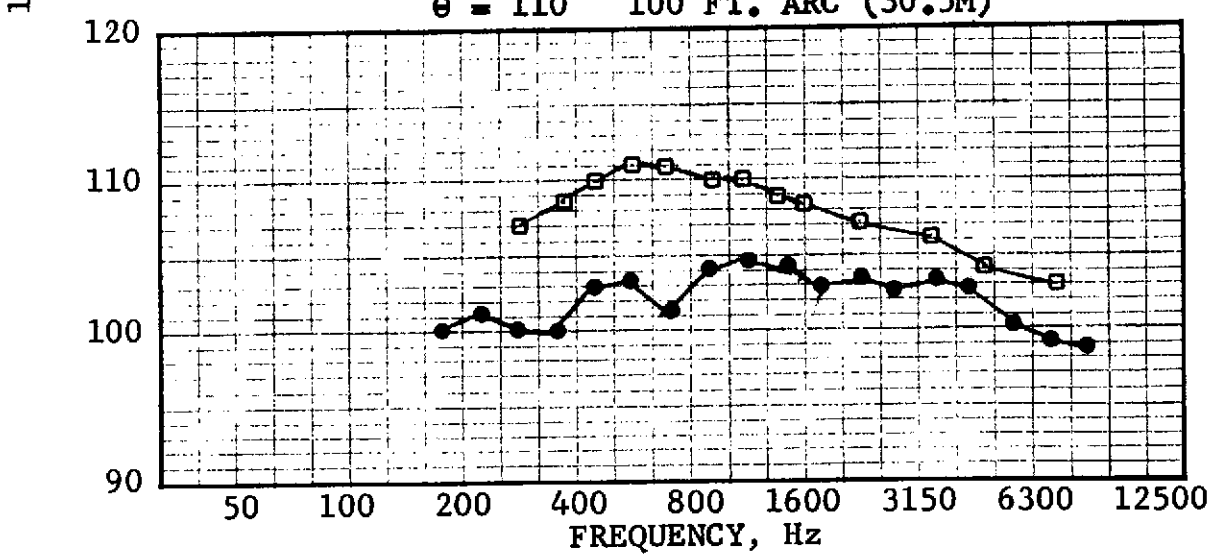

FIGURE 11.15 - ISOLATED NACELLE WIND TUNNEL TEST
V_∞ = 328 FT/SEC (100 M/SEC)
V_j^o = 1975 FT/SEC (602 M/SEC)
θ = 120° 100 FT. ARC (30.5M)

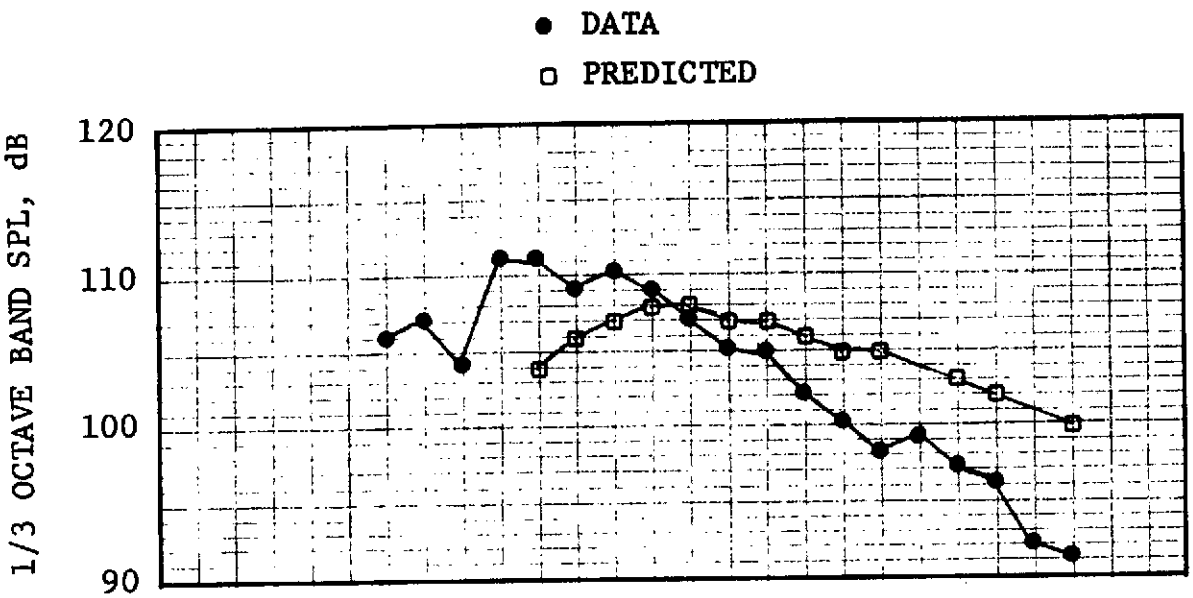

FIGURE 11.16 - ISOLATED NACELLE WIND TUNNEL TEST
V_∞ = 328 FT/SEC (100 M/SEC)
V_j^o = 1975 FT/SEC (602 M/SEC)
θ = 150° 100 FT. ARC (30.5M)

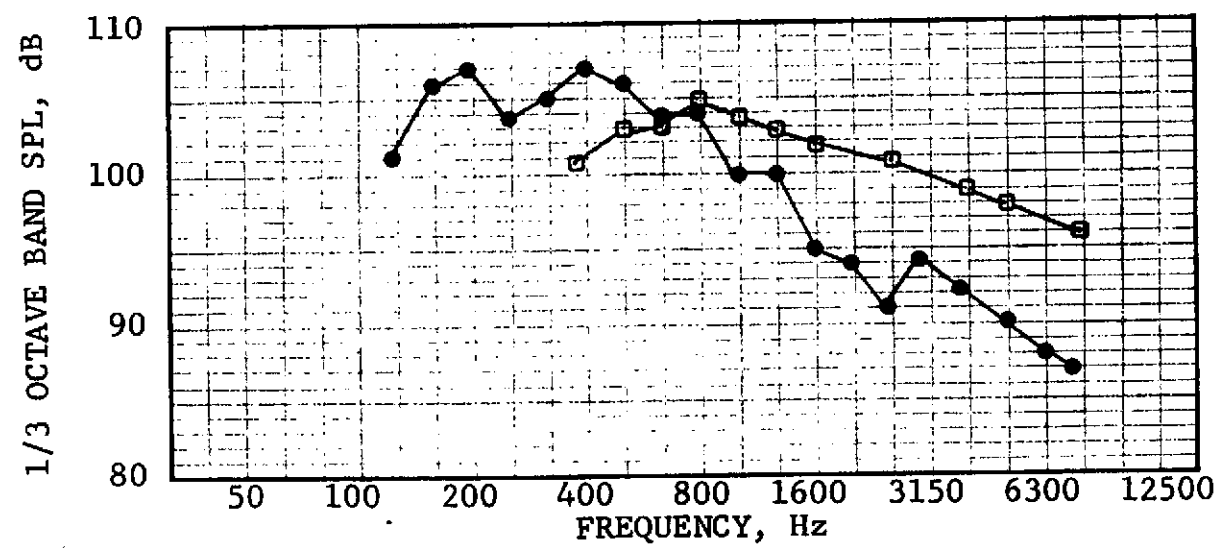

FIGURE 11.17 - ISOLATED NACELLE WIND TUNNEL TEST
V_∞ = 328 FT/SEC (100 M/SEC)
V_j^o = 1975 FT/SEC (602 M/SEC)
θ = 160° 100 FT. ARC (30.5M)

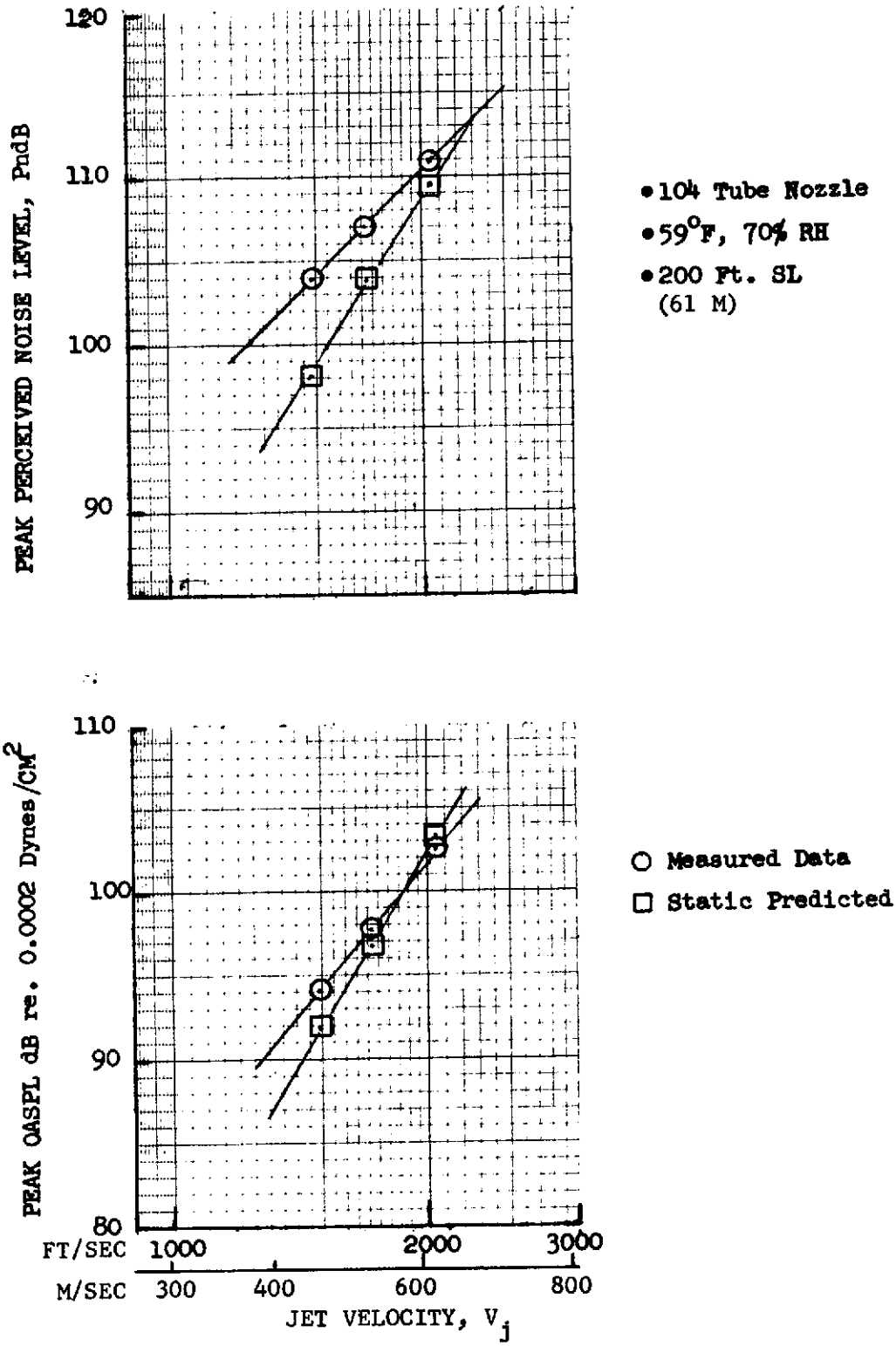

FIGURE 11.18 - COMPARISON OF MEASURED AND PREDICTED STATIC PEAK PNL AND OASPL

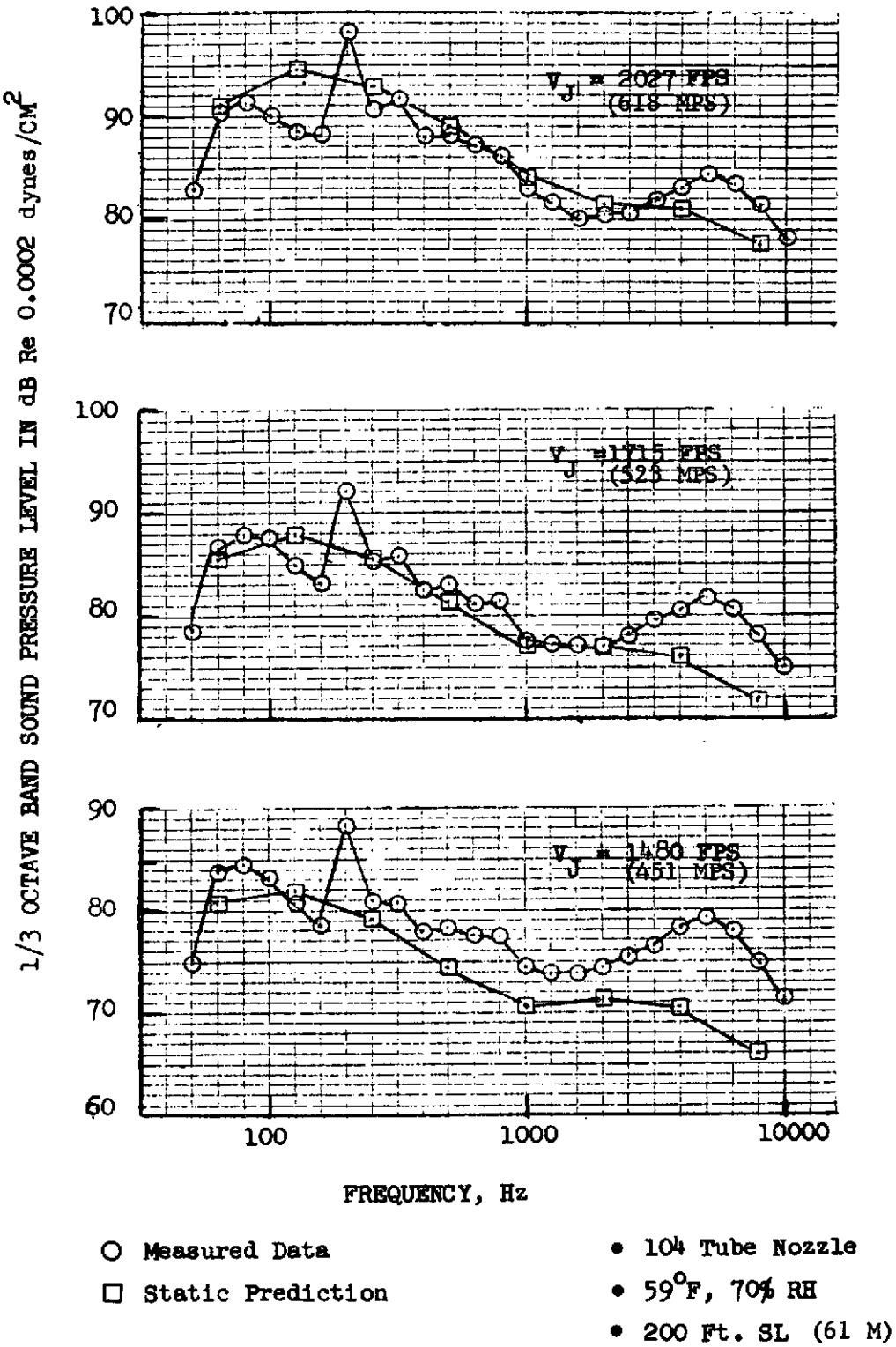

FIGURE 11.19 - COMPARISON OF MEASURED AND PREDICTED STATIC PEAK ANGLE SPECTRA

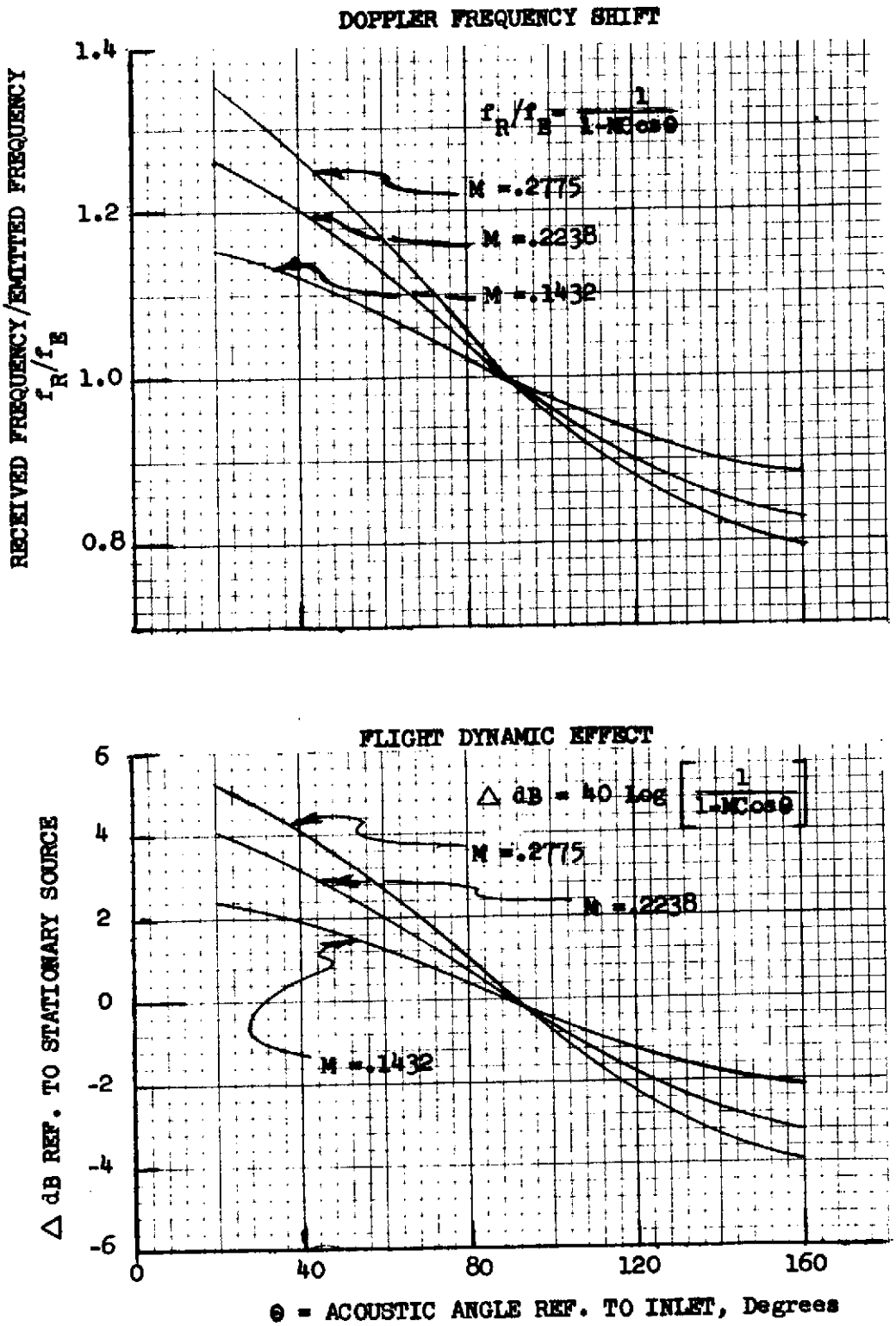

FIGURE 11.20 - DOPPLER AND DYNAMIC EFFECTS AT WIND TUNNEL MACH NUMBERS

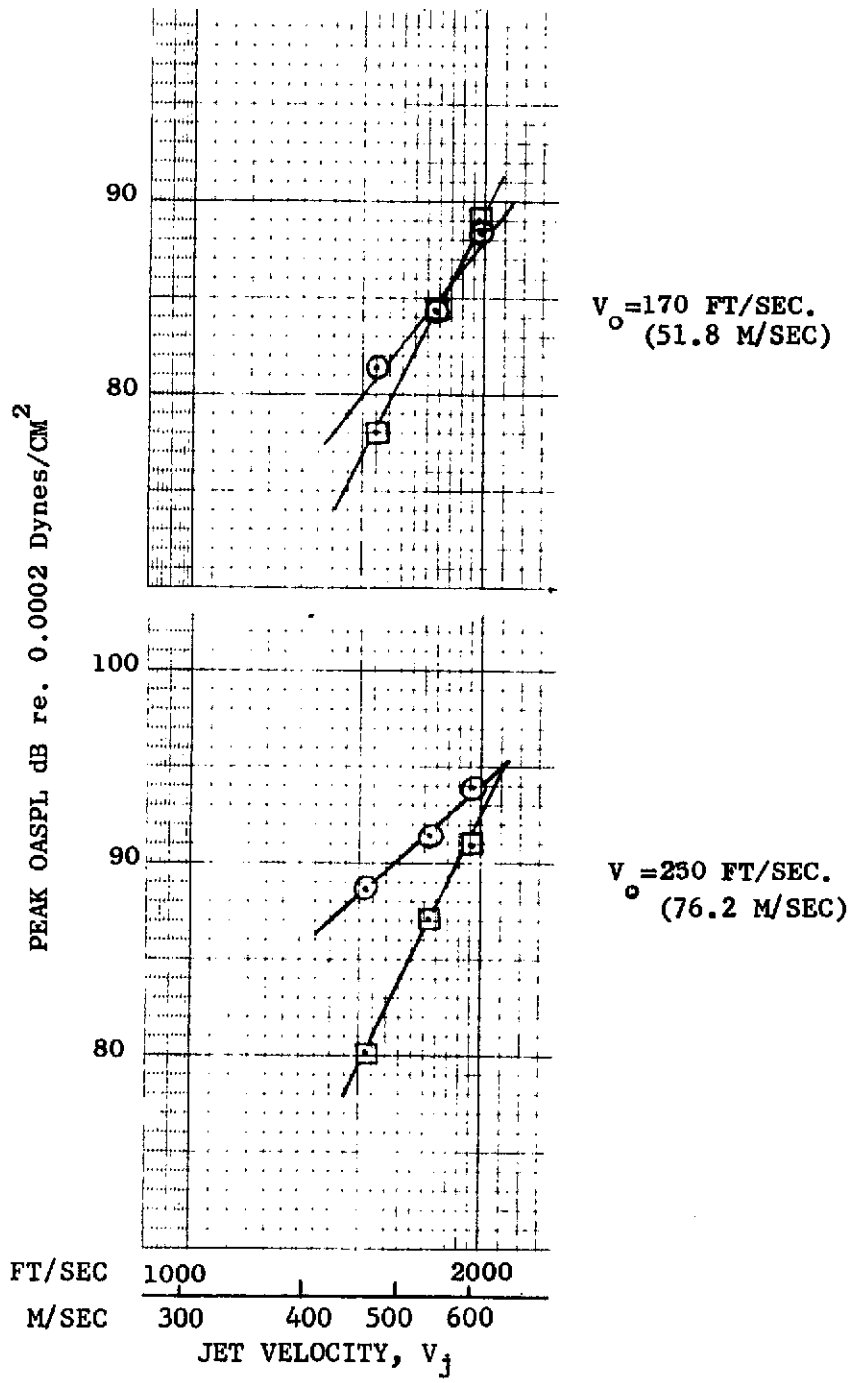

104 TUBE NOZZLE
59°F, 70%R.H.
200 FT. SIDELINE (61 M)

○ MEASURED DATA, CORRECTED FOR FLIGHT
□ FLIGHT PREDICTED

FIGURE 11.21 - COMPARISON OF PREDICTED AND MEASURED PEAK OASPL AT SIMULATED FLIGHT CONDITIONS

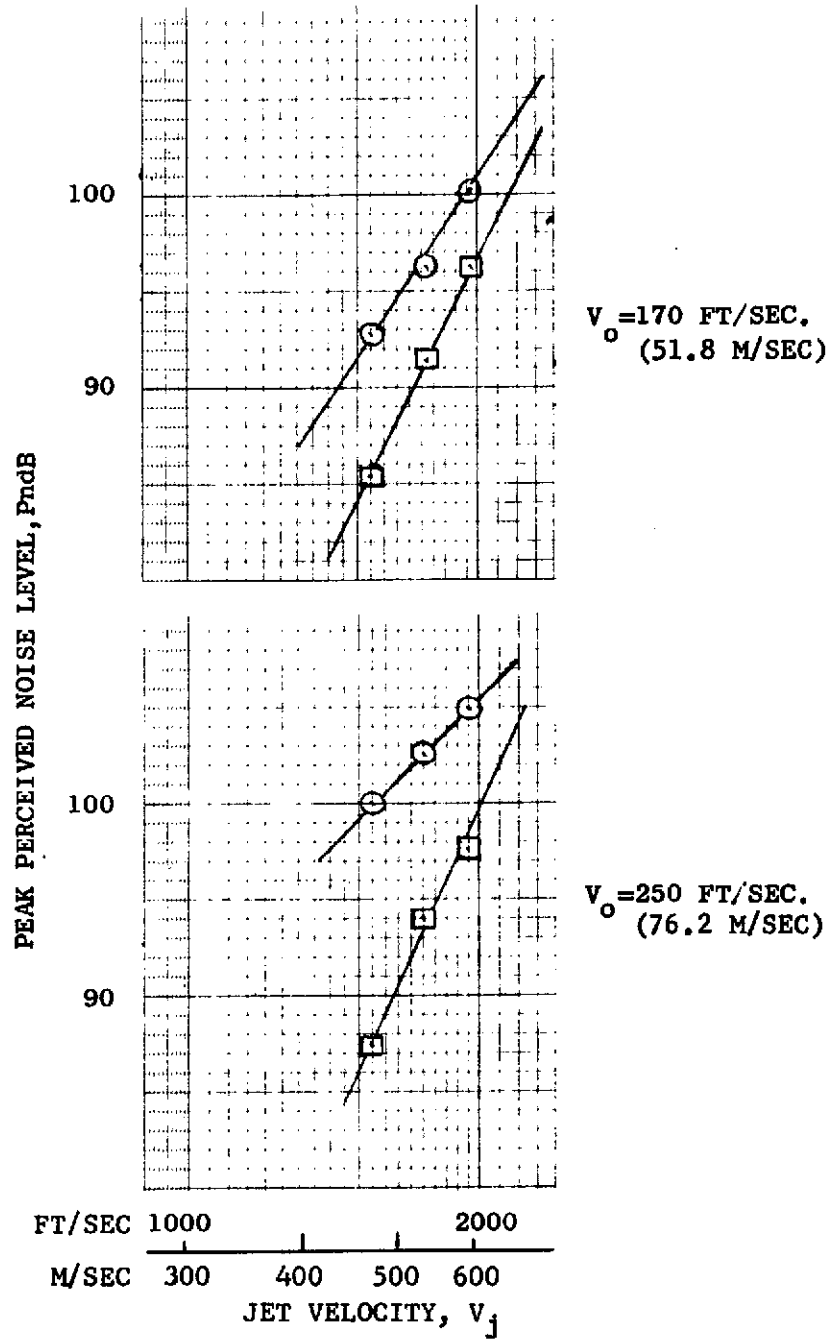

104 TUBE NOZZLE
59°F, 70% R.H.
200 FT. SIDELINE (61 M)

○ MEASURED DATA, CORRECTED FOR FLIGHT
□ FLIGHT PREDICTED

FIGURE 11.22 - COMPARISON OF PREDICTED AND MEASURED PEAK PNL AT SIMULATED FLIGHT CONDITIONS

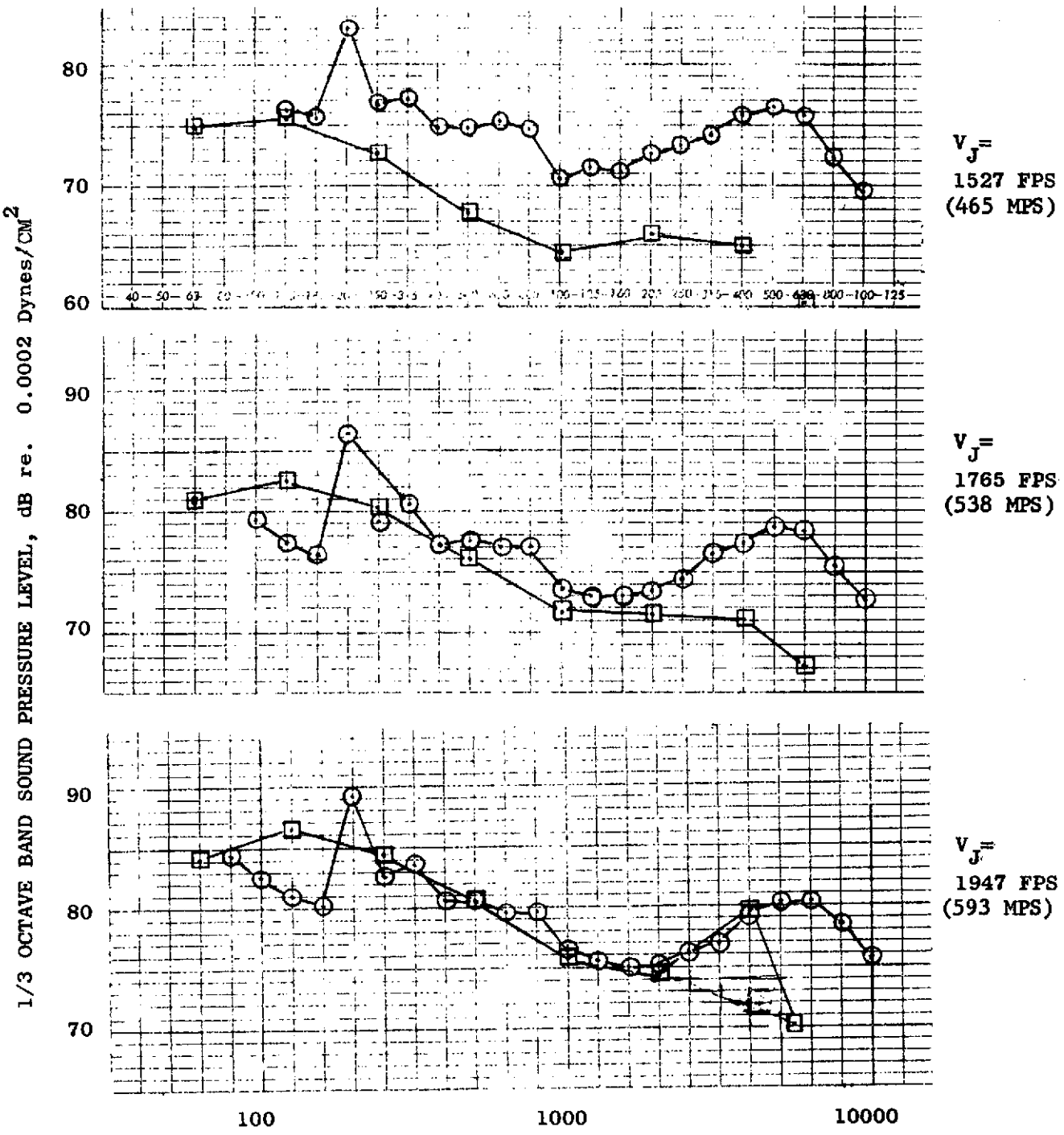

104 TUBE NOZZLE
59°F, 70% R.H.
200 FT. SIDELINE (61 M)
V_o=170 FT/SEC. (51.8 M/SEC)

○ MEASURED DATA, CORRECTED FOR FLIGHT
□ FLIGHT PREDICTED

FIGURE 11.23 - COMPARISON OF PREDICTED AND MEASURED PEAK ANGLE SPECTRA V_o = 170 FT/SEC (51.8 M/SEC)

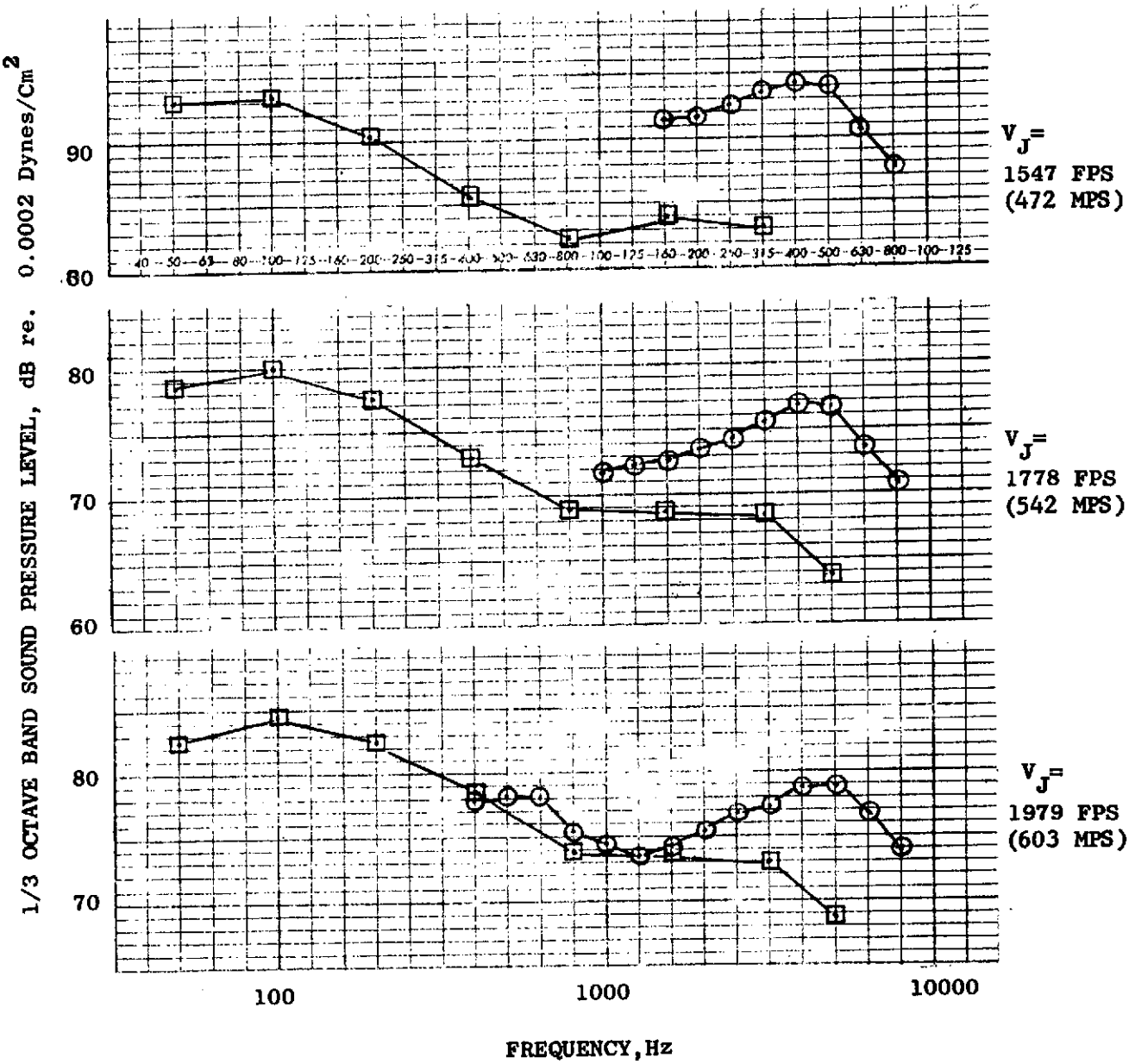

104 TUBE NOZZLE
59°F, 70% R.H.
200 FT. SIDELINE (61 M)
V_o= 250 FT/SEC. (76.2 M/SEC)

○ MEASURED DATA, CORRECTED FOR FLIGHT
□ FLIGHT PREDICTED

FIGURE 11.24 - COMPARISON OF PREDICTED AND MEASURED PEAK ANGLE SPECTRA V_o = 250 FT/SEC (76.2 M/SEC)

12.0 CONCLUSIONS

This series of wind tunnel and static tests has provided a comprehensive data bank for a variety of nozzle configurations. The data analysis has indicated that substantial changes in the jet noise signature of an exhaust nozzle configuration due to a simulated freestream velocity can be measured in a wind tunnel. The magnitude of the change is a function of the nozzle exhaust velocity, acoustic angle and the wind tunnel freestream velocity. The operating envelope for which this effect may be measured in the wind tunnel is a function of the following:

- The freestream velocity in the wind tunnel relative to the jet velocity of the exhaust nozzle.
- The type of nozzle configuration that is being evaluated. For example, a conical nozzle could be evaluated at a lower jet velocity than a suppressor nozzle because the conical nozzle would have a higher jet noise signature.
- The location of the microphones relative to the exhaust jet i.e. both the influence of reverberation and background noise can be minimized by making acoustic measurements close to the exhaust stream.

To successfully perform absolute level measurements in a wind tunnel, valid reverberation corrections must be defined. The results of the studies in this program indicated that the wind tunnel reverberation corrections determined using the dodecahedron sound source are not in agreement at the angle of maximum jet noise with those obtained by comparing indoor and outdoor static acoustic data. Two reasons for this disagreement are that the dodecahedron sound source is monopole and omidirectional. Also, the sound source was placed at only one location in the wind tunnel. In contrast, the exhaust jet may be visualized as a series of highly directional point sources extending along the axis of the jet. Therefore, if a speaker system is employed, the calibration procedure should account for the extended source effects.

Although reverberation corrections can be determined, the results of this study indicate that the most direct approach would be to minimize the effects.

This may be done by using directional microphones or locating the microphones in close proximity to the exhaust jet. The results of the farfield to near field comparisons indicate that this approach does yield meaningful results on the basis of a spectrum analysis above the minimum frequency where ground reflection corrections are valid.

In comparing the conical ejector nozzle data, the AIE nozzle data and the 104 tube suppressor nozzle data to determine the relative velocity effect, the following results are apparent:

- The addition of freestream velocity reduces the jet noise signature of the conical ejector nozzle, as well as the signature of other suppressor nozzles.
- The magnitude of this effect is a function of the freestream velocity and the jet velocity of the exhaust nozzle.
- The relative velocity effects are most apparent at the angles of max noise and do not have as strong an influence at the angles in the forward quadrant. The simulated freestream environment does not cause the suppressors to become ineffective. In fact, at the extreme acoustic angles in the aft quadrant the 104 tube nozzle becomes more effective.
- The comparisons indicate that the effectiveness of the AIE nozzle as a suppressor in a relative velocity environment is inconclusive with regards to the magnitude of suppression in a relative velocity field.
- The acoustically-treated shroud on the 104 tube nozzle provided an additional 4 - 6 dB suppression depending on the jet velocity and was essentially unaffected by the freestream velocity. The addition of the acoustically-treated shroud affects the high frequency portion of the spectra.

The results of the analytical studies indicate that the agreement between the predicted and measured results for the conical ejector nozzle are good on the basis of OAPWL as a function of jet velocity and power level spectra. The comparisons indicate that the one-third octave band spectra do not show good agreement in general and need further work to correct this problem.

The comparison for the 104 tube nozzle configuration indicates that the comparisons at the high jet velocity are in good agreement on an OASPL, PNL and spectrum basis. However, the comparisons at the lower jet velocity indicate a marked disagreement which can be explained by the fact that the effective number of tubes radiating to the far field change as a function of jet velocity. This effect needs to be incorporated into the semi-empirical prediction procedure.

13.0 RECOMMENDATIONS

This report has been an effort to document the results of a comprehensive series of wind tunnel and static tests using a variety of exhaust nozzle configurations. The analysis has been done in the areas that are felt to represent the critical problems that must be solved to determine the validity of wind tunnel measurements and the effect of relative velocity on a suppressor in a simulated freestream environment.

The nozzles used in this test series were also used in a series of flight tests conducted using a F106 aircraft. The results are presented in references 13.1 and 13.2. The first recommendation is that the results of these test series should be compared with these flyover test results. However, the data measured in the wind tunnel should be corrected for dynamic and doppler effect.

This validity of wind tunnel measurements is dependent on three critical areas which may be stated as follows:

1) Reverberation effects must be minimized or eliminated.

2) Background noise influence must be corrected for or eliminated.

3) The farfield to nearfield region must be defined as a function of frequency.

The problem stated in item 1 may be partially solved by using directional microphones. Using these microphones as a technique for wind tunnel measurements should be evaluated further. Also, treating the walls of the wind tunnel with standard acoustic treatment has been shown to have a significant effect on minimizing reverberation effects.

The effect of tunnel background noise, item 2, can be minimized by being close to the noise source. Therefore, it is recommended that emphasis be placed on solving the farfield to nearfield correlation problem. This is imperative because if the microphone can be placed extremely close to the exhaust jet, both the effects of background noise and reverberation can be virtually eliminated.

Finally, more detailed studies need to be conducted to define the mechanisms of jet noise generation in a complex suppressor system. For example, the change in the turbulent structure of the exhaust jet due to the addition of the various freestream velocities could be measured using a laser velocimeter. The results of this type of detailed study would then provide the required information for modifying existing prediction procedures.

14.0 REFERENCES

10.1 Bies, D.A., "Investigation of the Feasibility of Making Model Acoustic Measurements in the NASA/Ames 40 by 80 Foot Wind Tunnel", prepared under contract NASR-6206 by Bolt, Beranek, and Newman Inc.

10.2 Hoch, R. and Thomas, P., "The Effect of Reflections on Jet Sound Pressure Spectra", First Symposium on Aeronautical Acoustics, March 6, 7, 8, 1968.

10.3 Howes, Walton L., "Ground Reflection of Jet Noise", NASA TR R-35, 1959.

10.4 Atencio, Adolph Jr., Kirk, Jerry V., Soderman, Paul T., and Hall, Leo P., "Comparison of Flight and Wind Tunnel Measurements of Jet Noise for the XV-5B Aircraft", NASA TMX-62,182, October 1972.

11.1 Lee R. at al, "Research Investigation of Generation and Suppression of Jet Noise", General Electric Company, Flight Propulsion Lab. Dept., Cincinnati, Ohio, 1961.

11.2 Reichardt, H., "New Theory of Free Turbulence", Zeit. ang. Math, U. Mech. 21, 257 (1941), Roy. Aero. Soc. J. 47, 1967 (1943)

11.3 "Quarterly Progress Report No. 3, 'Supersonic Transport Noise Reduction Technology Program - Phase II'", FAA Contract No. DOT-FA72WA2894 December 1 through February 23, 1973.

11.4 Gray, V.; Gutierreo, D.A.; Walker, D.Q.; "Assessment of Jet as Acoustic Shields by Comparison of Single and Multitube Suppressor Nozzle Data", NASA TMX-71450, October 15, 1973.

13.1 Brausch, J.F.; "Flight Velocity Influence on Jet Noise of Conical Ejector, Annular Plug and Segmented Suppressor Nozzles", NASA CR120961, August, 1972.

13.2 Wilcox F.A.; "Comparison of Ground and Flight Test Results Using a Modified F106B Aircraft", NASA TMX-71439, November, 1973.